Cosmology and light particles in scalar and neutrino portal extensions of the Standard Model

A thesis submitted to The University of Manchester for the degree of Doctor of Philosophy in the Faculty of Science and Engineering

2022

Abigail R. Keats

School of Natural Sciences

Department of Physics and Astronomy

Contents

Word count: 41,600

List of Figures

List of Tables

Abstract

This thesis aims to tackle some of the unanswered questions in the Standard Models of cosmology and particles. The large-scale homogeneity, isotropy and flatness of the observable universe, and its small-scale primordial density perturbations that seed structure formation, can be explained with the addition of an inflationary period preceding the Hot Big Bang. We study an inflationary model that minimally extends the Standard Model (SM) with a Z_2 symmetric potential containing a single scalar field, serving as our inflaton, with a quartic self-coupling and a non-minimal coupling to gravity. With the addition of an inflaton-SM Higgs portal coupling, the universe is able to efficiently reheat. We study two variations of the model, with scale symmetry breaking in the inflaton sector and in both the inflaton and Higgs sectors.

In the model with scale symmetry breaking in just the inflaton sector we find two windows of inflaton masses that allow for successful reheating: light inflaton with masses ($0.16 \lesssim m_\chi \lesssim 16$) GeV reheat via two-to-two inflaton-Higgs scattering, and heavy inflaton with masses ($250 < m_\chi \lesssim 7600$) GeV reheat via their decay into Higgs particles. Light inflatons are more strongly coupled to the SM, and their mass is constrained by particle physics experiments to $m_\chi > 1$ GeV. Heavy inflaton are very weakly coupled to the SM, and evade direct observational constraints. In the model with scale symmetry breaking in both sectors, we find that only the light inflaton window is viable if we assume our universe is metastable. Inflaton masses in the range $O(10^{-3})$ GeV $\leq m_\chi \leq m_h$ evade all current cosmological, experimental and stability constraints.

There is a wealth of evidence that supports the existence of dark matter (DM), from the large scale structure of the universe, astrophysical phenomena and the Cosmic Microwave Background's power spectrum. We incorporate sterile neutrino DM into our inflationary model with the extension of a Neutrino Minimal Standard Model, modified with an inflaton-sterile neutrino Yukawa coupling. We study DM production via inflaton decay in the early universe, and find that the DM properties are determined by a complex interplay of constraints from cosmology and particle physics. Light inflaton produce warm DM and masses in the range $O(10 - 100)$ keV and heavy inflaton produce cold DM with masses $O(1 - 10)$ MeV; both DM windows satisfy the requirements for structure formation. With the addition of two heavier degenerate sterile neutrinos with masses $O(10^3 - 10^{10})$ GeV, the model is able to generate the baryon asymmetry of the universe via leptogenesis, and the SM neutrino masses via the see-saw mechanism.

Declaration

No portion of the work referred to in the thesis has been submitted in support of an application for another degree or qualification of this or any other university or other institute of learning.

Copyright

Acknowledgements

Thank you to my supervisors, Fedor Bezrukov and Jeffrey Forshaw, for imparting your knowledge, guidance and feedback throughout my PhD and the writing of my thesis. Thank you to the Science and Technology Facilities Council (STFC) for funding my studies. Thank you to all my friends for your unwavering belief in me. Thank you Lucy Simper, I am so grateful for your constant love and support. Thank you to my partner, Alex Simpson, your grounding presence and encouragement got me over the finish line.

Chapter 1

Introduction

1.1 The Standard Model of particles

The Standard Model (SM) of particles describes the fundamental forces that govern the universe: strong, weak and electromagnetic (EM). The model excludes gravity, as we currently have no quantum description of the force. Gravity is described at low energies by Einstein's effective field theory, General Relativity [1], which breaks down at scales above the Planck mass, $M_{\mathrm{Pl}} = 1.221 \times 10^{19}$ GeV. The SM has had unprecedented success in predicting and explaining almost all the results of particle physics experiments. There are, however, still some questions in particle physics that can not be answered by the SM: how did our universe become dominated by matter over antimatter; what mechanism generates the SM neutrino masses; what is dark matter (DM); and what are the mechanisms for SM and DM production?

We observe the universe to be filled with remnant matter leftover from matter-antimatter annihilation in the early stages of its evolution. The excess of matter is a consequence of sizeable charge-parity (CP) violating processes [2], which generates a matter-antimatter asymmetry. In the SM, quark mixing is the only source of CP violation, and has been observed in the decay of B, K and D mesons [3–7]. However, CP violation in the SM is many orders of magnitude too small to explain the matter-antimatter asymmetry of the universe [8–10] that produces a baryon-to-entropy ratio of $O(10^{-10})$ [11]. We therefore require extensions of the SM to provide new sources of CP violation.

In the gauge theory of the combined electromagnetic and weak (EW) interactions, explicit mass terms are impossible to add as they contradict gauge invariance. We can, however, maintain gauge invariance of the theory and generate the particle masses if the EW symmetry is spontaneously broken. This is achieved when a complex scalar field, the Higgs field, acquires a non-zero vacuum expectation value (VEV). The SM fermion masses are then generated through their Yukawa coupling with the Higgs field, which couples the left- and right- hand fermionic components. Post spontaneous symmetry breaking, the fermion mass term is then given by the Higgs VEV multiplied by the Yukawa coupling. As neutrinos have no right-handed

component, they can not acquire a mass through a Yukawa coupling, and so the SM predicts them to be massless. However, this is in contradiction to the observed neutrino oscillations, which was confirmed in 2001 by the Sudbury Neutrino Observatory [12, 13]. We therefore require a process beyond the SM to generate the SM neutrino masses.

Finally, there is a vast amount of evidence to support the existence of DM from observed gravitational effects [14–16], the CMB's power spectrum [17, 18], and structure formation [19, 20]. Although we have not directly observed DM, we have been able to infer that it makes up over 80% of the total matter density in the universe [21] and it has the following properties: DM must be weakly coupled (or decoupled) to the SM; it is a massive particle; and it is cool enough to form structures in the hot radiation-dominated epoch. There are no viable DM candidates in the SM, and within the bounds of our current knowledge, there are a rich variety of possible DM models that could extend the SM [22–30].

1.2 The Standard Model of cosmology

The observable universe is almost completely flat, homogeneous and isotropic. We have been able to deduce that the universe is expanding at an accelerating rate from measuring the red-shift of Type Ia supernovae [31, 32], which thereby requires the addition of a positive cosmological constant in Einstein's field equations [1]. In the Standard Model of cosmology (SMC) the positive cosmological constant is interpreted as 'dark energy', which dominates the energy density of the universe today. This discovery led to the 'Hot Big Bang model', as cosmologists theorized that the universe expanded and cooled from an initial highly dense and hot state. Additionally, we know that large scale-structures, such as galaxies and galaxy clusters, have a dominant dark matter component from observing its gravitational effects [14–16]. Our best fit cosmological model with dominant components of dark energy and cold dark matter [33] has very accurately predicted the results of key events in the history of the universe: the existence and properties of the CMB [34–36]; the abundance of light elements from Big Bang Nucleosynthesis (BBN) [37–39]; the number of neutrino species in the SM [40]; and the formation of large scale structures [41, 42]. However despite its success, the Hot Big Bang model is unable to explain the homogeneity, isotropy and flatness of the universe, and how primordial matter density perturbations that seed large scale structure formation were generated.

The Hot Big Bang model predicts that the observable universe is made up of many causally disconnected regions, which we would naturally expect to vary in temperature and density. However, the CMB revealed that our observable universe is remarkably homogeneous and isotropic, with small primordial density perturbations [34–36] that the Hot Big Bang model has no means to generate. Additionally, as curvature grows with the evolution of the universe,

until its recent dark energy dominated epoch, we require an extremely small initial curvature to produce a flat universe today. These initial conditions present cosmologists with complex fine-tuning problems in the Hot Big Bang model. A possible solution to which is 'inflation': a period of positive accelerating expansion prior to the Hot Big Bang.

1.3 Outline

In order to evade spoiling the success of the SM and SMC, it is preferable that solutions for problems such as inflation, SM and DM production, the generation of the baryon asymmetry of the universe (BAU) and SM neutrino masses, are provided for by minimal extensions to the models. The original work of this thesis [43, 44] studies a model of inflation that extends the SM by just a single scalar inflaton field. The main focus of the study is to constrain the model from cosmology, for successful inflation and reheating (SM production), and particle physics. However, the most general model is still very hard to constrain, and so we focus on two theoretically motivated variants, which we discuss below.

The measurement of particle masses tells us that the universe is not scale symmetric. The first variation of our inflationary model assumes scale symmetry is only broken in the inflaton sector by a single massive parameter, and an inflaton-Higgs portal coupling allows for the transfer of symmetry breaking into the SM sector [43, 45–48]. In the second variation of our inflationary model, scale symmetry is broken by two massive parameters in the inflaton and Higgs sectors [44]. The model is then tightly constrained under the assumption that the universe is metastable, which we motivate as follows. The measurement of the SM Higgs boson mass revealed that our universe is surprisingly close to the metastability/stability bound [49]. If the universe is stable, then the observation that its energy density is dominated by a positive cosmological constant [31, 32], known as 'dark energy', tells us that the universe will eternally expand at an accelerating rate. However, Dvali argues that an eternally accelerating universe would eventually lead to quantum inconsistencies from graviton-graviton scattering [50, 51], and so we require a mechanism for the universe to end before this moment is reached. We provide a possible solution to this problem by requiring our model to give rise to a metastable universe that is sufficiently long-lived.

The next part of original work [43] presented in this thesis incorporates DM in our inflationary model by extending the scalar sector with a modified νMSM [43, 45–47, 52]. Our DM candidate is a sterile neutrino, which is produced in the early universe via inflaton decay. The DM parameters are constrained by the observed DM abundance and the requirements for structure formation. Additionally, we find that the mechanisms for generating the BAU via leptogenesis and the SM neutrino masses studied in the original νMSM [53, 54] are not affected by our modifications.

The thesis begins with four theory and literature review chapters, which provide the reader with the foundational knowledge and experimental constraints that we need to build, analyse and constrain our cosmological models in the final three chapters.

We begin with the thermal history of the universe in chapter 2. Here we review the SMC, which accurately describes the large-scale evolution of the universe since the hot radiation-dominated epoch known as the Hot Big Bang. I define the equations that govern cosmological expansion and the thermal evolution of the universe, which will be necessary for modelling the periods of inflation, reheating and DM production in chapters 6−8. I review the key events in the timeline of the universe's history: neutrino decoupling, Big Bang Nucleosynthesis and photon decoupling. The SMC very accurately predicts the results of these events, and so any extensions to which are significantly constrained. The chapter ends with the best fit cosmological model we have today, with dominant components of dark energy and dark matter. We will use the relative abundance of matter and radiative components to determine when the universe transitioned from radiation to matter-domination, and the relative abundance of DM to constrain the parameters of our DM model.

Chapter 3 studies the theory of inflation, which aims to provide an explanation for the large-scale homogeneity, isotropy and flatness of our observable universe, and its small-scale density inhomogeneities, without the input of finely-tuned initial conditions. A finite period of positively accelerating expansion, called inflation, flattens curved space and ensures the observable universe has previously come into causal contact. I then study the conditions that would lead to inflation for a set of minimal large-field inflationary models, which extend the SM by a single scalar field. Next, I discuss the generation of scalar and tensor cosmological perturbations from the inflationary enhancement of quantum fluctuations of the inflaton field. Scalar perturbations generate density inhomogeneities, which seed the large-scale structure of the universe, and tensor perturbations generate gravitational waves. The inflationary potential is constrained by the measurement of the CMB's amplitude of scalar perturbations, and the limit on the scalar-to-tensor ratio. These constraints will be implemented in our light scalar inflaton model in chapter 6. The chapter ends with analysing the growth of density perturbations that evolve to form large scale structures.

In chapter 4 I review DM. First I discuss a few of the observed gravitational effects that support the existence of DM. I then analyse two DM production mechanisms, freeze-in and freeze-out, which provides us with the framework to constrain the DM abundance and the parameters of our DM model in chapter 7. In the last section I discuss the essential role DM plays in structure formation, and the constraints on models that produce relativistic DM from the smallest observed structures in the universe.

In the final theory chapter 5 we study neutrinos. The observation of SM neutrino oscil-

lations has revealed that the massless SM neutrino sector is incomplete. Here we discuss a possible solution: the Neutrino Minimal Standard Model (νMSM), which extends the neutrino sector by a minimum of two right-handed singlet Majorana (sterile) neutrinos, that generate the SM neutrino masses via the see-saw mechanism. We find that sterile neutrinos can also serve as a DM candidate. I analyse their production mechanisms via active-sterile neutrino mixing, and discuss the various astrophysical constraints on sterile neutrino DM models. Additionally, we analyse the model's mechanisms for leptogenesis, and bound the sterile neutrinos' parameter space by requiring they generate enough lepton asymmetry (LA) to generate the baryon asymmetry of the universe (BAU) via EW sphaleron processes. We will use the analysis carried out in this chapter to extend our light inflaton model with a modified νMSM in chapter 7.

In chapter 6 we begin with our basic inflationary model, which extends the SM by a single scalar inflaton field. The inflaton's quartic self-coupling is constrained from the measurement of the CMB's amplitude of scalar perturbations and upper limit on the tensor-to-scalar ratio. The addition of a symmetry breaking inflaton mass term and an inflaton-Higgs portal allows for efficient reheating and the transfer of symmetry breaking into the SM. We establish two windows in the inflaton parameter space that evade current cosmological and experimental constraints. First I review the work carried out in [45–48] on the 'light' inflaton window, and then present my original work in [43] on the 'heavy' inflaton window.

In chapter 7 we extend our basic inflaton model with a νMSM, modified with an additional inflaton-sterile neutrino Yukawa coupling. Symmetry breaking in the inflaton sector generates the sterile neutrino masses, and initiates sterile neutrino DM production via inflaton decay in the early universe. I review the work carried out in [45–47, 52], which constrains the DM parameter space in the 'light' inflaton window. I then present my original work in [43], which constrains the DM parameter space in the 'heavy' inflaton windows. We find that both regions of DM parameter space are within the bounds for structure formation. We apply the analysis and constraints from generating the SM neutrino masses and the BAU via leptogenesis mechanisms in the standard νMSM in chapter 5, to our modified νMSM.

In chapter 8 I present my work [44] analysing a generic Z_2 symmetric inflaton model, which extends our previous model with a symmetry breaking Higgs mass term. As a result, the measurement of the Higgs boson mass does not uniquely determine the Higgs quartic self-coupling and thus the stability of the EW vacuum. I assume the universe is metastable, and re-constrain the inflaton model in accordance with cosmological and experimental bounds.

I end with conclusions and outlook in chapter 9.

Chapter 2

Thermal history of the universe

The large-scale evolution of the universe from an initial highly dense and hot state to the present day is very successfully described by the Hot Big Bang theory [55–57]. The model was built after discovering that all galaxies are receding from us, which led to the conclusion that the universe is expanding [58–60]. Prior to this observation, it was assumed the universe was static and eternal.

In 1915 Einstein formulated a cosmological framework in his theory of General Relativity [1], in which his field equations describe how matter and energy curve spacetime. He later added a cosmological constant to his field equations to balance the effects of gravity, thus ensuring his model universe was static [61]. Meanwhile, de Sitter modelled a universe with no matter or radiation and dominated by the cosmological constant, which drives an accelerating rate of expansion [62]. It wasn't until 1922, when Friedmann proposed an intermediate model of an expanding universe filled with matter and radiation [63], that we had a good description of the real universe. From Einstein's field equations, he derived the Friedmann equations that relate cosmological expansion to the composition of a homogeneous and isotropic universe [63].

The recession of galaxies was first noted by Slipher in 1912, who observed a Doppler shift in their spectra [58, 59]. Following this result, Lemaître independently derived Friedmann's equations in 1927, and suggested the recession of galaxies was due to the expansion of the universe [64]. This was later confirmed experimentally by Hubble in 1929, who demonstrated that there was a positive linear relationship between the recession velocities of nearby galaxies and their distance to the observer [60], as shown in Figure 2.1. This came to be known as the Hubble-Lemaître law [60]:

$$v = H_0 d, \tag{2.1}$$

where v is the recessional velocity of the galaxy, d is the distance to the observer and H_0 is Hubble expansion rate of the universe today. Extrapolating the expansion backwards in time, the universe must have been denser and hotter, and according to General Relativity, originated from a singularity [65].

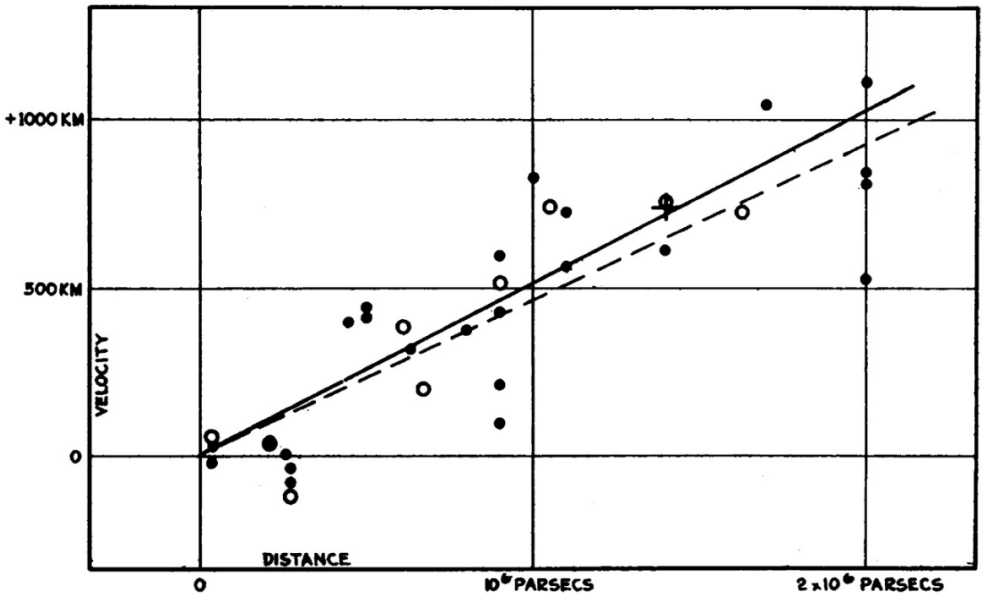

Figure 2.1: Radial velocity against distance of extra-galactic nebulae
Hubble's experimental results, plot taken from [60].

Following Hubble's results, Einstein's cosmological constant was abandoned and the universe was thought to only contain matter and radiation. As a result, cosmologists expected to find that the expansion rate was decelerating due to gravity, however the spectra of distant Type Ia supernovae, observed by The High-Z Supernova Search Team and the Supernova Cosmology Project in the late 1990s, revealed that the universe is in fact accelerating [31, 32]. The cosmological constant was thus reinstated as positive vacuum energy, which dominates the energy density of the universe today.

Whilst the Hot Big Bang theory is successful in its description of the large-scale evolution of the universe, it can not explain why the observable universe is almost completely flat, homogeneous and isotropic, nor the origin of its primordial scalar perturbations that seed large-scale structure. One solution may be that a period of positively accelerating expansion called inflation preceded the Hot Big Bang, which will be the subject of chapter 3.

This chapter will focus on the large scale evolution of the universe starting from the hot radiation-dominated epoch, known as the 'Hot Big Bang' epoch, and roughly following the general logic of the textbooks: 'Introduction to the Theory of the Early Universe: Hot Big Bang Theory' by D. S. Gorbunov and V. A. Rubakov [55], 'The Early Universe' by E. W. Kolb and M. S. Turner [56], and 'Particle Physics and Cosmology: The Fabric of Spacetime' by F. Bernardeau, C. Grojean and J. Dalibard [66]. Firstly, we will provide the reader with the framework of the Hot Big Bang model: the dynamics of cosmological expansion, described by Friedmann's equations, and the thermal evolution of the universe. In the following sections we will show that the model provides an extensive explanation and accurate description of key events in the universe's history, such as neutrino decoupling, Big Bang Nucleosynthesis and

photon decoupling. We will end with the details of the best-fit cosmological model of the real universe, which has dominant components of dark energy and cold dark matter.

2.1 Cosmological expansion

The dynamics of cosmological expansion are derived from Einstein's field equations:

$$G_{\mu\nu} + \Lambda g_{\mu\nu} = 8\pi G T_{\mu\nu}, \tag{2.2}$$

where G is the gravitational constant, and the cosmological constant is interpreted as the vacuum (or 'dark energy') energy density, $\Lambda = \rho_\Lambda$. The equations relate the density and flux of energy and momentum, encoded in the stress-energy tensor, $T_{\mu\nu}$, with spacetime curvature, encoded in the Einstein metric,

$$G_{\mu\nu} = R_{\mu\nu} - \frac{1}{2} g_{\mu\nu} R. \tag{2.3}$$

The 4D space-time metric, $g_{\mu\nu}$, describes the geometry of spacetime and tells us how to compute the distance between two points:

$$ds^2 = g_{\mu\nu} dx^\mu dx^\nu, \tag{2.4}$$

where $(\mu, \nu = 0)$ denotes the time component and $(\mu, \nu = 1, 2, 3)$ denotes the space components. Throughout the thesis we will refer to two 4D spacetime metrics that describe a homogeneous and isotropic universe: the Minkowski metric for a static universe,

$$ds^2 = dt^2 - \gamma_{ij} dx^i dx^j, \tag{2.5}$$

and the Friedmann–Lemaître–Robertson–Walker (FLRW) metric for an expanding universe,

$$ds^2 = dt^2 - a^2(t) \gamma_{ij} dx^i dx^j, \tag{2.6}$$

$$= a^2(\tau) \left(d\tau^2 - \gamma_{ij} dx^i dx^j \right), \tag{2.7}$$

where $(i, j = 1, 2, 3)$ and for a spatially flat universe $\gamma_{ij} = \delta_{ij}$. The scale factor $a(t)$ defines the scaling of the spatial coordinates with time, which is dependent on the composition of the universe. It is used to translate between the physical coordinate system in an expanding universe to the conformal coordinate system, which is equivalent to the physical coordinate system in a static universe. For example, the conformal time τ, given in equation (2.7), is

related to the physical time by

$$\tau = \int \frac{dt}{a(t)}. \tag{2.8}$$

Additionally, we can relate the scale factor to the redshift z of a photon by

$$\frac{a_0}{a(t)} = 1 + z(t) \equiv \frac{\lambda(t_0)}{\lambda(t)}, \tag{2.9}$$

which is defined as the ratio of a photon's wavelength measured today to its wavelength measured at time t.

The Friedmann and Raychaudhuri equations govern the dynamics of cosmological expansion. We derive them using the FLRW metric for a homogeneous and isotropic universe, which has an energy-momentum tensor of the form:

$$T_{\mu\nu} = \text{diag}\left(\rho, p, p, p\right), \tag{2.10}$$

where ρ is energy density and p is pressure. Then taking the 00 and ij components of the Einstein's field equations respectively, the Friedmann and Raychaudhuri equations are given by[1]:

$$\left(\frac{\dot{a}}{a}\right)^2 = \frac{\rho}{3M_{\text{P}}^2} - \frac{\kappa}{a^2}, \tag{2.11}$$

$$2\frac{\ddot{a}}{a} + \left(\frac{\dot{a}}{a}\right)^2 = -\frac{p}{M_{\text{P}}^2} - \frac{\kappa}{a^2}, \tag{2.12}$$

where we have substituted in for the reduced Planck mass:

$$M_{\text{P}} \equiv \frac{1}{\sqrt{8\pi G}} = 2.435 \times 10^{18} \text{ GeV}, \tag{2.13}$$

and the Hubble expansion rate is defined as

$$H(t) \equiv \frac{\dot{a}(t)}{a(t)}. \tag{2.14}$$

Spatial curvature can take values between $-1 \leq \kappa \leq +1$, where positively curved space is modelled as a 3-sphere and negatively curved space is modelled as a 3-hyperboloid. The curvature energy density measured today is[2] [33]

$$\Omega_\kappa \equiv -\frac{\kappa}{\left(a_0 H_0\right)^2} = 0.0007 \pm 0.0019, \tag{2.15}$$

[1] We use the notation $\dot{X} \equiv \partial X/\partial t,\ \ddot{X} \equiv \partial^2 X/\partial t^2$.

[2] Subscript 0 denotes the value of parameters as measured today.

and so we will assume the universe has no spatial curvature ($\kappa = 0$), in which case space is modelled as a 3-plane. The total energy density of a flat universe is called the critical energy density,

$$\rho_c = 3M_{\rm P}^2 H^2, \tag{2.16}$$

and the relative energy density of component i is given by

$$\Omega_i(t) \equiv \frac{\rho_i(t)}{\rho_c(t)}, \tag{2.17}$$

where $\sum_i \Omega_i = 1$ in a flat universe.

To close the set of equations (2.11) and (2.12), we require an additional equation from the conservation of the energy-momentum tensor:

$$\nabla_\mu T^{\mu\nu} = 0, \tag{2.18}$$

where ∇_μ is the covariant derivative[3]. The following equation is derived from the $\nu = 0$ component:

$$\dot{\rho}_{(i)} + 3\frac{\dot{a}}{a}(\rho_{(i)} + p_{(i)}) = 0, \tag{2.19}$$

which holds for individual non-interacting components i as well as for the total sum of components. For a universe in thermal equilibrium, equation (2.19) is equivalent to the statement that entropy in a co-moving volume, $V = a^3$, is conserved. The first law of thermodynamics for the conservation of energy in a co-moving volume is

$$d(\rho a^3) = Td(sa^3) - pda^3 - \sum_i \mu_i d(n_i a^3), \tag{2.20}$$

where ρ is energy density, s is entropy density and n_i is number density. We assume the chemical potentials, μ_i, are vanishing, as we only require a very small matter-antimatter asymmetry in the early universe to generate the matter-dominated universe today; we will argue that this is a plausible assumption in section 2.2. Then, by substituting equation (2.19) into equation

[3]The covariant derivative is related to the Christoffel symbols by $\nabla_\mu T^{\mu\nu} = \frac{\partial T^{\mu\nu}}{dx^\mu} + \Gamma^\mu_{\mu\sigma} T^{\sigma\nu} + \Gamma^\nu_{\mu\sigma} T^{\mu\sigma} = 0$.

(2.20), we have that entropy is conserved in a co-moving volume:

$$\begin{aligned} T\frac{d(sa^3)}{dt} &= (\rho + p)\,\frac{d(a^3)}{dt} + a^3\frac{d\rho}{dt}, \\ &= a^3\left[(\rho + p)\,3\frac{\dot{a}}{a} + \dot{\rho}\right] = 0, \qquad (2.21) \\ &\rightarrow sa^3 = \text{const.} \qquad (2.22) \end{aligned}$$

This conservation law will be particularly useful when we come to evaluate the present day abundance of particles species, such as dark matter (DM), that are decoupled from the thermal bath.

To find the relationship between the Hubble expansion rate and the energy composition of universe, we require the equation of state, which for an ideal fluid is given by

$$p_i = \omega_i \rho_i, \qquad (2.23)$$

where the constant of proportionality, ω_i, depends on the component i of the fluid. Substituting (2.23) into (2.19), we can evaluate the dependence of the energy density, and thus the Hubble expansion rate, on the scale factor:

$$\begin{aligned} \dot{\rho}_i + 3\,(1 + \omega_i)\,\frac{\dot{a}}{a}\rho_i &= 0, \\ \int \frac{d\rho_i}{\rho_i} &= -3\,(1 + \omega_i)\int \frac{da}{a}, \\ \rightarrow \rho_i &\propto a^{-3(1+\omega_i)}. \qquad (2.24) \end{aligned}$$

For non-relativistic matter (m), relativistic matter (γ) and vacuum (Λ) components,

$$\omega_i = \begin{cases} 0, & i = \text{m} \\ \frac{1}{3}, & i = \gamma \\ -1. & i = \Lambda \end{cases} \qquad (2.25)$$

Given equations (2.11) and (2.24), we can then determine the Hubble expansion rate's dependence on the scale factor when component i dominates the energy density of the universe:

$$H^2 \propto \rho_i \propto \begin{cases} a^{-3}, & i = \text{m} \\ a^{-4}, & i = \gamma \\ \text{const.} & i = \Lambda \end{cases} \qquad (2.26)$$

At the Big Bang epoch the universe is very hot and so its energy density is dominated by radiation. As the universe expands and cools, it then enters the matter dominated epoch

followed by the vacuum energy dominated epoch, as matter energy density decreases with expansion whilst the vacuum energy density remains constant.

2.2 Thermodynamics

During the Hot Big Bang epoch the universe is extremely hot, with temperatures up to $O(M_{\rm Pl})$, and all the SM particles are thermalized and relativistic. As the universe expands and cools, the particles fall out of chemical equilibrium once temperatures drop below the mass of the particles, and depart from thermal equilibrium (known as 'freeze-out') once their production rate is less than the expansion rate. It is therefore instructive to describe the history of the universe by its thermal evolution. In order to do so, we need to evaluate quantities of Bose and Fermi particles from equilibrium thermodynamics.

The Bose-Einstein $(-)$ and Fermi-Dirac $(+)$ distribution functions for Bose and Fermi gases in thermal equilibrium are

$$f_i(\mathbf{p}) = \frac{1}{(2\pi)^3} \frac{1}{\exp\left[\frac{E(\mathbf{p})-\mu}{T}\right] \mp 1}, \tag{2.27}$$

where μ is the chemical potential, T is the temperature of the thermal bath, and the energy of particle i is

$$E(\mathbf{p}) = \sqrt{|\mathbf{p}|^2 + m_i^2}, \tag{2.28}$$

where $\mathbf{p}$ is the momentum and m_i is the mass. We will now show that in the early universe the chemical potentials of thermal relativistic particles is vanishing.

Interactions of particles in thermal equilibrium conserve the sum of their initial and final chemical potentials. For example, the scattering process $p_1 + p_2 \leftrightarrow p_A + p_B$ has

$$\mu_1 + \mu_2 = \mu_A + \mu_B. \tag{2.29}$$

Thus we can demonstrate through the process of particle-antiparticle annihilation into photons, $p\bar{p} \to 2\gamma$, that the chemical potentials of particles and antiparticles have equal magnitudes but opposite signs:

$$\begin{aligned} \mu_p + \mu_{\bar{p}} = 2\mu_\gamma = 0, \\ \to \mu_p = -\mu_{\bar{p}}, \end{aligned} \tag{2.30}$$

as the chemical potential of photons is zero. The difference in chemical potentials of the particles and antiparticles gives rise to a difference in their number densities, n_p and $n_{\bar{p}}$. In

the early universe there is a very small excess of quarks over anti-quarks, otherwise known as the baryon asymmetry, which results in a matter-dominated universe today; we discuss this further in section 2.3. Additionally, as the universe is electrically neutral, leptons have the same excess over anti-leptons:

$$\frac{n_q - n_{\bar{q}}}{n_q + n_{\bar{q}}} = O(10^{-10}), \qquad \frac{n_{l^-} - n_{l^+}}{n_{l^-} + n_{l^+}} = O(10^{-10}). \tag{2.31}$$

The difference in the number densities of particles and anti-particles is extremely small, and thus so must be the difference in their chemical potentials ($\mu \ll T$). In the early universe it is therefore often valid to take chemical potentials as vanishing. We will now evaluate the densities and pressure of the gas in this limit.

The number density, energy density, pressure and entropy density of a thermal relativistic gas respectively is [67]:

$$n(T) = \sum_i g_i \int f_i(\mathbf{p}) \mathrm{d}^3\mathbf{p} = g_{*n}(T) \frac{\zeta(3)}{\pi^2} T^3, \tag{2.32}$$

$$\rho(T) = \sum_i g_i \int f_i(\mathbf{p}) E(\mathbf{p}) \mathrm{d}^3\mathbf{p} = g_{*\rho}(T) \frac{\pi^2}{30} T^4, \tag{2.33}$$

$$p(T) = \sum_i g_i \int f_i(\mathbf{p}) \frac{|\mathbf{p}|^2}{3E} \mathrm{d}^3\mathbf{p} = \frac{1}{3}\rho(T), \tag{2.34}$$

$$s(T) = \frac{\rho + p}{T} = g_{*s}(T) \frac{2\pi^2}{45} T^3. \tag{2.35}$$

The number of relativistic effective degrees of freedom for each of the following quantities is given by [67]:

$$\lim_{T \gg m_i} g_{*n}(T) = \sum_{\text{bosons, } i} g_i \left(\frac{T_i}{T}\right)^3 + \frac{3}{4} \sum_{\text{fermions, } i} g_i \left(\frac{T_i}{T}\right)^3, \tag{2.36}$$

$$\lim_{T \gg m_i} g_{*\rho}(T) = \sum_{\text{bosons, } i} g_i \left(\frac{T_i}{T}\right)^4 + \frac{7}{8} \sum_{\text{fermions, } i} g_i \left(\frac{T_i}{T}\right)^4, \tag{2.37}$$

$$\lim_{T \gg m_i} g_{*p}(T) = \sum_{\text{bosons, } i} g_i \left(\frac{T_i}{T}\right)^4 + \frac{7}{8} \sum_{\text{fermions, } i} g_i \left(\frac{T_i}{T}\right)^4, \tag{2.38}$$

$$\lim_{T \gg m_i} g_{*s}(T) = \sum_{\text{bosons, } i} g_i \left(\frac{T_i}{T}\right)^3 + \frac{7}{8} \sum_{\text{fermions, } i} g_i \left(\frac{T_i}{T}\right)^3, \tag{2.39}$$

where T_i is the temperature of particle species i and g_i is their number of intrinsic degrees of freedom, which counts the number of flavours, spin states, colours and particle-antiparticle pairs. The average thermal momentum of relativistic bosons and fermions is then approxi-

mately

$$\langle p \rangle \approx \frac{\rho_i}{n_i} \begin{cases} 2.70T, & \text{bosons} \\ 3.15T. & \text{fermions} \end{cases} \tag{2.40}$$

At $T \gtrsim 200$ GeV all SM particles are in thermal equilibrium, i.e. $T_i = T$ for all species. The SM has 28 bosonic and 90 fermionic intrisic degrees of freedom, and so the total number of relativistic effective degrees of freedom of the SM is

$$g_*(T \gtrsim 200 \text{ GeV}) = 28 + \left(\frac{7}{8} \cdot 90\right) = 106.75, \tag{2.41}$$

where $g_* \equiv g_{*\rho/p/s}$. The number of relativistic effective degrees of freedom is a decreasing function of temperature, as shown by Figure 2.2, as once the thermal bath temperature cools below the mass of a particle, the species does not contribute. Today the universe has cooled to $T_0 = 2.7$ K, and so only photons ($g_\gamma = 2$) and neutrinos ($g_\nu = 6$) are light enough to contribute to the number of relativistic effective degrees of freedom. Neutrinos departed from thermal equilibrium in the early universe when their interaction rate dropped below the Hubble expansion rate, and only photons remain in the thermal bath today:

$$g_{*s}(T_0) = g_\gamma + \frac{7}{8} \cdot g_\nu \cdot \left(\frac{T_{\nu,0}}{T_0}\right)^3 = 3.91; \tag{2.42}$$

we will evaluate the neutrino-to-photon temperature ratio in section 2.4.

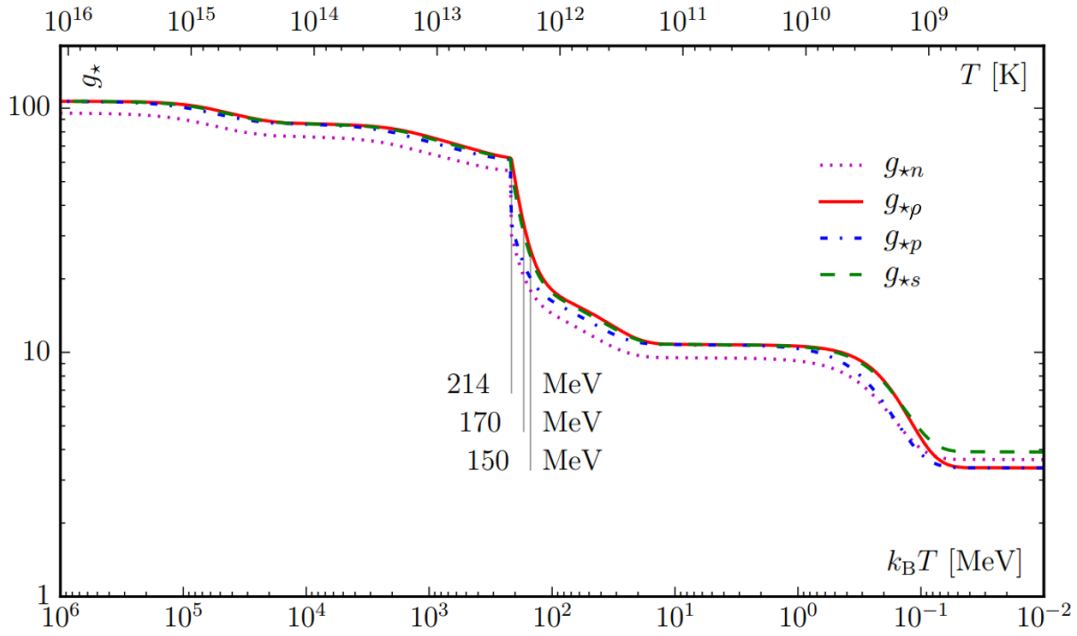

Figure 2.2: Number of effective degrees of freedom in SM against temperature

Plot of the number of effective degrees of freedom in the SM associated with number density (g_{*n}), energy density ($g_{*\rho}$), pressure (g_{*p}) and entropy density (g_{*s}), defined by equations (2.32)−(2.35) respectively, as a function of the temperature of the thermal bath; taken from [67].

For non-relativistic particles ($m_i \ll T$), the thermal distribution function in equation (2.27) is reduced to the Maxwell-Boltzmann distribution:

$$f(\mathbf{p}) = \frac{1}{(2\pi)^3} \exp\left[-\frac{E(\mathbf{p}) - \mu}{T}\right]. \tag{2.43}$$

The number density, energy density, pressure and entropy density of a non-relativistic particle species of type i are:

$$n_i = g_i \left(\frac{m_i T}{2\pi}\right)^{\frac{3}{2}} e^{\frac{\mu_i - m_i}{T}}, \tag{2.44}$$

$$\rho_i = m_i n_i + \frac{3}{2} n_i T_i, \tag{2.45}$$

$$p_i = T n_i, \tag{2.46}$$

$$s_i = n_i \left(\frac{5}{2} + \log\left[\frac{g_i}{n_i}\left(\frac{m_i T}{2\pi}\right)^{\frac{3}{2}}\right]\right). \tag{2.47}$$

We can see from equations (2.44)−(2.47) that once the temperature of the thermal plasma drops below the mass of the particle, the density and pressure of the particle is exponentially suppressed by a factor of $\exp\left[-\frac{m_i}{T}\right]$, as fewer particles have enough kinetic energy to create species i. At this moment the particles fall out of chemical equilibrium and their abundance depletes, as their production rate decreases whilst they continue to interact and decay; this is known as Boltzmann suppression.

2.3 Conditions for baryogenesis and leptogenesis

The early universe had large quantities of quarks and anti-quarks in thermal equilibrium, and yet today we observe the universe to be dominated by matter. We must therefore conclude that there was a very small excess of quarks over anti-quarks in the early, hot stages of its evolution. As the universe cooled, all the anti-quarks annihilated and only an excess of baryons remained, thus resulting in a maximally asymmetric universe today. We parameterize baryon asymmetry (BA) and lepton asymmetry (LA) in either of the following two ways,

$$\Delta_X \equiv \frac{n_X - n_{\bar{X}}}{n_X + n_{\bar{X}}}, \tag{2.48}$$

$$Y_X \equiv \frac{n_X - n_{\bar{X}}}{s}, \tag{2.49}$$

where $X = B/L$ for baryons/leptons. At $T \gtrsim 1$ GeV the BA of the universe (BAU) is [11]

$$\Delta_B \sim Y_B = O(10^{-10}). \tag{2.50}$$

Under the assumption that the universe was initially baryon-symmetric, we require processes that generate BA during the early universe. We can create BA or LA if the following three Sakharov conditions are satisfied [2]: 1) Baryon or lepton number violation, 2) charge conjugation (C) violation, and charge conjugation and parity (CP) violation, 3) Out of thermal equilibrium interactions.

1. Baryon or lepton number violation

Baryons and anti-baryons have equal and opposite baryon numbers, $B = \pm 1$, and likewise, leptons and anti-leptons have lepton numbers $L = \pm 1$. In order to generate BA/LA, we require processes that do not conserve baryon/lepton number.

2. C and CP violation

In order to generate a net BA/LA, we require processes with particles and antiparticles to be asymmetric, for example,

$$\Gamma(X \to qq) \neq \Gamma(\overline{X} \to \bar{q}\bar{q}). \tag{2.51}$$

We satisfy (2.51) if the processes violate C and CP symmetries[4]:

$$\Gamma(X \to q_L q_L) \neq \Gamma(\overline{X} \to \bar{q}_L \bar{q}_L), \tag{2.52}$$

$$\Gamma(X \to q_L q_L) \neq \Gamma(\overline{X} \to \bar{q}_R \bar{q}_R), \tag{2.53}$$

[4]Charge conjugation (C) transforms a particle into its corresponding antiparticle, e.g. $q_L \to \bar{q}_L$. Charge conjugation and parity (CP) transforms a particle into its corresponding antiparticle with a helicity flip, e.g. $q_L \to \bar{q}_R$.

where subscripts L/R refer to left/right-handed helicities.

3. Out of thermal equilibrium interactions

In order to generate a net BA/LA, processes need to be out of thermal equilibrium so that the rates of forward and backward reactions are different,

$$\Gamma(X \to q\bar{q}) \neq \Gamma(q\bar{q} \to X). \tag{2.54}$$

In section 5.3, we study a leptogenesis model in which LA is generated during the production and decay of right-handed singlet neutrinos. BA is then generated via electroweak (EW) sphaleron processes that violate $B + L$ at temperatures exceeding the EW symmetry breaking scale, $T_{\rm EW} = 160$ GeV [68]. The parameter space of the model is constrained by the BAU, and we implement the results in section 7.6, where we incorporate leptogenesis in an extension of our inflationary model. Additionally, we constrain our inflationary model by the requirement that the SM temperature exceeds $T_{\rm EW}$ in sections 6.8 and 6.9.

2.4 Neutrino decoupling

The aim of this section is to find the neutrino temperature today in order to evaluate the number of effective relativistic degrees of freedom in the SM. To do so, we need to find when the neutrinos decoupled from the thermal bath. The neutrinos are in thermal equilibrium at temperatures $T \gtrsim 10$ MeV, where their weak interaction rate exceeds the Hubble expansion rate. At temperature $T \sim 10$ MeV, the thermal plasma is composed of photons, electrons, positrons, protons, neutrons and neutrinos, and so the neutrinos are kept in equilibrium by the following 4-point weak interactions,

$$\begin{aligned} \nu_l + e^{\pm} &\longleftrightarrow \nu_l + e^{\pm} \\ \bar{\nu}_l + e^{\pm} &\longleftrightarrow \bar{\nu}_l + e^{\pm} \\ \nu_l + \bar{\nu}_l &\longleftrightarrow e^{\pm} + e^{\mp} \end{aligned} \tag{2.55}$$

which have a scattering cross-section of

$$\sigma_\nu \sim G_F^2 E_\nu^2, \tag{2.56}$$

where $G_F = 1.166 \times 10^{-5}$ GeV^{-2} is the Fermi constant and E_ν is the energy of the neutrino. They decouple from the thermal bath, or freeze-out, once their interaction rate decreases to

the order of the Hubble expansion rate:

$$\sigma_\nu(T_{\nu,f})n_\nu(T_{\nu,f})v \sim H(T_{\nu,f}), \tag{2.57}$$

where v is the neutrino velocity and $T_{\nu,f}$ is the neutrino freeze-out temperature. As their scattering cross-section is relatively small, they freeze-out early during the radiation dominated epoch whilst they are still relativistic. We estimate the neutrino interaction rate using the following approximations: $E_\nu \sim T$, $n \sim T^3$, and $v = c$. Then substituting equation (2.33) into Friedmann equation (2.11) for the Hubble expansion rate, the neutrino freeze-out temperature is given by

$$\begin{aligned} G_F^2 T_{\nu,f}^5 &\sim \left(\frac{g_{*\rho}\pi^2}{90}\right)^{\frac{1}{2}} \frac{T_{\nu,f}^2}{M_{\mathrm{P}}}, \\ T_{\nu,f} &\sim \left(M_{\mathrm{P}} G_F^2\right)^{-\frac{1}{3}} \sim 2 - 3 \text{ MeV}. \end{aligned} \tag{2.58}$$

The neutrinos freeze-out with a relativistic distribution, and their temperature remains the same as the thermal plasma whilst the electrons, positrons and photons remain in thermal equilibrium:

$$T_\nu(t) = T_{\nu,f}\frac{a(t_{\nu,f})}{a(t)} = T(t). \tag{2.59}$$

However, the neutrinos are entropy diluted by electron-positron annihilation at temperature

$$T_e \sim \frac{m_e}{3} = O(0.1) \text{ MeV}, \tag{2.60}$$

which effectively heats up the thermal plasma relative to the neutrinos. As a result, the neutrino temperature does not equal the thermal plasma temperature at $T < T_e$.

To find the neutrino temperature today we need to evaluate

$$T_{\nu,0} = T_{\nu,f}\frac{a(t_{\nu,f})}{a(t_0)} \tag{2.61}$$

by making use of the entropy conservation law stated in (2.22), which is equivalent to

$$g_{*s}(T)T^3a^3 = \text{const.}, \tag{2.62}$$

having substituted in for the relativistic entropy density, given by equation (2.35). We then apply (2.62) to the conservation of entropy in the electron-photon plasma to find the ratio of

the scale factors from neutrino freeze-out to today,

$$\frac{a(t_{\nu,f})}{a(t_0)} = \frac{T_0}{T_{\nu,f}} \left(\frac{g_{*s}^{e,\gamma}(T_0)}{g_{*s}^{e,\gamma}(T_{\nu,f})} \right)^{\frac{1}{3}}. \tag{2.63}$$

Given the number of entropic degrees of freedom at neutrino freeze-out,[5] $g_{*s}^{e,\gamma}(T_{\nu,f}) = g_\gamma + \frac{7}{8} \cdot g_{e^\mp} = \frac{11}{2}$, and after electron-positron annihilation, $g_{*s}^{e,\gamma}(T < T_e) = g_\gamma = 2$, the ratio of the neutrino temperature to the thermal photon temperature today is

$$\frac{T_{\nu,0}}{T_0} = \left(\frac{g_{*s}^{e,\gamma}(T_0)}{g_{*s}^{e,\gamma}(T_{\nu,f})} \right)^{\frac{1}{3}} = \left(\frac{4}{11} \right)^{\frac{1}{3}}. \tag{2.64}$$

Then using equations (2.42) and (2.35), we find that the total number of entropic degrees of freedom today is

$$\begin{aligned} g_{*s}(T_0) &= g_\gamma + \frac{7}{8} \cdot g_\nu \cdot \left(\frac{T_\nu}{T_0} \right)^3, \\ &= 2 + \frac{7}{8} \cdot 6 \cdot \frac{4}{11} = 3.91, \end{aligned} \tag{2.65}$$

and the entropy density today is

$$s_0 = \frac{2\pi^2}{45} g_{*s}(T_0) T_0^3 = 2.838 \times 10^3 \text{ cm}^{-3}, \tag{2.66}$$

where $T_0 = 2.7255 \pm 0.0006$ K [39].

The detection of relic neutrinos, called the cosmic neutrino background (CνB), would provide us with invaluable data from the earliest observable moments after the Big Bang [69]. As neutrinos are extremely weakly interacting and non-relativistic today, they may not be directly detectable for many years. However, there is indirect evidence of the CνB from their imprint on the Cosmic Microwave Background radiation (CMB) [70], (relic photons from the recombination epoch). In section 2.6 we will discuss how the CMB encodes information on the flatness and composition of the universe.

2.5 Big Bang Nucleosynthesis

The primordial abundances of light nuclei (hydrogen-2, helium-3, helium-4 and lithium-7) are dependent on the neutron-to-proton ratio at the time of neutron freeze-out, and their measurement ultimately allows us to constrain the number of effective degrees of freedom at the time of Big Bang Nucleosynthesis (BBN). The neutrons and protons are kept in thermal

[5] The number of intrinsic degrees of freedom of a photon and an electron-positron pair are $g_\gamma = 2$ and $g_{e^\mp} = 4$ respectively.

equilibrium at temperatures $T > 10$ MeV by the following weak interactions:

$$\begin{aligned} n + \nu_e &\longleftrightarrow p + e^- \\ n + e^+ &\longleftrightarrow p + \bar{\nu}_e \\ n &\longleftrightarrow p + e^- + \bar{\nu}_e \end{aligned} \tag{2.67}$$

Equation (2.48) implies that the electron chemical potential is vanishing in the early universe ($\mu_e \ll T$), and assuming that the lepton asymmetry of the universe is small, the neutrino chemical potential is also negligible ($\mu_{\nu_e} \ll T$). Then we obtain from (2.67) that the proton and neutron chemical potentials must be equal, $\mu_p = \mu_n$. As the protons and neutrons are thermal at temperatures well below their masses ($m_{n,p} \sim 900$ GeV), we use the thermal non-relativistic number density equation (2.44) to evaluate the ratio of the neutron-to-proton number density:

$$X_{n-p}(T) \equiv \frac{n_n(T)}{n_p(T)} = \exp\left(-\frac{\Delta m}{T}\right), \tag{2.68}$$

where $\Delta m \equiv m_n - m_p \sim 1.3$ MeV.

At temperatures $T \gg \Delta m, m_e$, the neutron interaction rate is

$$\Gamma_n = C_n G_F^2 T^5, \tag{2.69}$$

where $C_n \sim 1.2$. The neutrons freeze-out during the radiation dominated epoch, when $\Gamma_n(T_{n,f}) \sim H(T_{n,f})$, at temperature [71, 72]

$$\begin{aligned} C_n G_F^2 T_{n,f}^5 &\sim \left(\frac{g_{*\rho}\pi^2}{90}\right)^{\frac{1}{2}} \frac{T_{n,f}^2}{M_{\rm P}}, \\ \rightarrow T_{n,f} &= g_{*\rho}^{\frac{1}{6}} \left(\frac{\pi}{3\sqrt{10} C_n M_{\rm P} G_F^2}\right)^{\frac{1}{3}} \sim 0.8 \text{ MeV}. \end{aligned} \tag{2.70}$$

By the time the universe has cooled to $T_{n,f}$, the neutrinos have already decoupled from the thermal plasma, but as the electrons and positrons are still in thermal equilibrium, the neutrino temperature remains the same as the thermal temperature. The effective number of relativistic degrees of freedom in the SM at neutron freeze-out is therefore

$$g_{*\rho}^{\rm SM}(T_{n,f}) = g_\gamma + \frac{7}{8}\left(g_{e^\mp} + g_\nu\right) \tag{2.71}$$

$$= 2 + \frac{7}{8}\left(4 + 2 \cdot N_\nu^{\rm SM}\right) = 10.75, \tag{2.72}$$

where the number of neutrino species in the SM is $N_\nu^{\rm SM} = 3$.

As the neutron-proton mass difference is similar to the neutron freeze-out temperature,

$\Delta m \sim T_{n,f}$, the neutrons freeze-out with a relatively large abundance:

$$X_{n-p}(T_{n,f}) = \exp\left(-\frac{\Delta m}{T_{n,f}}\right) \sim \frac{1}{6}. \tag{2.73}$$

After neutron freeze-out, the neutron-to-proton ratio deviates slowly from its equilibrium value as the neutrons continue to deplete, predominantly via their decay. By the time light nuclei are formed at BBN at temperature

$$T_{\rm BBN} \sim 0.1 \text{ MeV}, \tag{2.74}$$

the neutron-to-proton ratio has decreased to

$$X_{n-p}(T_{\rm BBN}) \sim \frac{1}{7}. \tag{2.75}$$

The majority of neutrons are bound in helium-4, as it is the most stable light nucleus [39]. The primordial mass fraction of helium-4 is then approximately given by [37–39]:

$$Y_{\text{He-4}} = \frac{2X_{n-p}(T_{\rm BBN})}{1 + X_{n-p}(T_{\rm BBN})} \simeq 0.25; \tag{2.76}$$

hydrogen-2, helium-3 and lithium-7 make up a very small proportion with $Y \lesssim O(10^{-5})$, and so the primordial mass fraction is dominated by hydrogen-1 with $Y_{\text{H-1}} \simeq 0.75$. If the neutrons had a smaller (larger) cross-section or the number of effective degrees of freedom at the time of neutron freeze-out was larger (smaller), they would freeze-out earlier (later) and we would be left with a larger (smaller) abundance of helium-4.

The observed abundance of primordial helium-4 tightly constrains the deviation of the neutron-to-proton ratio from the SM predicted value, $\Delta(X_{n-p})$, at neutron freeze-out [35]:

$$\left.\frac{|\Delta(X_{n-p})|}{X_{n-p}}\right|_{T_{n,f}^{\rm SM}} \lesssim 0.025, \tag{2.77}$$

at the 68% C.L. This bound translates to a constraint on the number of additional relativistic degrees of freedom at time of neutron freeze-out, which is historically written as the number of extra neutrino species,

$$N_\nu = N_\nu^{\rm SM} + \Delta N_\nu. \tag{2.78}$$

To evaluate the bound on ΔN_ν, we first perform a linear expansion of the freeze-out temper-

ature, given by equation (2.70),

$$T_{n,f}(N_\nu^{\rm SM} + \Delta N_\nu) \sim T_{n,f}^{\rm SM} + \Delta T_{n,f}, \tag{2.79}$$

where $T_{n,f}^{\rm SM} \equiv T_{n,f}(N_\nu^{\rm SM})$, as a function of the number of degrees of freedom:

$$\begin{aligned} T_{n,f}(N_\nu^{\rm SM} + \Delta N_\nu) &\propto \left(g_{*\rho}^{\rm SM} + \frac{7}{4}\Delta N_\nu\right)^{\frac{1}{6}} \sim g_{*\rho}^{\rm SM}\left(1 + \frac{7}{24}\Delta N_\nu\right), \\ \rightarrow \Delta T_{n,f} &\sim \frac{7}{24}\frac{\Delta N_\nu}{g_{*\rho}^{\rm SM}(T_{n,f})} T_{n,f}^{\rm SM}. \end{aligned} \tag{2.80}$$

Then linearly expanding the neutron-to-proton ratio,

$$X_{n-p}(T_{n,f}^{\rm SM} + \Delta T_{n,f}) \sim X_{n-p}(T_{n,f}^{\rm SM}) + \Delta(X_{n-p}(T_{n,f}^{\rm SM})), \tag{2.81}$$

as function of temperature, we obtain the following expression for the first order approximation of the uncertainty on X_{n-p}:

$$\begin{aligned} X_{n-p}(T_{n,f}^{\rm SM} + \Delta T_{n,f}) = \exp\left[-\frac{\Delta m}{T_{n,f}^{\rm SM}}\left(1 + \frac{\Delta T_{n,f}}{T_{n,f}^{\rm SM}}\right)\right] &\sim X_{n-p}(T_{n,f}^{\rm SM})\left(1 + \frac{\Delta m \Delta T_{n,f}}{\left(T_{n,f}^{\rm SM}\right)^2}\right), \\ \rightarrow \left.\frac{\Delta(X_{n-p})}{X_{n-p}}\right|_{T_{n,f}^{\rm SM}} &\sim \frac{\Delta m \Delta T_{n,f}}{\left(T_{n,f}^{\rm SM}\right)^2} \sim \frac{7}{24}\frac{\Delta m}{g_{*\rho}^{\rm SM}(T_{n,f})}\frac{\Delta N_\nu}{T_{n,f}^{\rm SM}}. \end{aligned} \tag{2.82}$$

We can then translate (2.77) into a bound on the number of additional effective degrees of freedom at $T \sim 1$ MeV, parameterized in terms of number of neutrino species [40]:

$$|\Delta N_\nu| \lesssim 0.5. \tag{2.83}$$

2.6 The Cosmic Microwave Background radiation

The primordial universe was dominated by radiation, a hot plasma of charged particles and photons that are tightly coupled by Compton scattering [73, 74]. We assume that due to a preceding inflationary epoch, the plasma was almost completely homogeneous and isotropic, except for small variations in density that were seeded by inflationary enhanced quantum fluctuations of the inflaton field [75, 76], which we will discuss in detail in chapter 3. Baryonic density perturbations of wavelengths smaller than the causal horizon oscillated, as matter was attracted into the gravitational potential wells created in higher density regions, whilst radiation pressure, exerted by photons scattering off charged particles, acted to push baryonic matter into lower density regions [77, 78]. DM, which does not interact electromagnetically, collected in gravitational wells unimpeded by radiation pressure. The compression and rarefaction of

the baryonic matter density is known as the Baryonic Acoustic Oscillations (BAO).

Once the plasma temperature had dropped to[6]

$$T_{\text{rec}} = (1 + z_{\text{rec}})\, T_0 \sim 0.3 \text{ eV} \tag{2.84}$$

at redshift $z_{\text{rec}} \sim 1100$, which corresponds to the matter-dominated epoch, it was cool enough for protons to capture electrons and form neutral hydrogen in a process called recombination [79, 80]. The universe then became transparent to photons, thus ceasing radiation pressure and freezing the BAO in time. The decoupled relic photons free-streamed through the universe, their wavelength redshifting with the expansion. Those travelling from regions of compression are hotter whilst those travelling from regions of rarefaction are cooler. We observe them today as the CMB radiation, as shown in Figure 2.3.

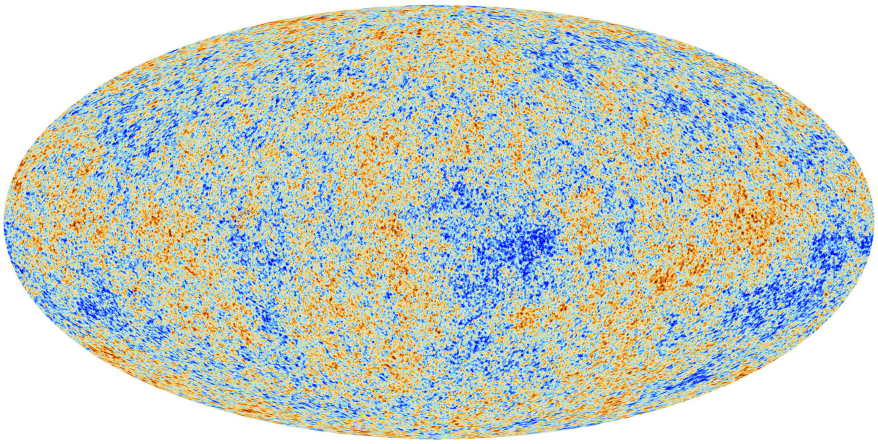

Figure 2.3: Anisotropies of the CMB

The Planck satellite's map of the small temperature fluctuations in the CMB radiation, $T = 2.72548 \pm 0.00057$ K [81]. These correspond to small fluctuations in matter density at the time of recombination, which seed the formation of large scale structure in the universe.

The CMB was first observed in 2003 by the Wilkinson Microwave Anisotropy Probe (WMAP) [34] and later in more detail by Planck in 2013 [35], which has provided us with an incredible insight into the composition and spatial curvature of the universe [82, 83]. This information is extracted from the positions and heights of the peaks in the CMB angular power spectrum [36] in Figure 2.4. The series of peaks show the variations in temperature at angular scales that have reached maximum compression (odd peaks) or maximum rarefaction (even peaks) at the time of recombination. Perturbations at angular scales larger than the sound horizon at recombination ($\theta \sim 1°$) are causally disconnected, and so we don't observe peaks in the power spectrum here [83].

The position of the first peak is sensitive to the spatial curvature of the universe, as it distorts the apparent angular size. Increasingly positive spatial curvature shifts the peaks to

[6]Comparing the radiation energy density's dependence on scale factor and temperature, given by equations (2.26) and (2.33), we can see that the radiation temperature decreases like $T \propto a^{-1}$.

the left and increasingly negative spatial curvature shifts the peaks to the right. The CMB power spectrum is shown to be consistent with a flat universe. Since the matter and radiation components do not make up the total critical energy density, we therefore infer that there is an additional missing component in the form of vacuum or 'dark' energy that explains the observed accelerated expansion [84, 85].

The second and third peaks of the CMB power spectrum provide evidence of DM and its relative energy density. Increasing the abundance of DM leads to the formation of deeper gravitational potential wells and so a larger radiation pressure is required to reverse the direction of the BAO at maximum compression [74]. This process is called baryon loading, and we observe its effects by the enhancement of compression amplitudes (odd peaks) relative to rarefaction amplitudes (even peaks). In particular, we can see an enhancement of the third peak relative to the second peak in Figure 2.4. Additionally, perturbations with small enough wavelengths to enter the horizon during the radiation dominated period are impacted by a process called radiation driving [74, 86]. During the matter-dominated period the dominant DM component creates fixed potential wells. However during the radiation-dominated period, radiation creates potential wells that decay with the expansion of the universe at the time of maximum compression, thus driving up the amplitude of the BAO [74]. The horizon scale at matter-radiation equality is determined by the scale that fluctuations are amplified by radiation driving, which then allows us to find the relative energy densities of matter and radiation in the universe [74]. Whilst the impact of baryon loading increases with the DM energy density, radiation driving decreases. From these two competing effects, we can conclude from the enhanced third peak that DM dominated at the time of recombination [74, 83]. Peaks at smaller scales are damped by radiative diffusion, as the wavelength of the density perturbations are smaller than the distance photons random walk at recombination [87, 88].

In Figure 2.4 the red dots plot the Planck results and the green curve plots the results of a dark energy and cold dark matter (ΛCDM) model that has around 5 times more cold dark matter than baryonic matter [36]. The two plots match with an incredible accuracy, and so the CMB provides us with a strong motivation for the ΛCDM model, which we will be discussed in detail in the following section.

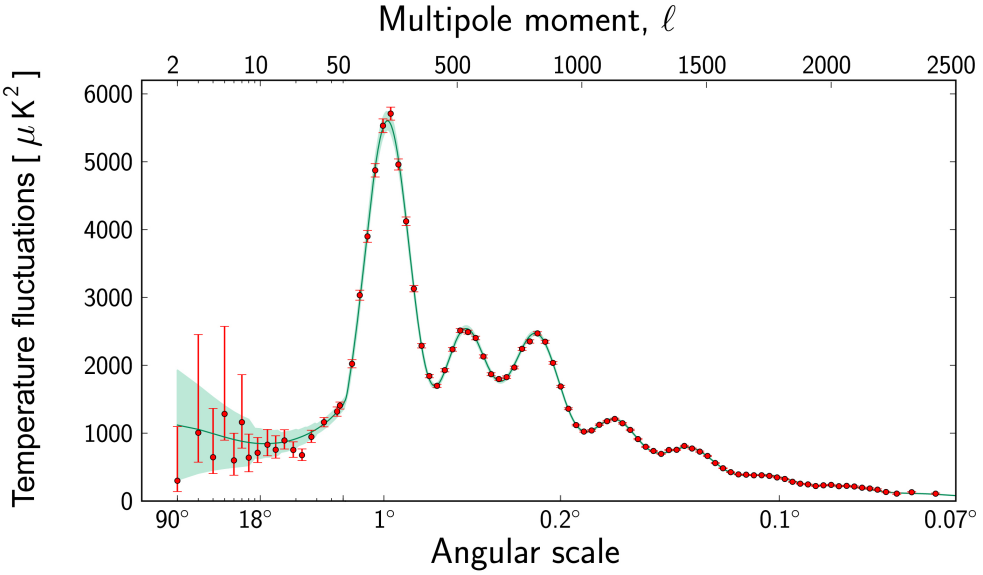

Figure 2.4: CMB angular power spectrum

Angular power spectrum of CMB temperature fluctuations plotted at different angular scales, taken from [36]. The temperature fluctuations are not sign sensitive. The red points mark the Planck 2013 data and the green curve marks the expected power spectrum from a ΛCDM model.

2.7 ΛCDM model

Planck's 2018 parameter fit of the relative energy densities as measured today for a flat ΛCDM model is [33]:

$$\Omega_{\Lambda,0} = 0.685 \pm 0.007, \quad \Omega_{\gamma,0} = (5.38 \pm 0.15) \times 10^{-5},$$
$$\Omega_{\mathrm{m},0} = \Omega_{\mathrm{b},0} + \Omega_{\mathrm{c},0} = 0.315 \pm 0.007, \begin{cases} \Omega_{\mathrm{b},0} = 0.0493 \pm 0.0006, \\ \Omega_{\mathrm{c},0} = 0.265 \pm 0.007, \end{cases} \tag{2.85}$$

where $\Omega_{\mathrm{b},0}$ and $\Omega_{\mathrm{c},0}$ are the baryon and cold DM energy densities respectively. Although cold DM provides us with a very good fit for the CMB, there is a suppression of small-scale structures relative to the model's predictions [89, 90]. We discuss DM and structure formation in detail in chapter 4, and show that this suppression may be an indication that DM is warm rather than cold [91–93].

We can use today's relative energy densities (2.85) to find an expression for the Hubble expansion rate at some previous time t. Substituting equation (2.14) and (2.17) into the

Friedmann equation (2.11), we find

$$H^2(t) = \frac{\rho_c(t)}{3M_{\rm P}^2} \sum_i \Omega_i(t). \tag{2.86}$$

Then, using (2.24) and (2.26), we can relate the relative energy densities measured at time t to today's:

$$\begin{aligned} H^2(t) &= \frac{\rho_{c,0}}{3M_{\rm P}^2} \sum_i \Omega_{i,0} \left(\frac{a_0}{a}\right)^{3(1+\omega_i)}, \\ &= H_0^2 \left[\Omega_{\rm m,0} \left(\frac{a_0}{a}\right)^3 + \Omega_{\gamma,0} \left(\frac{a_0}{a}\right)^4 + \Omega_{\Lambda,0}\right]; \end{aligned} \tag{2.87}$$

we will always assume the standard normalization of the scale factor, $a_0 = 1$. The critical energy density measured today is [33]

$$\rho_{c,0} = 3M_{\rm P}^2 H_0^2 = 1.054 \times 10^{-5} h^2 (\text{ GeV/c}^2)\text{cm}^{-3}, \tag{2.88}$$

where the Hubble expansion rate is $H_0 = 100\ h$ kms^{-1}Mpc^{-1} with $h = 0.674 \pm 0.005$. We can now use parameters (2.85) and equation (2.87) to find the time of matter-radiation equality and when the universe transitioned from decelerating to accelerating expansion.

Matter-radiation equality

Neglecting the vacuum energy component, matter-radiation equality approximately occurred when

$$\Omega_{\rm m,0} \left(\frac{a_0}{a}\right)^3 = \Omega_{\gamma,0} \left(\frac{a_0}{a}\right)^4, \tag{2.89}$$

which corresponds to a redshift and temperature of

$$z_{\rm eq} = \frac{\Omega_{\rm m,0}}{\Omega_{\gamma,0}} - 1 \sim 6 \times 10^3, \qquad T_{\rm eq} \sim 1 \text{ eV}. \tag{2.90}$$

Transition from decelerating to accelerating expansion

During the radiation and matter dominated epochs the universe had a decelerating expansion rate, however once the vacuum energy dominated, the expansion rate transitioned to an

accelerating rate:

$$\ddot{a} \propto \begin{cases} -t^{-\frac{4}{3}}, & \text{matter dom.} \\ -t^{-\frac{3}{2}}, & \text{radiation dom.} \\ e^{Ht}. & \text{vacuum energy dom.} \end{cases} \tag{2.91}$$

By the time the vacuum energy density dominated the radiation energy density was negligible as it redshifts the fastest. To find when the universe transitions from a decelerating to an accelerating expansion rate, we take the time derivative of the Friedmann equation (2.87):

$$\begin{aligned} \frac{d}{dt}\left(\dot{a}^2\right) &= H_0^2 \frac{d}{dt}\left[\Omega_{\Lambda,0} a^2 + \Omega_{\mathrm{m},0} a_0^3 a^{-1}\right], \\ \rightarrow \ddot{a} &= H_0^2 \frac{a}{2}\left[2\Omega_{\Lambda,0} - \Omega_{\mathrm{m},0}\left(\frac{a_0}{a}\right)^3\right]. \end{aligned} \tag{2.92}$$

Then by setting $\ddot{a} = 0$, we find the transition to an accelerating expansion rate occurred relatively recently, at a redshift and temperature of

$$z_{\mathrm{acc}} \sim \left(\frac{2\Omega_{\Lambda,0}}{\Omega_{\mathrm{m},0}}\right)^{\frac{1}{3}} - 1 \sim 0.6, \qquad T_{\mathrm{acc}} \sim 4 \text{ K}. \tag{2.93}$$

2.8 Summary and discussion

The theory in this chapter provides us with the essential framework to build and constrain our cosmological models in chapters 6, 7 and 8. Below we will summarise the main points from this chapter and discuss how they will be used later in our analysis.

Preceding the Hot Big Bang epoch, our cosmological models include a period of positively accelerating expansion called inflation, which is well approximated by the de Sitter universe (a universe dominated by vacuum energy). The conditions of inflation gives rise to a spatially flat ($\kappa = 0$), homogeneous and isotropic universe, which is described by FLRW metric,

$$ds^2 = dt^2 - a^2(t)\delta_{ij} dx^i dx^j. \tag{2.94}$$

After inflation there is a process called reheating, during which the inflationary energy is efficiently transferred into the SM.

The inflationary and reheating epochs are fully described by a closed set of differential equations that relate the Hubble expansion rate ($H \equiv \dot{a}/a$) and macroscopic properties of the universe (ρ, p) to the dynamics of the inflaton and SM particles. These are the Friedmann

and Raychaudhuri equations,

$$\left(\frac{\dot{a}}{a}\right)^2 = \frac{\rho}{3M_{\rm P}^2}, \tag{2.95}$$

$$2\frac{\ddot{a}}{a} + \left(\frac{\dot{a}}{a}\right)^2 = -\frac{p}{M_{\rm P}^2}, \tag{2.96}$$

the covariant conservation of the energy momentum tensor,

$$\dot{\rho} + 3H(\rho + p) = 0, \tag{2.97}$$

and the Boltzmann collision integral equations defined in section 7.3, which describe the dynamics of the system of particles. Since the universe reheats to very high temperatures, all SM particles are relativistic and in thermal equilibrium in the early universe. As SM interactions are very fast relative to the Hubble expansion rate, we make the approximation that SM particles instantaneously thermalize on production. We can then use thermodynamics to track the evolution of the SM temperature:

$$\rho_{\rm SM} = g_{\rm SM}\frac{\pi^2}{30}T_{\rm SM}^4, \tag{2.98}$$

where $g_{\rm SM}$ is the number of relativistic degrees of freedom in the SM associated with energy density. Our inflationary model will be constrained by the requirement that the reheating temperature exceeds the EW symmetry breaking scale, $T_{\rm EW} = 160$ GeV [68], so that EW sphaleron processes can generate the BAU [11],

$$Y_B \sim O(10^{-10}). \tag{2.99}$$

In chapter 7 we will introduce a DM candidate to our model, which is produced via inflaton decay in the early universe at time $t_{\rm prod}$. The relic abundance after production is related to the known present day abundance by [33]

$$\Omega_{\rm c,0} = \Omega_{\rm c}(t_{\rm prod})\left(\frac{a(t_{\rm prod})}{a_0}\right)^3 = 0.265 \pm 0.007. \tag{2.100}$$

Given that we can solve for $T_{\rm SM}$ and we know the present day entropy density,

$$s_0 = 2.838 \times 10^3 \text{ cm}^{-3}, \tag{2.101}$$

we will use the conservation of entropy,

$$sa^3 = \text{const.} \tag{2.102}$$

$$\rightarrow \left(\frac{a(t_{\text{prod}})}{a_0}\right)^3 = \frac{s_0}{\frac{2\pi^2}{45} g_{\text{SM}}(t_{\text{prod}}) T^3_{\text{SM}}(t_{\text{prod}})} \tag{2.103}$$

to constrain the DM parameters of the model.

The final important constraint from this chapter is the limit on the number of additional relativistic degrees of freedom to the SM at BBN, which is equivalent to less than half a neutrino species [40],

$$\Delta N_\nu \lesssim 0.5. \tag{2.104}$$

We must therefore ensure that any additional particles in our model are either heavy enough to be non-relativistic by the time of BBN, $m \gtrsim 0.1$ MeV, or have decayed prior to BBN [94–96], $\Gamma^{-1}_{\text{decay}} \lesssim O(0.1)$ s.

Chapter 3

Inflation and cosmological perturbations

The CMB has provided cosmologists with a complex problem: the observable universe is flat and almost completely homogeneous and isotropic on scales $\gtrsim 60$ Mpc [97]. Whilst the Hot Big Bang (HBB) model is successful in describing the evolution of the expanding universe from an initial state of hot dense gas moments before BBN, there is no explanation for these observations without the input of finely-tuned initial conditions. A possible solution is an initial period of positively accelerating expansion, namely inflation, which flattens curved space and ensures the observable universe has previously come into causal contact. Additionally, inflationary enhanced quantum fluctuations of the inflaton field generate the primordial scalar perturbations that seed structure formation.

In section 3.2 we adopt the slow roll formalism to define the conditions for inflation, and discuss a particular set of large-field inflationary models, which will provide the reader with the foundational knowledge for our inflaton model in chapter 6. Other types of inflationary models that are not discussed here are: small-field models, as they have an initial condition problem; and hybrid models, as they may generate isocurvature modes, which there is currently no evidence of in the CMB. Note that in this chapter, we only discuss purely inflationary models, however a realistic cosmological model must also provide mechanisms for reheating (SM production) and DM production. This will be discussed in detail in chapter 6, where we extend a minimal inflationary model with a scalar-Higgs portal coupling to provide a mechanism for reheating; and in chapter 7, where we couple the scalar field to a modified Neutrino Minimal Standard Model (νMSM) to provide a mechanism for DM production.

Whilst the background inflaton field governs the inflationary dynamics, inflationary enhanced quantum fluctuations of the inflaton field generate cosmological perturbations through perturbing the metric. This gives rise to scalar and tensor perturbations, which we observe as density inhomogeneities and gravitational waves in the universe. The aim of section 3.3 is to determine the relationship between the amplitude of inflaton and metric perturbations, which

we will use to constrain our inflationary model. We proceed by quantizing the canonically normalized inflaton fluctuations with a conformally flat FLRW metric, following the same procedure as that of the harmonic oscillator. We find that the solution of the field fluctuation is a Gaussian random field, thus allowing us to define its amplitude and power spectrum, which contains all the information of the properties of the field. On evaluating the power spectrum, we discover that single-field inflaton models produce adiabatic and scale-invariant perturbations, which is in agreement with CMB observations. The measurement of the CMB's amplitude of primordial scalar perturbations allows us to constrain the self-coupling of the inflaton field for a given model.

This chapter finishes by analysing the growth of density perturbations that evolve to form the large-scale structures in the universe. We choose to study the simplified case of a static universe, which provides us with reasonable estimates of the mass and scale of baryonic structures that begin to form after recombination.

The general logic of this chapter roughly follows the textbooks: 'Introduction to the theory of the early universe: cosmological perturbations and inflationary theory' by D. S. Gorbunov and V. A. Rubakov [78] and 'Cosmological Inflation and Large-Scale Structure' by A. R. Liddle and D. H. Lyth [98]; and lecture notes: 'TASI Lectures on Inflation' by Daniel Baumann [99].

3.1 Problems with the Hot Big Bang Model

3.1.1 Horizon problem

The measurement of the CMB temperature anisoptropies has revealed that the observable universe is almost completely homogeneous and isotropic, and so we would expect all parts of the region to have previously come into causal contact. The size of a causally connected region is defined by the cosmological horizon, l_H: the maximum distance light has travelled since the beginning of the universe. The size of a causally connected region at t_1 measured today at t_0 is given by the co-moving distance travelled by a photon at t_1, multiplied by the scale factor today:

$$l_{\mathrm{H},1}(t_0) = a_0 \int_0^{t_1} dt' \frac{1}{a(t')} = a_0 \int_0^{a_1} da' \frac{1}{Ha'^2} \tag{3.1}$$

$$\propto \begin{cases} a_0 a_1^{\frac{1}{2}} & \text{matter dom.} \\ a_0 a_1 & \text{radiation dom.,} \end{cases} \tag{3.2}$$

where the Hubble expansion rate is proportional to

$$H(t) \propto \begin{cases} a^{-\frac{3}{2}} & \text{matter dom.} \\ a^{-2} & \text{radiation dom.} \end{cases} \tag{3.3}$$

As the expansion rate is a rapidly decreasing function of the scale factor, we are able to see more regions that have not previously been in causal contact as time advances during periods of matter and radiation domination. In order to make comparisons with the CMB, we calculate[1] the angular size of a region in causal contact at recombination as measured today:

$$\theta_{\text{CMB}} = \frac{l_{\text{H,r}}(t_0)}{l_{\text{H},0}(t_0)} = \left(\frac{a_{\text{r}}}{a_0}\right)^{\frac{1}{2}} = (1+z_{\text{r}})^{-\frac{1}{2}} \sim 1.7^\circ, \tag{3.4}$$

where $z_r = 1100$. The HBB model therefore predicts that the CMB is made up of

$$\left(\frac{l_{\text{H},0}(t_0)}{l_{\text{H},r}(t_0)}\right)^2 \sim 10^3 \tag{3.5}$$

causally disconnected regions, however CMB temperature anisoptropies have been measured to be as small as $\Delta T/T \sim 10^{-4}$ [81]. As density perturbations grow during the radiation and matter dominated epochs, it would therefore require remarkable homogeneity between regions that haven't been in causal contact.

3.1.2 Flatness problem

At the Planckian epoch it is natural to expect the spatial curvature of the universe to be $\Omega_\kappa(t_{\text{Pl}}) \sim O(1)$, and at present we know the universe to be extremely flat, with $\Omega_{\kappa,0} < O(10^{-3})$. However, during the radiation and matter domination epochs, the curvature relative energy density is an increasing function of time:

$$\Omega_\kappa(t) \equiv -\frac{\kappa}{H(t)^2 a(t)^2} \propto \begin{cases} a(t) \propto t^{\frac{2}{3}}, & \text{matter dom.} \\ a(t)^2 \propto t, & \text{radiation dom.} \end{cases} \tag{3.6}$$

and so the HBB model requires an exceedingly small initial curvature in order to produce a flat universe today. At recombination, we estimate that the curvature is finely tuned to

$$\Omega_\kappa(t_{\text{r}}) \sim \left(\frac{t_{\text{r}}}{t_0}\right)^{\frac{2}{3}} \Omega_{\kappa,0} \lesssim 10^{-15}, \tag{3.7}$$

where $t_{\text{r}} \sim 1$ s and $t_0 \sim 10^{17}$ s.

[1] Note that we have ignored the recent period of dark energy domination in our estimation.

3.1.3 Primordial perturbation problem

Finally, and perhaps most importantly, the HBB model provides no mechanism to generate the primordial scalar perturbations observed in the CMB, shown in Figure 2.3, which seed the formation of large-scale structure in the universe.

3.2 Inflation

The problems of the HBB model may be solved with the addition of an initial finite period of positively accelerating expansion called inflation. Here, we will evaluate the inflationary conditions that would allow the entire observable universe to have been in causal contact and become spatially flat, using the slow roll formalism. Specifically we study a generic large-field inflationary model with a single scalar field serving as our 'inflaton'; the analysis will then be applicable to our quartic scalar model in chapter 6.

3.2.1 Slow roll formalism

Inflation is defined as a finite period of positively accelerating expansion, which is achieved when the universe has an equation of state similar to that of dark energy,

$$p \sim -\rho. \tag{3.8}$$

As a result, the Hubble expansion rate is approximately constant, and we have the following solution to the Friedmann equation (2.11),

$$a(t) = a_i \exp\left[\int_{t_i}^{t} dt' H(t')\right], \tag{3.9}$$

where we have assumed a flat universe ($\kappa = 0$). The period when (3.8) is satisfied is defined by the 'slow roll conditions', which we discuss below.

The action of the simplest inflationary model consists of a single scalar inflaton field, $\phi(\mathbf{x}, t)$, that is minimally coupled to gravity[2], and has potential $V(\phi)$ is[3]

$$S = \int \mathrm{d}^4x\sqrt{-g}\left[\frac{1}{2}g^{\mu\nu}\partial_\mu\phi\partial_\nu\phi - V(\phi)\right], \tag{3.11}$$

[2] A non-minimally coupled field is directly coupled to gravity, i.e. we have the following additional term in the Lagrangian:

$$\mathcal{L} \supset -\frac{1}{2}\xi R\phi^2, \tag{3.10}$$

where R is the Ricci scalar. A minimally coupled field is not directly coupled to gravity, i.e. $\xi = 0$.

[3] We use the notation $\partial_\mu \equiv \frac{\partial}{\partial x^\mu}$.

where $g \equiv \det(g_{\mu\nu})$. As the universe is almost completely homogeneous with small inhomogeneities, we can split our inflaton field into two component parts:

$$\phi(\mathbf{x}, t) = \phi_b(t) + \varphi(\mathbf{x}, t); \tag{3.12}$$

a homogeneous classical background field, $\phi_b(t)$, overlaid with quantum fluctuations, $\varphi(\mathbf{x}, t)$. The quantum fluctuations of the inflaton field source cosmological perturbations and will be the subject of the following section. In this section we will focus on studying the homogeneous background field, which governs the inflationary dynamics.

The equation of motion of a field is derived from the Euler-Lagrange equation:

$$\frac{\partial \mathcal{L}}{\partial \phi} - \partial_\mu \left(\frac{\partial \mathcal{L}}{\partial(\partial_\mu \phi)} \right) = 0, \tag{3.13}$$

where the Lagrangian density is related to the action by $S = \int \mathrm{d}^4 x \mathcal{L}$. The equation of motion of the background inflaton field is then

$$\ddot{\phi}_b + 3H\dot{\phi}_b + V_\phi(\phi_b) = 0, \tag{3.14}$$

where we use the FLRW metric for a homogeneous, isotropic and flat universe (for which $g = -a^6$), and assume the notation $V_\phi \equiv \partial V / \partial \phi$. Its energy density and pressure are evaluated using the energy-momentum tensor:

$$T_{\mu\nu} = \partial_\mu \phi_b \partial_\nu \phi_b - g_{\mu\nu}\mathcal{L}, \begin{cases} T_{00} = \rho = \frac{1}{2}\dot{\phi}_b^2 + V(\phi_b), \\ T_{ii} = p = \frac{1}{2}\dot{\phi}_b^2 - V(\phi_b), \end{cases} \tag{3.15}$$

thus giving a Hubble expansion rate of

$$H^2 = \frac{1}{3M_\mathrm{P}^2} \left(\frac{1}{2}\dot{\phi}_b^2 + V(\phi_b) \right). \tag{3.16}$$

The equation of state (3.8) is therefore satisfied when the kinetic energy of the field is much smaller than its potential, $\dot{\phi}^2 \ll |V(\phi)|$, hence inflation happens in the 'slow roll' regime. This period is then defined by the following two slow roll conditions, using equations (3.16) and (3.14) respectively:

1. The inflaton's kinetic energy is much smaller than its potential energy:

$$\left| \frac{\dot{\phi}_b^2}{2V} \right| \ll 1, \tag{3.17}$$

$$\rightarrow H \simeq \sqrt{\frac{V}{3M_\mathrm{P}^2}}. \tag{3.18}$$

2. The inflaton's kinetic term is much smaller than its friction term:

$$\left|\frac{\ddot{\phi}_b}{3H\dot{\phi}_b}\right| \ll 1, \tag{3.19}$$

$$\rightarrow \dot{\phi}_b \simeq -\frac{V_\phi}{3H}. \tag{3.20}$$

Then by substituting equations (3.18) and (3.20) into equations (3.17) and (3.19) respectively, we derive the slow roll parameters:

$$\epsilon = \frac{M_{\rm P}^2}{2}\left(\frac{V_\phi}{V}\right)^2, \qquad \eta = M_{\rm P}^2\left|\frac{V_{\phi\phi}}{V}\right|, \tag{3.21}$$

where $\epsilon, \eta \ll 1$, and inflation ends when $\epsilon, \eta \sim 1$

3.2.2 Large-field inflation

The simplest example of a large field inflationary model has a potential of the form

$$V(\phi) = \frac{\lambda\phi^n}{n}. \tag{3.22}$$

As the name suggests, the slow-roll conditions are satisfied when the field values are very large,

$$\phi \gg M_{\rm P}, \tag{3.23}$$

during which time the field rolls slowly down its potential until[4] $\phi_{\rm e} \sim M_{\rm P}$, when the slow roll conditions are violated and inflation ends. The field then rapidly rolls to the minimum of its potential, where it oscillates, and preheating/reheating[5] proceeds.

We will now evaluate the slow-roll parameters in terms of the number of e-foldings of expansion prior to the end of inflation:

$$N_{\rm e} \equiv \ln\left(\frac{a_{\rm e}}{a(\phi)}\right). \tag{3.24}$$

To find an expression for the field value in terms of $N_{\rm e}$, we first substitute equation (3.18) into (3.9):

$$N_e = \frac{1}{\sqrt{3M_{\rm P}^2}}\int_t^{t_{\rm e}} dt'\sqrt{V(\phi)}, \tag{3.25}$$

[4] We use the notation $X_{\rm e}$ to define the quantity X evaluated at the end of inflation.

[5] Preheating and reheating are periods of non-perturbative and perturbative particle production, which we will discuss in detail in sections 6.7, 6.8 and 6.9.

then make a change of variables from $t \to \phi$ using equation (3.20):

$$N_e = \frac{1}{M_{\rm P}^2}\int_{\phi_e}^{\phi} d\phi \frac{V}{V_\phi} \sim \frac{\phi^2}{2nM_{\rm P}^2}, \tag{3.26}$$

where we have evaluated the integral in the limit $\phi \gg \phi_e$. The slow-roll parameters (3.21) evaluated in terms of N_e are then given by

$$\epsilon = \frac{n}{4N_e}, \qquad \eta = \frac{(n-1)}{2N_e}. \tag{3.27}$$

In chapter 6 we present our multi-field inflationary model that couples a scalar inflaton field (X) to the SM Higgs doublet (Φ), in order to provide a mechanism for reheating (SM particle production). In our model the universe does not therefore necessarily inflate along $\Phi = 0$ in field space, but along a non-zero angle of rotation in the $X - \Phi$ plane. We assume the inflaton field has a very large initial field value that converges to the inflationary attractor solution long before perturbations within our comsological horizon today were generated. The parameters of our model are tuned so that the angle of the inflationary attractor solution is small, and the inflaton-Higgs quartic coupling gives rise to a large effective Higgs mass during inflation. As a result, fluctuations in the Higgs direction are suppressed and thus our inflationary dynamics can be well approximated by that of a single-field model.

3.2.3 Inflation as a solution to the horizon and flatness problems

To solve the horizon problem we require the size of the causally connected region at the end of inflation, as measured today, to be greater than the size of the observable universe:

$$\frac{l_{\rm H,e}(t_0)}{l_{H,0}(t_0)} = \frac{a_0}{l_{H,0}(t_0)}\int_{t_{\rm Pl}}^{t_{\rm e}} da' \frac{1}{Ha'^2} \sim \frac{a_0 H_0}{H(t_{\rm Pl})a(t_{\rm Pl})} > 1. \tag{3.28}$$

The integral here is saturated at the lower bound, and we have approximated $l_{H,0}(t_0) \sim H_0^{-1}$. To solve the flatness problem, we additionally require inflation to have flattened out a large spatial curvature at the Planckian epoch:

$$\frac{\Omega_\kappa(t_{\rm Pl})}{\Omega_\kappa(t_0)} \sim \frac{a_0^2 H_0^2}{H(t_{\rm Pl})^2 a(t_{\rm Pl})^2} > 1. \tag{3.29}$$

Both the horizon and flatness problems are therefore solved with the same condition, which we will use to find the minimum amount of inflationary expansion. We can re-express conditions (3.28) and (3.29) by the following:

$$\left(\frac{a_{\rm e}}{a(t_{\rm Pl})}\right)\left(\frac{a_0}{a_{\rm e}}\right)\left(\frac{H_0}{H(t_{\rm Pl})}\right) > 1, \tag{3.30}$$

then substituting in for the total number of e-foldings of inflationary expansion,

$$N_{\rm e}^{\rm tot} = \ln \frac{a_{\rm e}}{a(t_{\rm Pl})}, \tag{3.31}$$

we obtain a condition for the minimum number of e-foldings:

$$N_{\rm e}^{\rm tot} > N_{\rm e}^{\rm min} \sim \ln\left(\frac{a_{\rm e}}{a_0}\right) + \ln\left(\frac{H(t_{\rm Pl})}{H_0}\right) \sim \ln\left(\frac{T_0}{H_0}\right) + \ln\left(\frac{M_{\rm Pl}}{T_{\rm reh}}\right) \sim 70 - 100, \tag{3.32}$$

where $H(t_{\rm Pl}) \sim M_{\rm Pl}$ and the reheating temperature is in the range[6] $T_{\rm reh} = O(10^2 - 10^{19})$ GeV. We have assumed here that the start of reheating is instantaneous with the end of inflation, and so use the approximation $a_{\rm e} \propto T_{\rm reh}^{-1}$. However, reheating may proceed much later, in which case our estimate is too high. We will therefore continue to use a more conservative estimate of $N_{\rm e}^{\rm min} = 60$.

3.3 Generation of cosmological perturbations

In addition to explaining the flatness and homogeneity of the universe, inflation also provides a mechanism for generating the primordial scalar perturbations via the inflationary enhancement of quantum fluctuations of the inflaton field, φ. The fluctuations result in different parts of the universe ending inflation at slightly different times, i.e. for large-field inflation, a patch with negative φ violates the slow roll conditions sooner than a patch with positive φ. This gives rise to relative density perturbations in the universe, which provide the initial seeds for large-scale structure formation. Single-field inflationary models generate perturbations that are consistent with observations of the CMB anisotropies [100, 101]. The properties of these perturbations (high gaussianity, scale-invariance and adiabaticity) will be defined and explained later in this chapter. Multi-field models are less well motivated, as they can produced non-gaussian perturbations with isocurvature modes, and so we choose not to discuss them here.

We expand the action of the scalar inflaton field (3.11) with a spatially flat FLRW metric to second order in fluctuations to obtain the quadratic action of the quantum field:

$$S_\varphi = \int {\rm d}^4x\ a^3 \left[\frac{1}{2}\dot{\varphi}^2 - \frac{1}{2}\frac{(\partial_i\varphi)^2}{a^2} - \frac{1}{2}V_{\phi\phi}(\phi_b)\varphi^2\right], \tag{3.33}$$

where we use the notation $\partial_i \equiv \partial/\partial x_i$ $(i = 1, 2, 3)$. Then by making a Fourier expansion of the

[6] The universe reheats to a maximum reheating temperature of $T_{\rm reh}^{\rm max} = O(M_{\rm Pl}) = O(10^{19})$ GeV if reheating occurs immediately after inflation, $H(t_e) \sim H(t_{\rm reh})$. We restrict the reheating temperature to a minimum of [68] $T_{\rm reh,min} = T_{\rm EW} = O(10^2)$ GeV so that the baryon asymmetry of the universe can be produced via EW sphaleron processes.

quantum field, representing it as a sum of plane waves:

$$\varphi(\mathbf{x}, t) = \sum_{\mathbf{k}} \varphi(\mathbf{k}, t) e^{\pm i \mathbf{k} \cdot \mathbf{x}}, \tag{3.34}$$

we obtain a linearised equation of motion of the quantum field:

$$\ddot{\varphi} + 3H\dot{\varphi} + \left(\frac{k^2}{a^2} + V_{\phi\phi}(\phi_c) \right) \varphi = 0, \tag{3.35}$$

where k is the conformal momentum that is related to the physical momentum by

$$q = \frac{k}{a}. \tag{3.36}$$

3.3.1 Subhorizon and superhorizon modes

Quantum fluctuations of the inflaton field are created on all k-scales, and due to the very nature of inflationary expansion, some of these modes may exit the Hubble horizon during inflation. We are going to show that these modes are of particular cosmological significance, since inflation results in the enhancement of their amplitudes, which gives rise to observable cosmological perturbations.

Inflaton fluctuations are subhorizon when

$$k \gg aH, \tag{3.37}$$

where $(aH)^{-1}$ is defined as the comoving Hubble horizon. Here, the second and fourth terms in equation (3.35) are sub-dominant, as the slow roll conditions (3.21) enforce $V_{\phi\phi}(\phi_c)$ to be small:

$$V_{\phi\phi} = \frac{V}{M_{\mathrm{P}}^2} \eta = 3H^2 \eta. \tag{3.38}$$

The subhorizon modes thereby undergoes simple harmonic motion, unimpeded by the expansion of the universe. However whilst the conformal momentum remains constant, the comoving Hubble horizon is a decreasing function of time during inflation,

$$(aH)^{-1} \propto e^{-Ht}. \tag{3.39}$$

The fluctuations can therefore exit the horizon when $k = aH$, shown by the first crossing in Figure 3.1, and become superhorizon when

$$k < aH. \tag{3.40}$$

Whilst the wavelength and momentum of the mode red-shifts with the expansion of the universe, we show below that the amplitude is fixed at horizon crossing, $k = a(t_*)H(t_*)$, as the mode is outside the region of causality. During this period, the amplitude of superhorizon modes is therefore enhanced relative to the subhorizon modes, which decay with the expansion of the universe. The superhorizon modes re-enter the horizon during the radiation or matter dominated periods, shown by the second crossing in Figure 3.1, as the co-moving Hubble horizon during these epochs is an increasing function of time:

$$(aH)^{-1} \propto \begin{cases} a, & \text{radiation dom.} \\ a^{\frac{1}{2}}. & \text{matter dom.} \end{cases} \tag{3.41}$$

Next we are going to formally evaluate the inflationary enhancement of superhorizon modes, which give rise to cosmological perturbations and ultimately the large scale structure of the universe.

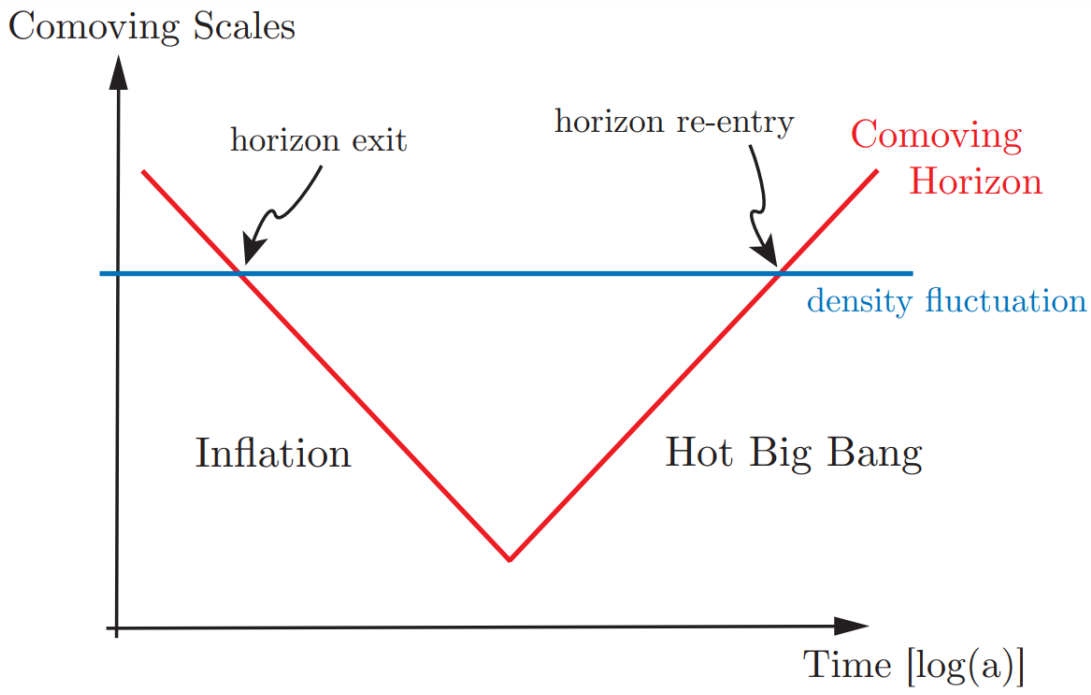

Figure 3.1: Evolution of cosmological perturbations

Log-log plot of the co-moving horizon $(aH)^{-1}$, in red, and the inverse conformal momentum, k^{-1}, in blue, against the scale factor; plot is taken from [99]. If we have exponential inflaton ($H = \text{const.}$), the gradient of the red line is equal to -1. During radiation and matter domination, the gradient of the red line is equal to 1 and 1/2 respectively, as in (3.41). Note that we do not show the kink at the transition between radiation and matter domination in this plot. The red and blue lines crossing represent fluctuations exiting and entering the horizon. Regions where $k^{-1} < (aH)^{-1}$, fluctuations are subhorizon, and regions where $k^{-1} > (aH)^{-1}$, fluctuations are superhorizon.

3.3.2 Quantum fluctuations of the inflaton perturbations

In order to evaluate the inflationary enhanced amplitude of the quantum fluctuation of the inflaton field, we will proceed by writing the action (3.33) in conformal time, τ, and the canonically normalised field, $\chi = a(\tau)\varphi$. From the action, we then derive the equation of motion of χ, which during slow roll inflation is analogous to the harmonic oscillator. As a result, the field can then be quantized following the standard quantization procedure for the harmonic oscillator. Thus we can solve for φ, and show that the amplitudes of superhorizon modes are frozen during inflation. The scalar field is a Gaussian random field, which by definition has a power spectrum that fully determines the properties of the field. On evaluation of the power spectrum, we show that it is scale-invariant, which is in agreement with CMB measurements [100, 101].

Using the metric with conformal time (2.7), the action of the massless scalar field is

$$S_\chi = \frac{1}{2}\int \mathrm{d}^3x\, d\tau\, a^2(\tau)\left[\varphi'^2 - (\partial_i\varphi)^2\right], \tag{3.42}$$

$$= \frac{1}{2}\int \mathrm{d}^3x\, d\tau\left[\chi'^2 - (\partial_i\chi)^2 + \frac{a''}{a}\chi^2\right], \tag{3.43}$$

where we use the notation $X' \equiv \partial X/\partial\tau$, $X'' \equiv \partial^2 X/\partial\tau^2$, and we can neglected the term $V_{\phi\phi}$ during slow roll inflation (3.38). We decompose the scalar field into a Fourier expansion of modes, χ_k, and vice versa:

$$\chi(\mathbf{x},\tau) = \int \frac{\mathrm{d}^3k}{(2\pi)^{\frac{3}{2}}}\chi_k(\tau)e^{i\mathbf{k}\cdot\mathbf{x}}, \tag{3.44}$$

$$\chi_k(\tau) = \int \frac{\mathrm{d}^3x}{(2\pi)^{\frac{3}{2}}}\chi(\mathbf{x},\tau)e^{-i\mathbf{k}\cdot\mathbf{x}},$$

where the Fourier integral is defined in the limit of an infinite sum,

$$\lim_{\mathbf{k}\to\infty}\sum_{\mathbf{k}} \to \int \frac{\mathrm{d}^3k}{(2\pi)^{\frac{3}{2}}}. \tag{3.45}$$

The equation of motion of the Fourier mode is thereby

$$\chi_k'' + \left(k^2 - \frac{a''}{a}\right)\chi_k = 0. \tag{3.46}$$

We can only numerically solve for χ_k during inflation as a''/a has a complex dependence on the background field dynamics. Here, we will instead find an analytical approximation for χ_k by taking the limit of a purely de Sitter universe, a spatially flat universe dominated by vacuum

energy, in which

$$\frac{a''}{a} = \frac{2}{\tau^2} = 2(aH)^2. \tag{3.47}$$

The equation of motion of χ_k is analogous to the harmonic oscillator, and so we will quantize the field following the standard quantization procedure for the harmonic oscillator.

Quantization of the inflaton field in a de Sitter universe

The scalar field χ and its fourier components $\chi_{\mathbf{k}}$ are promoted to operators with the following decomposition:

$$\hat{\chi}(\mathbf{x}, \tau) = \int \frac{\mathrm{d}^3 k}{(2\pi)^{\frac{3}{2}}} \left(\chi_k(\tau) \hat{A}_{\mathbf{k}} e^{i\mathbf{k}\cdot\mathbf{x}} + \chi_k^*(\tau) \hat{A}_{\mathbf{k}}^\dagger e^{-i\mathbf{k}\cdot\mathbf{x}} \right), \tag{3.48}$$

$$\hat{\chi}_{\mathbf{k}} = \chi_k(\tau) \hat{A}_{\mathbf{k}} + \chi_{-k}^*(\tau) \hat{A}_{-\mathbf{k}}^\dagger. \tag{3.49}$$

The creation and annihilation operators, $A_{\mathbf{k}}^\dagger$ and $A_{\mathbf{k}}$ respectively, obey the canonical commutation relation:

$$\left[\hat{A}_{\mathbf{k}}, \hat{A}_{\mathbf{k}'}^\dagger \right] = \delta^3 \left(\mathbf{k} - \mathbf{k}' \right), \tag{3.50}$$

if the modes are normalized as follows:

$$i \left(\chi_k^* \chi_k' - \chi_k^{*\prime} \chi_k \right) = 1. \tag{3.51}$$

The vacuum state of the fluctuations $|0\rangle$ is defined by

$$A_{\mathbf{k}} |0\rangle = 0. \tag{3.52}$$

In the subhorizon limit ($k\tau \gg 1$), the solution to the equation of motion of χ_k (3.46) has the general form:

$$\chi_k = \alpha \frac{e^{-ik\tau}}{\sqrt{2k}} \left(1 - \frac{i}{k\tau} \right) + \beta \frac{e^{ik\tau}}{\sqrt{2k}} \left(1 + \frac{i}{k\tau} \right). \tag{3.53}$$

The coefficients α and β are then fixed by our normalization condition (3.51):

$$\chi_k = \frac{e^{-ik\tau}}{\sqrt{2k}} \left(1 - \frac{i}{k\tau} \right). \tag{3.54}$$

In the subhorizon limit, χ_k behaves as a simple harmonic oscillator in Minkowski space, oscillating with time-independent frequency $\omega_k = k$, whilst in the superhorizon limit ($k\tau \ll 1$),

the field behaves as $\chi_k \propto a(\tau)$. Next we will show that the inflaton field is a Gaussian random field, and thus define its power spectrum.

Gaussianity of vacuum fluctuations

A field is a Gaussian random field if its variables obey Gaussian statistics. If this is true, its properties can then be completely determined by its 2-point correlation function, i.e. the vacuum expectation value of the field operators[7]:

$$\langle 0|\hat{\varphi}(\mathbf{x},t)\hat{\varphi}(\mathbf{y},t)|0\rangle \equiv \langle \hat{\varphi}(\mathbf{x},t)\hat{\varphi}(\mathbf{y},t)\rangle; \tag{3.55}$$

or alternatively by its power spectrum, which we will define later. Here we will use the central limit theorem to show that the vacuum fluctuations of the inflaton field are a Gaussian random field, which is in agreement with CMB observations.

The Fourier components of the scalar field, $\hat{\chi}_{\mathbf{k}}$, are uncorrelated, i.e. their real and imaginary parts have independent probability distributions equal to

$$\langle\ |\hat{\chi}_{\mathbf{k}}|^2\rangle = |\chi_k(\tau)|^2. \tag{3.56}$$

We can decompose the scalar field into a sum of plane waves with Fourier coefficients, $\chi_k(\tau)$, that have uniformly distributed random phases, as written in equation (3.48). Then by the central limit theorem, which states that the normalized sum of independent random variables tends to a Gaussian distribution, the vacuum fluctuations of the scalar field are by definition Gaussian random fields.

Power spectrum and amplitude of the inflaton field

The power spectrum gives us the relative amplitude of each Fourier mode, which we compute by taking the Fourier transform of the correlation function,

$$P_\varphi(k)\delta^3(\mathbf{k}-\mathbf{k}') = \int \frac{\mathrm{d}^3x}{(2\pi)^{\frac{3}{2}}} \int \frac{\mathrm{d}^3y}{(2\pi)^{\frac{3}{2}}} e^{-i\mathbf{k}\cdot\mathbf{x}} e^{-i\mathbf{k}'\cdot\mathbf{y}} \langle\hat{\varphi}(\mathbf{x},t)\hat{\varphi}(\mathbf{y},t)\rangle. \tag{3.57}$$

The right hand side of (3.57) is then by definition just the 2-point correlation function of the Fourier modes:

$$P_\varphi(k)\delta^3(\mathbf{k}+\mathbf{k}') = \langle\hat{\varphi}_{\mathbf{k}}(t)\hat{\varphi}_{\mathbf{k}'}(t)\rangle, \tag{3.58}$$

[7] We will continue to use the notation $\langle X\rangle \equiv \langle 0|X|0\rangle$, as we only deal with vacuum fluctuations.

where $\hat{\varphi}_{\mathbf{k}} \equiv \hat{\chi}_{\mathbf{k}}/a$. Using the definition of the vacuum (3.52) and the canonical commutation relation (3.50), we are able to evaluate (3.58):

$$\begin{aligned}\langle\hat{\varphi}_{\mathbf{k}}(t)\hat{\varphi}_{\mathbf{k}'}(t)\rangle &= \frac{e^{-i(k+k')\tau}}{2a^2\sqrt{-kk'}}\left(1-\frac{i}{k\tau}\right)\left(1-\frac{i}{k'\tau}\right)\langle\, \hat{A}_{\mathbf{k}}\hat{A}^{\dagger}_{-\mathbf{k}'}\rangle, \\ &= \frac{1}{2ka^2}\left(1+\frac{1}{k^2\tau^2}\right)\delta^3\left(\mathbf{k}+\mathbf{k}'\right), \\ &= \frac{H^2}{2k^3}\left(1+k^2\tau^2\right)\delta^3\left(\mathbf{k}+\mathbf{k}'\right), \end{aligned} \tag{3.59}$$

where we have inserted equation (3.54) as our solution for χ_k. In the superhorizon limit ($k\tau \ll 1$), our inflaton field power spectrum is given by

$$P_{\varphi}(k) = \frac{H_k^2}{2k^3}. \tag{3.60}$$

A power spectrum that has the relation $P(k) \propto k^{-d}$, where $d = 3$ is the number of spatial dimensions, has the special property of being scale-invariant, i.e. the field fluctuations have the same correlation on every scale:

$$\begin{aligned}\langle\hat{\varphi}(\lambda\mathbf{x},t)\hat{\varphi}(\lambda\mathbf{y},t)\rangle &= \int_{-\infty}^{\infty}\frac{\mathrm{d}^3k}{(2\pi)^{\frac{3}{2}}}\int_{-\infty}^{\infty}\frac{\mathrm{d}^3k'}{(2\pi)^{\frac{3}{2}}}e^{i\lambda\mathbf{k}\cdot\mathbf{x}}e^{i\lambda\mathbf{k}'\cdot\mathbf{y}}\frac{H^2}{2k^3}\delta^3\left(\mathbf{k}+\mathbf{k}'\right) \\ &= \int_{-\infty}^{\infty}\frac{d(\lambda k)}{(2\pi)^2}\frac{H^2}{(\lambda k)}e^{i\lambda\mathbf{k}\cdot(\mathbf{x}-\mathbf{y})} \\ &= \langle\hat{\varphi}(\mathbf{x},t)\hat{\varphi}(\mathbf{y},t)\rangle. \end{aligned} \tag{3.61}$$

This is a feature observed in the CMB, and thus one of the strong motivations for inflation. Additionally, as the correlation function only depends on $|\mathbf{x}-\mathbf{y}|$, it is also invariant under translations and rotations. The vacuum fluctuations are therefore defined as adiabatic perturbations, as they are homogeneously and isotropically distributed in space.

Due to the scale-invariance of the power spectrum, it is standard to use the following definition of the power spectrum that removes the k-dependence:

$$\Delta^2_{\varphi}(k) = \frac{k^3}{2\pi^2}P_{\varphi}(k), \tag{3.62}$$

and $\delta\varphi \equiv \Delta_{\varphi}(k)$ defines the amplitude of the field fluctuation. The power spectrum and amplitude of superhorizon vacuum fluctuations of the inflaton field is then given by

$$\Delta^2_{\varphi}(k) = \left(\frac{H_*}{2\pi}\right)^2, \qquad \delta\varphi = \frac{H_*}{2\pi}, \tag{3.63}$$

where $*$ indicates that the term needs to be evaluated at horizon crossing, $a(t_*)H(t_*) = k$. Whilst the amplitude of superhorizon modes remains roughly constant during inflation, the

amplitude of subhorizon modes ($k\tau \gg 1$) decay with the expansion of the universe:

$$\delta\varphi_{\text{sub}} = \frac{k}{2\pi a}. \tag{3.64}$$

The amplitudes of superhorizon modes are therefore vastly enhanced relative to subhorizon modes by a factor of

$$\frac{\delta\varphi}{\delta\varphi_{\text{sub}}} = \frac{H_*}{q(t_e)} \sim \frac{a(t_e)}{a(t_*)} \sim e^{N_e}, \tag{3.65}$$

where N_e is the number e-foldings prior to the end of inflation that the mode exited the horizon.

3.3.3 Metric perturbations

During inflation, the energy density of the universe is dominated by the inflaton field. As a result, fluctations of the inflaton field perturb the stress-energy tensor, $\delta T_{\mu\nu}$, thus giving rise to perturbations of the metric, $\delta g_{\mu\nu}$, through Einstein's equations of motion:

$$\left[\delta R_{\mu\nu} - \frac{1}{2}\delta\left(g_{\mu\nu}R\right)\right] = 8\pi G\delta T_{\mu\nu}. \tag{3.66}$$

Likewise, metric perturbations backreact on to the inflaton perturbations via the perturbed equation of motion of the inflaton field:

$$\delta\left(\partial_\mu\partial^\mu\phi - V_\phi(\phi)\right) = 0, \tag{3.67}$$

and so perturbations of the metric and inflaton field are tightly coupled.

Metric perturbations are categorised into 3 types based on their spin number: scalar (spin 0), vector (spin 1), and tensor (spin 2). We observe scalar perturbations as density perturbations and tensor perturbations as gravitational waves; vector perturbations decay with the expansion of the universe and so we will not discuss them here. The aim of sections 3.3.3.1 and 3.3.3.2 are to provide the reader with the observables of the scalar and tensor perturbations (i.e power spectrums, amplitudes and spectral tilts) that allow us to constrain inflationary models.

3.3.3.1 Scalar perturbations

Generally scalar perturbations are a composition of adiabatic and isocurvature modes. Adiabatic perturbations give rise to total density fluctuations throughout the universe, but the relative densities between different particle species are the same. For example, matter and

radiation components must satisfy the condition:

$$\delta\left(\frac{n_{\rm m}}{n_\gamma}\right)=0, \qquad \frac{\delta\rho_{\rm m}}{\rho_{\rm m}}=\frac{3}{4}\frac{\delta\rho_\gamma}{\rho_\gamma}. \tag{3.68}$$

Adiabatic perturbations are sometimes referred to as curvature perturbations, as small overdense regions with density ρ' give rise to local changes in curvature:

$$H^2-\frac{\rho'}{3M_{\rm P}^2}=-\frac{\kappa}{a^2}. \tag{3.69}$$

Given that the overall curvature of the universe with average density $\bar{\rho}$ is negligibly small:

$$H^2-\frac{\bar{\rho}}{3M_{\rm P}^2}=-\frac{\kappa}{a^2}\sim 0, \tag{3.70}$$

the density perturbation is then related to the curvature perturbation by:

$$\frac{\delta\rho}{\rho}\equiv\frac{\rho'-\bar{\rho}}{\bar{\rho}}=\frac{\kappa}{(Ha)^2}. \tag{3.71}$$

On the other hand, isocurvature modes have zero total density fluctuations and relative density perturbations between different particle species:

$$\delta\rho=0, \qquad \frac{\delta\rho_{\rm m}}{\rho_{\rm m}}\neq\frac{3}{4}\frac{\delta\rho_\gamma}{\rho_\gamma}. \tag{3.72}$$

Next we will show that single-field inflaton models produce adiabatic modes with no admixture of isocurvature modes, which is currently in agreement with CMB measurements [100, 101]. Isocurvature modes may be produced by multi-field models, however as this is not well motivated by observations, we will continue to review single-field inflationary models only.

The inflaton field is homogeneous on constant-time hypersurfaces[8], and so quantum fluctuations of the field can be expressed as a time-shift, $\delta t(\mathbf{x},t)$, along the trajectory of the homogeneous background field. Positive (negative) fluctuations result in different parts of the universe exiting inflation at later (earlier) times and thus having a greater (lower) density. For single-field inflation, the time-shift induces the same relative density fluctuation for every species, as during reheating energy is transferred from the inflaton field into other particles species via the same mechanism everywhere in the universe. The model therefore produces adiabatic modes exclusively:

$$\delta\varphi(\mathbf{x},t)=\dot{\phi}_b(t)\delta t(\mathbf{x},t), \qquad \delta\rho(\mathbf{x},t)=\dot{\rho}\delta t(\mathbf{x},t). \tag{3.73}$$

[8]We study fluctuations of gauge-invariant quantities, i.e. the value of the perturbation does not arbitrarily depend on our choice of gauge.

The energy density behaves in the same way as the scale factor,

$$\dot{\rho} \sim -H\rho, \tag{3.74}$$

and so we can express the relative energy density fluctuation in terms of the amplitude of the inflaton fluctuation:

$$\frac{\delta\rho}{\rho} \sim \frac{H}{\dot{\phi}_b}\delta\varphi. \tag{3.75}$$

It is conventional to use the following parameterization for the scalar power spectrum

$$\Delta_s^2(k) = A_\varphi(k_*)\left(\frac{k}{k_*}\right)^{n_s-1}, \tag{3.76}$$

where n_s is the spectral index. The power spectrum and amplitude of superhorizon scalar perturbations generated by fluctuations of the inflaton field is then given by

$$\Delta_s^2 = \left(\frac{H_*^2}{2\pi\dot{\phi}_b}\right)^2, \qquad \Delta_s = \frac{H_*^2}{2\pi\dot{\phi}_b}, \tag{3.77}$$

with $n_s \sim 1$, which is in agreement with Planck's measurement [33]. The measurement of the amplitude of the primordial scalar perturbations [33],

$$\Delta_s^{\mathrm{CMB}}(k_*) \sim 4.7 \times 10^{-5} \tag{3.78}$$

at $k_* = 0.05\ \mathrm{Mpc}^{-1}$, allows us to constrain the self-coupling of the inflaton field for a given model. Using the slow-roll conditions, (3.20) and (3.18), the amplitude can be expressed in terms of the inflationary potential:

$$\Delta_s = \frac{\sqrt{3}}{6\pi}\frac{1}{M_{\mathrm{P}}^3}\frac{V^{\frac{3}{2}}}{V_\phi}. \tag{3.79}$$

Then for a large-field inflationary models with a potential of the form given in (3.22), the self-coupling is constrained by

$$\lambda = \frac{12\pi^2 M_{\mathrm{P}}^{4-n}}{\sqrt{(2N_e)^{n+2}n^{n-4}}}\Delta_s^2. \tag{3.80}$$

We use $N_e = 60$, as we are probing modes with a wavelength the size of cosmological horizon, which exited the horizon 60 e-foldings prior to the end of inflation. Our inflationary model, to be discussed in chapter 6, has a quartic scalar potential ($n = 4$). The CMB measurement (3.78) then constrains the quartic self-coupling to $\lambda \sim 1.5 \times 10^{-13}$, if we assume the inflaton field is minimally coupled to gravity.

3.3.3.2 Tensor perturbations

Tensor perturbations, h_{ij}, are free excitations of spacetime:

$$ds^2 = a^2(\tau)\left[d\tau^2 - (\delta_{ij} + h_{ij})\, dx^i dx^j\right], \tag{3.81}$$

that manifest as unsourced gravitational waves, with the action:

$$S_h = \frac{M_{\rm P}^2}{8}\int \mathrm{d}^3x\; d\tau\; a^2(\tau)\left[(h'_{ij})^2 - (\partial_i h_{ij})^2\right]. \tag{3.82}$$

The action of the tensor perturbations is the same as the action of the massless scalar field given in (3.42), except with the addition of an overall factor of $M_{\rm P}^2/4$. We can therefore follow the same quantization procedure outlined in section 3.3.2, and so will leave out some details here.

The tensor mode is composed of two transverse polarisations, ($s = +, \mathrm{x}$), and their Fourier transform is given by

$$h_{ij} = \int \frac{\mathrm{d}^3k}{(2\pi)^3}\sum_{s=+,\mathrm{x}} \epsilon^s_{ij}(k) h^s_k(\tau) e^{i\mathbf{k}\cdot\mathbf{x}}. \tag{3.83}$$

Given the following properties of the polarization tensors:

$$\epsilon_{ii} = k^i\epsilon_{ij} = 0, \qquad \epsilon^s_{ij}(k)\epsilon^{s'}_{ij}(k) = 2\delta_{ss'}, \tag{3.84}$$

the canonically normalized Fourier modes ($a(\tau)h^s_k$) obey the same equation of motion of the massless scalar field given by (3.46), but have a different overall normalization factor:

$$h^s_k = \frac{2}{M_{\rm P}}\varphi_k. \tag{3.85}$$

The power spectrum of tensor perturbations is parameterized analogous to the scalar perturbations:

$$\Delta^2_T(k) = A_T(k_*)\left(\frac{k}{k_*}\right)^{n_T}, \tag{3.86}$$

where n_T is the tensor spectral index, and the power spectrum sums over both polarization states $\Delta^2_T(k) = 2\Delta^2_h(k)$. The superhorizon tensor power spectrum generated by inflation is then

$$\Delta^2_T = 2\times\frac{4}{M_{\rm P}^2}\Delta^2_\varphi = \frac{2}{\pi^2}\left(\frac{H_*}{M_{\rm P}}\right)^2, \tag{3.87}$$

with $n_T = 0$, inflation also predicts a flat power spectrum for tensor modes. We have not yet been able to detect tensor modes as their amplitude is extremely small; a factor of $M_{\rm P}^{-1}$ smaller than scalar perturbations. The potential to make a measurement in the future is an exciting prospect as it would provide us with direct evidence of inflation, since we know of no other way of generating tensor perturbations. The tensor amplitude only depends on the inflationary potential, as $H \propto \sqrt{V(\phi)}$ during inflation, so it would allow us to determine the energy scale of inflation and the inflationary model. So far we only have an upper-bound on the tensor-to-scalar ratio:

$$r \equiv \frac{\Delta_T^2(k_*)}{\Delta_s^2(k_*)} = 8M_{\rm P}^2 \left(\frac{V_\phi}{V}\right)^2 = \frac{4n}{N_e}, \tag{3.88}$$

where at the 95% confidence limit [33]

$$r < r_{\rm CMB} = 0.13. \tag{3.89}$$

Given equation (3.88), the tensor-to-scalar ratio of a quartic model ($n = 4$) exceeds this bound, with $r \sim 0.27$. However by non-minimally coupling the inflaton field to gravity, we can achieve $r < r_{\rm CMB}$; this analysis will be carried out in section 6.3.

3.4 Structure formation

We have shown that inflationary enhanced quantum fluctuations of the inflaton field generate density inhomogeneties, which seed the formation of large scale structures. We are now going to provide the reader with a very simplified but intuitive description of how perturbations evolve and form structures in a static universe, using Newtonian mechanics. Although this treatment is naive, it does provide us with a good approximation for baryonic structure formation in the real universe, and the results will be useful in section 4.3 where we study dark matter structure formation.

Overdense regions of the universe gravitationally attract matter from surrounding regions. Using our result from equation (3.71), we can see that density perturbations grow like

$$\frac{\delta\rho}{\rho} = \frac{\kappa}{(H(t)a(t))^2} \propto \begin{cases} t, & \text{radiation dom.} \\ t^{\frac{2}{3}}, & \text{matter dom.} \end{cases} \tag{3.90}$$

during the radiation and matter dominated periods, whilst $\delta\rho/\rho < 1$. The critical scale at which perturbations reach hydrostatic equilbrium is defined as the Jeans length, R_J. At scales beyond the Jeans length the perturbation density grows exponentially, quickly reaching $\delta\rho/\rho \sim 1$ where perturbations undergo non-linear gravitational collapse and form compact

objects such as stars and galaxies. We will derive the Jeans length using the Virial theorem, which states that for a stable system of particles, the total kinetic energy, K, is equal to half of the total potential energy, V:

$$K(R_J) = -\frac{1}{2}V(R_J). \tag{3.91}$$

In the context of star and galaxy formation, the Jeans length is the radius of a spherical cloud of hydrogen in which the gravitational potential energy is balanced by the pressure of the gas. When $K > -V/2$, the perturbations undergo acoustic oscillations, and when $K < -V/2$, the perturbations gravitationally collapse.

Using Newton's law of gravitation, the gravitational potential energy of a spherical cloud of gas with mass M and radius R is

$$V = -\frac{3}{5}\frac{GM^2}{R}, \tag{3.92}$$

and assuming classical thermodynamics, the total kinetic energy of N particles is

$$K = \frac{3}{2}Nk_BT = \frac{3}{2}\frac{M}{m_H}k_BT. \tag{3.93}$$

Next we equate equations (3.92) and (3.93) using the Virial theorem and then substitute in for mass, assuming constant density, $M = \frac{4\pi}{3}R^3\rho$. Then rearranging for the Jeans length gives

$$R_J = \left(\frac{15}{4\pi}\frac{k_BT}{m_H}\frac{1}{G\rho}\right)^{\frac{1}{2}}. \tag{3.94}$$

Alternatively, the Jean's length written in terms of the speed of sound within the gas cloud,

$$u_s^2 = \frac{k_BT}{\gamma m_H}, \tag{3.95}$$

where we assume the adiabatic index of an ideal gas, $\gamma = \frac{5}{3}$:

$$R_J = \frac{3}{2\sqrt{\pi}}\frac{u_s}{\sqrt{G\rho}}; \begin{cases} R < R_J, & \text{acoustic oscillations} \\ R > R_J. & \text{gravitational collapse} \end{cases} \tag{3.96}$$

Then defining the Jeans mass as

$$M_J = \frac{4\pi}{3}R_J^3\rho,$$

substituting in for R_J gives

$$M_J = \frac{9}{2\sqrt{\pi}} \frac{u_s^3}{\sqrt{G^3\rho}}; \begin{cases} M < M_J, & \text{acoustic oscillations} \\ M > M_J. & \text{gravitational collapse} \end{cases} \tag{3.97}$$

We can therefore deduce from (3.96) and (3.97) that cooler and denser clouds are less stable, so they will gravitationally collapse at smaller masses and form smaller stars. On the other hand, hotter and less dense clouds are more stable, so they require more mass to gravitationally collapse and thus form larger stars.

The static universe approximations are applicable to the real universe in the regime when the time it takes for a perturbation to collapse,

$$t_J = \frac{\lambda_J}{u_s} \sim (G\rho)^{-\frac{1}{2}}, \tag{3.98}$$

is less than the Hubble time, $H^{-1} \sim (G\rho_T)^{-\frac{1}{2}}$, as we can ignore the effects of expansion. This is the case when the perturbation fluid dominates the total energy density of the universe, ρ_T. In particular, the Jeans analysis is accurate in predicting the scale that baryonic structures begin to form at recombination, when radiation pressure has ceased and gravitational forces can dominate:

$$M_J(T_r) \sim 10^6 M_\odot, \tag{3.99}$$

where T_r is the temperature at recombination and $M_\odot = 1.2 \times 10^{57}$ GeV is the solar mass; this result gives the approximate size of the smallest dwarf galaxies in the universe. On the other hand, the Jeans analysis is not applicable when the perturbation fluid is a sub-dominant component of the total energy density, as when $t_J > H^{-1}$ the expansion of the universe can not be ignored. The Jeans analysis is therefore not applicable to cold (or warm) DM, which can form structures in the radiation-dominated epoch as it does not feel the effect of radiation pressure. We will discuss DM structure formation in detail in section 4.3.

3.5 Summary and discussion

In this chapter we show how an initial period of positively accelerating expansion called inflation is able to explain the flatness, homogeneity and isotropy of our observable universe, without the need to implement finely tuned initial conditions. We specifically study a minimal single large-field inflationary model, with a potential of the form

$$V(\phi) = \frac{\lambda\phi^n}{n}. \tag{3.100}$$

The slow-roll conditions are satisfied for this model whilst the field values are very large, $\phi \gg M_{\rm P}$, and inflation ends once the slow-roll conditions are violated, when $\phi_e = O(M_{\rm P})$. If inflation is to solve the horizon and flatness problems, we require a minimum of 60 e-foldings of expansion,

$$N_e^{\rm tot} = \ln \frac{a_e}{a(t_{\rm pl})} \gtrsim 60. \tag{3.101}$$

Inflation also provides us with a mechanism to generate small inhomogeneities that seed the large-scale structure of the universe, through inflationary enhanced quantum fluctuations of the inflaton field. Single-field inflationary models generate highly gaussian, scale-invariant and adiabatic perturbations, which is in agreement with CMB observations [100, 101]. Multi-field models are less well-motivated, as they can lead to non-gaussianity and the generation of isocurvature modes. Although the models we present in chapters 6, 7 and 8 are multi-field inflationary models, we carefully tune our parameters so that the inflationary dynamics can be approximated by that of a single-field model.

Quantum fluctuations of the inflaton field generate scalar and tensor metric perturbations with power spectrums that we parameterize in the following form,

$$\Delta_s^2(k) = A_\varphi(k_*) \left(\frac{k}{k_*}\right)^{n_s - 1}, \qquad \Delta_T^2(k) = A_T(k_*) \left(\frac{k}{k_*}\right)^{n_T}. \tag{3.102}$$

Inflation predicts that the power spectrums for both scalar and tensor perturbations are flat, with spectral indexes $n_s \sim 1$ and $n_T \sim 0$ respectively. Planck's measurement of the amplitude of the primordial scalar perturbations [33],

$$\Delta_s^{\rm CMB}(k_*) \sim 4.7 \times 10^{-5} \tag{3.103}$$

at $k_* = 0.05$ Mpc^{-1}, allows us to constrain the self-coupling of the inflaton field,

$$\lambda = \frac{12\pi^2 M_{\rm P}^{4-n}}{\sqrt{(2N_e)^{n+2} n^{n-4}}} \Delta_s^2, \tag{3.104}$$

which we evaluate at the relevant $N_e = 60$ e-foldings prior to the end of inflation.

So far we only have an upper-bound on the tensor-to-scalar ratio [33],

$$r \equiv \frac{\Delta_T^2(k_*)}{\Delta_s^2(k_*)} < r_{\rm CMB} = 0.13, \tag{3.105}$$

at the 95% confidence limit. The large-field inflationary model predicts a tensor-to-scalar ratio

of

$$r = \frac{4n}{N_e}. \tag{3.106}$$

Later we study our inflationary model with a quartic potential ($n = 4$), which gives a tensor-to-scalar ratio that exceeds the CMB bound (3.105). However, we will show that by non-minimally coupling the inflaton field to gravity, we can achieve $r < r_{\rm CMB}$; this analysis will be carried out in section 6.3.

Chapter 4

Dark matter

We now have a vast amount of evidence to support the existence of DM: from the large scale structure of the universe [19, 20], the CMB's power spectrum [17, 18] and a catalogue of observed gravitational effects [14–16], we infer that DM makes up over 80% of the total matter density in the universe [21]. DM is fundamentally different to baryonic matter as we can only indirectly observe it from its gravitational effects. Since we can not see it, we know that it does not interact much via electromagnetic or strong forces, and as DM has proven to be extremely difficult to detect, it is not yet known whether it is weakly interacting with the SM or decoupled entirely. Finally, for DM models to be compatible with structure formation, their free-streaming length, or 'hotness', is constrained by the scale of the smallest old structures in the universe [92, 102].

Within these constraints lies a rich variety of possible DM models, many of which look to solve additional problems within the SM. To name a few, there are hidden sector models that generate baryon asymmetry [22, 23], axion-like particles (ALPs) that may solve the strong charge-parity (CP) problem [24–26], and the dark Higgs (scalar) DM which is motivated by the electroweak (EW) hierarchy problem [27, 28]. In chapter 7, we extend our inflaton model with a modified Minimal Neutrino Standard Model (νMSM) [43], in which our DM candidate is a right-handed singlet neutrino, otherwise known as a sterile neutrino. Sterile neutrinos have historically been a well-motivated addition to the SM as they provide a mechanism for generating SM neutrino masses via the see-saw mechanism [53, 54], and the baryon asymmetry of the universe (BAU) via leptogenesis [103–105]. There are many models for sterile neutrino DM production [106], for example, the Dodelson-Widrow [29] and Shi-Fuller [30] mechanisms produce DM via active-sterile neutrino oscillations. Both of these models will be discussed in section 5.2, where we will show that they are very strongly constrained by the active-sterile neutrino mixing angle and their free-streaming length. We present an alternative model, whereby DM is produced via scalar inflaton decay [43]. The parameter space is less constrained, as the DM production mechanism does not depend on the coupling strength to the SM neutrino sector.

The aim of this chapter is to motivate the need for DM and introduce the reader to the

background theory that is required to constrain our sterile neutrino DM model. First we present the main pieces of gravitational evidence of DM, followed by the freeze-out and freeze-in production mechanisms, which are necessary to constrain the relic abundance and thus the parameters of the DM model. Finally, we will discuss why DM is fundamental to the large scale structure of the universe, and how small-scale structures, probed by the Lyman-α forest, constrain the DM free-streaming length.

4.1 Gravitational evidence of dark matter

4.1.1 Galactic rotational curves

The baryonic matter within a galaxy is divided between two components: a very dense region of stars at the centre of the galaxy called the galactic bulge, and surrounding it, a sparsely populated region of stars and dust called the galactic disc. To approximate the dynamics within these two regions, we will assume the total mass of the galaxy is contained within the central bulge of mass M_0, radius r_0 and constant density. Then using Newton's law of gravitation, the force acting on a star of mass m is

$$F_{\text{grav}} = \frac{GM_0 m}{r^2}, \tag{4.1}$$

and stars inside and outside the central bulge have rotational velocities [107]

$$v_{\text{rot}} \propto \begin{cases} r, & r < r_0, \\ r^{-\frac{1}{2}}, & r > r_0. \end{cases} \tag{4.2}$$

In 1933 Zwicky measured the average redshift of each member galaxy in the Coma galaxy cluster. He found that their rotational velocities greatly exceeded the expected value calculated from the gravitational mass of the luminous matter in the cluster [108]. As a result, he concluded that the majority of the mass in the cluster must be made up of non-luminous matter, called dark matter [108]. Following Zwicky's discovery, in the 1970s Rubin and Ford investigated this result further by using a high-resolution spectrograph to measure the rotational velocities of individual galaxies. Their results revealed that the rotational velocities of galaxies outside their central bulge remained constant out to very large radii [14, 109], as shown in Figure 4.1. Without modifying gravity, they concluded that the flat rotational curves can only be explained if the galaxies are embedded within an extended dark matter halo, which makes up over 80% of the total mass [110–112].

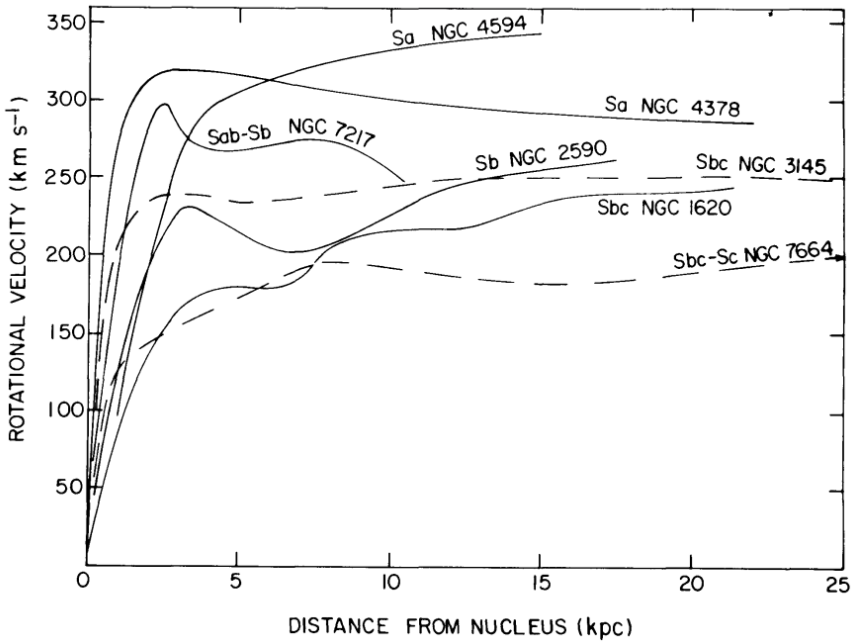

Figure 4.1: Rotational velocities of galaxies plotted against distance from the centre, taken from [109].

4.1.2 Gravitational lensing

Gravitational lensing is the bending of light within a gravitational field, predicted by Einstein's theory of General Relativity. We can use this as a tool to map out the distribution of DM by observing the light from very distant bright objects, such as quasars and galaxies, that has been bent by a nearby 'lensing' galaxy. This allows us to determine the gravitational field produced by the lensing galaxy, and from which we can infer the mass and distribution of DM within it.

The Sloan Digital Sky Survey (SDSS) has been able to map out the DM distribution within galaxies at distances up to 200 kpc from the centre, which is far beyond what is achievable using rotational velocity curves [113, 114]. Since discovering that DM halos are far larger and more massive than we had first anticipated, we can now appreciate the extent to which the formation and evolution of a galaxy's observable structure (the baryonic matter) depends on the properties of their host DM halo [15].

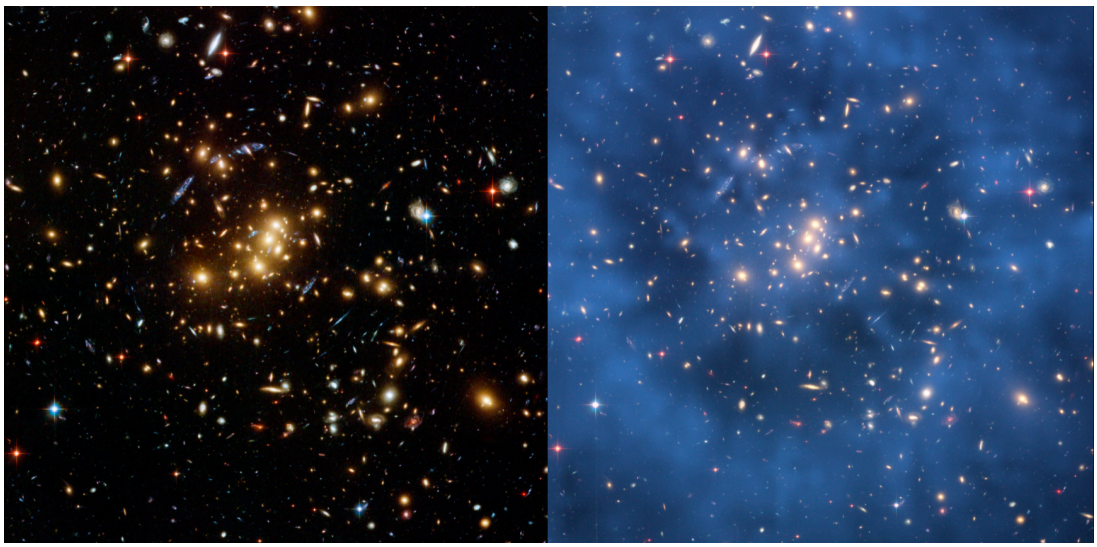

Figure 4.2: Distribution of DM in galaxy cluster Cl 0024+17

On the left is the Hubble Space Telescope image of the galaxy cluster Cl 0024+17. On the right is the same image with a superimposed blue map of the cluster's DM distribution. The map is derived by observing how the light from distant galaxies is distorted by Cl 0024+17's gravitational lens. Images are taken from [115].

4.1.3 Bullet Cluster

The Bullet Cluster is two previously collided galaxy clusters moving past each other. Figure 4.3 is a composite image of the Bullet Cluster containing X-ray data taken by NASA's Chandra X-ray Observatory in pink and a gravitational lensing map in blue, overlaying the Hubble Space and Magellan Telescope optical images [116]. The galaxies within the clusters mostly pass straight through, however the hot intergalactic gas is slowed down by its electromagnetic interactions. This is shown in Figure 4.3 by the x-ray emissions (in pink) that are displaced relative to the galaxies. The blue maps the region containing most of the mass of the cluster from observing the effects of gravitational lensing of distant galaxies. Most of the baryonic mass is contained within the intergalactic gas, however the cluster's centre of mass peak spatially offsets the baryonic mass peak by a statistical significance of 8σ [16, 117]. This observation is evidence of weakly interacting DM, which passes relatively unimpeded through the colliding galaxy clusters.

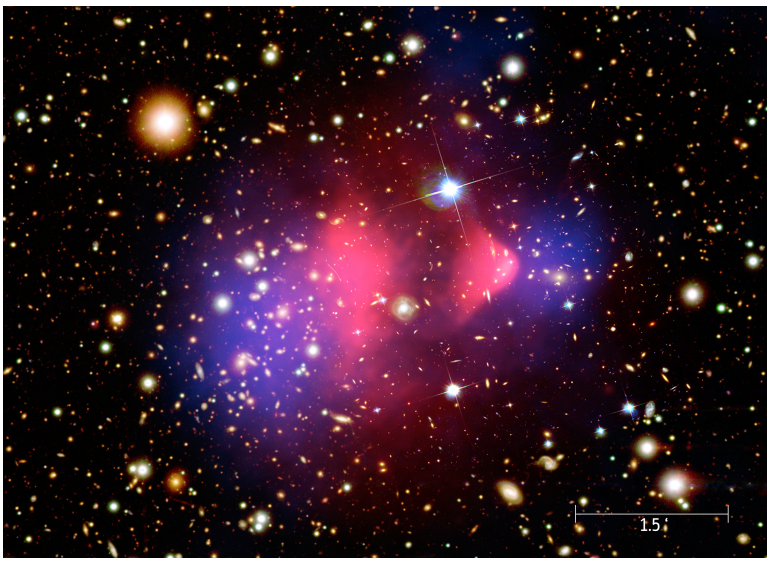

Figure 4.3: Bullet cluster

A composite image of the galaxy cluster 1E 0657-56, known as the Bullet Cluster, taken from [116]. The optical image of the galaxy cluster (taken by the Hubble Space and Magellan Telescope) is superimposed with maps of the x-ray emissions in pink (data taken by NASA's Chandra X-ray Observatory) and mass distribution in blue.

4.2 Dark matter production mechanisms

In this section we are going to analyse two DM production mechanisms: freeze-in [118] and freeze-out [55, 56]. Freeze-in DM has an initially negligible abundance due to its very weak coupling to the bath particles. The DM is produced via decay/scattering of bath particles, and remains decoupled from the bath throughout. On the other hand, freeze-out DM is more strongly coupled with the thermal bath. It has an initially large thermal abundance, which later departs from thermal equilibrium at the time of freeze-out.

Figure 4.4 below plots the evolution of the freeze-in and freeze-out DM yields, which is defined as the ratio of the DM number density over the total entropy,

$$Y_{\mathrm{DM}} \equiv \frac{n_{\mathrm{DM}}}{s}, \tag{4.3}$$

with the expansion of the universe [118], which is given as a function of the DM particle mass over the thermal bath temperature. The evolution of thermal DM yield is given by the solid black line; the yield remains constant whilst temperatures exceed the DM mass, and decreases rapidly once temperatures drop below the DM mass due to Boltzmann suppression. The evolution of freeze-in and freeze-out DM is given by the dashed and solid coloured lines respectively, and the arrows on the plots show the direction of increasing DM coupling strength with the thermal bath. Whilst the freeze-in DM yield increases with increasing coupling strength, the freeze-out DM yield decreases, as the DM departs from thermal equilibrium later when their

abundance is more strongly Boltzmann suppressed. The DM yield remains constant once their production and annihilation ceases.

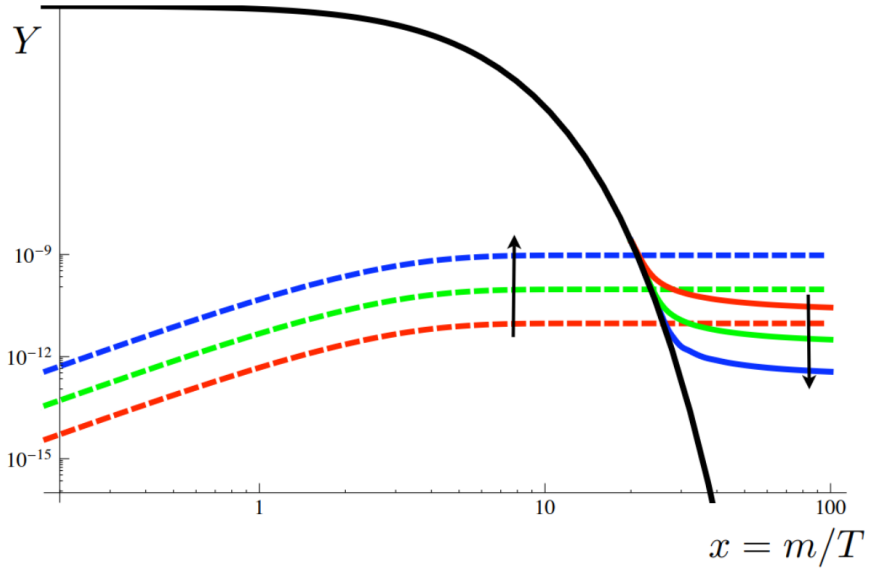

Figure 4.4: Evolution of freeze-in and freeze-out DM yields

Plot of the DM yield, $Y \equiv n/s$, against the DM particle's mass over temperature, $x = m/T$, taken from [118]. The black solid line is the yield if equilibrium is maintained; and the coloured solid/dashed lines are the evolution of the freeze-out/in yields. The coupling strength of the DM increases in the direction of the arrows.

The initial conditions of freeze-out DM are erased when the particles come into thermal equilibrium, which is to be expected due to the high temperatures that are reached during the reheating period. Freeze-in DM is therefore an unusual case as it remains out of thermal equilibrium and as a result, its relic abundance intrinsically depends on the initial conditions of the model. Although this makes freeze-out models arguably more robust, freeze-in models are able to produce lighter and warmer DM, which is favourable for structure formation [91–93]. In chapter 7 we present our sterile neutrino DM candidate that is produced via freeze-in. As the DM is an extension to a cosmological model that fully describes inflation and reheating, we can be sure of the initial conditions and can constrain its relic abundance.

In the following analysis we evaluate the yield of freeze-out and freeze-in DM particles and constrain the DM model parameters by equating their relative energy density today,

$$\Omega_{\mathrm{DM},0} = \frac{m_{\mathrm{DM}} n_{\mathrm{DM},0}}{\rho_{c,0}}, \tag{4.4}$$

with the known DM abundance, given in (2.85). The number density of particles today, $n_{\mathrm{DM},0}$, is evaluated by diluting the number density of particles at the end of freeze-in/freeze-out, $n_{\mathrm{DM},f}$, by the expansion of the universe,

$$n_{\mathrm{DM},0} = n_{\mathrm{DM},f} \left(\frac{a_f}{a_0}\right)^3. \tag{4.5}$$

Then, as the co-moving entropy density is a conserved quantity, $s_f a_f^3 = s_0 a_0^3$, the relative energy density is related to the DM yield by

$$\Omega_{\mathrm{DM},0} = \frac{m_{\mathrm{DM}} Y_{\mathrm{DM},f} s_0}{\rho_{c,0}}. \tag{4.6}$$

4.2.1 Freeze-out production

In the early hot universe, DM particles (A) are kept in thermal and chemical equilibrium through their weak coupling to a thermal bath of particles (B); this particular class of DM particles are therefore referred to as weakly interacting massive particles (WIMPs) [55, 56]. We will assume here that particles B are lighter than A, and that they annihilate and pair-create via the following scattering process:

$$AA \leftrightarrow BB. \tag{4.7}$$

The WIMP abundance is governed by the Boltzmann equation [55, 56]:

$$\frac{d(n_{\mathrm{DM}} a^3)}{dt} = -\langle \sigma_{\mathrm{ann}} \cdot v \rangle \cdot \left(n_{\mathrm{DM}}^2 - n_{\mathrm{DM,eq}}^2 \right) a^3, \tag{4.8}$$

where $n_{\mathrm{DM,eq}}$ is the number density of A in thermal equilibrium and $\langle \sigma_{\mathrm{ann}} \cdot v \rangle$ is the thermally averaged annihilation cross-section. The WIMPs have a thermal abundance, given by the black line in Figure 4.4, whilst their annihilation rate,

$$\Gamma_{\mathrm{ann}} = \langle \sigma_{\mathrm{ann}} \cdot v \rangle n_{\mathrm{DM}}, \tag{4.9}$$

exceeds the Hubble expansion rate. At high temperatures, $T > m_{\mathrm{DM}}$, the WIMPs also maintain chemical equilibrium, i.e. the DM production and annihilation rates are equal. As a result, we see that their thermal yield remains constant in Figure 4.4, or equivalently from equation (4.8), their co-moving number density remains constant whilst they remain in thermal and chemical equilibrium.

The WIMPs freeze-out once the annihilation rate drops to the order of the Hubble expansion rate,

$$\Gamma_{\mathrm{ann}}(T_f) \sim H(T_f). \tag{4.10}$$

At temperatures $T < T_f$, the expansion rate is too fast for the DM particles to collide and annihilate, and so their yield remains constant. WIMPs with a small coupling to the thermal bath freeze-out whilst they are still in chemical equilibrium, $T_f > m_{\mathrm{DM}}$ and are therefore

still relativistic. On the other hand, WIMPs with a relatively large cross-section freeze-out after departing from chemical equilibrium, at $T_f < m_{\rm DM}$, once they are non-relativistic. As a result, their number density is Boltzmann-suppressed, thus yielding a smaller final abundance. We will now evaluate the yields of both cases separately, in order to constrain the WIMP parameters using the known abundance of DM in the universe.

4.2.1.1 Freeze-out of relativistic particles

The yield of relativistic DM particles at freeze-out is the ratio of their thermal number density, given by equation (2.32), over the total entropy, given by equation (2.35) [55, 56, 119],

$$Y_{\rm DM,f} = \frac{45\zeta(3)}{2\pi^4}\frac{g_{*n}^{\rm DM}}{g_{*s}(T_f)}; \tag{4.11}$$

the freeze-out temperature is defined by $\Gamma_{\rm ann}(T_f) \sim H(T_f)$. The yield is independent of temperature, as shown in Figure 4.4 by the flat thermal yield in the region $m/T \lesssim 1$, and so we can easily calculate the relative energy density of DM:

$$\Omega_{\rm DM}h^2 = \frac{g_{*n}^{\rm DM}}{g_{*s}(T_f)}\frac{m_{\rm DM}}{13.4\ {\rm eV}}. \tag{4.12}$$

4.2.1.2 Freeze-out of non-relativistic particles

Constraining the parameters of non-relativistic WIMPs is more involved, since they depart from chemical and thermal equilibrium prior to freeze-out, which results in their yield crucially depending on the mass-to-temperature ratio at the time of freeze-out [55, 56, 119].

Once the universe has expanded and cooled to temperatures below the mass scale of the WIMP, $T < m_{\rm DM}$, their production becomes kinematically unviable and they drop out of chemical equilibrium. The WIMP's departure from chemical equilibrium is shown in Figure 4.4 where their thermal yield starts to decrease, which is known as Boltzmann suppression, as the DM particles continue to annihilate. Once their annihilation rate drops below the Hubble expansion rate, the DM then departs from thermal equilibrium, which is shown by the coloured lines branching from the thermal yield in Figure 4.4. Once the universe is expanding too fast for the particles to annihilate, the DM freezes out and their yield remains constant. Next we are going to carefully track the DM abundance between departing from chemical and thermal equilibrium to freeze-out.

Chemical equilibrium is lost when [55]

$$\frac{dn_{\rm DM,eq}}{dt} \gtrsim \langle\sigma_{\rm ann}\cdot v\rangle n_{\rm DM,eq}^2. \tag{4.13}$$

The non-relativistic thermal number density is given by equation (2.44), and its differential is

[55, 119]

$$\frac{dn_{\rm DM,eq}}{dt} \sim -\frac{m_{\rm DM}}{T}\frac{\dot{T}}{T} n_{\rm DM,eq} \sim xH(T) n_{\rm DM,eq}, \tag{4.14}$$

where $x_i \equiv m_{\rm DM}/T_i$. Then by equating equations (4.13) and (4.14), we can determine when the WIMPs depart from chemical equilibrium [55, 119]:

$$x_f H(T_f) = \langle \sigma_{\rm ann} \cdot v \rangle n_{\rm DM,eq}(T_f), \tag{4.15}$$

$$\rightarrow x_f \sim \ln\left[\frac{g_{\rm DM}}{\sqrt{g_{*\rho}}} M_{\rm P} \langle \sigma_{\rm ann} \cdot v \rangle m_{\rm DM}\right], \tag{4.16}$$

to logarithmic accuracy. We assume here that annihilation of A is efficient, and so the temperature they depart from chemical equilibrium is approximately equal to the temperature that they freeze-out, T_f.

To carefully track the abundance between exiting chemical and thermal equilibrium and freeze-out, we must solve the Boltzmann equation (4.8), which we will reparameterize from $n_{\rm DM} \rightarrow Y_{\rm DM}$:

$$\frac{dY_{\rm DM}}{dt} = \frac{1}{a^3 s}\frac{d}{dt}\left(n_{\rm DM} a^3\right), \tag{4.17}$$

$$= -s\langle \sigma_{\rm ann} \cdot v \rangle \cdot \left(Y^2_{\rm DM} - Y^2_{\rm DM,eq}\right).$$

Then using the relation $dx/dt = Hx$, derived from the conservation of conformal entropy density[1], we transform coordinates from $t \rightarrow x$ to obtain the following expression [55, 119]:

$$\frac{dY_{\rm DM}}{dx} = -\frac{\lambda \langle \sigma_{\rm ann} \cdot v \rangle}{x^2} \cdot \left(Y^2_{\rm DM} - Y^2_{\rm DM,eq}\right), \tag{4.20}$$

where $\lambda \sim \frac{4\pi}{3\sqrt{10}} \frac{g_{*s}}{\sqrt{g_{*\rho}}} M_{\rm P} m_{\rm DM}$. At freeze-out $Y_{{\rm DM},f} \sim Y_{\rm DM,eq}$, then using equation (4.15) [55, 119],

$$Y_{{\rm DM},f} = \frac{1}{s(T_f)} \frac{x_f H(T_f)}{\langle \sigma_{\rm ann} \cdot v \rangle}, \tag{4.21}$$

$$= \frac{x_f^2}{\lambda \langle \sigma_{\rm ann} \cdot v \rangle}.$$

[1] Given that entropy density is conserved in a co-moving volume, and assuming $g_{*s}(T)$ is constant, we obtain the following relation:

$$\frac{d(s(T)a^3)}{dt} = \frac{d}{dt}\left(\frac{2\pi^2}{45} g_{*s} T^3 a^3\right) = 3s(T)a^3\left(\frac{\dot{T}}{T} + \frac{\dot{a}}{a}\right) = 0,$$

$$\rightarrow \frac{\dot{T}}{T} = -\frac{\dot{a}}{a} = -H. \tag{4.18}$$

Then substituting equation (4.18) into the time derivative of x, we have

$$\frac{dx}{dt} = m_{\rm DM}\frac{d}{dt}\left(\frac{1}{T}\right) = -x\frac{\dot{T}}{T} = Hx. \tag{4.19}$$

In the limit $T_0 \ll T_f$, we have $Y_{\mathrm{DM},0} \gg Y_{\mathrm{DM,eq}}$ and $x_0 \gg x_f$, and thus we can neglect $Y^2_{\mathrm{DM,eq}}$ in equation (4.20) [55, 119]:

$$\begin{aligned}\int_{Y_{\mathrm{DM},f}}^{Y_{\mathrm{DM},0}} dY_{\mathrm{DM}}\ \frac{1}{Y^2_{\mathrm{DM}}} &= -\int_{x_f}^{x_0} dx\ \frac{\lambda\langle\sigma_{\mathrm{ann}}\cdot v\rangle}{x^2},\\ &\to \frac{1}{Y_{\mathrm{DM},0}} \sim \frac{\lambda\langle\sigma_{\mathrm{ann}}\cdot v\rangle}{x_f} + \frac{1}{Y_{\mathrm{DM},f}},\\ &\to Y_{\mathrm{DM},0} \sim \frac{x_f}{\lambda\langle\sigma_{\mathrm{ann}}\cdot v\rangle}.\end{aligned} \tag{4.22}$$

The annihilation of WIMPs between exiting thermal equilibrium and freeze-out will therefore deplete their yield by $Y_{\mathrm{DM},0}/Y_{\mathrm{DM},f} = x_f^{-1}$. Using result (4.22), the relative energy density of DM today is

$$\Omega_{\mathrm{DM}}h^2 \sim \frac{1.68\times10^{-10}\ \mathrm{GeV}^{-2}}{\langle\sigma_{\mathrm{ann}}\cdot v\rangle}\left(\frac{100}{g_*(T_f)}\right)^{\frac{1}{2}}\left(\frac{x_f}{20}\right); \tag{4.23}$$

here we use the notation $g_* \equiv g_{*s/\rho}$, since at high temperatures $g_{*s} = g_{*\rho}$. As we have previously argued, we can see explicitly here that the freeze-out yield decreases with increasing coupling strength. Particle A is known as a 'WIMP miracle' when $x_f \sim 20$ as it reproduces the observed DM abundance [55, 56, 119].

4.2.2 Freeze-in production

Now we will consider the scenario where in the early hot universe there is a negligible abundance of DM particles (A) that are very weakly, or feebly, coupled to a bath of particles (B); this class of DM particles are therefore referred to as feebly interacting massive particles (FIMPs). Their production rate, Γ_{prod}, is far less than the Hubble expansion rate throughout the course of the universe's history. As a result, we see in Figure 4.4 that the FIMPs yield, given by the coloured dashed lines, does not coincide with the thermal abundance [118]. We will consider the following two processes for the production of A:

$$BB \to AA, \qquad B \to AA, \tag{4.24}$$

where the two-to-two scattering process has coupling strength λ and the decay process has coupling strength λm_B. The FIMP abundance is governed by the Boltzmann equation [118]:

$$\frac{d(n_{\mathrm{DM}}a^3)}{dt} = 2\Gamma_{\mathrm{prod}}\ n_B a^3, \tag{4.25}$$

with production rate:

$$\Gamma_{\mathrm{prod}} = \Gamma_{BB\to AA} + \Gamma_{B\to AA}. \tag{4.26}$$

The FIMP number density remains low during production, since $\lambda_{\rm prod} \ll H(T)$, so we can neglect the reverse reactions $AA \to BB/B$. We will assume the limit $m_B \gg m_{\rm DM}$, in which case the decay process usually dominates, and we can neglect the two-to-two scattering in our calculation of the final yield. Additionally, if the bath of particles B is not in thermal equilibrium the yield of A is model-dependent. This is the case in chapter 7, where we analyse DM sterile neutrino production from the decay of inflaton with a highly infra-red distribution [43]. Here we will present the model-independent result, thereby assuming particles B have reached thermal equilibrium prior to the production of A.

At temperatures $T \gg m_B$, the conformal number density of particles B is constant, $n_B a^3 = c.$, and so we can approximate the integration of equation (4.25) by[2]

$$\begin{aligned} n_{\rm DM} &\sim 2\Gamma_{B\to AA} n_B t, \\ &\sim \frac{\Gamma_{B\to AA} n_B}{H}; \end{aligned} \tag{4.28}$$

where in the second line we have used the inverse relation between the Hubble expansion rate and time in a radiation-dominated universe, $H = 1/2t$. In the limit $m_B \gg m_{\rm DM}$, the decay rate is

$$\Gamma_{B\to AA} = \frac{\lambda^2 m_B}{8\pi}. \tag{4.29}$$

Then substituting equation (2.32) for the thermal number density of B, we obtain the following expression for the FIMP number density:

$$n_{\rm DM} \sim \xi(3)\frac{3\sqrt{10}}{8\pi^4}\frac{g_B}{\sqrt{g_{*\rho}}}\lambda^2 M_{\rm P} m_B T, \tag{4.30}$$

and expression for the FIMP yield:

$$Y_{\rm DM} \sim \xi(3)\frac{135\sqrt{10}}{16\pi^6}\frac{g_B}{g_{*s}\sqrt{g_{*\rho}}}\frac{M_{\rm P} m_B}{T^2}\lambda^2; \tag{4.31}$$

we will assume particle B is a scalar and so $g_B = 1$. When the bath particles are in thermal equilibrium, freeze-in production is most efficient when the temperature is of the order of the most massive particle at the interaction vertex, and so in our case when $T_f \sim m_B$ [118]. When $T < m_B$, the number density of particles B are Botzmann suppressed; and when $T > m_B$,

[2] To more precisely solve for $n_{\rm DM}$, we need to integrate over the distribution functions of the particles (f_A, f_B) in the Boltzmann equation [118]:

$$\begin{aligned} \dot{n}_{\rm DM} + 3Hn_{\rm DM} = \int & d\Pi_A^2 d\Pi_B (2\pi^4)\delta^4(2p_A - p_B) \\ & \times \left[|M_{B\to AA}|^2 f_B(1+f_A)^2 - |M_{AA\to B}|^2 f_A^2(1+f_B)\right]; \end{aligned} \tag{4.27}$$

where $d\Pi_i = {\rm d}^3 p_i/(2\pi)^3 2E_i$ are the phase space elements. This results in a final yield less than a factor of 2 different from our approximation, given in (4.32). See [118] for the details.

the universe's expansion rate is larger and therefore so is the rate the FIMP number density is diluted. Particles A freeze-in with a final yield of

$$Y_{\mathrm{DM},f} \sim \left(3.33 \times 10^{-2}\right) \frac{1}{g_{*s}\sqrt{g_{*\rho}}} \frac{M_{\mathrm{P}}}{m_B} \lambda^2, \tag{4.32}$$

evaluated when $T_f = m_B$, which corresponds to a relative energy density of

$$\Omega_{\mathrm{DM}} h^2 \sim \left(2.18 \times 10^{25}\right) \frac{1}{g_{*s}\sqrt{g_{*\rho}}} \frac{m_{\mathrm{DM}}}{m_B} \lambda^2, \tag{4.33}$$

$$\sim O(0.1) \left(\frac{100}{g_*(m_B)}\right)^{\frac{3}{2}} \left(\frac{m_{\mathrm{DM}}}{m_B}\right) \left(\frac{\lambda}{2 \times 10^{-12}}\right)^2. \tag{4.34}$$

Here we have abbreviated $g_* \equiv g_{*s/\rho}$, since at high temperatures $g_{*s} = g_{*\rho}$. Unlike the freeze-out DM abundance given in equation (4.23), the freeze-in DM abundance increases with increasing coupling strength.

4.3 Structure formation

DM plays an essential role in creating the network of galaxy clusters, filaments and voids that form the large scale structure of the universe [19, 20], which is shown by the Sloan Digital Sky Survey (SDSS) in Figure 4.5. We will first explain how baryonic structures are formed, and the discrepancies of purely baryonic matter models with cosmological observables. We will then discuss how this is rectified with an additional DM component.

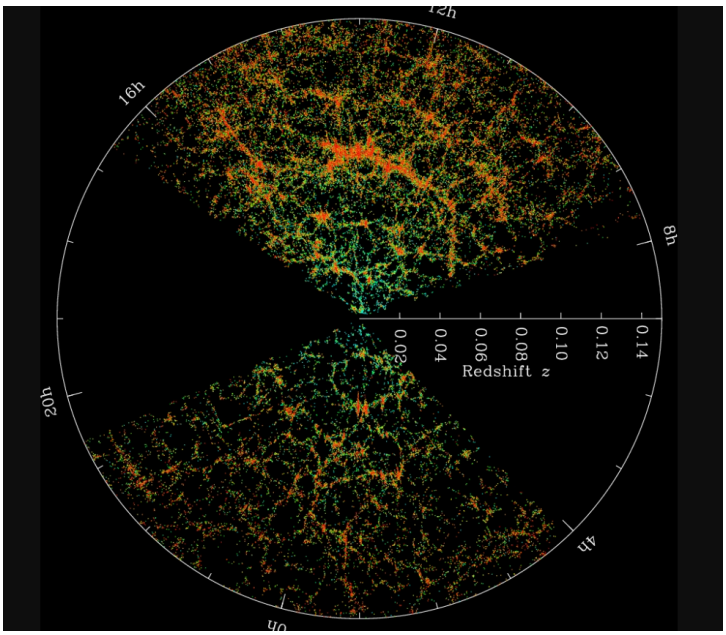

Figure 4.5: SDSS map of galaxy distribution

The distribution of galaxies in the universe mapped by the SDSS out to distances ~ 600 Mpc. The galaxies are represented by dots, and colour-coded from green to red to show low to high local density respectively. The data in the image is from Data Release 17 of the SDSS-IV [120].

Before recombination, protons and electrons were coupled to photons by Thomson scattering, which created a large radiation pressure that prevented the gravitational collapse of density fluctuations. At scales below the Jeans' length, given by equation (3.96), this gave rise to the baryonic acoustic oscillations that we observe in the CMB [83, 121]. At recombination, photons decouple and subsequently free-stream through the universe. As a result, radiation pressure ceased, allowing gravitational forces to dominate, thus leading to the collapse of perturbations. Before the consideration of DM, there were two competing theories that assumed matter was purely baryonic: Zel'dovich's pancake model, containing only adiabatic perturbations [122]; and Peeble's hierarchical clustering model, containing only isothermal perturbations [123] (which evolve in the same way as isocurvature perturbations during radiation domination). In Zeldovich's model [122], perturbations collapse into large pancake-like structures, and small-scale perturbations are smoothed out by Silk damping [87], as photons diffuse out of overdense regions, dragging baryons with them. In order for there to be sufficient time for the large structures to fragment and form the small-scale filamentary structures, the model requires large perturbation amplitudes at recombination ($\Delta T/T > 10^{-3}$ [124]), which we now know exceed those measured by the CMB [125]. Alternatively, Peeble's model [123] assumes only isothermal perturbations and so there is no Silk damping, thereby allowing smaller perturbations to collapse after recombination. However we now know CMB anisotropies are adiabatic, there is currently no evidence of any admixture of isocurvature modes [126]. We will now discuss how an additional dominant DM matter component is able to reproduce the observed large scale structure.

By definition, DM does not interact electromagnetically and so it does not feel the effect of radiation pressure prior to recombination. DM that is produced at relativistic speeds (defined as 'hot' or 'warm' DM) damps perturbations below their 'free-streaming length', thus limiting the minimum scale of structures that can form [127, 128]; this will be the subject of the following section. However perturbations of 'cold' or 'warm' DM are able to collapse long before recombination in the radiation-dominated epoch, thus enabling small-scale structures to form [41, 42]. After matter-radiation equality, DM then dominates the evolution of matter perturbations, and creates the gravitational potential wells for baryonic matter to fall into after recombination, thus negating the impact of Silk damping [78]. Initially, matter perturbations larger than the Jeans length grow linearly, whilst $\delta\rho/\rho < 1$. Small-scale perturbations reach $\delta\rho/\rho \sim 1$ first, at which time their growth becomes non-linear, and they gravitationally collapse to form stars and galaxies. Large-scale perturbations remain in the linear regime until today, as once the cosmological constant dominates their growth competes with cosmological expansion. Smaller structures then later merge to form larger structures, such as filaments and clusters, whilst underdense regions form vast voids [78]. Whilst baryonic matter is able to form very

compact objects, such as stars, due to radiative cooling, DM is dissipationless, and so maintains a diffuse halo structure [113, 129].

4.3.1 Free-streaming length

The free-streaming scale of DM plays a crucial role in structure formation, as it defines the length below which DM density fluctuations are damped. DM particles that decouple from the thermal bath at relativistic speeds, when $T_{\mathrm{DM},f} \gg m_{\mathrm{DM}}$, have enough kinetic energy to escape the gravitational potential wells in small over-dense regions. As a result of the free-streaming DM, small primordial inhomogeneities are smoothed out, thereby preventing structure formation on these scales. However, once the universe expands and cools to temperatures $T \sim m_{\mathrm{DM}}$, the DM particles become non-relativistic. Subsequently, they are entrapped by the gravitational potential wells and structures begin to form. The distance travelled by the DM particles between decoupling and their non-relativistic transition defines the free-streaming length. The maximum free-streaming length for any given DM model is constrained by the smallest observable structures in the universe.

As DM is very weakly interacting, it is described by a collisional fluid with a free-streaming wavenumber and free-streaming length of [127, 128, 130]

$$k_{\mathrm{FS}}(t) = \frac{\left(4\pi G\rho(t)a^2(t)\right)^{\frac{1}{2}}}{\langle v\rangle} = \sqrt{\frac{3}{2}}\frac{H(t)a(t)}{\langle v\rangle}, \tag{4.35}$$

$$\lambda_{\mathrm{FS}}(t) = \frac{2\pi a(t)}{k_{\mathrm{FS}}(t)}. \tag{4.36}$$

Note that where the Jeans length (3.96) defines the scale below which perturbations in a collisional fluid undergo adiabatic oscillations, the free-streaming length (4.36) is the scale below which perturbations are damped in a collisionless fluid. They are defined very similarly up to a small numerical factor, except the velocity dispersion, $\langle v\rangle$, of a collisionless fluid replaces the speed of sound, c_{s}, in a collisional fluid. For this example, we will assume the DM particle is fermionic and after decoupling it free-streams with a thermal velocity. At $T \gg m_{\mathrm{DM}}$, the DM particle is relativistic and therefore travels at the speed of light. However once $T \sim m_{\mathrm{DM}}$, the velocity of the particle decays with the expansion of the universe [127, 128]:

$$\begin{aligned}\langle v\rangle \equiv \frac{\langle p\rangle}{m_{\mathrm{DM}}} &= \frac{3.15T_{\mathrm{DM}}}{m_{\mathrm{DM}}} = \frac{3.15T_{\mathrm{DM},0}}{m_{\mathrm{DM}}}\left(\frac{a_0}{a}\right) = \frac{3.15T_0}{m_{\mathrm{DM}}}\left(\frac{g_{*s}(T_0)}{g_{*s}(T)}\right)^{\frac{1}{3}}\left(\frac{a_0}{a}\right)\left(\frac{\langle p\rangle}{3.15T}\right), \\ &= 350\ \mathrm{kms}^{-1}(1+z)g_{*s}(T)^{-\frac{1}{3}}\left(\frac{1\ \mathrm{eV}}{m_{\mathrm{DM}}}\right)\left(\frac{\langle p\rangle}{3.15T}\right).\end{aligned} \tag{4.37}$$

The DM particle's velocity transitions from relativistic to non-relativistic when $\langle v\rangle = 1$, which

corresponds to red-shift [127, 128]

$$1 + z_{\rm nr} = 856\ g_{*s}(T \approx m_{\rm DM})^{\frac{1}{3}} \left(\frac{m_X}{1\ \text{eV}}\right) \left(\frac{3.15T}{\langle p \rangle}\right)_{T \approx m_{\rm DM}}. \tag{4.38}$$

Next we will calculate the free-streaming length for DM that becomes non-relativistic during matter domination ($z_{\rm nr} < z_{\rm eq}$) and radiation domination ($z_{\rm nr} > z_{\rm eq}$), where $z_{\rm eq}$ defines the red-shift where matter-radiation equality occurs [55]:

$$1 + z_{\rm eq} = \frac{\Omega_{\rm m,0}}{\Omega_{\gamma,0}} \sim 6 \times 10^3. \tag{4.39}$$

Note that the analysis needs to be carried out separately for both regimes as the expansion rates have a different dependence on the scale factor. We define DM as 'hot' if it becomes non-relativistic during the matter-dominated period, and 'warm' if it becomes non-relativistic during the radiation-dominated period. In addition there may be 'cold' DM particles, which have large masses and low velocities, and so their free-streaming lengths are insignificant on cosmological scales.

4.3.1.1 Hot DM

During the matter-dominated period, the Hubble expansion rate is

$$H(t) = H_0 \sqrt{\Omega_{\rm m,0}(1+z)^3}, \tag{4.40}$$

where $\Omega_{\rm m,0}$ is the relative energy density of matter in the universe today. Next we need to find when the free-streaming length of the hot DM reaches its maximum, as this will determine the scale below which structure formation is suppressed. During matter-domination, the scale factor's dependence on time is

$$a \propto t^{\frac{2}{3}}. \tag{4.41}$$

Then substituting equation (4.40) into (4.36), and using relation (4.41), we evaluate the co-moving free-streaming length's dependence on time whilst the DM is initially relativistic and once it has cooled to non-relativistic speeds:

$$\lambda_{\rm FS}/a \propto \begin{cases} \frac{1}{Ha} \propto t^{\frac{1}{3}}, & \text{relativistic} \\ \frac{1}{Ha^2} \propto t^{-\frac{1}{3}}. & \text{non-relativistic} \end{cases} \tag{4.42}$$

Therefore the maximum co-moving free-streaming length, or minimum wavenumber, is at the moment the DM transitions from being relativistic to non-relativistic [127, 128] at redshift $z_{\rm nr}$

evaluated in (4.38). By evaluating the average thermal velocity (4.37) at the non-relativistic transition, we obtain the following for the minimum free-streaming wavenumber [127, 128]:

$$(k_{\mathrm{FS,min}})^{-1} = \sqrt{\frac{2}{3}}\frac{350\ \mathrm{kms}^{-1}}{H_0\sqrt{\Omega_{\mathrm{m},0}}}(1+z_{\mathrm{nr}})^{\frac{1}{2}} g_{*s}(T\approx m_{\mathrm{DM}})^{-\frac{1}{3}}\left(\frac{1\ \mathrm{eV}}{m_{\mathrm{DM}}}\right)\left(\frac{\langle p\rangle}{3.15T}\right)_{T\approx m_{\mathrm{DM}}}. \quad (4.43)$$

Then substituting in equation (4.38) for z_{nr}, the maximum free streaming length of hot DM today is

$$\lambda_{\mathrm{FS},0} \equiv \frac{2\pi a_0}{k_{\mathrm{FS,min}}} \approx 1.39\times 10^3\ \mathrm{Mpc}\ g_{*s}(T\approx m_{\mathrm{DM}})^{-\frac{1}{6}}\left(\frac{1\ \mathrm{eV}}{m_{\mathrm{DM}}}\right)^{\frac{1}{2}}\left(\frac{\langle p\rangle}{3.15T}\right)^{\frac{1}{2}}_{T\approx m_{\mathrm{DM}}}, \quad (4.44)$$

where the scale factor today is $a_0 = 1$.

4.3.1.2 Warm DM

Thermal DM with masses of $O(\mathrm{keV})$ transition to non-relativistic speeds at a redshift much larger than the red-shift at matter-radiation equality,

$$z_{\mathrm{nr}} = O(10^6) \gg z_{\mathrm{eq}}, \quad (4.45)$$

during the radiation-dominated period. During the radiation-dominated period, the Hubble expansion rate is

$$H(t) = H_0\sqrt{\Omega_{\gamma,0}}(1+z)^2, \quad (4.46)$$

where $\Omega_{\gamma,0}$ is the relative energy density of radiation in the universe today. During radiation-domination, the scale factor's dependence on time is

$$a \propto t^{\frac{1}{2}}. \quad (4.47)$$

Then substituting equation (4.46) into (4.36), and using relation (4.47), we evaluate the co-moving free-streaming length's dependence on time whilst the DM is initially relativistic and once it has cooled to non-relativistic speeds:

$$\lambda_{\mathrm{FS}}/a \propto \begin{cases} \frac{1}{Ha} \propto t^{\frac{1}{2}}, & \text{relativistic} \\ \frac{1}{Ha^2} \propto \text{const.} & \text{non-relativistic} \end{cases} \quad (4.48)$$

Therefore whilst the DM is relativistic the co-moving free streaming length increases until the DM transitions to non-relativistic speeds, where it reaches its maximum value and maintains

a constant value there after. The minimum wavenumber is therefore given by [130]:

$$(k_{\rm FS,min})^{-1} = \sqrt{\frac{2}{3}}\frac{0.350\ {\rm kms}^{-1}}{H_0\sqrt{\Omega_{\gamma,0}}} g_{*s}(T \approx m_{\rm DM})^{-\frac{1}{3}} \left(\frac{1\ {\rm keV}}{m_{\rm DM}}\right)\left(\frac{\langle p\rangle}{3.15T}\right)_{T\approx m_{\rm DM}}, \tag{4.49}$$

which corresponds to the following maximum free-streaming length of warm DM today [130]:

$$\lambda_{\rm FS,0} \equiv \frac{2\pi a_0}{k_{\rm FS,min}} \approx 3.64\ {\rm Mpc}\ g_{*s}(T \approx m_{\rm DM})^{-\frac{1}{3}} \left(\frac{1\ {\rm keV}}{m_{\rm DM}}\right)\left(\frac{\langle p\rangle}{3.15T}\right)_{T\approx m_{\rm DM}}. \tag{4.50}$$

However, strictly speaking the better parameter for defining the scale that is affected by the free-streaming of warm dark matter is the free-streaming horizon, which is just the present day value of the particle horizon [130],

$$\lambda_{\rm FSH,0} = \int_0^{t_0} dt \frac{\langle v\rangle}{a}. \tag{4.51}$$

The free-streaming horizon is larger than the free-streaming length, as whilst $\lambda_{\rm FS,0}$ remains constant after the non-relativistic transition, $\lambda_{\rm FSH,0}$ continues to grow, typically by one order of magnitude [130]. The calculation of $\lambda_{\rm FSH,0}$ is more involved (see [130] for details), and so we use $\lambda_{\rm FS,0}$ in our analysis, which provides a weaker constraint on our warm DM models.

4.3.2 Lyman-α forest

The Lyman-α forest examines structure formation in the early universe by using light emitted from highly redshifted and luminous quasars [131–136]. As the photons travel through the universe, they are red-shifted with its expansion, and those with the Lyman-α transmission energy that come in contact with neutral hydrogen are absorbed, exciting an electron from its ground state to its first excited state. On returning to the ground state, the photon is scattered away from our line of sight, and so we observe a Lyman-α absorption line in the quasar's spectrum. The redshift of the line tells us the distance the photon is absorbed, thereby allowing us to map the distribution of neutral hydrogen in the universe.

In the early universe the neutral hydrogen clouds are large and diffuse, and so there are a larger number of absorption lines at high redshifts, as seen in Figure 4.6. Over time, the hydrogen clouds becomes smaller and denser until they eventually collapse under gravity to form stars and galaxies, and so we see fewer absorption lines at low redshifts [134, 135]. The broad peak at the far right of the spectrum in Figure 4.6 is the characteristic Lyman-α emission intrinsic to the quasar, therefore all the absorption lines at lower redshifts are due to intervening matter [133].

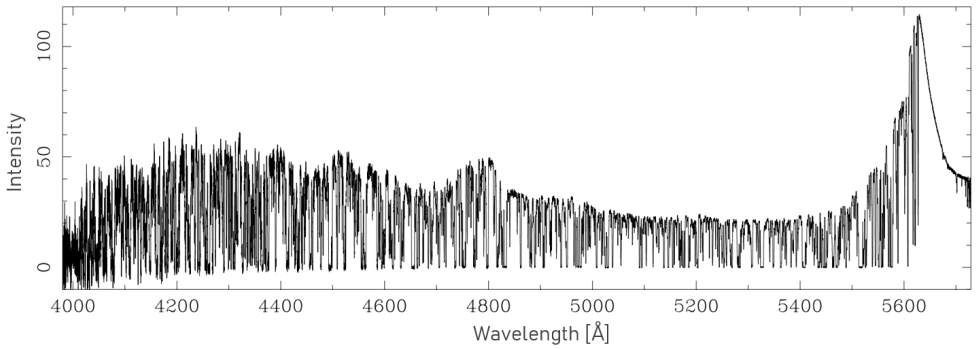

Figure 4.6: Lyman-α forest
Redshifted Lyman-α absorption lines in the spectra of quasar QSO 1422+23, taken from [134].

The Lyman-α forest is able to probe high redshifts ($z = 2 - 6$) that are undetectable by telescopes, making it a powerful tool for studying the matter power spectrum in the non-linear regime and thus constraining DM models [92, 93, 137, 138]. Hot DM is excluded as a viable DM candidate due to its large free-streaming length, calculated in (4.44), that would prevent the formation of MPc-scale structures [124, 139]. Although cold DM has been very successful in describing the large scale self-similar structure of the universe [41], testing the model in simulations of Milky Way sized galaxy formation revealed that it over-predicted the abundance of satellite galaxies [89, 90]. Small-scale structures may have been suppressed by reionization, which increased the pressure of the intergalactic medium at the time when the first stars and galaxies began to form [140–142]. Alternatively, the discrepancies may be resolved if our DM is warm, as their free-streaming suppresses the abundance of small-scale structures [91–93]. The Lyman-α spectra from the High Resolution Echelle Spectrometer (HIRES) [136] and the Sloan Digital Sky Survey (SDSS) [135] tightly constrains the free streaming length of warm DM, calculated in (4.50), to be within the bound [92, 102, 130, 138, 143, 144]:

$$\lambda_{\mathrm{FS},0} < \lambda_{\mathrm{FS},0}^{\mathrm{max}} = 0.1 \text{ Mpc}, \tag{4.52}$$

which translates to a lower mass bound for a given model. In Section 5.2.2 we will show that the Lyman-α constraint excludes a particular keV-scale sterile neutrino DM model (assuming the DM makes up the total observed abundance), where the DM is produced via non-resonant active neutrino mixing, known as the Dodelson-Widrow (DW) mechanism [29]. On the other hand, the DM model that we present in chapter 7 is within the Lyman-α constraint [43].

4.4 Summary and discussion

In this chapter we have shown that a dominant DM component is essential for large-scale structure formation [19, 20], reproducing the CMB's power spectrum [17, 18] and explaining

many gravitational effects, such as galactic rotational curves and gravitational lensing [14–16]. In order for our cosmological model to be consistent with these results, we introduce a sterile neutrino DM candidate in chapter 7 by minimally extending our inflationary potential with a modified νMSM. The model couples the inflaton field to three sterile neutrinos, and the lightest, N_1, is our DM candidate. We will now summarise the key results from this chapter that will allow us to constrain the parameter space of our model.

The analysis carried out on the freeze-in and freeze-out production mechanisms will be required to constrain the DM relic abundance and inflaton parameters of our model. Freeze-in DM has an initially negligible abundance and remains decoupled from the thermal bath, as its production rate is much smaller than the Hubble expansion rate. Their relic abundance is therefore proportional to their coupling strength. On the other hand, freeze-out DM has an initially thermal abundance, as in the early universe their production rate exceeds the Hubble expansion rate. Their relic abundance decreases with increasing coupling strength, as DM that is more strongly coupled remains in thermal equilibrium longer after departing from chemical equilibrium, when their yield is Boltzmann suppressed.

In our cosmological model, the sterile neutrino DM is produced via inflaton (χ) decay in the early universe. As the DM production rate, $\Gamma_{\rm prod}$, is far less than the Hubble expansion rate throughout the course of the universe's history, the DM is produced via the freeze-in mechanism, and so its abundance is governed by the following Boltzmann equation [118],

$$\frac{d(n_{\rm DM}a^3)}{dt} = 2\Gamma_{\rm prod} n_\chi a^3. \tag{4.53}$$

In section 4.2.2 we analysed the freeze-in production mechanism under the assumption that the decaying particle is in thermal equilibrium. In our model, however, only the lightest inflaton particles have thermalised prior to DM production, whilst the heaviest inflaton particles have a highly non-thermal infrared distribution. In section 7.4, we provide analytical approximations at the extremeties of our inflaton parameter space, and in section 7.5, we provide a detailed numerical analysis in which we solve the Boltzmann equations precisely across the entire inflaton parameter space. We then equate the known the relative energy density of DM today, $\Omega_{\rm c,0} = 0.265 \pm 0.007$ [33], with the relic abundance of our sterile neutrino DM,

$$\Omega_{\rm DM,0} = \frac{m_{\rm DM} Y_{{\rm DM},f} s_0}{\rho_{c,0}}, \tag{4.54}$$

in order to constrain the parameters of our model.

In section 8.4.2, we investigate whether an inflaton with a zero vacuum expectation value could be a possible source of WIMP (freeze-out) DM. However, using the following results for

the freeze-out abundance of relativistic particles,

$$\Omega_{\rm DM}h^2 = \frac{g_{*n}^{\rm DM}}{g_{*s}(T_f)}\frac{m_{\rm DM}}{13.4\ {\rm eV}}, \tag{4.55}$$

and non-relativistic particles,

$$\Omega_{\rm DM}h^2 \sim \frac{1.68\times10^{-10}\ {\rm GeV}^{-2}}{\langle\sigma_{\rm ann}\cdot v\rangle}\left(\frac{100}{g_*(T_f)}\right)^{\frac{1}{2}}\left(\frac{x_f}{20}\right), \tag{4.56}$$

we show that this situation is fully excluded, as it leads to overclosure of the universe.

The size of the smallest scale structures that can form in the universe is determined by how relativistic DM is on production. 'Hot' or 'warm' DM particles are produced with relativistic velocities, and become non-relativistic during the matter and radiation dominated periods respectively. The distance the particles travel at relativistic velocities defines their free-streaming length, during which they have enough kinetic energy to escape the gravitational wells of small over-dense regions. As a result, DM perturbations below the free-streaming length are damped, and we observed a suppression of small-scale structures in the universe. 'Cold' DM particles are produced with non-relativistic velocities, and so their free-streaming length is insignificant.

The Lyman-α forest is our most sensitive probe for measuring the smallest scale structures in the universe, and imposes the following bound on the maximum free-streaming length [92, 102, 130, 138, 143, 144],

$$\lambda_{\rm FS,0} < \lambda_{\rm FS,0}^{\rm max} = 0.1\ {\rm Mpc}. \tag{4.57}$$

The bound fully excludes hot DM as a viable candidate and tightly constrains warm DM models, which have a free-streaming length of

$$\lambda_{\rm FS,0} \equiv \frac{2\pi a_0}{k_{\rm FS,min}} \approx 3.64\ {\rm Mpc}\ g_{*s}(T\approx m_{\rm DM})^{-\frac{1}{3}}\left(\frac{1\ {\rm keV}}{m_{\rm DM}}\right)\left(\frac{\langle p\rangle}{3.15T}\right)_{T\approx m_{\rm DM}}. \tag{4.58}$$

Whilst cold DM models are unconstrained by the Lyman-α bound, model simulations suggest that they may over-predict the abundance of small-scale structures [89, 90].

Chapter 5

Neutrinos

Since the observation of neutrino oscillations we have known that the massless SM neutrino sector is incomplete. In this chapter we will study a possible solution: we extend the SM neutrino sector by the Neutrino Minimal Standard Model (νMSM) with three right-handed singlet neutrinos, which generate the SM neutrino masses via the 'see-saw' mechanism. Moreover, the lightest right-handed neutrino is an ideal dark matter candidate, and two heavier right-handed neutrinos are able to generate the observed BAU via leptogensis. Here, we aim to provide the reader with the background theory and astrophysical bounds of the SM neutrino sector and the νMSM, which will be implemented in a modified νMSM that extends our light inflaton model in chapter 7. Section 5.1 outlines the SM neutrino sector, νMSM and the generation of SM neutrino masses. Section 5.2 analyses non-resonant and resonant DM production mechanisms, and the astrophysical constraints that tightly bound the DM parameter space. In section 5.3 we study various mechanisms for leptogenesis in νMSM, and how EW sphaleron processes convert LA to BA. We then bound the parameter space of the two heavier right-handed neutrinos by requiring they generate the total BAU.

5.1 Neutrinos in the Standard Model and beyond

5.1.1 Neutrinos in the Standard Model

Neutrinos are spin$-1/2$ fermions that are singlets of the spontaneously broken SM gauge symmetry $SU(2)_L \bigotimes U(1)_Y \xrightarrow{\text{SSB}} U(1)_{\text{EM}}$. The SM has three flavours of neutrino (electron, muon and tau), which is consistent with the primordial elemental abundances at Big Bang Nucleosynthesis [55, 145] and collider experiments [146]. We only observe left-handed neutrinos, which form part of the left-handed lepton douplet:

$$L_{Ll} = \begin{pmatrix} \nu_l \\ l \end{pmatrix}_L , \tag{5.1}$$

where $l = e, \mu, \tau$.

Masses are included in the SM through Yukawa interactions, which couple fermion states of opposite helicities, $f_{L/R}$, to the SM Higgs doublet, Φ,

$$-\mathcal{L}_f = g_f \left(\bar{f}_L f_R + \bar{f}_R f_L\right) \Phi. \tag{5.2}$$

Dirac mass terms that couple left- and right-handed fermions are then generated post EW symmetry breaking, $\Phi \to \langle\Phi\rangle + \frac{\phi}{\sqrt{2}}$,

$$-\mathcal{L}_f = \frac{g_f}{\sqrt{2}} \left(\bar{f}_L f_R + \bar{f}_R f_L\right) \phi + m_f \left(\bar{f}_L f_R + \bar{f}_R f_L\right), \tag{5.3}$$

where ϕ is the SM Higgs boson, the fermion mass is

$$m_f = \frac{g_f v}{\sqrt{2}}, \tag{5.4}$$

and the SM Higgs vacuum expectation value (VEV) is $v \equiv \sqrt{2}\langle\Phi\rangle = 246$ GeV [147]. Since we don't observe right-handed neutrinos, the SM predicts left-handed neutrinos to be massless particles. Additionally, neutrino masses cannot be generated via loop-level processes since they violate lepton number and $B - L$ conservation. The neutrinos are therefore precisely massless if they are to obey all SM symmetries. The neutrinos only interact via weak charged currents (CC) and neutral currents (NC). The corresponding Lagrangian densities are

$$\begin{aligned} -\mathcal{L}_{\text{CC}} &= \frac{g}{\sqrt{2}} \sum_l \bar{\nu}_{Ll} \gamma^\mu l_L^- W_\mu^+ \; + \; l_L^+ \gamma^\mu \nu_{Ll} W_\mu^-, \\ -\mathcal{L}_{\text{NC}} &= \frac{g}{2\cos\theta_W} \sum_l \bar{\nu}_{Ll} \gamma^\mu \nu_{Ll} Z_\mu^0. \end{aligned} \tag{5.5}$$

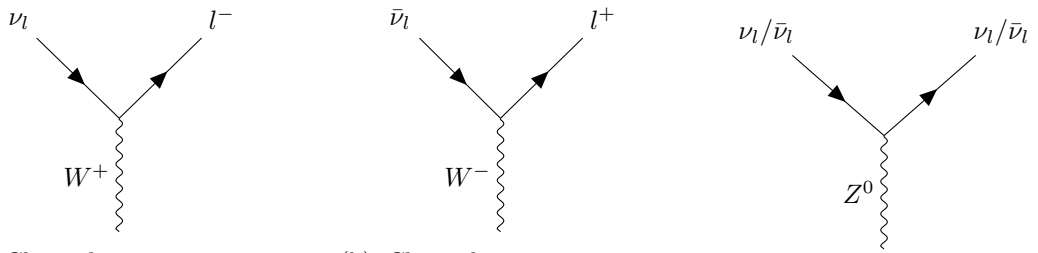

(a) Charged current interaction

(b) Charged current interaction

(c) Neutral current interaction

Figure 5.1: Neutrino interactions

5.1.2 Neutrino oscillations

The Homestake mine experiment was the first experiment to detect the electron neutrinos created by thermonuclear reactions in the Sun [148], referred to as solar neutrinos, and notice a discrepancy between the flux observed and the Standard Solar Model (SSM) theoretical

prediction [149]. Referred to as the solar neutrino problem, the experiment measured only a third of the expected flux. It was then theorised that if the SM neutrinos had mass they'd be able change flavour (or 'oscillate') [150–152]. This was later confirmed by the Sudbury Neutrino Observatory experiment that measured the total neutrino flux to be consistent with SSM, whilst the flux of individual neutrino flavours were not [12, 13].

Neutrinos produced via weak interactions in a given flavour eigenstate, $|\nu_\alpha\rangle$ ($\alpha = e, \mu, \tau$), propagate in a mass eigenstate, $|\nu_i\rangle$ ($i = 1, 2, 3$), which on detection, then collapse back into a flavour eigenstate. The linear composition of mass states that make up a given flavour state is determined by the PMNS matrix [153], U,

$$|\nu_\alpha\rangle = \sum_{i=1}^{3} U_{\alpha i} |\nu_i\rangle, \tag{5.6}$$

that diagonalises the neutrino mass matrix,

$$m_{ij}\delta_{ij} = \sum_{\alpha,\beta=e,\mu,\tau} (U^T)_{i\alpha} m_{\alpha\beta} U_{\beta j}, \tag{5.7}$$

where m_{ij} is the mass matrix of the neutrino mass eignestates. The PMNS matrix is given by

$$U = \begin{pmatrix} U_{e1} & U_{e2} & U_{e3} \\ U_{\mu 1} & U_{\mu 2} & U_{\mu 3} \\ U_{\tau 1} & U_{\tau 2} & U_{\tau 3} \end{pmatrix}, \tag{5.8}$$

$$= \begin{pmatrix} 1 & 0 & 0 \\ 0 & c_{L23} & s_{L23} \\ 0 & -s_{L23} & c_{L23} \end{pmatrix} \cdot \begin{pmatrix} c_{L13} & 0 & s_{L13} e^{-i\delta_L} \\ 0 & 1 & 0 \\ -s_{L13} e^{i\delta_L} & 0 & c_{L13} \end{pmatrix} \cdot \begin{pmatrix} c_{L21} & s_{L12} & 0 \\ -s_{L12} & c_{L12} & 0 \\ 0 & 0 & 1 \end{pmatrix} \cdot \begin{pmatrix} e^{i\alpha_1} & 0 & 0 \\ 0 & e^{i\alpha_2} & 0 \\ 0 & 0 & 1 \end{pmatrix}. \tag{5.9}$$

If neutrinos are Dirac particles, the PMNS matrix has 4 independent parameters: 3 mixing angles ($c_{Lij} \equiv \cos\theta_{Lij}$ and $s_{Lij} \equiv \sin\theta_{Lij}$), and 1 charge-parity violating phase, δ_L. If the neutrinos are Majorana particles, there are an additional 2 phases, $\alpha_{1,2}$; we will discuss Majorana neutrinos in the last part of this section.

The probability of a neutrino oscillating from flavour α to β in time t is

$$P_{\alpha\beta} = |\langle \nu_\beta | \nu_\alpha(t) \rangle|^2 = \Big| \sum_{i=1}^{3} \sum_{j=1}^{3} U_{\alpha i} U^*_{\beta j} \langle \nu_j | \nu_i(t) \rangle \Big|^2. \tag{5.10}$$

The quantum mechanical propagation from time $t = 0$ to some time t when the state is

measured, is given by

$$|\nu_i(t)\rangle = e^{-iq\cdot x}|\nu_i(0)\rangle, \tag{5.11}$$

where

$$\begin{aligned} q\cdot x &= Et - \mathbf{p}\cdot\mathbf{x}, \\ &= L\sqrt{p^2+m_i^2} - pL, \\ &\sim \frac{m_i^2 L}{2E}; \end{aligned} \tag{5.12}$$

as the neutrinos are relativistic, $p_i \gg m_i$, we take the approximation $p_i \sim E_i$, and L is the distance travelled by the neutrino in time t. The probability amplitude of $\nu_\alpha \to \nu_\beta$ is then given by

$$\begin{aligned} P_{\alpha\beta} &= \sum_{i=1}^{3}|U_{\alpha i}|^2|U_{\beta i}|^2 + \sum_{i=1}^{3}\sum_{j=1}^{3}U_{\alpha i}U_{\beta i}^*U_{\alpha j}^*U_{\beta j}e^{-2iX_{ij}}, \\ &= \delta_{\alpha\beta} - 4\sum_{i<j}^{3}\mathrm{Re}\left[U_{\alpha i}^*U_{\beta i}U_{\alpha j}U_{\beta j}^*\right]\sin^2 X_{ij} + 2\sum_{i<j}^{3}\mathrm{Im}\left[U_{\alpha i}^*U_{\beta i}U_{\alpha j}U_{\beta j}^*\right]\sin 2X_{ij}, \end{aligned} \tag{5.13}$$

where we have used the orthogonality of mass eigenstates, $\langle\nu_j|\nu_i\rangle = \delta_{ij}$, and define [39]

$$X_{ij} = \frac{\Delta m_{ij}^2 L}{4E} = 1.27\frac{\Delta m_{ij}^2\,[\mathrm{eV}^2]\,L\,[\mathrm{km}]}{E\,[\mathrm{GeV}]}, \tag{5.14}$$

with $\Delta m_{ij}^2 \equiv m_i^2 - m_j^2$. The rate of neutrino oscillations is therefore proportional to the squared mass splitting and the probability amplitude is proportional to the neutrino mixing angles. The largest disappearance of α neutrinos occurs when $X_{ij} = \frac{\pi}{2}$, which for a given mass splitting and distance travelled, is when the neutrinos have energy

$$E = 0.81\Delta m_{ij}^2 L. \tag{5.15}$$

As we can only determine the magnitude of Δm_{32}^2, we define a 'normal' hierarchy (NH) with mass orderings $m_1 < m_2 < m_3$, and 'inverted' hierarchy (IH) with mass orderings $m_3 < m_1 < m_2$. The active neutrino mass splittings are [39]

$$\Delta m_{21}^2 \equiv \Delta m_{\mathrm{sol}}^2 = (7.53 \pm 0.18)\times 10^{-5}\ \mathrm{eV}^2, \tag{5.16}$$

$$\Delta m_{32}^2 \equiv \Delta m_{\mathrm{atm}}^2 = \begin{cases} (2.453 \pm 0.033)\times 10^{-3}\ \mathrm{eV}^2, & \text{(NH)} \\ (-2.536 \pm 0.034)\times 10^{-3}\ \mathrm{eV}^2. & \text{(IH)} \end{cases} \tag{5.17}$$

Neutrinos produced from different sources have varying energies and travel different distances

to the point of their detection, and so the measurement of their flux is sensitive to different neutrino mass splittings, as shown by equation (5.15). Solar neutrinos have $E \sim 1$ MeV and travel $L \sim O(10^{10})$ km to reach Earth, and so their flux is sensitive to the measurement of Δm^2_{21}, which is otherwise referred to as the solar mass splitting $\left(\Delta m^2_{\text{sol}}\right)$. Although the probability amplitude of neutrino oscillations is only sensitive to the magnitude of Δm^2_{ij}, the matter effects, otherwise known as the Mikheyev–Smirnov–Wolfenstein (MSW) effect[1] [151, 152], caused by solar neutrino interactions within the electron-dense Sun, induce sensitivity to the sign of Δm^2_{21}. On the other hand, atmospheric neutrinos produced by pion and kaon decays have $E \sim \left(0.1 - 10^2\right)$ GeV and travel $L = O\left(10 - 10^4\right)$ km to reach Earth, and so their flux is sensitive to Δm^2_{32}, which is otherwise referred to as the atmospheric mass splitting $\left(\Delta m^2_{\text{atm}}\right)$. Additionally, neutrinos produced from reactor and accelerator experiments with short and long baselines can access a wide range of Δm^2_{ij} and θ_{ij}. The active neutrino mixing angles are [39]

$$\sin^2\theta_{12} = 0.307 \pm 0.013, \tag{5.18}$$

$$\sin^2\theta_{23} = \begin{cases} 0.546 \pm 0.021, & \text{(NH)} \\ 0.539 \pm 0.022, & \text{(IH)} \end{cases} \tag{5.19}$$

$$\sin^2\theta_{13} = (2.20 \pm 0.07) \times 10^{-2}. \tag{5.20}$$

As we explained earlier in this section, Dirac neutrino masses cannot be generated via the Higgs mechanism due to the absence of right-handed neutrinos. However, if neutrinos and anti-neutrinos are the same particle, neutrino masses may be incorporated into the SM via a Majorana mass term [155],

$$-\mathcal{L}_M = \frac{m_M}{2}\left(\overline{\nu_L^C}\nu_L + \overline{\nu_L}\nu_L^C\right), \tag{5.21}$$

where superscript C denotes charge conjugation of the field. The observation of neutrinoless double-beta decay would provide confirmation that neutrinos are Majorana particles [**2019Beta**, 156]. Whilst Dirac neutrinos and anti-neutrinos are distinct, with equal and opposite quantum numbers (lepton number $L = \pm 1$, weak isospin $I_3 = \pm 1/2$ and weak hypercharge $Y = \mp 1$), Majorana particles and antiparticles are indistinguishable, and so they have the same quantum numbers. As a result, the Majorana neutrino mass term violates lepton number by $\Delta L = \pm 2$, weak isospin by $\Delta I_3 = 1$ and weak hypercharge $\Delta Y = -2$. To form a Majorana mass term that is gauge invariant, we require new physics beyond the SM, i.e. coupling the neutrinos to a Higgs field with $I_3 = -1$ and $Y = +2$ [157].

[1] The interaction between electron neutrinos and the high density of electrons in the Sun increases the electron neutrino's effective mass relative to their mass in a vacuum. As a result, their effective mixing angle is different to their vacuum mixing angle, and depends on the sign of Δm^2_{21} [154].

As we have not obtained any observational evidence of Majorana neutrinos, in the following section we consider an alternative way to generate Dirac SM neutrino masses through the addition of right-handed singlet neutrinos [53, 54]. As the right-handed neutrinos have no charge, a Majorana mass term can be added without violating local gauge symmetries. The term does still, however, violate lepton number conservation. The SM neutrino masses can then be generated via the 'see-saw' mechanism [158, 159]. This model can also solve other problems within the SM by providing a viable DM candidate [160, 161], and a mechanism for leptogenesis [11, 104, 162–166] that can generate the BAU.

5.1.3 The Neutrino Minimal Standard Model

The Neutrino Minimal Standard Model (νMSM) [53, 54] aims to explain the origin of the SM neutrino masses through the addition of right-handed singlet neutrinos, N_I ($I = 1, \mathcal{N}$). It is common to refer to SM neutrinos as 'active' neutrinos, as they interact via the weak force, and right-handed neutrinos as 'sterile' neutrinos, as they are decoupled from the weak force. This is considered to be a rather natural extension since the SM neutrino is the only fermion which does not have a right-handed component. The most general renormalizable Lagrangian is:

$$L_{\nu\text{MSM}} = \overline{N}_I i\partial_\nu \gamma^\nu N_I - F_{\alpha I}\overline{L}_\alpha N_I \Phi - \frac{1}{2}(M_M)_I \overline{N}_I^C N_I + h.c.. \tag{5.22}$$

The left-handed lepton doublet and right-handed sterile neutrino is coupled to the SM Higgs doublet, Φ, by a Yukawa coupling that generates the Dirac mass, $(m_D)_{\alpha I} = F_{\alpha I}\langle\Phi\rangle$, post EW symmetry breaking; M_M is the Majorana mass of the sterile neutrinos. In the limit $m_D \ll M_M$, we perform a block diagonalization of the total $(3+\mathcal{N}) \times (3+\mathcal{N})$ neutrino mass matrix,

$$\begin{pmatrix} \mathbb{0}_{\alpha\beta} & (m_D)_{\alpha J} \\ (m_D^{\mathrm{T}})_{I\beta} & (M_M)_I \delta_{IJ} \end{pmatrix} \rightarrow \begin{pmatrix} m_{\alpha\beta} & \mathbb{0}_{\alpha J} \\ \mathbb{0}_{I\beta} & M_{IJ} \end{pmatrix}, \tag{5.23}$$

from which we obtain the 3×3 Majorana mass matrix for the active neutrinos [167],

$$m_{\alpha\beta} = -\sum_{I=1}^{N} \frac{(m_D)_{\alpha I}\left(m_D^T\right)_{I\beta}}{(M_M)_I}. \tag{5.24}$$

As larger Majorana neutrino masses generate lighter active neutrino masses, the mechanism is called the 'see-saw' mechanism [158, 159]. Up to first order in m_D/M_M, the sterile neutrino mass matrix is $M_{IJ} = (M_M)_{IJ}\delta_{IJ}$. To simplify our notation going forward, we will just use

M_I for sterile neutrino mass and Majorana mass. The active-sterile neutrino mixing angle is

$$\theta_{\alpha I} = \frac{(m_D)_{\alpha I}}{M_I}, \tag{5.25}$$

and the total interaction strength between a sterile neutrino and all active neutrino species is

$$\theta_I^2 \equiv \sum_{\alpha=e,\mu,\tau} |\theta_{\alpha I}|^2. \tag{5.26}$$

One sterile neutrino with a non-zero mixing angle is required to generate each non-zero active neutrino mass. The minimal νMSM therefore requires the addition of only 2 sterile neutrinos to account for the 2 observed neutrino mass splittings, assuming the lightest neutrino is massless. If we require all three neutrinos to have mass, we need at least 3 sterile neutrinos [168]. Next we will consider the situation where the lightest sterile neutrino is dark matter. In this case, the mixing angle of the DM sterile neutrino is too small to contribute sufficiently to the active neutrino masses and leptogenesis, and so an additional 2 heavier sterile neutrinos are required [53, 54]. Moreover, since there are are 3 fermionic generations in the SM, an additional 3 sterile neutrinos appears to be a natural choice.

5.2 Sterile neutrino dark matter

We will first investigate whether active neutrinos are a plausible WIMP dark matter candidate. In section 2.4, we showed that active neutrinos decouple from the SM whilst they are still relativistic, at $T_{\nu,f} = 2-3$ MeV. We can then evaluate their present energy density using equation (4.12):

$$\Omega_\nu h^2 = \frac{g^\nu_{*n}}{g_{*s}(T_f)} \frac{\sum m_\nu}{13.4 \text{ eV}} = \frac{\sum m_\nu}{96 \text{ eV}}; \tag{5.27}$$

where $g^\nu_{*n} = \frac{3}{4} \times 2 = \frac{3}{2}$ and $g_{*s}(T_{\nu,f}) = 10.75$ are evaluated using equations (2.36) and (2.39) respectively. If we require the SM neutrino energy density to make-up the total DM abundance, the neutrinos need to have a mass of $m_\nu \sim O(10)$ eV. Given that neutrinos have a thermal distribution, $\langle p \rangle / T_\nu = 3.15$, we use equation (4.50) to evaluate their free-streaming length:

$$\begin{aligned} \lambda_{\text{FS}} &\approx 3.64 \text{ Mpc } g_{*s}(T \approx 10 \text{ eV})^{-\frac{1}{3}} \times 10^2 \left(\frac{10 \text{ eV}}{m_\nu}\right) \left(\frac{T_\nu}{T}\right)_{T \approx 10 \text{ eV}}, \\ &\sim 1.65 \times 10^2 \text{ Mpc } \left(\frac{10 \text{ eV}}{m_\nu}\right), \end{aligned} \tag{5.28}$$

where $g_{*s}(T \approx 10 \text{ eV}) = 3.91$, and $T_\nu/T = (4/11)^{\frac{1}{3}}$ at $T \approx 10$ eV. The SM neutrino free-streaming length greatly exceeds the Lyman-α bound on the maximum free streaming length given in (4.52) and so they are too hot to account for the small scale structures in the universe.

We therefore conclude that they are not a viable DM candidate.

On the other hand, sterile neutrinos are heavier than active neutrinos and can be produced non-thermally; the lightest and therefore the most stable sterile neutrino (N_1) is an ideal dark matter candidate if it is sufficiently long-lived [160, 161]. Sterile neutrinos can decay through active-sterile mixing into three active neutrinos via a neutral current, $N \to \nu_\alpha \nu_\beta \overline{\nu}_\beta$, and radiatively via $N \to \nu\gamma$, emitting a photon with energy $E_\gamma \sim M_I/2$ [169], as shown in Figure 5.2.

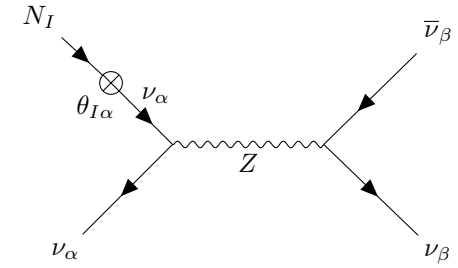

(a) Sterile neutrino decay via active-sterile mixing into three active neutrinos via a neutral current.

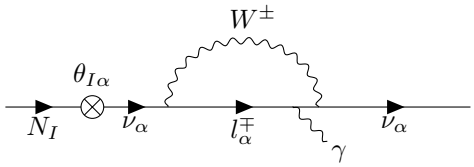

(b) Sterile neutrino decay via active-sterile mixing into an active neutrino and photon via a charged current.

Figure 5.2: Sterile neutrino decay channels

The dominant sterile neutrino decay channel, $N \to \nu_\alpha \nu_\beta \overline{\nu}_\beta$, constrains the maximum DM interaction strength in equation (5.26) [106, 170],

$$\theta_1^2 < \theta_{1,\max}^2 = 3.4 \times 10^{-4} \left(\frac{10 \text{ keV}}{M_I} \right)^4, \tag{5.29}$$

by the requirement that N_1's lifetime exceeds the age of the universe. However, we will later show that the absence of x-rays observed from radiatively decaying sterile neutrinos imposes a more stringent constraint on the DM active-sterile neutrino mixing angle [171]. Additionally, the sterile neutrino DM is tightly constrained by two other independent astrophysical bounds: its maximum phase space density [172] and the Lyman-α maximum free-streaming length [102].

Next we study resonant and non-resonant production of DM sterile neutrinos via active-sterile neutrino oscillations, and show that x-ray, Lyman-α and phase space density bounds tightly constrain their parameter space. In chapter 7 I present an alternative model that evades these constraints, in which DM sterile neutrinos are produced via inflaton decay in the early universe.

5.2.1 Dark matter production

In the νMSM, the active-sterile neutrino Yukawa coupling gives rise to DM sterile neutrino production. Below the EW scale, production is via active-sterile neutrino oscillations with a rate approximately given by [168, 173]

$$\Gamma_N \sim \Gamma_\nu \theta^2_{M_1}, \tag{5.30}$$

where the rate of active neutrino production is $\Gamma_\nu \sim G_F^2 T^5$, and $\theta^2_{M_1}$ is the modified active-sterile mixing angle for particles travelling through a medium of finite temperature and density [168, 173],

$$\theta^2_{M_1}(T) \simeq \frac{\theta_1^2}{\left(1 + \frac{2p}{M_1^2}\left(b\left(p,T\right) \pm c\left(T\right)\right)\right)^2 + \theta_1^2}, \tag{5.31}$$

where p is the momentum of the DM sterile neutrino. In a vacuum the active-sterile neutrino mixing angle, θ_1, is suppressed due to their large difference in mass. However, by the MSW effect [174, 175], active neutrinos propagating through a medium acquire an effective mass due to their weak interactions with the plasma, whilst sterile neutrinos do not, thereby decreasing their effective mass difference. As a result, the active-sterile neutrino mixing angle in a medium is enhanced relative to the active-sterile neutrino mixing angle in a vacuum. The function $b(p,T)$ accounts for the MSW effects induced by the active neutrinos' weak interactions with the thermal plasma. The main contributions are from gauge boson resonances in $\nu\overline{\nu}$, $\nu_e e^-$, $\overline{\nu}_e e^+$ scatterings [168, 174],

$$b(p,T) = \frac{16 G_{\rm F}^2}{\pi \alpha_{\rm W}} p \left(2 + \cos^2\theta_{\rm W}\right) \frac{7\pi^2 T^4}{360}, \tag{5.32}$$

where $\theta_{\rm W}$ is the Weinberg angle, $G_{\rm F}$ is the Fermi constant and $\alpha_{\rm W}$ is the weak coupling constant. The term $b(p,T)$ dominates over $c(p,T)$ in a CP-symmetric plasma. The function $c(T)$ accounts for the lepton-number driven MSW effect that is present if the plasma is CP-asymmetric [30, 168],

$$c(T) = 3\sqrt{2} G_F \left(1 + \sin^2\theta_W\right)\left(n_{\nu_e} - \overline{n}_{\nu_e}\right), \tag{5.33}$$

where $n_{\nu_e}(\overline{n}_{\nu_e})$ is the number density of background (anti-)electron-neutrinos. In equation (5.31) $c(T)$ contributes with an opposite sign for N_1 mixing with active neutrinos and anti-neutrinos [168].

Next, we will consider regions of the sterile neutrino parameter space where $\theta^2_{M_1} \ll O(1)$ and $\theta^2_{M_1} \sim O(1)$, which give rise to non-resonant and resonant production respectively. These cases

will be analysed separately, since the sterile neutrinos have different momentum distributions. We will then constrain the DM sterile neutrino parameter space using various astrophysical bounds in section 5.2.2.

Non-resonant production

DM sterile neutrinos are non-resonantly produced (NRP) when their active-sterile neutrino mixing angle is $\theta_{M_1} \ll O(1)$, which is known as the Dodelson-Widrow (DW) mechanism [29] . This physically corresponds to when the CP-asymmetry in the plasma is small, in which case the function $b(p,T)$ dominates over $c(T)$ in (5.31). Their momentum distribution function is well approximated by that of the active neutrino, a relativistic thermal Fermi-Dirac distribution, suppressed by a factor χ,

$$f_{N_1} \simeq \frac{g_N}{(2\pi)^3} \frac{\chi}{e^{\frac{p}{T_\nu}} + 1}. \tag{5.34}$$

The number of internal degrees of freedom of N_1 is $g_N = 2$, the active neutrino temperature is T_ν, and the suppression factor is approximately $\chi \sim \theta_1^2$. With a more careful analysis, we find that the momentum distribution is actually slightly shifted towards the infrared relative to the thermal distribution with $\langle p \rangle = 3.15T$. The sterile neutrinos are therefore slightly cooler, with an average momentum of [29, 143]

$$\left(\frac{\langle p \rangle}{3.15T} \right)_{T \approx \text{keV}} = 0.8 - 0.9. \tag{5.35}$$

NRP sterile neutrinos with a mass of $O(\text{keV})$ are classified as warm DM candidates, which may well be favoured over cold DM for structure formation [176, 177]. Their production temperature, defined when the production rate (5.30) has reached a maximum, is [29]

$$T_{\text{prod}} \simeq 133 \left(\frac{M}{\text{keV}} \right)^{\frac{1}{3}} \text{MeV}. \tag{5.36}$$

As $\Gamma_N(T_{\text{prod}}) \ll H(T_{\text{prod}})$, the DM sterile neutrinos remain out of thermal equilibrium.

Resonant production

The resonant production (RP) of DM sterile neutrinos, known as the Shi-Fuller mechanism [30], occurs when the effective mass of the active neutrino is approximately equal to the mass of the sterile neutrino, which corresponds to when [168]

$$1 + \frac{2p}{M_1^2} \left(b\left(p,T\right) \pm c\left(T\right) \right) = 0. \tag{5.37}$$

For the functions $b(p,T)$ and $c(p,T)$ to cancel, we require the LA of the plasma to be large. When equation (5.37) is satisfied, the effective active-sterile neutrino mixing angle, given by equation (5.31), is $\theta_{M_1} \sim 1$, and thus we generate the maximum abundance of RP sterile neutrino DM for a given LA [168, 178]:

$$Y_{1,\max} \sim Y_L, \tag{5.38}$$

where $Y_1 \equiv n_1/s$ and Y_L is the LA defined in equation (2.49). The maximal amount of LA generated by the thermally-decoupled decay of heavy sterile neutrinos ($N_{2,3}$) is [178, 179]

$$\Delta_{L,\max} = \frac{4}{(9\times 2)+4} = \frac{2}{11}, \tag{5.39}$$

where 4 is the total number of spin states of $N_{2,3}$ and 9 is the number of spin states of 3 leptonic generations. In equation (5.39) we have used the LA paramerization defined in equation (2.48), which corresponds to

$$Y_{L,\max} \sim 7\times 10^{-4}. \tag{5.40}$$

The RP sterile neutrinos populate a highly non-thermal, infra-red momentum distribution, with an average momentum of [30, 143]

$$\left(\frac{\langle p\rangle}{3.15T}\right)_{T\approx \mathrm{keV}} \approx 0.6, \tag{5.41}$$

RP sterile neutrinos are therefore colder than NRP sterile neutrinos, but with a mass of $O(\mathrm{keV})$, they are also classified as warm DM candidates. Their maximum abundance is constrained by the observed DM abundance [168, 178],

$$Y_1 \leq Y_{\mathrm{DM}} \sim 10^{-6}\left(\frac{\mathrm{keV}}{M_1}\right), \tag{5.42}$$

therefore resonant effects do not significantly contribute to the DM abundance if $Y_L < O(10^{-6})$ for keV sterile neutrinos. For resonant effects to significantly contribute to the production of DM, we require lepton flavour asymmetries that greatly exceed[2] the BAU, $Y_B = O(10^{-10})$. The majority of the LA must therefore be generated after the EW phase transition, once sphalerons are frozen-out, in order to prevent the overproduction of BA [30].

[2]The total LA may be of the order of the BAU if there is a cancellation between different neutrino species.

5.2.2 Astrophysical dark matter constraints

Next we evaluate two independent astrophysical bounds: the phase space density and x-ray bounds, which we then apply to RP and NRP sterile neutrino models. We show that with the addition of the Lyman-α bound, their parameter space is strongly constrained.

Phase space density bound

DM particles have a maximum allowed phase-space density (PSD) that can be constrained either by Liouville's theorem or the Pauli Exclusion Principle (PEP), if the DM is fermionic. Using a DM-dominated object with a known density and velocity dispersion, such as dwarf spheroidal galaxies (dSphs), we can then obtain a lower mass bound of the DM particle, which is defined when the PSD of the object corresponds to the maximum PSD of the DM particle [180].

By PEP, the PSD of fermionic DM can not exceed that of a degenerate Fermi gas. The maximum number of fermionic DM particles allowed within a sphere of momentum-space of radius k_F is

$$N = \frac{g \cdot \frac{4}{3}\pi k_F^3}{\left(\frac{2\pi}{L}\right)^3}, \tag{5.43}$$

where g is the number of internal degrees of freedom of the DM particle and L is a unit of length. The Fermi vector, k_F, is then given by

$$k_{\rm F} = \left(\frac{6\pi^2\rho(r)}{gm}\right)^{\frac{1}{3}}, \tag{5.44}$$

where m is the mass of the DM particle, and $\overline{\rho} \equiv mN/L^3$ is the average mass density. For the DM particles to be gravitationally bound within a spherical object, the Fermi velocity [172, 180],

$$v_{\rm F} \equiv \frac{\hbar k_F}{m} = \hbar\left(\frac{6\pi^2\rho(r)}{gm^4}\right)^{\frac{1}{3}}, \tag{5.45}$$

must be less than the escape velocity of the object [172],

$$v_\infty(r) = \left(8\pi G\int_r^{r_{\rm max}}\frac{dx}{x^2}\int_0^x \rho(y)y^2dy + \frac{2GM(<r_{\rm max})}{r_{\rm max}}\right)^{\frac{1}{2}}. \tag{5.46}$$

$r_{\rm max}$ is some cut-off scale in the density profile of the object and $M(<r_{\rm max})$ is the mass contained within $r_{\rm max}$. As a result, the following lower mass bound of a DM particle is obtained

from the dSh Leo II data at the 95% C.L. [172],

$$M_1 \geq M_{\rm PEP} = \left(\frac{6\pi^2\hbar^3\rho(r)}{g v_\infty(r)^3}\right)^{\frac{1}{4}} = 0.13 \text{ keV}. \tag{5.47}$$

The Leo II dSph was used in [172] to obtain all the DM mass bounds since its data provided the strongest constraint of all the dSphs.

For specific DM models, such as RP and NRP sterile neutrinos, for which we know the primordial DM (fine-grained) distribution function, we are able to obtain a more stringent mass bound using Liouville's theorem, which states "the phase-space distribution function does not change in the course of dissipationless, collisionless dynamics" [180]. The maximum of the fine-grained primordial distribution, $f_{\rm max}$, therefore remains constant as the system evolves. Physical measurements, however, can only probe the course-grained distribution of the dSph, $F \equiv {\rm d}\rho/{\rm d}^3v$, i.e. the phase-space density averaged over some region of momentum space [172]. The course-grained distribution is related to the fine-grained distribution, $f \equiv dn/{\rm d}^3p$, by

$$F = m^4 \frac{{\rm d}\left(\rho/m\right)}{{\rm d}^3\left(mv\right)} = m^4 f. \tag{5.48}$$

Using Liouville's theorem, we are then required to satisfy the following inequality [172, 180],

$$\overline{F}_{\rm max} \leq m^4 f_{\rm max}, \tag{5.49}$$

which translates into a lower mass bound of the DM particle. This was originally evaluated by Tremaine and Gunn (TG) [181], however we will refer to a modified version from [172], which assumes the DM halo has a multivariate Gaussian velocity distribution:

$$\overline{F}_{\rm max} = \frac{\rho(r)}{(2\pi)^{\frac{3}{2}}\sigma_r(r)\sigma_t^2(r)}, \tag{5.50}$$

where σ_r and σ_t are the radial and tangential velocity dispersions respectively. The maximum of the Fermi-Dirac distribution function for relativistic and thermal fermions is

$$f_{\rm max,FD} = \frac{g}{2(2\pi\hbar)^3}. \tag{5.51}$$

NRP sterile neutrinos have a distribution function that is well-approximated by (5.34), the Fermi-Dirac distribution normalised by $\chi \sim \theta_1^2$, and so its maximum is [172, 180]:

$$f_{\rm max,NRP} \sim \chi f_{\rm max,FD} = \frac{g\chi}{2(2\pi\hbar)^3}. \tag{5.52}$$

Then equating the abundance of NRP sterile neutrinos with the total DM abundance [182],

$$\omega_{\rm DM} \equiv \Omega_{\rm DM} h^2 = g\chi \frac{M_{\rm NRP}}{94 \text{ eV}}, \tag{5.53}$$

allows us to re-express equation (5.52) as [172, 180]

$$f_{\rm max,NRP} \sim \frac{\omega_{\rm DM}}{2(2\pi)^3} \frac{94 \text{ eV}}{M_{\rm NRP}}, \tag{5.54}$$

where $\omega_{\rm DM} \simeq 0.12$. Equating equations (5.50) and (5.54) using Liouville's theorem, given by equation (5.49), the lower mass bound for NRP sterile neutrino at the 95% C.L. is [172]

$$M_1 \geq M_{\rm NRP} = 1.74 \text{ keV}. \tag{5.55}$$

The distribution function of RP sterile neutrinos is highly non-thermal and dependent on the LA. A detailed numerical analysis is therefore necessary to obtain the lower mass bound as a function of the mixing angle; the results from [172] are shown in Figure 5.3 below. Across the full parameter space of RP sterile neutrinos, we require [180]

$$M_1 \gtrsim M_{\rm RP} = 1 \text{ keV}. \tag{5.56}$$

The model-dependent bounds for NRP and RP sterile neutrinos are more stringent than the model-independent PEP bound.

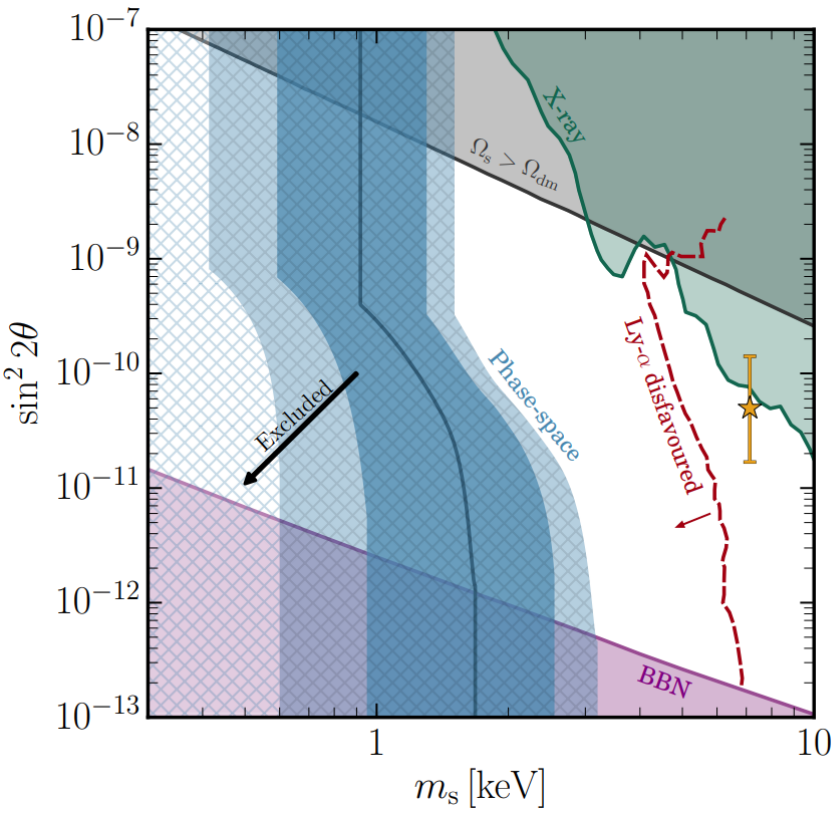

Figure 5.3: Phase space density exclusion plot of RP sterile neutrino DM

Plot of RP sterile neutrino mixing angle against mass, taken from [172]. The blue hatched region is ruled out by PSD bounds based on Liouville's theorem, and assuming the DM has a Gaussian velocity dispersion. The solid blue line is the central value of the bound, and the dark/light regions are $\pm 1/2\sigma$ confidence intervals. The region above the solid black line, which defines where $\Omega_{N_1} = \Omega_{\rm DM}$ for NRP sterile neutrinos, is excluded since $\Omega_{N_1} > \Omega_{\rm DM}$. The purple region at the bottom is excluded by the maximum lepton asymmetry allowed by BBN [183]. The region to the left of the red-dashed line is disfavoured by structure formation given by Lyman-α data [102, 184]. The green region in the top right is excluded by the absence of x-ray emissions from the radiative decay of sterile neutrinos [185]. The yellow star is an interpretation of the unidentified 3.55 keV x-ray signal if it was emitted via the radiative decay of a sterile neutrino [186], details of which will follow in the section below.

X-ray bound

Sterile neutrinos decay radiatively via $N \to \nu\gamma$, as shown in Figure 5.2b, emitting photons with energy $E_\gamma \sim M_1/2$. For DM sterile neutrinos of mass $\sim O(\text{keV} - \text{MeV})$, we would therefore expect to see a narrow x-ray line in the spectrum of DM dominated objects. The DM line can be distinguished from other x-ray emissions as its brightness is proportional to the density of DM in the object [168].

Extensive searches for the DM line (for example, by XMM-Newton and Chandra [187–189]), have placed strong constraints on the active-sterile neutrino mixing angle by reliably estimating the amount of DM in the observed object. Their radiative decay width is [106, 190,

191]

$$\Gamma_{N_1\to\nu\gamma} = \frac{9\alpha G_F^2}{1024\pi^4}\sin^2(2\theta_1)M_1^5 \simeq 5.5\times10^{-22}\theta_1^2\left(\frac{M_1}{\text{keV}}\right)^5 \text{s}^{-1}, \tag{5.57}$$

and in the absence of x-rays [171, 185],

$$\theta_1^2 \lesssim \theta_{1,\text{x-ray}}^2 = 3\times10^{-5}\left(\frac{\text{keV}}{M_1}\right)^5, \tag{5.58}$$

which is equivalent to $\Gamma^{-1}_{N_1\to\nu\gamma} \sim O(10^8)$ times the age of the universe.

An unidentified x-ray line of energy 3.52 ± 0.02 keV was observed in spectra of the Andromeda (M31) galaxy and the Perseus galaxy cluster [186]. The signal may be attributed to DM sterile neutrinos of mass $M_1 = 7.14 \pm 0.07$ keV and $\sin^2 2\theta_1 = 4.9^{+1.3}_{-1.6}\times10^{-11}$, as plotted in Figures 5.3 and 5.4, [172, 184, 186, 192], however the possibility that this signal is an instrumental effect or an atomic line can not be ruled out. If sterile neutrino DM of this mass is to remain within the current x-ray bound and make up the total DM abundance, they must be produced resonantly, and so we require a non-zero LA. Alternatively, 7.1 keV sterile neutrinos may be produced non-resonantly ($Y_L = 0$) and be consistent with x-ray bounds if they do not constitute more than $\sim 15\%$ of the total DM abundance [106]. However, recently improved Lyman-α bounds using combined data from SDSS, XQ and HR excludes both possibilities by over 3σ [184], as shown by the shaded red region of parameter space in Figure 5.4.

We can conclude from Figure 5.4 that the x-ray and Lyman-α bounds rule out the possibility of NRP sterile neutrinos making up the total DM abundance. RP sterile neutrinos with mass of $O(10)$ keV may make up the total DM abundance if the LA is at least $O(10^5)$ times greater than the BAU, which would therefore require the majority of the LA to be generated post sphaleron freeze-out. In chapter 7 we present our modified νMSM, in which DM sterile neutrino production does not depend on the active-sterile neutrino mixing angle, rather the strength of its coupling to a scalar inflaton field. As a result, the model evades the x-ray constraints.

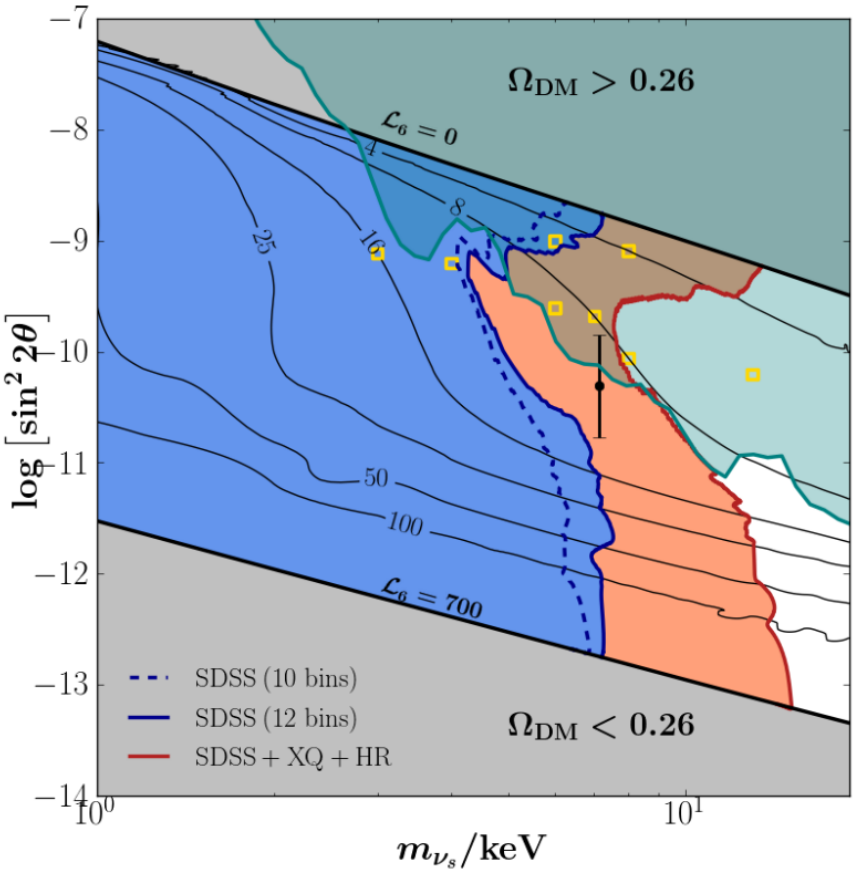

Figure 5.4: X-ray and Lyman-α exclusion plot of RP sterile neutrino DM

Plot of RP sterile neutrino mixing angle against mass, taken from [184]. Black lines are isocurves of constant LA, where $L_6 \equiv 10^6 Y_L$. The mixing angle is bounded from below by the maximum LA that can be produced in νMSM ($L_6 = 700$), and from above by the overproduction of NRP sterile neutrino DM ($L_6 = 0$). The green shaded region is the bound from the absence of x-rays, and the black dot is the sterile neutrino interpretation of the unidentified 3.55 keV x-ray signal [186]. The blue and red regions are excluded by over 3σ by SDSS and SBSS + XQ + HR Lyman-α forest power spectrums respectively.

5.3 Leptogenesis

Sterile neutrino interactions can generate a LA if the three Sakharov conditions stated in section 2.3 are satisfied. As sterile neutrinos are singlets under the SM gauge transformations, a lepton number violating Majorana mass term is allowed whilst still conserving the SM gauge symmetries. As a result, sterile neutrinos can undergo lepton number violating Yukawa interactions, such as $N \to \bar{\phi}\bar{L}$ ($\Delta L = 2$). These interactions may then generate a LA if the Yukawa couplings contain a complex CP-violating phase and are small enough for the sterile neutrinos to depart from equilibrium [11]. In the following sections we will discuss the two mechanisms by which LA can be generated: during sterile neutrino production (freeze-in) via neutrino oscillations, and during sterile neutrino decay (freeze-out). There is a maximal lepton asymmetry bound from Big Bang Nucleosynthesis [178, 183], where electron neutrinos have $Y_{\nu_e}^{\rm BBN} \lesssim 2.5 \times 10^{-3}$. Any larger will change the primordial abundance of light elements, due

to their sensitive dependence on the neutron to proton ratio at the time weak interactions freeze-out. For the νMSM model, this bound is weaker than the maximum LA that can be produced, which is given in (5.40). Recent observations of the abundance of ^{4}He suggests that the universe may well have a large LA [193], however the focus of this section will be to examine how leptogenesis can generate the BAU, and what constraints this puts on the νMSM.

EW sphaleron processes violate $B+L$, and can therefore generate a net BA from an initial LA. Here, sphalerons convert the LA in left-handed leptons to BA in left-handed quarks, which then gets redistributed to right-handed particles via SM interactions [194]. Sphaleron scatterings are frozen-out after EW symmetry breaking [11], once $T < T_{\rm EW}$, and so the LA must be generated during the symmetric Higgs phase, when $T > T_{\rm EW}$. During this period, the $B-L$ conserving sphaleron processes are fast enough to be in thermal equilibrium, and so there are only N_F conserved global charges [195, 196]:

$$X_l = \frac{1}{N_F} B - L_l; \tag{5.59}$$

where the number of fermion families is $N_F = 3$, and $l = e, \mu, \tau$. By imposing the conservation of X_l, the neutrality of the system with respect to $SU(2)$ and $U(1)$ gauge charges, and requiring the EW sphaleron processes to be in thermal equilibrium, we obtain the following expression for the BA in the symmetric Higgs phase [197, 198]:

$$Y_B = \left(\frac{8N_f + 4N_\Phi}{22N_f + 13N_\Phi} \right) (Y_B - Y_L)\,; \tag{5.60}$$

when $N_f = 3$ and the number of Higgs doublets is $N_\Phi = 1$, this yields $Y_B = 28/79\,(Y_B - Y_L)$.

During the freeze-out and freeze-in periods, the sterile neutrinos have departed from thermal equilibrium, and so the necessary Sakharov conditions to generate a LA are satisfied. Next, we will look at the mechanisms that generate LA during these periods: thermal and resonant leptogenesis generate LA through sterile neutrino decay, and leptogenesis via neutrino oscillations generate LA during sterile neutrino production. Requiring that at least some LA is generated prior to the EW phase transition and that it is large enough to produce the observed BAU, we will constrain the sterile neutrino parameter space for each mechanism accordingly.

5.3.1 Thermal leptogenesis

The thermal leptogenesis process assumes an initial thermal abundance of sterile neutrinos hierarchical in mass ($M_1 \ll M_2 \ll M_3$), which generate a lepton asymmetry via their out-of-equilibrium decay at temperature $T_{\rm decay} \sim M_I$ [11, 162, 163].

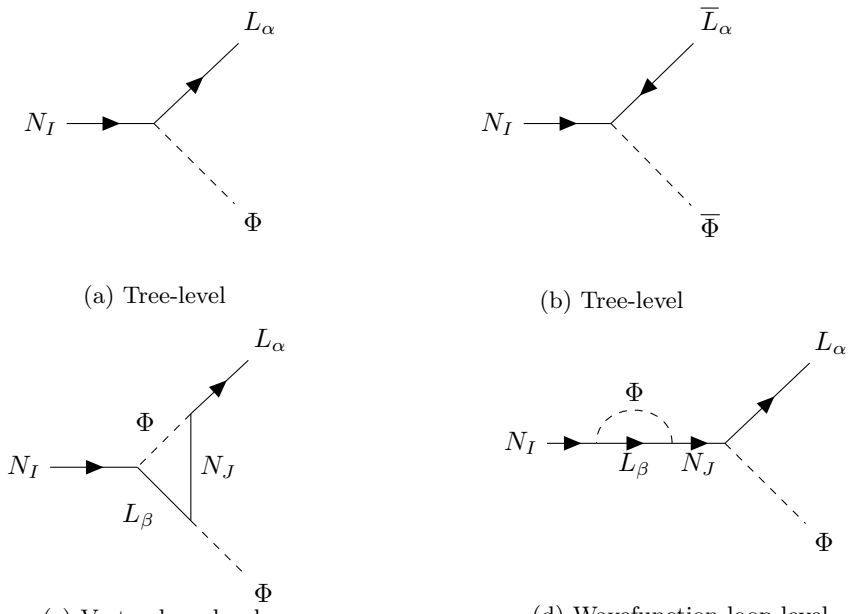

(a) Tree-level

(b) Tree-level

(c) Vertex loop-level

(d) Wavefunction loop-level

Figure 5.5: Sterile neutrino decay channels

The tree-level contribution to the amplitude of the process $N_I(\mathbf{p}_1, \sigma_1) \to L(\mathbf{p}_2, \sigma_2)\phi(\mathbf{p}_3)$, as shown in Figures 5.5a and 5.5b, is:

$$\begin{aligned} M^{\mathrm{TL}}_{N_I \to L\phi} &= \overline{u}_2 F_I u_1, \\ \overline{|M^{\mathrm{TL}}_{N_I \to L\phi}|}^2 &= \frac{\left(F^\dagger F\right)_{II}}{2} \sum_{\sigma_{1,2}} [\overline{u}_2 u_1][\overline{u}_1 u_2], \\ &= 2\left(F^\dagger F\right)_{II} (p_1 \cdot p_2), \\ &= \left(F^\dagger F\right)_{II} \left(M_I^2 - m_\phi^2\right); \end{aligned} \tag{5.61}$$

therefore the tree-level decay width is CP-symmetric, i.e. $\Gamma_{N_I \to L\phi} = \Gamma_{N_I \to \bar{L}\bar{\phi}}$. Following the notation used in [197, 199],

$$\left(F^\dagger F\right)_{II} = \frac{M_I}{\langle \Phi \rangle^2} \tilde{m}_I \tag{5.62}$$

and

$$\tilde{m}_I = \sum_J m_J |R_{IJ}|^2, \tag{5.63}$$

where R_{IJ} is any orthogonal matrix and m_J is the active neutrino mass. The tree-level con-

tribution to the total decay width of neutrino N_I is thereby [103]

$$\Gamma_I^{\rm TL} \equiv \Gamma^{\rm TL}_{N_I\to L\phi} + \Gamma^{\rm TL}_{N_I\to \bar{L}\bar{\phi}} = \frac{\left(F^\dagger F\right)_{II}}{8\pi} M_I \left(1-\frac{m_\phi^2}{M_I^2}\right)^2 \sim \frac{M_I^2 \tilde{m}_I}{4\pi v^2}; \tag{5.64}$$

we implicitly sum over all contributions, defining $\Gamma_{N_I\to L\Phi} \equiv \sum_\alpha \Gamma_{N_I\to L_\alpha\Phi}$, where all charged and neutral components of the Higgs doublet are physical.

CP asymmetry is generated by the interference of tree-level and loop-level decay processes. The 1 loop-level processes have a vertex and wavefunction contribution, as shown in Figures 5.5c and 5.5d respectively. The decay asymmetry is defined by [103]

$$\epsilon_I \equiv \frac{\Gamma_{N_I\to L\Phi} - \Gamma_{N_I\to \bar{L}\bar{\Phi}}}{\Gamma_{N_I\to L\Phi} + \Gamma_{N_I\to \bar{L}\bar{\Phi}}}. \tag{5.65}$$

The vertex contribution to the decay asymmetry is [103]

$$\epsilon_I^{\rm V} = \frac{1}{8\pi}\sum_{J\neq I} f\left(\frac{M_K^2}{M_I^2}\right) \frac{{\rm Im}\left[\left(F^\dagger F\right)^2_{JI}\right]}{\left(F^\dagger F\right)_{II}}, \tag{5.66}$$

where $f(x) = \sqrt{x}\left(1-(1+x){\rm ln}\left[\frac{1+x}{x}\right]\right)$, and the wavefunction contribution to the decay asymmetry is [103]

$$\epsilon_I^{\rm WF} = -\frac{1}{8\pi}\sum_{J\neq I} \frac{M_I M_J}{M_J^2 - M_I^2} \frac{{\rm Im}\left[\left(F^\dagger F\right)^2_{JI}\right]}{\left(F^\dagger F\right)_{II}}, \tag{5.67}$$

in the limit that the neutrinos are hierarchical, $|M_I - M_J| \gg |\Gamma_I - \Gamma_J|$.

In the limit $M_J^2 \gg M_I^2$, the CP asymmetry generated by the wavefunction component is twice as large as the vertex component [103]:

$$\begin{aligned}\epsilon_I = \epsilon_I^{\rm V} + \epsilon_I^{\rm WF} &\sim \sum_{J\neq I}\left[-\frac{1}{16\pi}\frac{M_I}{M_J}\frac{{\rm Im}\left[\left(F^\dagger F\right)^2_{JI}\right]}{\left(F^\dagger F\right)_{II}} - \frac{1}{8\pi}\frac{M_I}{M_J}\frac{{\rm Im}\left[\left(F^\dagger F\right)^2_{JI}\right]}{\left(F^\dagger F\right)_{II}}\right] \\ &= -\frac{3}{16\pi}\sum_{J\neq I}\frac{M_I}{M_J}\frac{{\rm Im}\left[\left(F^\dagger F\right)^2_{JI}\right]}{\left(F^\dagger F\right)_{II}}.\end{aligned} \tag{5.68}$$

As N_1 is the lightest sterile neutrino, it is still in thermal equilibrium after N_2 and N_3 have decayed. As a result, any LA generated by N_2 and N_3 decays will be washed out by the lepton number violating interactions of N_1 [162, 197] shown in Figure 5.6; therefore only the LA generated by N_1 decays contribute significantly to the final LA [162].

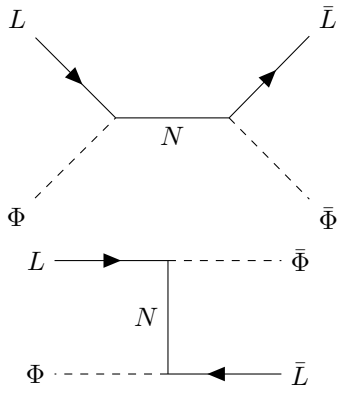

(a) $L\Phi \to \bar{L}\bar{\Phi}$

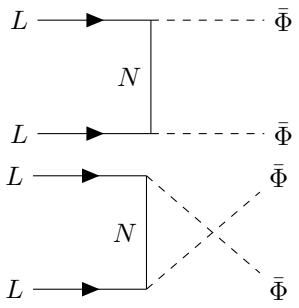

(b) $LL \to \bar{\Phi}\bar{\Phi}$

Figure 5.6: Lepton number violating interactions, $\Delta L = 2$

Substituting equation (5.62) into (5.68) and using the orthogonality of R, the upper bound on the decay asymmetry generated by the lightest sterile neutrino, N_1, is [199]

$$\begin{aligned} |\epsilon_1| &\lesssim \frac{3}{4\pi}\frac{M_1}{v^2}\left(m_3 - m_1\right), \\ &\lesssim \frac{3}{4\pi}\frac{M_1}{v^2} m_{\text{atm}}; \end{aligned} \tag{5.69}$$

where we have used the notation $m_{\text{atm}} \equiv \sqrt{\Delta m^2_{\text{atm}}}$. We will then use approximation (5.69) to obtain the lower mass bound on N_1 that generates the observed BAU.

Assuming an initial thermal abundance of N_1 at $T \gg M_1$, the LA generated is [103]

$$Y_L = \epsilon_1 \eta Y_{N,\text{eq}}(T \gg M_1), \tag{5.70}$$

where η is the decay efficiency of N_1. The equilibrium abundance of N_1 is [103]

$$Y_{N,\text{eq}} = \frac{45 g_N}{2 g_{*s} \pi^4} \sim 4 \times 10^{-3}, \tag{5.71}$$

where the number of spin degrees of freedom of Majorana neutrino is $g_N = 2$, and the effective number of relativistic degrees of freedom that contributes to entropy is $g_{*s} \sim 100$. The decay efficiency of N_1 is $\eta \sim 1$ if $\Gamma_1(T_{\text{decay}}) < H(T_{\text{decay}})$, as the neutrinos decay out of equilibrium; and $\eta < 1$ if $\Gamma_1(T_{\text{decay}}) > H(T_{\text{decay}})$, as there is a wash-out of LA whilst the neutrinos decay in thermal equilibrium [197]. To achieve $\eta \sim 1$, the active neutrino mass is required to be within the following bound [197, 199]:

$$m_1 < \tilde{m}_1 < \frac{4\pi^2}{\sqrt{90}} \frac{\sqrt{g_*} v^2}{M_{\text{P}}} \sim 10^{-3} \text{ eV}, \tag{5.72}$$

where due to orthogonality of R, the active neutrino mass is well approximated by $m_1 \lesssim \tilde{m}_1$. It is however unlikely that $\eta \sim 1$ if the Yukawa coupling is large enough to produce a thermal

abundance. Even so, the decay efficiency of thermal neutrinos only mildly suppresses the LA when $T < M$, since inverse sterile neutrino decays are Boltzmann suppressed [194]. We will use the estimate $\eta \sim 0.1$, as given in [199], to approximate the lower mass bound of N_1.

The maximum LA that can be generated from the decay of N_1, obtained from substituting the maximum decay asymmetry calculated in (5.69) into equation (5.70), is

$$Y_L \lesssim 8\eta \left(\frac{M_1}{\text{GeV}}\right) \times 10^{-19}. \tag{5.73}$$

Assuming that thermal leptogenesis generates the total BAU, we use equation (5.60) to obtain the lower mass bound on the lightest sterile neutrino,

$$M_1 > \left(\frac{0.1}{\eta}\right) \times O(10^9)\ \text{GeV}, \tag{5.74}$$

which is known as the Davidson-Ibarra bound [199]. Here we approximated $Y_B - Y_L \sim -Y_L$ in equation (5.60), as sphaleron processes that convert LA to BA are inefficient at very high temperatures ($T > 10^{12}$ GeV) [197, 199].

5.3.2 Resonant leptogenesis

Thermal leptogenesis presents problems for both experimentalists and theorists: the theory is untestable by experiment, since it is unfeasible to detect sterile neutrinos at the required mass scale; and it presents a hierarchy problem for theorists [200], as the Yukawa couplings give large radiative corrections to the bare Higgs mass parameter, μ_Φ^2.

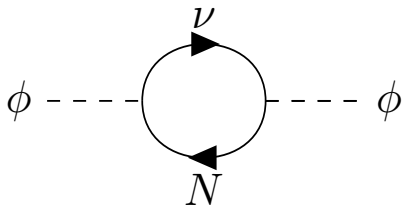

Figure 5.7: Radiative correction to Higgs mass parameter

The radiative correction to μ_Φ^2, given by the Feynman diagram in Figure 5.7, is of the order [200]

$$\delta\mu_\Phi^2 \sim \frac{\left(F^\dagger F\right)_{II}}{4\pi^2} M_I \log\left(\frac{q}{M_I}\right) \sim \frac{m_i M_I^3}{2\pi^2 v^2} \log\left(\frac{q}{M_I}\right), \tag{5.75}$$

for external momenta[3] $q < M_I$. For the theory to produce the active neutrino mass splitting,

[3]Here q is the renormalization group scale, which is just the typical energy scale that the Higgs mass is observed. The value of the observed Higgs mass ($\mu_\Phi^2 + \delta\mu_\Phi^2$) thus changes with energy due to the $\delta\mu_\Phi^2$ dependence on q. The relation between the bare and observed mass for a given q is determined by the renormalization group equations.

we require $m_i > m_{\rm atm}$, and for the radiative corrections to be sub-dominant, we need $\delta\mu^2 < O(10^4)$ GeV^2. To satisfy both requirements, the sterile neutrino mass needs to be within the range [11, 200]

$$M_I < O(10^7) \text{ GeV}, \tag{5.76}$$

which is below the lower mass bound (5.74) required for thermal leptogenesis to generate the BAU. To reproduce the Higgs mass with larger sterile neutrino masses requires higher order loop corrections with finely-tuned tree values.

However, if the sterile neutrinos are degenerate in mass rather than hierarchical, the wavefunction contribution to the decay asymmetry (5.67) is singular as $M_I \to M_J$, which is an artefact of the assumption that sterile neutrinos are asymptotic states [104, 165, 166, 201]. In the limit $\Delta M_{32} \ll M_2$ ($\Delta M_{ij} \equiv M_i - M_j$), using out-of-equilibrium QFT methods [201–205], the wavefunction decay asymmetry gains a finite regulator term, $A \sim M_I\Gamma_I$ [104, 165, 166, 201]:

$$\epsilon^{\rm WF} = \frac{\text{Im}\left[\left(F^\dagger F\right)_{32}\right]^2\left[\left(F^\dagger F\right)_{22}+\left(F^\dagger F\right)_{33}\right]}{16\pi\left(F^\dagger F\right)_{22}\left(F^\dagger F\right)_{33}}\frac{M_2M_3\Delta M_{23}^2}{\left(\Delta M_{23}^2\right)^2+A^2}. \tag{5.77}$$

Going forward, we assume the lightest sterile neutrino, N_1, is DM, which necessarily has a lifetime that exceeds the age of the universe. The LA is therefore resonantly produced via the decay of two heavier degenerate sterile neutrinos, N_2 and N_3. The resonant enhancement of CP violation occurs when $\Delta M_{32} \sim \Gamma_2/2$ [104, 164–166], which gives the following wavefunction contribution to the decay asymmetry [104, 165, 166, 206],

$$|\epsilon^{\rm WF}| \simeq \frac{1}{2}\frac{\text{Im}\left[\left(F^\dagger F\right)_{32}\right]^2}{\left(F^\dagger F\right)_{22}\left(F^\dagger F\right)_{33}}. \tag{5.78}$$

Resonant leptogenesis can achieve a decay asymmetry that is independent of the sterile neutrino mass with a magnitude of up to $|\epsilon^{\rm WF}| \leq \frac{1}{2}$, and is therefore far more efficient than the thermal leptogenesis process for lighter sterile neutrinos [104, 165, 166, 206]. The Davidson-Ibarra bound (5.74) is then relaxed and we may have $M_{2/3}$ as small as 1 TeV, which is bounded by the requirement that the LA is created at $T > T_{\rm EW}$ [11, 104, 164–166, 201]. Such sterile neutrinos may have evaded experimental detection due to their weak Yukawa coupling. If we require the model to generate the active neutrino masses, the typical value of a Yukawa coupling, given equation (5.62), is

$$|F_I|^2 \sim \frac{M_I}{v^2/2}m_{\rm atm}, \tag{5.79}$$

which for $M_{2/3} = O(1)$ TeV is as small as $|F_I|^2 \sim O(10^{-12})$.

Important variations of the standard resonant leptogensis model based on lepton flavour symmetries are presented in [207–210], in which the BAU is produced from the sphaleron conversion of individual lepton numbers. In these scenarios, $M_{2/3}$ can be as light as 100 GeV.

5.3.3 Leptogenesis via neutrino oscillations

Now we will consider an initial zero abundance of sterile neutrinos that are produced out-of-equilibrium in the early universe via their Yukawa interactions with the SM. As these interactions are CP-conserving, the universe has an initial equal abundance of Majorana neutrinos with opposite helicities, and so the total lepton number is $L_{\rm tot} = L + L_1 + L_2 + L_3 = 0$, where L is the lepton number in the active species and $L_I = 0$ ($I = 1, 2, 3$) are the lepton numbers of the individual Majorana neutrino states [53, 105]. However, since the neutrinos are produced in their gauge basis, which doesn't coincide with their mass basis, they change states via CP violating oscillations, thereby redistributing the lepton number between the active neutrino sector ($L \neq 0$) and sterile neutrino sector ($L_I \neq 0$). As the total lepton number is conserved ($L_{\rm tot} = 0$), we have [53, 105]

$$\Delta L = -\sum_{I=1,2,3} \Delta L_I. \tag{5.80}$$

The LA generated in the active neutrino sector is then converted into BA via EW sphalerons processes at $T > T_{\rm EW}$.

The dark matter sterile neutrino, N_1, does not contribute to the generation of LA as the x-ray bound, given in equation (5.58), requires the Yukawa coupling to be extremely small, $|F_1|^2 < O(10^{-21})$ [53]. As a result, N_1 is effectively decoupled from the plasma in the early universe [53]. The dominant mechanism for generating LA in the active and sterile neutrino sectors is CP violating $N_2 - N_3$ oscillations, mediated by a lepton and Higgs doublet loop [53, 105], as shown in Figure 5.8. Oscillations between sterile and active species and between active neutrinos of different flavours are strongly suppressed due to their very different effective masses [53]. Additionally, active neutrino oscillations that violate lepton number and sterile neutrino oscillations that change helicity are also suppressed [53].

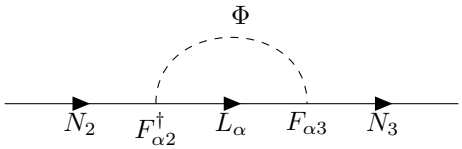

Figure 5.8: CP violating $N_2 - N_3$ oscillations mediated by a lepton and Higgs doublet loop

Although the rate of the CP violating $N_2 - N_3$ oscillations is strongly suppressed by their Yukawa couplings, $|F_{\alpha 2}|^2 |F_{\alpha 3}|^2$, we are able to resonantly produce a large LA if $N_{2,3}$ are

degenerate in mass [53, 105]. Next we will determine the mass range of $N_{2,3}$ that are out of thermal equilibrium prior to EW symmetry breaking, and can therefore generate the BAU.

The main contribution to the sterile neutrino interaction rate with the SM is the two-to-two Higgs-mediated scattering process, $t\bar{t} \leftrightarrow N_I \overline{L}_\alpha$:

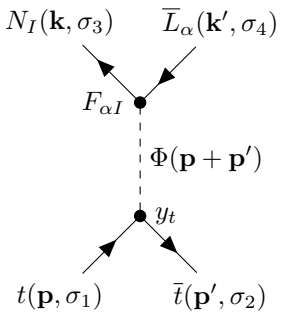

Figure 5.9: Scattering process $t\bar{t} \leftrightarrow N_I \overline{L}_\alpha$, mediated by the Higgs boson

The amplitude of the process in the centre of mass frame, $p = (E, 0, 0, \mathbf{E})$ and $p' = (E, 0, 0, -\mathbf{E})$, is

$$|M_{t\bar{t}\to N\overline{L}}| = [\overline{u}_3 v_4] \cdot F_{\alpha I} \cdot \frac{g^{\mu\nu} - \frac{E^\mu E^\nu}{m_h^2}}{4E^2 - m_h^2} \cdot y_t \cdot [\overline{v}_2 u_1], \tag{5.81}$$

which gives an average squared amplitude of

$$\overline{|M_{t\bar{t}\to N\overline{L}}|}^2 \sim (F_{\alpha I} y_t)^2 \cdot \left(\frac{E}{m_h}\right)^4, \tag{5.82}$$

where we define $\overline{|M|}^2 \equiv \frac{1}{4}\sum_{\sigma_1,\sigma_2}\sum_{\sigma_3,\sigma_4}|M|^2$. The rate of the scattering process, summing over all active lepton flavours (α) is [53, 105]

$$\begin{aligned}\Gamma_{t\bar{t}\to N\overline{L}} \equiv n_t \cdot \sigma_{t\bar{t}\to N\overline{L}} &\sim \frac{3}{4} g_t \frac{\xi(3)}{\pi^2} T^3 \cdot \frac{F_I^2 y_t^2}{64\pi} \frac{E^2}{m_h^4}, \\ &\sim \frac{9}{64\pi^3} F_I^2 T,\end{aligned} \tag{5.83}$$

where n_t is the relativistic thermal number density of top quarks, which have $g_t = 12$ degrees of freedom and a Yukawa coupling $y_t \sim 1$. We then take the approximation $\langle E \rangle \sim m_h \sim T$, since we are evaluating the rate prior to EW symmetry breaking. The temperature at which N_I thermalizes with the SM ($\Gamma_{t\bar{t}\to N\overline{L}}(T_{\rm eq}) \sim H(T_{\rm eq})$) is:

$$T_{\rm eq} = \frac{27\sqrt{10}}{64\pi^4} \frac{M_{\rm P}}{\sqrt{g_{\rm SM}}} |F_I|^2 . \tag{5.84}$$

We will assume the typical value of a Yukawa coupling that can explain the active neutrino

mass splitting, which given the see-saw relation in equation (5.62) is

$$|F_I|^2 \sim \frac{m_{\rm atm} M_I}{v^2/2}. \tag{5.85}$$

Then, by requiring $T_{\rm eq} < T_{\rm EW}$, we obtain the following upper bound on $M_{2,3}$ [53, 105],

$$M_{2,3} < \frac{32\pi^4}{27\sqrt{10}} \frac{v^2\sqrt{g_{\rm SM}}}{M_{\rm P}\ m_{\rm atm}} T_{\rm EW} \sim 30 \text{ GeV}. \tag{5.86}$$

Additionally, for the model to be consistent with the BBN predictions, $N_{2/3}$ must decay prior to this epoch. Post EW symmetry breaking, the main decay channels of sterile neutrinos with $M_I < M_W$ are $N \to \nu_\alpha \overline{\nu}_\beta \nu_\beta / l_\alpha^- l_\beta^+ \nu_\beta / \nu_\alpha l_\beta^+ l_\beta^- / l_\alpha^- U \overline{D} / \nu_\alpha q \overline{q}$, which has decay width [211, 212]:

$$\Gamma_{N_I} \geq \frac{G_F^2 M_I^5}{192\pi^3} \theta_I^2. \tag{5.87}$$

The inequality $\Gamma_{N_I} > H\left(T_{\rm BBN}\right)$, where $T_{\rm BBN} \sim$ few MeV, translates into a lower mass bound of [53, 105]

$$M_{2,3} > \text{few GeV}. \tag{5.88}$$

The late-time decay of sterile neutrinos within this mass range does not release a large amount of entropy into the SM, which would subsequently lead to a dilution of the BA. The details of this analysis is given later in section 7.7.

The majority of the BA is generated when the $N_2 - N_3$ oscillation rate [11, 53, 105, 168],

$$\omega \sim \frac{\left|\Delta M_{23}^2\right|}{E} \sim \frac{\left|\Delta M_{23}^2\right|}{T}, \tag{5.89}$$

is of the order of the Hubble expansion rate ($\omega(T_B) \sim H(T_B)$); we assume in (5.89) the typical energy of a sterile neutrino is $E \sim T$. When $T > T_B$ ($\omega < H$) CP violation has no time to develop, and once $T < T_B$ ($\omega > H$) the neutrino oscillations are out of resonance and the LA is strongly suppressed by averaging effects [11, 53, 105, 168]. The BA is therefore generated at temperature [11, 53, 105, 168]

$$T_B = \left(\frac{3\sqrt{10}}{\pi\sqrt{g_{\rm SM}}} M_{\rm P} \left|\Delta M_{23}^2\right|\right)^{\frac{1}{3}} \sim O\left(10^6\right) \times \left(\frac{\left|\Delta M_{23}^2\right|}{\text{GeV}^2}\right)^{\frac{1}{3}} \text{ GeV}, \tag{5.90}$$

if $\omega(T_B) \sim H(T_B)$ occurs prior to EW symmetry breaking ($T_B \gtrsim T_{\rm EW}$) and the thermalization of the sterile neutrinos ($T_B \gtrsim T_{\rm eq}$).

The evolution of the lepton asymmetries generated in the active and sterile neutrino sectors are tracked by the kinetic equations of the neutrino density matrix. The quantitative analysis

is beyond the scope of this review, and is found in [53, 105]. Below we quote the final result for the BA generated via neutrino oscillations [11, 53]:

$$Y_B = 2 \times 10^{-10} \delta_{\rm CP} \left(\frac{10^{-6}}{|\Delta M^2_{23}| / M^2_3} \right)^{\frac{2}{3}} \left(\frac{M_3}{10 \text{ GeV}} \right)^{\frac{5}{3}}, \tag{5.91}$$

which shows that $N_{2,3}$ must be highly degenerate in mass in order to produce the total BAU. The CP violation parameter [11, 53],

$$\begin{aligned} \delta_{\rm CP} = 4 s_{R23} c_{R23} \big[& s_{L12} s_{L13} c_{L13} \left(\left(c^4_{L23} + s^4_{L23} \right) c^2_{L13} - s^2_{L13} \right) \cdot \sin\left(\delta_L + \alpha_2 \right) \\ & + c_{L12} c^3_{L13} s_{L23} c_{L23} \left(c^2_{L23} - s^2_{L23} \right) \cdot \sin \alpha_2 \big], \end{aligned} \tag{5.92}$$

can have a magnitude of up to $O(1)$ according to current neutrino oscillation data, and is non-zero even when there is no CP violation in active neutrino oscillations (i.e. when $\theta_{L13} = 0$). The mixing angles θ_{Lij}, CP violating phase δ_L, and Majorana phase α_2 are parameters of the active neutrino PMNS mixing matrix, given in (5.8), whilst the mixing angles θ_{Rij} are parameters of the analogous PMNS mixing matrix ($L \to R$) for sterile neutrinos.

5.3.4 Unification of leptogenesis mechanisms

Until recently, resonant leptogenesis (freeze-out LA production) and leptogenesis via neutrino oscillations (freeze-in LA production) were considered as two separate mechanisms that operate in two distinct sterile neutrino mass scales: $M_{2,3} = O(10^2 - T_{\rm reh})$ GeV and $M_{2,3} = O(1 - 10)$ GeV respectively. Conversely, the work carried out in [201] suggests that the generation of LA via both mechanisms could be described by the same set of quantum kinetic equations operating in different regions of the sterile neutrino parameter space, with a significant overlap between them. We will present the results from [201] in this section, however there is still a debate over whether the two mechanisms of mixing and oscillations are distinct or the same phenomenon [204, 213]

The analysis carried out in [201] showed that contradictory to what was originally thought, the mass scales of the two mechanisms are not completely separate. Sterile neutrinos with masses as small as $O(1)$ GeV cause a significant deviation from equilibrium during freeze-out. Additionally, LA can be produced via freeze-in by sterile neutrinos that thermalize prior to sphaleron freeze-out, which is the case for $M_{2,3} > O(10)$ GeV [201]. Although thermal sterile neutrinos washout the generated LA, once temperatures drop below their mass scale, the washout is strongly suppressed by the Boltzmann factor, proportional to $\exp\left[-M_I/T\right]$ [197, 201]. As a result of these two effects, LA can be generated during freeze-out by sterile neutrinos that are lighter than expected, and during freeze-in by sterile neutrinos that are heavier than expected.

The results are summarized in Figure 5.10 below, which plots the squared active-sterile neutrino mixing angle, $U^2 \equiv \sum_{\alpha I} |\theta_{\alpha I}|^2$, against the average sterile neutrino mass, M; the left and right plots assume active neutrinos have a normal and inverted hierarchy respectively [201]. The coloured gradient in the legend to the right of the plots gives the maximum mass splitting of N_2 and N_3 that can produce the total BAU, the white regions in the plot require $\Delta M/M < 10^{-6}$. The solid black curve bounds the parameter space where both freeze-in and freeze-out mechanisms produce the observed BAU, assuming an initial zero abundance of sterile neutrinos [201]. The blue dashed curve bounds the parameter space where an initial thermal abundance of sterile neutrinos is assumed, and so the BAU can only be produced via freeze-out; and the red dotted line bounds the parameter space where sterile neutrinos with an initial zero abundance don't deviate from equilibrium due to the expansion of the universe, and so the BAU can only be produced via freeze-in [201]. The active-sterile neutrino mixing angle is bounded from below by requiring the active neutrino masses to be produced via the see-saw mechanism; and as the LA washout rate increases with U^2, the active-sterile neutrino mixing angle is bounded from above by requiring the sterile neutrinos to produce the total BAU [201].

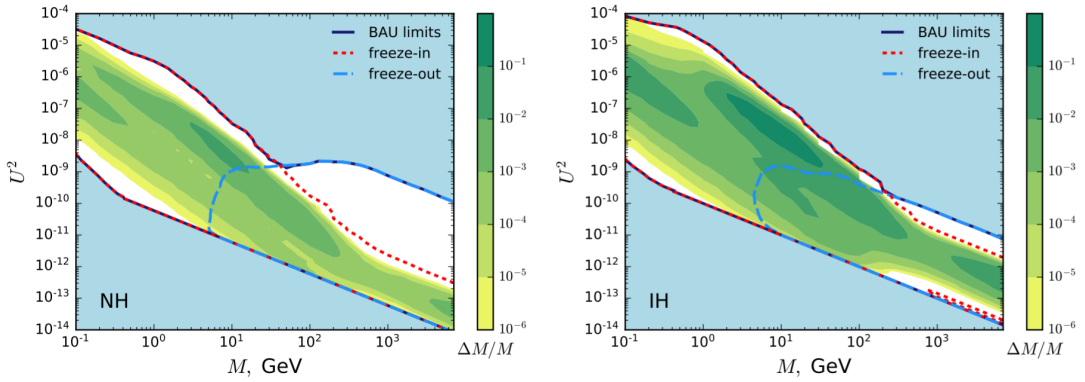

Figure 5.10: Exclusion plot of sterile neutrino parameter space for production of BAU via leptogenesis

Plots of the squared active-sterile neutrino mixing angle, U^2, against the average sterile neutrino mass, M, for normal and inverted active neutrino masses on the left and right plots respectively, taken from [201]. The notation used is $U^2 \equiv \sum_{\alpha I} |\theta_{\alpha I}|^2$, where $\theta_{\alpha I}$ is given in equation (5.25). The red dotted and blue dashed line bounds the sterile neutrino parameter space where freeze-in and freeze-out mechanisms produce the BAU respectively, and the solid back line is the region where both mechanisms contribute to the production of the BAU. The colour of the shaded regions within the bounds give the maximum sterile neutrino mass splitting that could produce the BAU, as labelled by the legend to the right of the plots; the white regions are where $\Delta M/M < 10^{-6}$ is required.

5.4 Summary and discussion

Here we present a summary of the νMSM constraints that allow the model to reproduce the active neutrino masses via the type-1 see-saw mechansism, produce a viable DM candidate,

and explain the origin of the BAU.

The solar and atmospheric active neutrino mass splittings are

$$m_{\rm sol} = 8.68 \times 10^{-3} \text{ eV}, \tag{5.93}$$

$$m_{\rm atm} = 4.95 \times 10^{-2} \text{ eV}, \tag{5.94}$$

where $m_{\rm x} \equiv \sqrt{\Delta m^2_{\rm x}}$, and we assume a normal mass hierarchy ($m_1 < m_2 < m_3$). The typical value of the active-sterile neutrino Yukawa coupling that would explain the origin of the active neutrino mass splitting is

$$|F_I|^2 \sim \frac{m_{\rm atm} M_I}{v^2/2}. \tag{5.95}$$

In the νMSM, the DM candidate is the lightest sterile neutrino, N_1. The average momentum and mass range of DM sterile neutrinos that are NRP and RP are tabulated below.

DM production mechanism	$\frac{\langle \mathbf{p} \rangle}{\mathbf{3.15T}}$	$\mathbf{M_1}$
Non-resonant	0.8-0.9	O(1-10) keV
Resonant	0.6	O(1-10) keV

Table 5.1: Average momentum and mass range of non-resonantly and resonantly produced sterile neutrino DM

The astrophysical bounds that constrain the DM sterile neutrino parameter space are:

- Lyman-α bound: maximum DM free-streaming length that would reproduce the smallest known structures in the universe, given by (4.52).
- Phase-space density bound: Maximum phase space density determined using Liouville's theorem, for NRP and RP DM sterile neutrinos

$$M_1 \gtrsim 1 \text{ keV}.$$

- X-ray bound: Absence of x-rays observed from the radiative decay of sterile neutrinos

$$\theta_1^2 \lesssim 3 \times 10^{-5} \left(\frac{\text{keV}}{M_1}\right)^5.$$

Note that both the Lyman-α and phase-space density bounds are dependent on the momentum distribution of the DM, whereas the x-ray bound is not. These astrophysical bounds are stated here as rough estimates of the precise bounds, which have a complex dependence on the momentum distribution and mass of the DM. For the exact astrophysical bounds for NRP and RP DM sterile neutrinos, consult Figures 5.3 and 5.4. We conclude that RP and NRP sterile

neutrinos are only viable DM candidates if they do not make up the total DM abundance, or the plasma has a LA that greatly exceeds the BAU.

In chapter 7 we extend a light scalar inflaton model with a modified νMSM, in which DM is produced via inflaton decay in the early universe. We are able to produce cooler DM than RP and NRP mechanisms that is within the Lyman-α bound. Additionally, our DM production mechanism is independent of the active-sterile neutrino mixing angle so the parameter space is also unconstrained by the x-ray bound.

The two heavier sterile neutrinos, $N_{2,3}$, produce LA during their out-of-equilibrium decay and production. If the two sterile neutrinos are degenerate in mass, the LA is produced efficiently by resonant leptogenesis and leptogenesis via neutrino oscillations. $N_{2,3}$ in the following mass ranges,

$$M_{2,3} = \begin{cases} O(10^2 - T_{\rm reh})\ \text{GeV}, & \text{resonant leptogensis} \\ O(1-10)\ \text{GeV}, & \text{leptogensis via neutrino oscillations} \end{cases} \tag{5.96}$$

generate a large enough LA to account for the BAU,

$$Y_B \sim O(10^{-10}). \tag{5.97}$$

Note that (5.96) are conservative mass bounds that we will apply to our modified νMSM in chapter 7. Less stringent mass bounds are discussed in section 5.3.4, which are based on the work carried out in [201].

Chapter 6

Scalar inflaton model

6.1 Introduction

The observable universe is homogeneous and isotropic, and almost completely flat. It is filled with matter and radiation and has an almost scale invariant spectrum of primordial density perturbations. These seemingly finely tuned initial conditions can be explained by the presence of an inflationary epoch prior to the Hot Big Bang [214–218]. Viable inflationary models should also provide a mechanism to initiate a reheating period post-inflation, during which the SM particles are produced.

This chapter studies an extension of the SM by a scalar inflaton with quartic self-interaction, which was suggested in [45]. With the addition of a small, non-minimal coupling to gravity, this model provides inflationary predictions in agreement with the CMB observations [48, 219, 220]. We assume that the scale symmetry in the scalar sector is broken only by the symmetry breaking mass term of the inflaton [43, 45–48, 52]. A negative quartic inflaton-Higgs coupling then allows for the transfer of symmetry breaking into the SM sector. Thus, the scalar provides symmetry breaking in the Higgs sector, as well as inflation.

Section 6.2 outlines the scalar quartic inflationary model with a non-minimal coupling, followed by the cosmological constraints on the inflaton self-coupling given by the scalar density perturbation amplitude and limits on the tensor-to-scalar ratio in section 6.3. We define three rotation angles in the inflaton-Higgs field space with respect to the gauge basis: the inflationary direction in section 6.3.1; the angle of rotation of the vacuum in section 6.4; and the inflaton-Higgs mixing angle in section 6.5. In section 6.6 we address the domain wall problem by breaking the Z_2 symmetry of our model through the addition of a small cubic inflaton term.

Defining the inflationary, vacua and mixing angles is essential for analysing the preheating and reheating periods, which describe the non-perturbative and perturbative transfer of inflationary energy into the SM. In section 6.7 we show that turbulent preheating proceeds via parametric resonance, and that the misalignment of the inflationary and vacuum angles does not transfer a significant amount of inflationary energy into the SM. In sections 6.8 and 6.9 we

study the reheating period, in which we use the inflaton-Higgs mixing angle to find the inflaton decay width in order to bound the inflaton parameter space. In section 6.8 we review the reheating analysis carried out in previous works [45–48] that focus on the region of parameters where the inflaton is lighter than the Higgs boson. Here, the dominant reheating mechanism is two-to-two inflaton-Higgs scattering. The inflaton mass is bounded from below by the minimum reheating temperature, which is required to exceed the EW symmetry breaking scale, and from above by ensuring quantum corrections to the inflaton's quartic self-coupling are small. Section 6.9 covers my own work [43] that focuses on the region of parameters where the inflaton is heavier and the channel of its direct decay to a pair of Higgs bosons is open, which allows for a more efficient reheating. The inflaton mass is also bounded from below by the minimum reheating temperature, and from above by the kinematics of the decay. In section 6.8 an analytical approach is sufficient, as the inflaton is not far from thermal equilibrium at the time of reheating. In section 6.9, however, the inflaton has a highly non-thermal distribution, and so it is necessary to solve the Boltzmann equations numerically. The inflaton distribution resulting from turbulent preheating in section 6.7.2 provides the initial condition for the reheating study.

6.2 The model

A minimal extension of the SM that incorporates mechanisms for inflation and reheating can be achieved with the addition of a single scalar field serving as our inflaton, X, which couples to the SM Higgs doublet,

$$\Phi = \frac{1}{\sqrt{2}} \begin{pmatrix} \varphi_1 + i\varphi_2 \\ \phi + i\varphi_3 \end{pmatrix}, \tag{6.1}$$

where ϕ is the SM Higgs boson, and φ_i $(i = 1, 2, 3)$ are the EW Goldstone bosons. The action and Lagrangian of the inflaton model expressed in the Jordan frame is [43, 45–47]:

$$S_{X\mathrm{SM}} = \int \sqrt{-g}\mathrm{d}^4x \left(\mathcal{L}_{\mathrm{SM}} + \mathcal{L}_X + \mathcal{L}_{\mathrm{grav}}\right), \tag{6.2}$$

$$\mathcal{L}_X = \frac{1}{2}\partial_\mu X \partial^\mu X + \frac{1}{2}\mu_X^2 X^2 - \frac{\beta}{4}X^4 - \lambda(\Phi^\dagger\Phi - \frac{\alpha}{\lambda}X^2)^2, \tag{6.3}$$

$$\mathcal{L}_{\mathrm{grav}} = -\frac{M_{\mathrm{P}}^2 + \xi X^2}{2}R, \tag{6.4}$$

where $\mathcal{L}_{\mathrm{SM}}$ is the SM Lagrangian and R is the Ricci scalar. The inflaton potential[1] requires parameters that will lead to symmetry breaking of the Higgs field, tuned to the SM expected

[1] The Z_2 symmetry of the inflaton potential gives rise to a domain wall problem. This may be resolved with the addition of a small cubic term, μX^3, without influencing the dynamics of inflation and reheating. This will be discussed in section 6.6, where we define the range of μ that satisfies these requirements.

value. We assume the only source of scale symmetry violation is due to the negative mass term in the inflaton sector; the negative quartic inflaton-Higgs coupling then allows for the transfer of symmetry breaking into the SM sector.

6.3 Inflation

During slow-roll inflation, the quartic[2] inflaton term dominates the energy density of the universe as field values exceed $O(M_{\rm P})$. We can therefore simplify our model to a single-field quartic scalar potential, and apply the standard slow-roll formalism [78, 221] as in section 3.2. In section 3.3.3, we showed that the self-coupling of a minimally coupled inflaton field is fixed from the measurement of the CMB's amplitude of the primordial scalar perturbations by equation (3.80), from which we obtain a quartic self-coupling of $\beta = O(10^{-13})$. Using equation (3.88), we find the tensor-to-scalar ratio of the model is $r \sim 0.27$, which exceeds the CMB's upper bound on the tensor-to-scalar ratio, $r_{\rm CMB} = 0.13$ [33].

We will now analyse the scenario where we have a non-minimally coupled inflaton field, $\xi > 0$, for which we are able to achieve $r < r_{\rm CMB}$ for a given range of the quartic self-coupling, β. Additionally, we assume no new scales below the Planck scale[3], so we require $\xi < 1$. In order to obtain the inflationary parameters (β, r) for $\xi \neq 0$ using the standard slow-roll formalism, we need to transform (6.2) from the Jordan frame to the Einstein frame via the following conformal transformation of the metric [46, 48, 219, 220]:

$$g_{\mu\nu} \to \tilde{g}_{\mu\nu} = \Omega^2 g_{\mu\nu}, \qquad \Omega^2 = 1 + \xi X^2/M_{\rm P}^2; \tag{6.5}$$

$\tilde{g}_{\mu\nu}$ corresponds to the metric in the Einstein frame, in which the inflaton field couples minimally to gravity, and the inflaton potential is [46, 48]

$$U(X) = \frac{\beta X^4}{4\Omega^4}. \tag{6.6}$$

The kinetic term is then conformally transformed using the following relation [46, 48]:

$$\frac{d\tilde{X}}{dX} = \sqrt{\frac{\Omega^2 + 6\xi^2 X^2/M_{\rm P}}{\Omega^4}}, \tag{6.7}$$

after which we can obtain the slow-roll parameters (ϵ, η) using the standard formalism [78, 221] (given by equations 3.21) for the canonically normalized inflaton field $\tilde{X}$. Following the

[2] We choose a quartic inflationary potential as the dimensionless self-coupling evades additional new energy scales below $M_{\rm P}$.

[3] Our model is UV complete up to the cutoff scale, $\Lambda \sim \frac{M_{\rm Pl}}{\sqrt{\xi}} / \frac{M_{\rm Pl}}{\xi}$, and at energy scales $E > \Lambda$, scattering processes violate perturbative unitarity [222–225]. We want our model to be UV complete up to the scale of quantum gravity, $M_{\rm Pl}$, and so without complicating our theory, we conservatively require $\xi < 1$. Note that this is not a stringent bound in our model, and $\xi > 1$ could only be ruled out by a measurement of r.

analysis given in section 3.3, the tensor-to-scalar ratio is then given by [46, 48]:

$$r = \frac{16\,(1+6\xi)}{(N_e+1)\,(1+8\,(N_e+1)\,\xi)}. \tag{6.8}$$

In Figure 6.1a, we plot r as a function of ξ, given by the blue line, and the CMB bound ($r_{\rm CMB} = 0.13$ [33]), given by the red dashed line. We show that for $\xi \geq O(10^{-2})$, r is sufficiently suppressed ($r < r_{\rm CMB}$) when evaluated at the relevant number e-foldings prior to the end of inflation for our model, $N_e \sim 60$. The scalar's quartic self-coupling is fixed by the CMB measurement of the primordial scalar perturbation amplitude [226] given in (3.78), and if we assume no new scales below the Planck scale, $\xi < 1$, we obtain the following range [46, 48]:

$$\begin{aligned}\beta &= \frac{3\pi^2\Delta_s^2}{2}\frac{(1+6\xi)(1+6\xi+8(N_e+1)\xi)}{(1+8(N_e+1)\xi)(N_e+1)^3)}, \\ &= O(10^{-12}-10^{-9}),\end{aligned} \tag{6.9}$$

where the lower bound corresponds to the excessive production of tensor modes ($r > r_{\rm CMB}$), and the upper bound would require $\xi > 1$ and introduces additional scales below Planck.

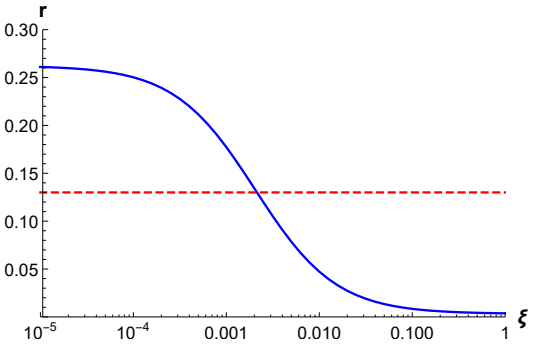

(a) Blue curve plots the tensor-to-scalar ratio, r, against non-minimal coupling, ξ. The red dashed line plots the CMB's upper bound, $r_{\rm CMB} = 0.13$.

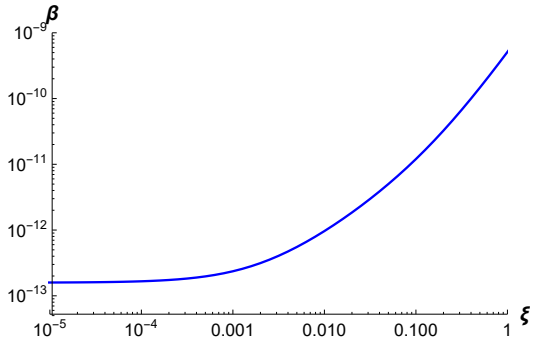

(b) Inflaton quartic self-coupling, β, against non-minimal coupling, ξ.

Figure 6.1: Tensor-to-scalar ratio and inflaton self-coupling plotted as functions of the inflaton's non-minimal coupling

6.3.1 Inflationary attractor solution

During the slow-roll inflationary epoch, we decompose the fields into a homogeneous classical component and a quantum component,

$$\begin{aligned}X(x,t) &= X_b(t) + \chi(x,t), \\ \Phi(x,t) &= \Phi_b(t) + \frac{h(x,t)}{\sqrt{2}}.\end{aligned} \tag{6.10}$$

The classically evolving background fields converge towards the inflationary attractor solution, which is found by evaluating the gradient of the potential[4], $V_{\theta_{\rm inf}} \equiv \frac{\partial V}{\partial \theta_{\rm inf}} = 0$, using the following field transformations,

$$\begin{aligned} X_b &\to R\cos\theta_{\rm inf}, \\ \sqrt{2}\Phi_b &\to R\sin\theta_{\rm inf}, \end{aligned} \tag{6.11}$$

where R is a coordinate along the inflationary direction. Neglecting the quadratic terms in the potential, the direction of the inflationary attractor solution in field space is then given by [43],

$$\tan\theta_{\rm inf} \equiv \frac{\sqrt{2}\Phi_b}{X_b} \sim \sqrt{\frac{\beta+2\alpha}{\lambda}}, \tag{6.12}$$

in the limit $\alpha, \beta \ll \lambda$. We verify our analytical result by numerically solving the Friedmann and Raychaudhuri equations, (2.11) and (2.12) respectively, derived from the Einstein's equations assuming a homogeneous and isotropic universe with zero spatial curvature:

$$\left(\frac{\dot{a}}{a}\right)^2 = \frac{1}{3M_{\rm P}^2}\left(V(X_b,\Phi_b) + \frac{\dot{\Phi}_b^2}{2} + \frac{\dot{X}_b^2}{2}\right), \tag{6.13}$$

$$\frac{2\ddot{a}}{a} + \left(\frac{\dot{a}}{a}\right)^2 = \frac{1}{M_{\rm P}^2}\left(V(X_b,\Phi_b) - \frac{\dot{\Phi}_b^2}{2} - \frac{\dot{X}_b^2}{2}\right); \tag{6.14}$$

and the Euler-Lagrange equations, which govern the background field dynamics:

$$\ddot{X}_b + 3H\dot{X}_b + V_X = 0, \tag{6.15}$$

$$\ddot{\Phi}_b + 3H\dot{\Phi}_b + V_\Phi = 0. \tag{6.16}$$

The blue curves in Figure 6.2 give the numerical evolution of the fields from an initial random point in field space, and are shown to converge to our analytical result (6.12), given by the red dashed line.

[4]Going forward we will use the notation $V_X \equiv \frac{\partial V}{\partial X}$ implicity.

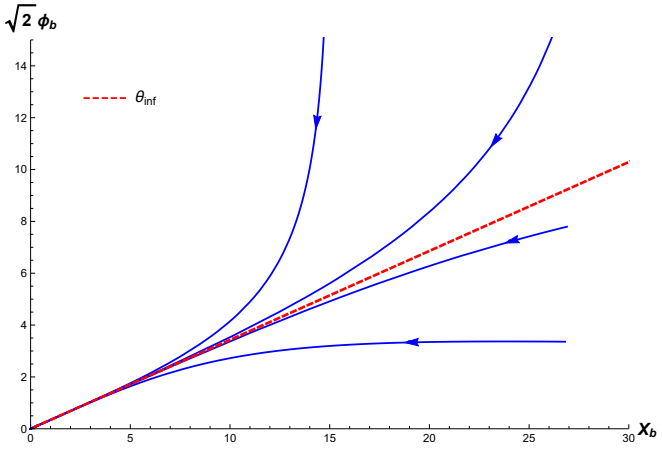

Figure 6.2: Inflationary attractor solution

The blue curves give the numerical evolution of the classical background fields from various initial random points in field-space, whose dynamics are governed by equations (6.13), (6.14), (6.15) and (6.16). The field lines are shown to converge towards the red dashed line $\theta_{\rm inf}$, which is the analytical inflationary attractor solution given by equation (6.12). We use the following parameters ($\lambda = 0.1,\ \alpha = 10^{-2},\ \beta = 10^{-3}$), and the field values ($X_b, \sqrt{2}\Phi_b$) are given in units of $M_{\rm P}$.

6.4 Symmetry breaking

As far as we are only interested in the situation where both fields have broken symmetry in order to correspond to observations, then $v \equiv \sqrt{2}\langle\Phi\rangle$ is fixed by the SM Higgs vacuum expectation value (VEV) equal to 246 GeV [147], and we can write the following formula for any non-zero VEV of the inflaton field, $v_X \equiv \langle X\rangle$ [46–48]:

$$v_X = \pm\sqrt{\frac{\mu_X^2 + 2\alpha v^2}{\beta + \frac{4\alpha^2}{\lambda}}} = \pm v\sqrt{\frac{\lambda}{2\alpha}}, \tag{6.17}$$

which is evaluated by solving for the inflaton field value at the minimum of its potential, $V_\Phi(v, v_X) = 0$. The vacuum angle, defined as the angle of rotation of the vacuum with respect to the gauge basis $(h, \chi) = (\sqrt{2}\Phi - v, X - v_X)$ is given by

$$\tan\theta_{\rm V} \equiv \frac{v}{v_X} = \sqrt{\frac{2\alpha}{\lambda}}. \tag{6.18}$$

6.5 Mass basis

By definition, the mass basis $(\tilde{\chi}, \tilde{h})$ diagonalises the matrix of second derivatives of the gauge fields, evaluated at their VEVs:

$$M = \left(\tilde{\chi}, \tilde{h}\right) \begin{pmatrix} V_{XX} & \frac{V_{X\Phi}}{\sqrt{2}} \\ \frac{V_{\Phi X}}{\sqrt{2}} & \frac{V_{\Phi\Phi}}{2} \end{pmatrix} \begin{pmatrix} \tilde{\chi} \\ \tilde{h} \end{pmatrix} = \begin{pmatrix} m_\chi^2 & 0 \\ 0 & m_h^2 \end{pmatrix}, \tag{6.19}$$

$$\text{where } \begin{pmatrix} V_{XX} & \frac{V_{X\Phi}}{\sqrt{2}} \\ \frac{V_{\Phi X}}{\sqrt{2}} & \frac{V_{\Phi\Phi}}{2} \end{pmatrix} = \begin{pmatrix} \frac{3v^2\beta\lambda}{2\alpha} + 4v^2\alpha - \mu_X^2 & -2\sqrt{2\alpha\lambda} \\ -2\sqrt{2\alpha\lambda} & 2v^2\lambda \end{pmatrix}. \tag{6.20}$$

The mass basis is rotated with respect to the gauge basis $(h, \chi) \equiv (\sqrt{2}\Phi - v, X - v_X)$,

$$\begin{aligned} \tilde{h} &= h\cos\theta_{\rm m} - \chi\sin\theta_{\rm m}, \\ \tilde{\chi} &= \chi\cos\theta_{\rm m} + h\sin\theta_{\rm m}. \end{aligned} \tag{6.21}$$

by mixing angle[5] [43, 46–48]

$$\theta_{\rm m} = \theta_{\rm V}\,\frac{2\alpha}{2\alpha - \beta}. \tag{6.22}$$

The eigenvalues of M are the masses of the physical inflaton and Higgs states (i.e. the excitations of the fields on top of the vacua in the mass basis) that are generated post spontaneous symmetry breaking [43, 46–48]:

$$m_{\rm h} = \sqrt{2\lambda}v, \qquad m_\chi = m_{\rm h}\sqrt{\frac{\beta}{2\alpha}}. \tag{6.23}$$

The measurement of $m_{\rm h} = 125$ GeV [147] constrains the SM Higgs boson self coupling $\lambda \simeq 0.1$. Later we will analyse separately the 'light' inflaton parameter space, $m_\chi \ll 2m_h$ ($\equiv (\beta \ll 8\alpha)$), and the 'heavy' inflaton parameter space, $m_\chi > 2m_h$ ($\equiv (\beta > 8\alpha)$), since they define regions where the universe reheats via different mechanisms.

6.6 Domain wall problem

As the inflaton potential is Z_2 symmetric, the field resides in one of two degenerate vacua states post spontaneous symmetry breaking:

$$v_X = \pm\frac{\mu_X}{\sqrt{\beta + \frac{4\alpha^2}{\lambda}}}, \tag{6.24}$$

[5] $\theta_{\rm m}$ reduces to the angle given in [46–48] in the limiting case of light inflaton, where $\beta \ll 8\alpha$.

at temperatures exceeding the EW symmetry breaking scale, when $\langle\Phi\rangle = 0$. Regions where fields occupy the same vacuum state form bubbles, which are separated by those with a different vacuum state by problematic topological defects called domain walls. In the case of degenerate vacuum states, the domain wall bubbles are stable and pressureless, and expand under their own surface tension until there is roughly one wall per horizon scale, where they remain and dominate the universe's energy density. In order for our model to be consistent with cosmology, we therefore need to destablise the domain walls. This can be achieved by softly breaking the Z_2 symmetry of the model with the addition of a cubic term, μX^3, thereby making one vacuum state more energetically favourable:

$$V(X, \Phi = 0) = \left(\frac{\beta}{4} + \frac{\alpha^2}{\lambda}\right) X^4 - \frac{\mu_X^2}{2} X^2 + \mu X^3, \tag{6.25}$$

where the energy density difference between the two vacua is

$$\delta V = V(+v_X) - V(-v_X) \approx 2\mu v_X^3. \tag{6.26}$$

The energy of a domain wall bubble of radius R and surface tension σ is

$$E_{\mathrm{b}}(R) = -\frac{4}{3}\pi R^3 \delta V + 4\pi R^2 \sigma. \tag{6.27}$$

For the domain wall bubbles to collapse we require the pressure exerted on the wall by the difference in energy density between the two vacua to exceed the surface tension of the bubble [227], which is satisfied when

$$\begin{aligned} \delta E_{\mathrm{b}} =& E_{\mathrm{b}}(R - \delta R) - E_{\mathrm{b}}(R) > 0, \\ \rightarrow \delta V >& \frac{2\sigma}{R}, \end{aligned} \tag{6.28}$$

where the surface energy density is [228]

$$\sigma \sim \frac{2\sqrt{2}}{3}\left(\beta + \frac{4\alpha^2}{\lambda}\right)^{\frac{1}{2}} v_X^3, \tag{6.29}$$

assuming the width of the bubble wall is negligible in comparison to its radius, R. If the domain walls expand to the maximum scale, their curvature is of the order of the Hubble horizon [229],

$$R \sim \frac{1}{H} = \sqrt{\frac{90}{\pi^2 g_{\mathrm{SM}}}} \frac{M_{\mathrm{P}}}{T^2}. \tag{6.30}$$

We require inequality (6.28) to be true at the moment spontaneous symmetry breaking occurs, so that the walls immediately collapse before they affect the evolution of the universe.

The inflationary potential at finite temperatures includes an additional term called the thermal mass,

$$V_T(X) = \frac{m_T^2}{2} X^2, \tag{6.31}$$

the dominant contributions to which are [228]

$$m_T^2 \sim \left(\frac{\beta}{4} + \frac{\alpha^2}{\lambda}\right) T^2. \tag{6.32}$$

The universe transitions to its broken symmetric phase once the squared inflaton mass is negative, i.e. when the thermal mass contribution is subdominant to the negative bare mass term, which occurs once the universe has cooled below the critical temperature

$$T_c \sim 2v_X. \tag{6.33}$$

Using (6.28), we then evaluate the lower bound on the inflaton cubic coupling, $\mu_{\min}$, to ensure the immediate collapse of the domain walls at the moment the inflaton sector's symmetry is spontaneously broken:

$$\begin{aligned} \mu > \mu_{\min} &= \sqrt{\frac{4\pi^2 g_{\rm SM}}{405}} \left(\beta + \frac{4\alpha^2}{\lambda}\right)^{\frac{1}{2}} \frac{T_c^2}{M_{\rm P}}, \\ &= \sqrt{\frac{16\pi^2 g_{\rm SM}}{405}} \frac{v^2}{M_{\rm P}} \left(\frac{\beta\lambda^2}{\alpha^2} + 4\lambda\right)^{\frac{1}{2}}, \\ &\sim 1.55 \times 10^{-13} \left(\frac{g_{\rm SM}}{100}\right)^{\frac{1}{2}} \left(\frac{\beta\lambda^2}{\alpha^2} + 4\lambda\right)^{\frac{1}{2}} \text{ GeV}. \end{aligned} \tag{6.34}$$

To ensure the addition of the cubic term doesn't influence the reheating dynamics, we require the cubic coupling contribution to the three-inflaton scatterings on top of the vacuum to be small compared to that of the quartic coupling post symmetry breaking. Additionally we require the cubic coupling's contribution to the inflaton mass to be negligible,

$$\begin{aligned} \frac{\partial^2 V}{\partial X^2}\Big|_{X=v_X, \sqrt{2}H=v} &= 3\beta v_X^2 - \mu_X^2 - 2\alpha v^2 + \frac{12\alpha^2}{\lambda} v_X^2 + 6\mu v_X, \\ &= \left(2\beta + \frac{4\alpha^2}{\lambda}\right) v_X^2 + 6\mu v_X. \end{aligned} \tag{6.35}$$

Since $\beta > \alpha^2/\lambda$, both of these requirements are satisfied when

$$\beta v_X \gg \mu, \tag{6.36}$$

from which we obtain the following upper bound on μ:

$$\mu < \mu_{\max} = O(10^{-2}) \times \beta v \sqrt{\frac{\lambda}{2\alpha}}. \tag{6.37}$$

The cubic coupling does not have any one-loop corrections to the running of the inflaton quartic self-coupling, which has the beta function

$$\beta_\beta = N_1 \beta^2 + N_2 \beta\alpha + N_3 \alpha^2, \tag{6.38}$$

where N_i are numerical factors. The one-loop beta function of the cubic coupling is

$$\beta_\mu = N_1 \mu\beta + N_2 \mu\alpha. \tag{6.39}$$

In sections 6.8 and 6.9, we determine the $\beta - \alpha$ parameter space of the model that has successful inflation and reheating, and find that $\beta \leq O(10^{-9})$ and $\alpha \leq O(10^{-5})$. The cubic coupling therefore remains small and the theory is self-consistent at all energy scales. We will evaluate the allowed range of μ using the bounds defined by (6.34) and (6.37).

6.7 Preheating

Following the inflationary epoch, which is terminated by the violation of the slow-roll conditions once $X_b = O(M_{\rm P})$, is a period of non-perturbative particle production called preheating. In this section we study inflationary attractor misalignment and parametric resonance preheating, and show that neither mechanism efficiently transfers inflationary energy into the SM sector. The non-thermal inflaton distribution resulting from parametric resonance provides us with the initial condition for the reheating study in sections 6.8 and 6.9.

6.7.1 Inflationary attractor misalignment

Prior to the transfer of inflationary energy into excitations of the inflaton and Higgs fields, the inflaton's quartic self-coupling dominates the potential, and so the classical equation of motion of the inflaton background field is well approximated by

$$\ddot{X}_b + 3H\dot{X}_b + \beta X_b^3 = 0, \tag{6.40}$$

where the Hubble expansion rate is

$$H^2 \simeq \frac{1}{3M_{\rm P}^2}\left(\frac{1}{2}\dot{X}_b^{\,2} + \frac{\beta}{4}X_b^4\right), \tag{6.41}$$

and $M_{\rm P}$ is the reduced Planck mass. At the end of inflation the Hubble friction term, $3H\dot{X}$, is subdominant to the kinetic term, $\ddot{X}$, in (6.40), and so the inflaton background field rolls to the minimum of its potential. Whilst the amplitude of the zero mode inflatons greatly exceeds its VEV, the field homogeneously oscillates about the origin along the direction of the inflationary attractor, as shown by the blue curves in Figure 6.3. The initial amplitude[6] of the inflaton field after inflation ($\mathbf{X}_{b,0} \sim 0.1 M_{\rm P}$ [230]) is damped by Hubble expansion and asymptotically approaches [230]

$$\mathbf{X}_b(t) \approx \frac{1}{\sqrt{t}} \left(\frac{3M_{\rm P}^2}{\beta} \right)^{\frac{1}{4}} \propto a^{-1}, \tag{6.42}$$

in the limit $t \to \infty$. The full solution of X_b is a function of the elliptical cosine[7] [230],

$$X_b(t) = \mathbf{X}_b(t)\ cn\left(x - x_0, \frac{1}{\sqrt{2}} \right) \tag{6.45}$$

where $x \equiv 2\left(3\beta M_{\rm P}^2\right)^{\frac{1}{4}} \sqrt{t}$ and $x_0 \approx 2.44$. Note that the energy density of the field is proportional to a^{-4}, and so it decreases at the same rate as the radiation energy density given in (2.26). Once the amplitude is sufficiently damped by Hubble expansion and particle production, symmetry is spontaneously broken and the fields oscillate on top of the vacuum along the direction of the inflationary attractor. For a light inflaton ($\beta \ll 8\alpha$) the angle of the inflationary attractor (6.12) aligns with the angle of rotation of the vacua (6.17), so preheating proceeds with the total inflationary energy residing in the oscillations of the inflaton field. However, for a heavy inflaton ($\beta > 8\alpha$) the angle of the inflationary attractor is misaligned with the angle of rotation of the vacua. As a result, Figure 6.3 shows that the direction of field oscillations on top of the vacuum, given by the double headed black arrow, is misaligned with the inflaton-like direction of the vacuum, given by the red dashed-line, and therefore some of the inflationary energy is deposited in oscillations of the Higgs field.

[6] Here we use bold font to denote the amplitude of the inflaton field, not a vector quantity.

[7] The Jacobi elliptical cosine function is

$$cn(u,k) = \cos\left(\mathrm{amp}(u,k)\right), \tag{6.43}$$

where the Jacobi amplitude is $\mathrm{amp}(u,k) = F^{-1}(u,k)$, and $F^{-1}(u,k)$ is inverse of the elliptic integral:

$$F(u,k) = \int_0^u \frac{\mathrm{d}t}{\sqrt{1-k^2\sin^2 t}}. \tag{6.44}$$

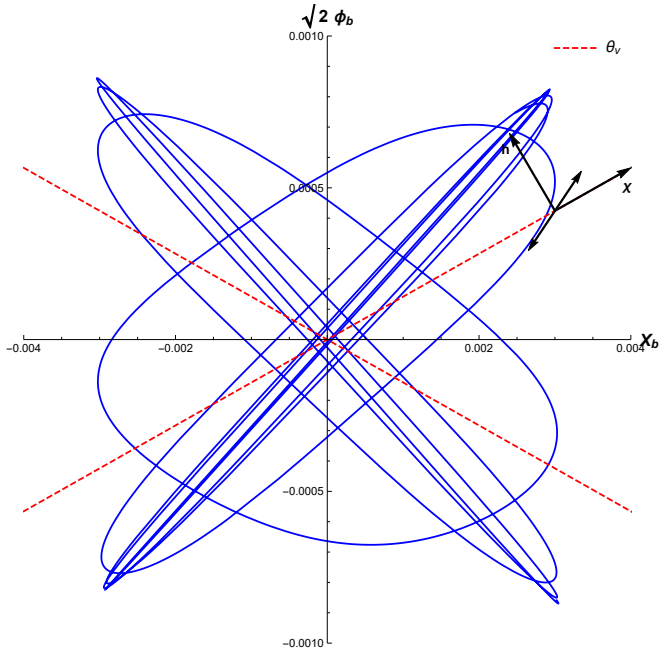

Figure 6.3: Field oscillations at preheating

Blue lines (numerical results) show the oscillations of the fields above their VEVs along the direction of the inflationary attractor, given by equation (6.12). The red dashed lines are the angles of rotation of the vacua, given by equation (6.17). The double headed black arrow gives the direction of the field oscillations on top of the vacuum after inflation, which is in the direction of the inflationary attractor solution. As the direction of the field oscillations are misaligned with the angle of rotation of the vacua, some of the inflationary energy is deposited in the Higgs direction. We use the following parameters: $\lambda = 0.1,\ \alpha = 10^{-2},\ \beta = 10^{-3}$, and the field values are given in units of $M_{\rm P}$.

We can approximate the magnitude of the energy transferred into the SM as a result of the misalignment of the inflationary attractor with the vacua by evaluating the ratio of the inflaton to Higgs fields' energy densities (for simplicity we take $\alpha \ll \beta$, so the Higgs field in the vacuum (6.17) is negligible compared to its value along the inflationary attractor (6.12)):

$$\frac{\rho_X}{\rho_\Phi} \sim \frac{\beta X^4}{\lambda \Phi^4} \sim O\left(\frac{\lambda}{\beta}\right) \sim O(10^8 - 10^{12}). \tag{6.46}$$

Therefore, this mechanism does not transfer noticeable energy into the Higgs-like direction during the early stages of preheating.

6.7.2 Parametric resonance

The preheating stage continues with energy transfer from oscillations of the zero mode into quantum excitations of the Higgs and inflaton fields via the Higgs portal coupling, $2\alpha X^2 \Phi\Phi^\dagger$, and the inflaton self-coupling, $\beta/4X^4$, respectively. During the period which defines preheating, this process is enhanced by a non-stochastic production mechanism called parametric resonance as a result of the periodically varying energy source that is our classical background inflaton [46]. To investigate this effect, we use the Heisenberg representation for the quantum fields,

which for the inflaton field is given by

$$\chi(t,\mathbf{x}) = \frac{1}{(2\pi)^{\frac{3}{2}}}\int \mathrm{d}^3\mathbf{k}\left(\hat{a}_k\chi_k(t)e^{-i\mathbf{k}.\mathbf{x}} + \hat{a}_k^\dagger\chi_k(t)e^{i\mathbf{k}.\mathbf{x}}\right), \tag{6.47}$$

where $\hat{a}_k$ and $\hat{a}_k^\dagger$ are annihilation and creation operators and k is the conformal momentum. The equation of motion of the temporal eigenmodes, $\chi_k(t)$, is then [230]

$$\ddot{\chi_k} + 3H\dot{\chi_k} + \left(\frac{k^2}{a^2} + 3\beta X_b^2(t)\right)\chi_k(t) = 0. \tag{6.48}$$

To simplify (6.48), we remove the field's dependence on the expansion of the universe through a conformal transformation, $\chi_k(t) \to X_k(t)/a(t)$, thereby reducing the problem to an equivalent one in Minkowski space-time [230],

$$X_k'' + \omega_k^2 X_k = 0, \tag{6.49}$$

where $X_k'' \equiv \frac{\partial^2 X_k}{\partial x^2}$. The conformal eigenmodes, X_k, oscillate with frequency [230]

$$\omega_k^2 = \kappa^2 + 3cn\left(x - x_0, \frac{1}{\sqrt{2}}\right), \tag{6.50}$$

where κ is the conformal momentum rescaled by $\tilde{\mathbf{X}}_b(t) = a(t)\mathbf{X}_b(t)$ and the inflaton self-coupling [230]:

$$\kappa^2 = \frac{k^2}{\beta\tilde{\mathbf{X}}_b^2}. \tag{6.51}$$

A defining feature of the X_k is that they oscillate with a frequency, ω_k, that varies periodically with the frequency of the zero-mode oscillations. Equation (6.49) therefore has the same form as the Mathieu equation, which has exponentially unstable solutions for modes with momenta that lie within the resonance bands. Physically, this corresponds to the exponential production of inflaton particles to occupy a highly non-thermal infra-red distribution function. However, since the resonance bands are narrow, the exponential production of particles is halted fairly promptly [230] due to the decaying amplitude of the zero-mode, as a result of the energy lost through particle production, and backreaction effects, which give an effective mass to the inflaton particles ($m_{\mathrm{eff}}^2 \sim 3\beta\langle\chi^2\rangle$). These two effects cause the position of the resonance bands to shift, thereby preventing the growth of the initial resonant modes [230]. However, it is the rescattering of particles out of their resonance bands that terminates parametric resonance all together. This becomes effective once the comoving number density of the particles, n_k, is of the order of the reciprocal of their self-coupling, which for inflatons is $n_k \sim \beta^{-1}$. It is for this reason that parametric enhancement can not take effect in transferring energy into

Higgs particles, since they promptly re-scatter from their resonance bands due to their large self-coupling, $\lambda \gg \alpha$ [230–232].

Rescattering of inflatons from their resonance bands becomes significant once roughly half of the energy of the inflaton condensate has been transferred, after which the inflaton enters a phase of free-turbulence. During this period the inflaton distribution evolves self-similarly towards thermalisation, and so the following ansatz is used [232, 233]:

$$f_\chi(k,\tau) = \tau^{-q} f_{\chi,0}(k\tau^{-p}); \tag{6.52}$$

$\tau = t/t_0$ is a dimensionless time scale, where t_0 is some arbitrarily late time, and k is conformal momentum. Exponent p is related to the number of m-particle scatterings by [232]

$$p = \frac{1}{2m-1} = \begin{cases} \frac{1}{5}, & m = 3 \\ \frac{1}{7}, & m = 4 \end{cases} \tag{6.53}$$

and exponent $q \approx 3.5p$ is approximated numerically using lattice simulations [232]. Comparative analysis of lattice simulations with wave kinetic theory verify that particle interactions with the zero-mode are important for most of the free-turbulence period, and so the evolution of the inflaton towards thermalisation is primarily driven by three-particle scatterings ($p = 1/5$). Only at later times, once the majority of the energy in the zero-mode has been transferred into excitations of the field, do four-particle scatterings ($p = 1/7$) dominate the evolution [232, 233].

The momentum distribution follows a power law at low momenta, k^{-s}, with exponent [232]

$$s = d - \frac{m}{m-1} = \begin{cases} \frac{3}{2}, & m = 3 \\ \frac{5}{3}, & m = 4 \end{cases} \tag{6.54}$$

where $d = 3$ is the number of spatial dimensions. Larger momenta are bounded by an ultraviolet cut-off [232, 233], which we will model in the form of an exponential function, parameterised by k_0:

$$f_\chi(k,t) = \left(\frac{t}{t_0}\right)^{-q} \left(\frac{k}{k_0}\left(\frac{t}{t_0}\right)^{-p}\right)^{-s} \times \exp\left[-\frac{k}{k_0}\left(\frac{t}{t_0}\right)^{-p}\right]. \tag{6.55}$$

Our analysis proceeds in the perturbative reheating period, during the later stages of thermalisation, from $t \sim t_0$. Once the Hubble expansion rate has decreased to the order of the inflaton decay width, the inflaton can efficiently transfer its energy into the SM via the Higgs portal. Light inflaton ($m_\chi \ll 2m_h$) and heavy inflaton ($m_\chi > 2m_h$) have different kinetmatically favourable reheating mechanisms, therefore we carry out the analysis of these two regimes

separately.

6.8 Reheating: light inflaton ($m_\chi \ll 2m_h$)

Here we review the reheating analysis carried out in the previous works [45–48] that focus on the region of parameters with the inflaton mass below the Higgs boson mass.

The dominant reheating mechanism for a light inflaton in the EW restored symmetry regime ($\Phi = 0$) is the two-to-two scattering process $\chi\chi \to hh/\varphi_i\varphi_i$ [46, 47], with an amplitude of

$$\begin{aligned} V(X,\Phi) &\supset -\alpha\left(h^2+\varphi_1^2+\varphi_2^2+\varphi_3^2\right)\chi^2, \\ &\to |M_{\chi\chi\to hh/\varphi_i\varphi_i}| = 4\alpha; \end{aligned} \tag{6.56}$$

where the combinatorial factor $2\cdot 2$ accounts for the 2 identical particles in the initial and final state. The total cross-section of the two-to-two scattering process is

$$\sigma_{\rm SM} = \sigma_{\chi\chi\to hh} + \sum_{i=1}^{3}\sigma_{\chi\chi\to\varphi_i\varphi_i} \sim \frac{\alpha^2}{\pi p_{\rm avg}^2},$$

where $p_{\rm avg}$ is the average momentum of the inflaton. The universe reheats when the mean free path of the inflaton,

$$\Gamma_{\rm SM}(T) \sim n_\chi \sigma_{\rm SM}, \tag{6.57}$$

is comparable with the Hubble expansion rate, $\Gamma_{\rm SM}(T_{\rm reh}) \sim H(T_{\rm reh})$. If we first assume that the inflaton is in thermal equilibrium at the time of reheating, then a thermal estimate of the reheating temperature can be found analytically using the number density for a thermal, relativistic inflaton, given by equation (2.32), with $g_\chi = 1$, and $p_{\rm avg} \sim T$ [44, 46]:

$$T_{\rm reh,T} \sim \frac{\zeta(3)\alpha^2}{\pi^4}\sqrt{\frac{90}{g_*}}M_{\rm P}; \tag{6.58}$$

the total number of effective degrees of freedom is $g_* = g_{\rm SM} + g_\chi \sim 10^2$. We require the reheating temperature to exceed the EW symmetry breaking scale, $T_{\rm EW} = 160$ GeV [68], so that the BAU can be produced via EW sphaleron processes. In the thermal limit, the minimum reheating temperature translates to the following lower bound on α [44, 46]:

$$\alpha > \alpha_{\rm min,T} \approx \left(\frac{\pi^4}{\zeta(3)}\sqrt{\frac{g_{\rm SM}}{90}}\frac{T_{\rm EW}}{M_{\rm P}}\right)^{\frac{1}{2}} \sim 7.5\times 10^{-8}. \tag{6.59}$$

However, since the inflaton distribution slowly evolves self-similarly toward thermal equilibrium [232, 233], a better approximation of the reheating temperature assumes a non-thermal

inflaton, which has an average momentum suppressed with respect to the thermal estimate, $p_{\rm avg} \sim T$:

$$\frac{p_{\rm avg}}{T} = \left(\frac{M_{\rm P}}{T}\right)^{p} \beta^{\frac{1+p}{4}}. \tag{6.60}$$

As a result, the inflaton number density and cross-section are enhanced with respect to their thermal estimates by factors $(T/p_{\rm avg})$ and $(T/p_{\rm avg})^2$ respectively, thereby increasing the thermal approximation of the reheating temperature (6.58) by a factor of $(T/p_{\rm avg})^3$. This gives the more realistic non-thermal estimate of the lower bound on α [44, 46],

$$\alpha > \alpha_{\rm min} \approx \left(\frac{M_{\rm P}}{T_{\rm EW}}\right)^{\frac{3p}{2}} \left(\frac{\pi^4}{\zeta(3)}\sqrt{\frac{g_{\rm SM}}{90}}\frac{T_{\rm EW}}{M_{\rm P}}\right)^{\frac{1}{2}} \beta^{\frac{3(1+p)}{8}} \sim (1.6\times 10^{-9}) \left(\frac{\beta}{10^{-12}}\right)^{\frac{3}{7}}, \tag{6.61}$$

where $g_{\rm SM} \sim 100$, and we take $p = 1/7$ to evaluate the most conservative bound to use in our analysis.

Additionally, to ensure quantum corrections to the inflaton's quartic self-coupling are sufficiently small and the inflationary analysis above holds, we require $\alpha^2 < 0.1\beta$ [45], leading to

$$\alpha < \alpha_{\rm max} = (0.1\beta)^{\frac{1}{2}}. \tag{6.62}$$

6.8.1 Analytical results

The $\beta - \alpha$ parameter space is fully closed by cosmological constraints, which determine the allowed range of β given in (6.9); and the reheating and inflationary constraints, which determine the upper and lower bounds of α given by (6.61) and (6.62) respectively. The results are summarised in Table 6.1 [44].

β	α
10^{-9}	$(3.1\times 10^{-8}) - (1.0\times 10^{-5})$
10^{-10}	$(1.1\times 10^{-8}) - (3.2\times 10^{-6})$
10^{-11}	$(4.2\times 10^{-9}) - (1.0\times 10^{-6})$
10^{-12}	$(1.6\times 10^{-9}) - (3.2\times 10^{-7})$

Table 6.1: Light inflaton $\beta - \alpha$ parameter space that allows for successful inflation and reheating. $\lambda \simeq 0.1$ is constrained by the measurement of the SM Higgs boson mass [147].

For non-thermal inflaton, (6.58) and (6.60) are used to estimate the reheating temperature,

$$\begin{aligned} T_{\rm reh} &\sim \left(\frac{T}{p_{\rm avg}}\right)^3 T_{\rm reh,T}, \\ &\sim \left(\frac{T_{\rm reh}}{M_{\rm P}}\right)^{\frac{3}{7}} \beta^{-\frac{6}{7}} \frac{\zeta(3)\alpha^2}{\pi^4}\sqrt{\frac{90}{g_*}} M_{\rm P}; \end{aligned} \tag{6.63}$$

then substituting in for $\alpha_{\min}$ using equation (6.61), the reheating temperatures within the bounds of the parameter space stated in Table 6.1 are [44]

$$\begin{aligned} T_{\rm reh} &\sim \left(\frac{\alpha}{\alpha_{\min}}\right)^{\frac{7}{2}} T_{\rm EW}, \\ &= O(T_{\rm EW} - 10^{10}) \text{ GeV}. \end{aligned} \tag{6.64}$$

The inflaton mass, given by equation (6.23), is inversely proportional to α, and so is bounded from below by $\alpha_{\max}$ and from above by $\alpha_{\min}$:

$$m_\chi \sim \left[0.16\left(\frac{\beta}{10^{-12}}\right)^{\frac{1}{4}} - 2.2\left(\frac{\beta}{10^{-12}}\right)^{\frac{2}{7}}\right] \text{ GeV}. \tag{6.65}$$

The range of the trilinear inflaton self-coupling, μ, is bounded by the constraints (6.34) and (6.37), which ensure μ is large enough to prevent domain walls forming and small enough to not significantly alter the reheating dynamics and inflaton mass. In Table 6.2 we evaluate the allowed range of μ using the bounds on light inflaton parameter space given in Table 6.1.

β	$\mu_{\min}(\alpha_{\min}) - \mu_{\max}(\alpha_{\min})$ [GeV]	$\mu_{\min}(\alpha_{\max}) - \mu_{\max}(\alpha_{\max})$ [GeV]
10^{-9}	$O(10^{-11} - 10^{-6})$	$O(10^{-13} - 10^{-7})$
10^{-10}	$O(10^{-11} - 10^{-6})$	$O(10^{-13} - 10^{-8})$
10^{-11}	$O(10^{-11} - 10^{-7})$	$O(10^{-13} - 10^{-8})$
10^{-12}	$O(10^{-11} - 10^{-8})$	$O(10^{-13} - 10^{-9})$

Table 6.2: Light inflaton trilinear coupling

Allowed range of the trilinear inflaton coupling, μ, in the light inflaton parameter space, where $\lambda \sim 0.1$ and the allowed ranges of β and α are given in Table 6.1. $\mu_{\min}$ is the lower bound to ensure the immediate collapse of the domain walls at the time of the phase transition, and $\mu_{\max}$ is the upper bound to ensure the coupling is small enough so that inflationary and reheating dynamics are not affected.

6.8.2 Light inflaton search

The light inflaton can be produced via rare meson decays. The most sensitive bound on the light inflaton parameter space is from searches for invisible scalars produced via kaon decay [234, 235], $K^\pm \to \pi^\pm \chi$, for inflaton with mass in the kinematically viable region $m_\chi \lesssim 0.3$ GeV. Having applied the necessary constraints for inflation and reheating to our model, equation (6.65) shows that the inflaton is only light enough when $\beta = \left(10^{-12} - 10^{-11}\right)$. Due to a discrepancy between the $K^+ \to \pi^+ \chi$ amplitude given in [236] and [47, 237–239], we carry out the calculation in the Appendix. First, at the free-quark level, we obtain the amplitude of the weak-contribution to the quark self-energy, where the flavour-changing neutral current ($s \to d$) is mediated by the W-boson or Faddeev-Popov unphysical scalar (Φ^+), and an internal quark

line [238, 239]. The largest contribution to the $K^+ \to \pi^+\chi$ amplitude is from the internal quark radiating a Higgs boson that then mixes with an inflaton [47, 239], as shown by Figure 6.4. As we can presume a soft Higgs boson emission, we approximate the Higgs as an external field [239].

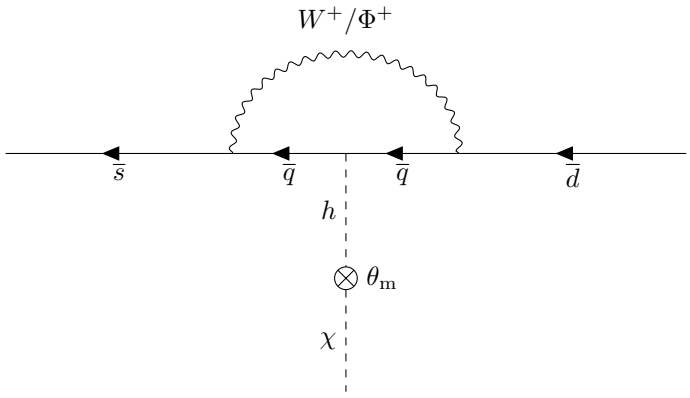

Figure 6.4: Quark-level process of dominant contribution to $K^+ \to \pi^+\chi$.

Quark-level process of $K^+ \to \pi^+\chi$. The neutral quark current ($\bar{s} \to \bar{d}$) changes flavour via the W boson (W^+) or unphysical scalar (Φ^+) loop. The Higgs boson (h) is emitted from the internal quark, which then mixes to produce an inflaton particle (χ).

The subdominant contributions to the $K^+ \to \pi^+\chi$ amplitude from the above flavour-changing neutral current process [47, 239, 240] are given below in Figure 6.5.

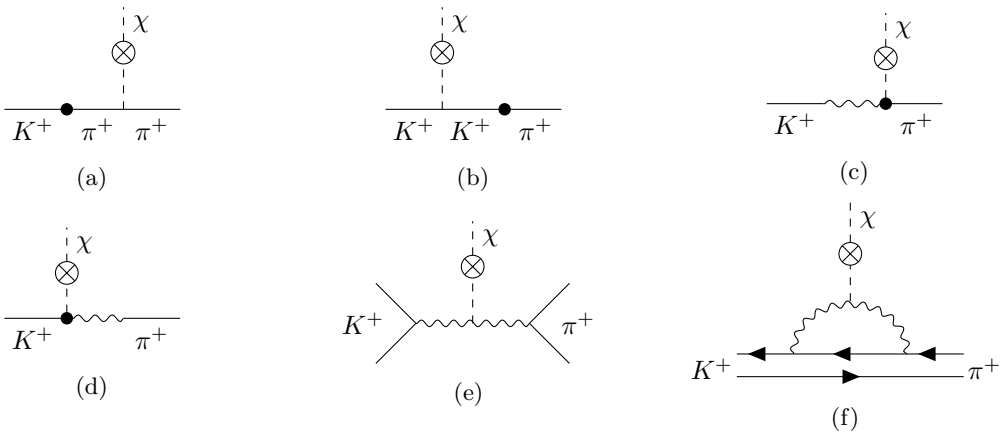

Figure 6.5: Sub-dominant contributions to $K^+ \to \pi^+\chi$.

The sub-dominant contributions to $K^+ \to \pi^+\chi$ amplitude [240]. The wavy line represents the W^+/Φ^+ boson, the filled dot denotes an effective vertex and the crossed dot denotes the Higgs boson (h) mixing into an inflaton (χ). Figures 6.5a and 6.5b are pole diagrams, which at quark-level is the emission of a Higgs boson from the bound-state quarks of π^+ and K^+ respectively. Figures 6.5c-6.5e are non-spectator diagrams. In Figures 6.5c and 6.5d the effective $\pi^+hW^+(\Phi^+)$ and $K^+hW^+(\Phi^+)$ vertices denote the contribution from the heavy quark traingle diagram with external gluons, see [240] for details. Figure 6.5f is the one-loop spectator diagram.

We do not include the contributions from the subdominant processes in our analysis.

Next we implement chiral perturbation theory [241–243] to obtain the meson interaction amplitude from the free-quark approximation [238, 239]. Our calculation reproduces the result

given in [47, 237–239], which gives the following branching ratio of $K^+ \to \pi^+\chi$,

$$\mathrm{Br}(K^+ \to \pi^+\chi) = \frac{\Gamma(K^+ \to \pi^+\chi)}{\Gamma_{\mathrm{total}}(K^+)} \approx 1.3 \times 10^{-3} \left(\frac{2|\mathbf{p}_\chi|}{M_K} \right) \theta_{\mathrm{m}}^2, \tag{6.66}$$

where $\mathbf{p}_\chi$ is the inflaton momentum in the centre of mass frame, M_K is the kaon mass and $\Gamma_{\mathrm{total}}(K_+)$ is the total decay width of K^+.

Figure 6.6 shows regions of the light inflaton parameter space that are excluded by searches for scalars produced via meson decays. The black dashed lines are of constant β, and the region between $\beta = 10^{-12}$ and $\beta = 10^{-9}$ defines the light inflaton parameter space. Lighter inflatons with mass below the muon threshold ($m_\chi \lesssim 2m_\mu$) have a long enough lifetime to decay outside the detector, whilst heavier inflatons have a short enough lifetime to decay within the detector [47]. The main decay channels of inflatons with masses in the range $2m_\mu < m_\chi < 1$ GeV are $\chi \to \mu^-\mu^+/\pi\pi$ [47]. In Figure 6.6 the solid coloured lines are the exclusion plots from searches for invisible scalars [235, 244–246], and the dotted coloured lines are the exclusion plots from searches for scalars that decay visibly within the detector via $\chi \to \mu^-\mu^+$ [247–250]; current bounds from LHCb limits $m_\chi > 1$ GeV.

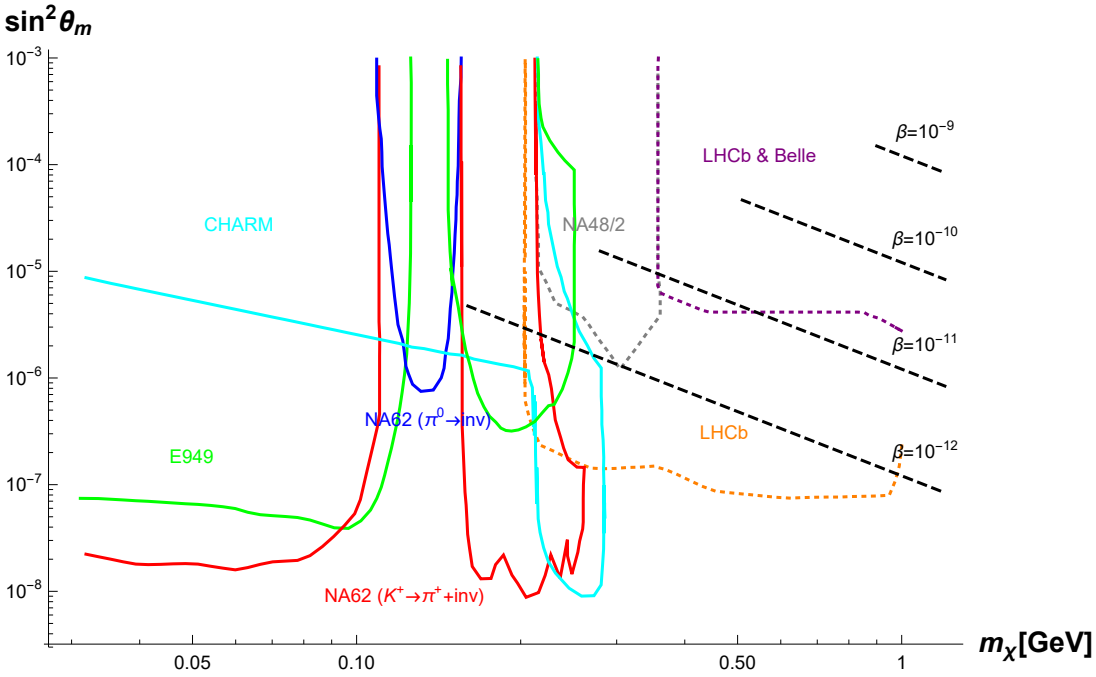

Figure 6.6: Exclusion plot of light inflaton parameter space from searches for invisible scalars produced via meson decay

Plot of the squared inflaton-Higgs mixing angle against inflaton mass. The black dashed lines plot the parameter space for the light inflaton model ($m_\chi \ll m_h$) with given values of the inflaton's quartic self-coupling, $\beta = \left(10^{-12} - 10^{-9}\right)$. The solid coloured lines are exclusion regions from searches for an invisible scalar produced via meson decay. Bounds are given from the following experiments: NA62 ($K^+ \to \pi^+ + \mathrm{inv.}$) in red [235]; NA62 ($\pi_0 \to \mathrm{inv.}$) in blue [244]; E949 in green [245]; CHARM in cyan [246]. The dotted coloured lines are exclusion regions from searches for a visible scalar produced via meson decay, which then decays in the detector via $\chi \to \mu^-\mu^+$. Bounds are given from the following experiments: NA48/2 in grey [247]; LHCb in orange and purple [248, 249]; and Belle in purple [250].

6.9 Reheating: heavy inflaton ($m_\chi > 2m_h$)

In this section we focus on my own work [43], where the inflaton is heavier and the channel of its direct decay to a pair of Higgs bosons is open, which allows for a more efficient reheating.

The dominant reheating process for heavy inflaton ($m_\chi > 2m_\mathrm{h}$) in the restored EW symmetry regime ($\Phi = 0$) is via the decay process $\chi \to hh/\varphi_i\varphi_i$ [43, 46], thereby kinematically bounding α from above:

$$\alpha < \alpha_{\max} = \frac{\beta}{8}. \tag{6.67}$$

The amplitude of the decay process is

$$V(X,h) \supset -2\alpha v_X \left(h^2 + \varphi_1^2 + \varphi_2^2 + \varphi_3^2\right)\chi, \tag{6.68}$$

$$\to |M_{\chi\to hh/\varphi_i\varphi_i}| = 4\alpha v_X, \tag{6.69}$$

where a symmetry factor of 2 accounts for the two identical particles in the final state. The total decay width of the process is

$$\Gamma_{\mathrm{SM}} = \Gamma_{\chi\to hh} + \sum_{i=1}^{3}\Gamma_{\chi\to\varphi_i\varphi_i} = \frac{\beta}{4\pi}\frac{m_h^4}{m_\chi^3}K(T),$$

where the kinematic factor is

$$K(T) = \left(1 - \frac{4m_h^2(T)}{m_\chi^2}\right)^{\frac{1}{2}}. \tag{6.70}$$

The heavy inflaton decays prior to thermalization, when its distribution is highly non-thermal from turbulent preheating. As a result, the reheating temperature can not be well approximated analytically, as in the light inflaton case. Instead, we solve the Boltzmann equations numerically to evaluate the inflaton upper mass bound (and therefore $\alpha_{\min}$), which is provided by ensuring the minimum reheating temperature is greater than the EW symmetry breaking scale.

6.9.1 Boltzmann equations for reheating

Three Boltzmann collision integral equations fully describe the dynamics of the system of particles during reheating [251, 252]:

$$\frac{\mathrm{d}f_\chi}{\mathrm{d}t} = C^{\chi}_{\chi\leftrightarrow hh/\varphi_i\varphi_i} + C_{\chi\chi\leftrightarrow hh/\varphi_i\varphi_i}, \tag{6.71}$$

$$\frac{\mathrm{d}f_{\mathrm{SM}}}{\mathrm{d}t} = C^{\mathrm{SM}}_{\chi\leftrightarrow hh/\varphi_i\varphi_i} + C^{\mathrm{SM}}_{hh/\varphi_i\varphi_i\leftrightarrow\mathrm{SMSM}} + C^{\mathrm{SM}}_{h/\varphi_i\leftrightarrow\mathrm{SMSM}}, \tag{6.72}$$

where φ_i $(i = 1, 2, 3)$ are the EW Goldstone bosons. The rate of particles x scattering in and out of their distribution functions, f_x, is calculated using the quantum collision integral; the standard definition for a general two-to-two scattering process, $a(p)a'(p') \leftrightarrow b(q)b(q')$, with amplitude $M_{aa'\to bb'}$ is

$$C^a_{aa'\leftrightarrow bb'} = \frac{1}{2E^a_p}\int \frac{g_{a'}\,\mathrm{d}^3p'}{2E^{a'}_{p'}(2\pi)^3}\frac{g_b\,\mathrm{d}^3q}{2E^b_q(2\pi)^3}\frac{g_{b'}\,\mathrm{d}^3q'}{2E^{b'}_{q'}(2\pi)^3}(2\pi)^4\delta^4(p+p'-q-q')|M_{aa'\to bb'}|^2 \quad (6.73)$$
$$\Big[f_b(q,t)f_{b'}(q',t)\big(1\pm f_a(p,t)\big)\big(1\pm f_{a'}(p',t)\big)$$
$$- f_a(p,t)f_{a'}(p',t)\big(1\pm f_b(q,t)\big)\big(1\pm f_{b'}(q',t)\big)\Big].$$

E^x_p is the energy of particle x with physical momentum p, and g_x is the number of effective degrees of freedom of particle x. The $(1 \pm f)$ term is to account for the probability that the final state boson $(+)$ or fermion $(-)$ is free to scatter into, which is determined by Bose-Einstein and Fermi-Dirac statistics respectively.

Equations (6.71) and (6.72) are simplified using the following:

- $\Gamma_{\rm SM} \gtrsim O(10^7)\Gamma_{\chi\chi\to hh/\varphi_i\varphi_i}$, so $C_{\chi\chi\leftrightarrow hh/\varphi_i\varphi_i}$, is neglected.
- Number conserving and violating interactions between $W^\pm/Z$ bosons are at rates of at least $O(10^{11})$ times greater than the Hubble expansion rate during reheating. As a result, kinetic and chemical equilibrium are reached very quickly, and so $C^{\rm SM}_{hh/\varphi_i\varphi_i\leftrightarrow \rm SMSM}$ and $C^{\rm SM}_{h/\varphi_i\leftrightarrow \rm SMSM}$ are neglected. Additionally, we assume the SM thermalises instantaneously on production to some temperature $T_{\rm SM}$, and therefore implement the detailed balance condition.
- We verified numerically that the density of inflaton particles at the start of the reheating period (when $\Gamma_{\rm SM} \sim H$) is small, and up until the end of the reheating period, the density of Higgs particles is also small. As a result, we take the classical limit of equation (6.73), where $f \ll 1$, and ignore the $(1 \pm f)$ terms .

The above simplifications reduce the Boltzmann equations (6.71) and (6.72) to [253, 254]

$$\frac{\partial f_\chi(k,t)}{\partial t} = \frac{am_\chi}{\sqrt{(am_\chi)^2+k^2}}\Gamma_{\rm SM}\Big[f^{eq}_\chi(T_{\rm SM}) - f_\chi(k,t)\Big], \quad (6.74)$$

where k is the conformal inflaton momentum. $f^{\rm eq}_\chi(k,t)$ is the Bose-Einstein distribution function of the inflaton thermalised at the SM temperature, $T_{\rm SM}(t)$:

$$f^{eq}_\chi(k,t) = \frac{1}{(2\pi)^3}\frac{1}{\exp\Big[\frac{\sqrt{(am_\chi)^2+k^2}}{aT_{\rm SM}(t)}\Big]-1}. \quad (6.75)$$

The differential equation for $a(t)$ is found using the Friedmann equation for the Hubble

expansion rate:

$$H(t) = \frac{\dot{a}(t)}{a(t)} = \sqrt{\frac{\rho_\chi(t) + \rho_{\rm SM}(t)}{3M_P^2}}; \tag{6.76}$$

where $\dot{a}(t) = \frac{da}{dt}$, $M_{\rm P}$ is the reduced Planck mass and the energy densities of the inflaton and SM are:

$$\rho_\chi(t) = \frac{4\pi g_\chi}{a^4}\int_{k=0}^{\infty} dk\ k^2\sqrt{k^2 + (am_\chi)^2}f_\chi(k,t), \tag{6.77}$$

$$\rho_{\rm SM}(t) = \frac{\pi^2 g_{\rm SM}}{30}T_{\rm SM}^4(t). \tag{6.78}$$

The number of degrees of freedom of the inflaton is $g_\chi = 1$. We take the number of effective degrees of freedom of the SM as constant throughout reheating, at $g_{\rm SM} = 100$.

Next we want to find the differential equation for $T_{\rm SM}$ to replace the Boltzmann equation (6.72), which we derive from the covariant conservation of the energy-momentum tensor given in equation (2.19):

$$\dot{\rho}_T + 3H\left(\rho_T + p_T\right) = 0, \tag{6.79}$$

where T denotes the sum of the inflaton and SM components. The time-derivative of the inflaton energy density,

$$\dot{\rho}_\chi = \frac{d}{dt}\int \frac{\mathrm{d}^3k}{a^3}E_k f_\phi(k,t), \tag{6.80}$$

$$= -3H\left(\rho_\chi + p_\chi\right) + \int \frac{\mathrm{d}^3k}{a^3}E_k\frac{\partial f_\chi(k,t)}{\partial t}, \tag{6.81}$$

is substituted into equation (6.79) to obtain the time-derivative of the SM energy density,

$$\dot{\rho}_{\rm SM} = -3H\left(\rho_{\rm SM} + p_{\rm SM}\right) - \int \frac{\mathrm{d}^3k}{a^3}E_k\frac{\partial f_\chi(k,t)}{\partial t}. \tag{6.82}$$

We then use the relation $p_{\rm SM} = \frac{1}{3}\rho_{\rm SM}$ and substitute equations (6.74) and (6.78) into (6.82) to find the differential equation for $T_{\rm SM}$,

$$\frac{dT_{\rm SM}}{dt} = -HT_{\rm SM} - \frac{30}{g_{\rm SM}\pi(aT_{\rm SM})^3}\int_0^\infty dk\ k^2 m_\chi\Gamma_{\rm SM}\Big[f_\chi^{eq}(T_{\rm SM}) - f_\chi(k,t)\Big]. \tag{6.83}$$

(6.74), (6.76) and (6.83) form a closed set of differential equations.

Next, we solve the Boltzmann equations numerically across the entire inflaton parameter space; here the inflaton mass is constrained, for a given self-coupling, from below by kinematics of the decay and from above by the electroweak symmetry breaking scale.

6.9.2 Numerical results

The non-thermal inflaton distribution resulting from turbulent preheating, detailed in section 6.7.2, provides the initial condition for the reheating study. Motivated by the works carried out in [232, 233], we assume the free turbulent evolution of the inflaton is driven by three particle scatterings up to some moment $t = t_0$, leading to the distribution function (6.55), with $q = 1/5$ and $s = 3/2$,

$$f(k, t_0) = \left(\frac{k}{k_0}\right)^{-\frac{3}{2}} e^{-\frac{k}{k_0}}. \tag{6.84}$$

Starting from a universe filled with only inflaton particles at t_0, the initial Hubble expansion rate is approximated by

$$H(t_0) = \sqrt{\frac{\rho_\chi(t_0)}{3M_{\rm P}^2}} \sim \sqrt{\frac{m_\chi k_0^3}{3M_{\rm P}^2 a(t_0)^3}}. \tag{6.85}$$

The parameter k_0 is chosen so that $H(t_0) \gtrsim \Gamma_{\rm SM}$, i.e. we choose the moment slightly before the inflaton decays. When the Hubble expansion rate has decreased to $H(t) \sim \Gamma_{\rm SM}$, the universe will start to reheat.

In Figure 6.7 we show that a heavy inflaton with self-couplings in the range $O(10^{-12}) \leqslant \beta \leqslant O(10^{-9})$ is constrained to the mass range $(250 < m_\chi \lesssim 7600)$ GeV. The inflaton mass is bounded from below by the kinematics of the decay, $\chi \to hh/gg$, requiring $m_\chi > 2m_{\rm h}$. The inflaton mass is bounded from above by the minimum reheating temperature, which is required to exceed the EW symmetry breaking scale, $T_{\rm EW} = 160$ GeV [68]. Here we define the reheating temperature, $T_{\rm eq}$, as the temperature when the energy densities of the inflaton and the SM are equal. For inflaton that entered thermal equilibrium, we can roughly estimate

$$T_{\rm eq} \propto \sqrt{\Gamma_{\rm SM}} \propto \sqrt{\frac{\beta}{m_\chi^3}}. \tag{6.86}$$

However, the proper equilibrium temperature for inflaton starting from a non-thermal distribution is found by solving the Boltzmann equation numerically.

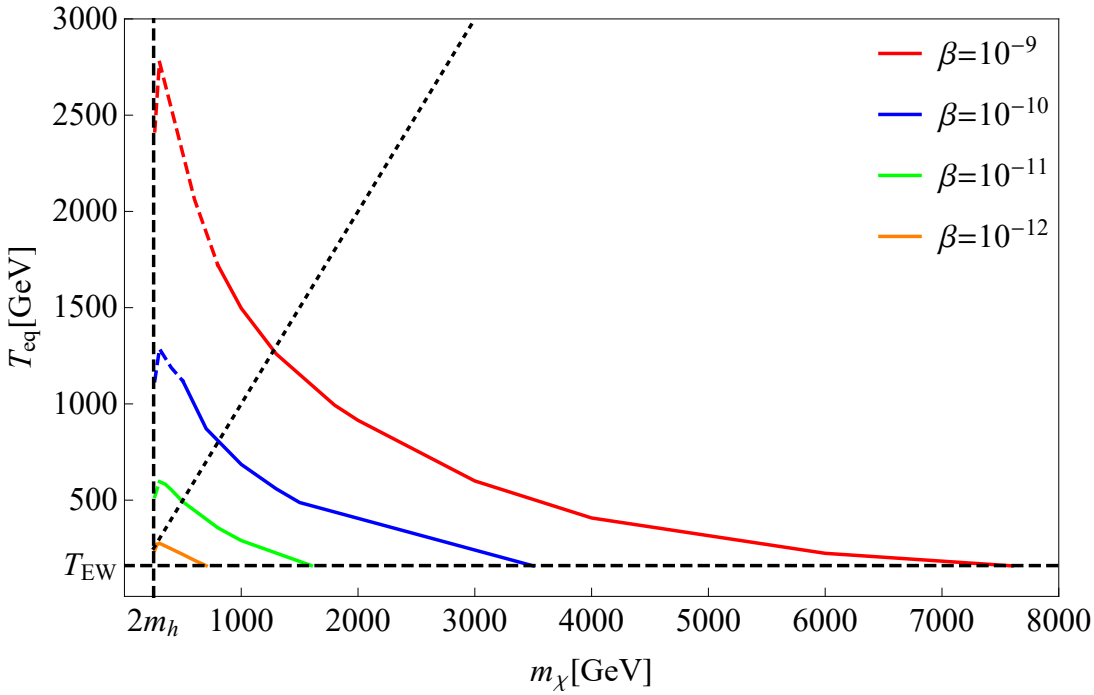

Figure 6.7: Reheating temperature against inflaton mass

Reheating temperature, $T_{\rm eq}$, defined when the energy densities of the SM and inflaton are equal, against the inflaton mass. The black dashed lines give the lower inflaton mass bound, at $2m_{\rm h} = 250$ GeV, and the lower reheating temperature bound at the EW symmetry breaking scale, $T_{\rm EW} = 160$ GeV [68].The diagonal black dotted line plots $T_{\rm eq} = m_\chi$.

The coloured dashed lines in Figure 6.7 give the area of parameter space where we would expect the thermal mass of the Higgs boson in the kinematic term (6.70) to suppress the inflaton decay width. We approximate the region using the leading contributions to the thermal Higgs mass:

$$\begin{aligned} m_h^2(T_{\rm eq}) &\sim \Big(\frac{\lambda}{2} + \frac{g_t^2}{4}\Big) T_{\rm reh}^2 - 2\alpha v_X^2, \\ &\sim \Big(\frac{\lambda}{2} + \frac{g_t^2}{4}\Big) T_{\rm eq}^2 - \lambda v^2, \\ \rightarrow T_{\rm eq} &\gtrsim m_\chi, \end{aligned} \tag{6.87}$$

where the Yukawa top coupling is $g_t \sim 1$. Precise analysis of this region requires a full thermal quantum treatment of the evolution, which is beyond the scope of this thesis, so the precise results here should be treated with caution. As the majority of the parameter space has $T_{\rm reh} < m_\chi$, we take the kinematic factor to be $K(T) = 1$ in our analysis.

Now we have obtained the bounds of the heavy inflaton's parameter space, we evaluate the range of the trilinear inflaton self-coupling that solves the domain wall problem in Table 6.2, using the constraints (6.34) and (6.37).

β	$\mu_{\min}(\alpha_{\min}) - \mu_{\max}(\alpha_{\min})$ [GeV]	$\mu_{\min}(\alpha_{\max}) - \mu_{\max}(\alpha_{\max})$ [GeV]
10^{-9}	$O(10^{-6} - 10^{-3})$	$O(10^{-9} - 10^{-5})$
10^{-10}	$O(10^{-6} - 10^{-4})$	$O(10^{-8} - 10^{-5})$
10^{-11}	$O(10^{-6} - 10^{-5})$	$O(10^{-8} - 10^{-6})$
10^{-12}	$O(10^{-6} - 10^{-5})$	$O(10^{-7} - 10^{-6})$

Table 6.3: Heavy inflaton trilinear coupling

Allowed range of the trilinear inflaton coupling, μ, in the heavy inflaton parameter space. $\mu_{\min}$ is the lower bound to ensure the immediate collapse of the domain walls at the time of the phase transition, and $\mu_{\max}$ is the upper bound required for $m_\chi > 2m_h \equiv \alpha < \beta/8$.

The heavy inflaton parameter space evades all current experimental constraints, due to extremely low mixing of the inflaton with the Higgs sector.

6.10 Discussion and conclusion

We studied a singlet scalar model with a quartic self-interaction and a coupling to the Higgs sector. With the addition of a non-minimal coupling of the scalar field to gravity, this model can successfully produce inflation within CMB bounds of the tensor-to-scalar ratio and the amplitude of primordial scalar perturbations, for self-coupling in the range $\beta = O(10^{-12} - 10^{-9})$. With scale invariance only broken in the scalar sector, the inflaton-Higgs coupling gives rise to symmetry breaking in the Higgs sector and provides the mechanism to initiate reheating.

The parameter space of light inflaton particles ($m_\chi \ll m_h$) is constrained to the mass range ($0.16 \lesssim m_\chi \lesssim 16$) GeV. The inflaton mass is bounded from below by equation (6.62), which ensures radiative corrections to the inflaton's quartic self-coupling from the inflaton-Higgs quartic coupling are small enough to evade spoiling the inflationary potential. The inflaton mass is bounded from above by requiring the universe is efficiently heated above the EW scale via two-to-two inflaton-Higgs scattering. However in addition to cosmological constraints, experimental searches for scalars in meson decays [235, 244–250] further constrain the light inflaton mass range to $m_\chi > 1$ GeV. In the parameter space of heavy inflaton particles ($m_\chi > 2m_h$), the mixing angle with the Higgs sector is very small, thus evading direct experimental constraints. Our analysis restricts the heavy inflaton mass range to ($250 < m_\chi \lesssim 7600$) GeV, by ensuring efficient reheating of the universe above the EW scale, via inflaton decay into two Higgs bosons. We find in both regions of parameter space that we can solve the domain wall problem with the addition of a small trilinear inflaton term, without influencing the inflationary and reheating dynamics.

Let us turn to the limitations of our analysis. First, our results depend on the assumption that the initial heavy inflaton distribution is governed by turbulence driven by 3-particle

scatterings, as suggested in [232, 233]. We assessed the level of influence of these assumptions by comparing the results of the three-particle scattering function to a 4-particle scattering function (the power law distribution k^{-s} in (6.55) with $s = 5/3$ instead of $s = 3/2$) in the non-analytical region of the parameter space. We found a relatively weak dependence on the initial distribution function, with up to a $(10 - 20)\%$ difference between the results. Secondly, we ignored the details of symmetry restoration in the EW sector after preheating, which would require a full thermal field theory treatment. Thus our results for inflaton masses approaching the kinematic limit of decay into two Higgs bosons may be modified by exact study.

A potentially interesting region of inflaton masses could be when $m_\chi \simeq m_\mathrm{h}$, when the mixing angle (8.5) becomes large. However, we expect that reheating in this range is still inefficient. Although this would significantly enhance the inflaton decay rate via inflaton-Higgs mixing, such processes can not contribute to reheating in restored EW symmetry, and $\chi\chi \to hh$ is inefficient for an inflaton in this mass range. Nonetheless, we can not rule out the possibility of significant SM production here as a result of the misalignment of the inflationary attractor with the vacuum, without a careful study of the preheating period.

Future work on this model may also include studying the effects of adding the renormalisable trilinear inflaton-Higgs coupling, $\chi\Phi^\dagger\Phi$. A sizeable coupling may significantly enhance $\chi \to hh$ in the heavy inflaton parameter space, thus reheating the universe more efficiently and extending the upper mass bound of the inflaton. Additionally there are experimental motivations if θ_m is significantly larger, as new detection channels in particle colliders, such as $\chi \to q\bar{q}$, may become accessible.

In the following chapter we extend our inflationary model with three sterile neutrinos in a modified νMSM model. We require the model parameters to be consistent with the SM neutrino mass splittings, and incorporate mechanisms for DM production via inflaton decay in the early universe, and leptogenesis to generate the BAU. We utilise the theory and relevant bounds from chapters 4 and 5 to constrain our model.

Chapter 7

Inflaton model + νMSM

7.1 Introduction

A more realistic model of nature should have a DM candidate and a means to produce it, to give over 80% of the total matter energy density today [255, 256]. In this chapter we minimally extend the light scalar inflaton model of chapter 6 with a modified version of the νMSM [53]. Here, symmetry breaking in the scalar sector gives Majorana masses to three sterile neutrinos, the lightest of which can be used as DM [43, 45, 52]. The DM is produced from direct inflaton decay during the reheating process, leading to a non-thermal velocity distribution for DM. Moreover, the additional two heavier sterile neutrinos are able to generate the SM neutrino masses via the seesaw mechanism, as in section 5.1.3, and produce the BAU via leptogenesis, as in section 5.3.

This chapter first outlines the scalar inflaton and νMSM model with a scalar-sterile neutrino Yukawa coupling, which generates the sterile neutrino mass post scalar symmetry breaking. We derive the DM production rate via inflaton decay. We argue that DM production via active-sterile neutrino mixing is negligible due to the absence of x-rays observed from the radiative decay of sterile neutrinos [106, 187]. Sections 7.3, 7.4 and 7.5 are concerned with evaluating the DM mass and average momentum across the inflaton parameter windows defined in chapter 6 by successful inflation and reheating. First we review DM production via light inflaton decay ($m_\chi \ll m_h$) from previous works [45–47, 52]. In this case, the DM properties are determined analytically across the entire light inflaton parameter space as the inflaton thermalizes prior to DM production. The light inflaton produces DM sterile neutrinos with mass $O(10-100)$keV, and an average momentum over temperature at the end of reheating of 2.45. Next we focus on my own work [43] that analyses DM production via heavy inflaton decay ($m_\chi > 2m_h$). Across the majority of the heavy inflaton parameter space the inflaton has a non-thermal distribution, resulting from turbulent preheating, at the time of DM production. As a result, we can only make analytical estimates in the limit reheating temperatures are much less/greater than the inflaton mass [45, 257]. We then solve the Boltzmann equations numerically across the entire

heavy inflaton parameter space; the analytical and numerical results are comparable only at the extremities of the parameter space. Our final results conclude that a heavy inflaton produces MeV sterile neutrinos, with an average momentum over temperature at the end of reheating of $O(1-10)$. On evaluation of the DM free-streaming length, we find that keV DM from a light inflaton is classified as warm DM and MeV DM from a heavy inflaton is classified as cold DM, and both are within the Lyman-α free-streaming bound (4.52).

In section 7.6, we make use of our analysis in section 5.3 to constrain the masses of the two heavier sterile neutrinos, by requiring they generate sufficient LA to account for the BAU and their masses are consistent with the SM neutrino mass splittings. In section 7.7, we then evaluate the entropy dilution from the late time decay of the two heavier sterile neutrinos. This is important to check, as a large entropy could be problematic if it dilutes the generated BA, but may be beneficial if it cools the DM, thereby relaxing the Lyman-α free-streaming bound (4.52). We conclude from our analysis, however, that the entropy dilution in our model is negligible.

7.2 The model and DM production

The νMSM can explain the origin of the BAU and DM [53] through the addition of three sterile neutrinos, N_I $(I = 1, 2, 3)$, to the SM. We reviewed the standard νMSM model in section 5.2, in which DM sterile neutrinos are NRP or RP via active-sterile neutrino oscillations. The review concluded that the total DM abundance can not be made up of NRP sterile neutrinos due to constraints from unobserved x-rays emissions (5.58) and the Lyman-α free-streaming bound (4.52). Although it is possible for RP sterile neutrinos to make up the total DM abundance, the model is complicated by the requirement that the LA exceeds the BAU by at least 5 orders of magnitude. The aim of this section is to offer an alternative mechanism for DM sterile neutrino production that is not tightly constrained by these astrophysical and cosmological bounds.

We extend our light inflaton model in chapter 6 with a νMSM that is modified with the addition of a $N_I - X$ Yukawa coupling [43, 45–47, 52]:

$$L_{\nu MSM+X} = L_{\nu MSM} + \frac{1}{2}(\partial_\mu X)^2 - \frac{f_I}{2}\overline{N_I}^c N_I X + h.c. + V(X, \Phi), \tag{7.1}$$

where $L_{\nu MSM}$ is the Lagrangian of the standard νMSM given in equation (5.22), and $V(X, \Phi)$ is the potential of our light scalar inflaton model given in equation (6.3). Spontaneous symmetry breaking in the inflaton sector, $X \to v_X + \chi$, generates the sterile neutrino mass,

$$M_I = v_X f_I, \tag{7.2}$$

and a coupling to the inflaton field; we assume the normal mass hierarchy ($M_1 < M_2 < M_3$). As in the scalar sector, we assume that the massive parameters enter only in the inflaton operators, i.e. we do not add bare Majorana masses for N_I. As discussed in section 5.2.2, the active-sterile neutrino coupling is strongly constrained from above by the absence of x-rays observed from the radiative decay of sterile neutrinos [106, 187]:

$$|F_{\alpha 1}| \lesssim 3 \times 10^{-11} \left(\frac{\text{keV}}{M_1}\right)^{\frac{3}{2}}. \tag{7.3}$$

We can therefore assume $F_{\alpha I} \ll f_I$, and neglect N_I production from active-sterile neutrino oscillations. In this limit, all sterile neutrinos with $M_I < m_\chi/2$ are produced via the freeze-in mechanism from inflaton decay in the early universe. The amplitude of the process $\chi(\mathbf{q_1}) \to N_I(\mathbf{p_1}, \sigma_1)\overline{N}_I(\mathbf{p_2}, \sigma_2)$ is

$$|M_{\chi \to N\overline{N}}| = f_I \overline{u}_{\sigma_1} v_{\sigma_2}, \tag{7.4}$$

where a symmetry factor of 2 accounts for the two identical Majorana particles in the final state. The squared amplitude summed over all possible spin states (σ_1, σ_2), and evaluated in the centre of mass frame is

$$\begin{aligned} \sum_{\sigma_1,\sigma_2} |M|^2 &= f_1^2 \text{Tr}\big[(\not{p}_1 + M_I)(\not{p}_2 - M_I)\big], \\ &= 4f_I^2(p_1 \cdot p_2 - M_I^2), \\ &= 2f_I^2 m_\chi^2 \left(1 - \frac{4M_I^2}{m_\chi^2}\right). \end{aligned} \tag{7.5}$$

The corresponding decay width is [43, 45, 47]

$$\Gamma_{N_I} = \frac{f_I^2 m_\chi}{16\pi}\left(1 - \frac{4M_I^2}{m_\chi^2}\right)^{\frac{3}{2}} \simeq \frac{\beta}{8\pi}\frac{M_I^2}{m_\chi}, \tag{7.6}$$

in the limit $m_\chi \gg M_I$. Γ_{N_I} is much less than the Hubble expansion rate throughout reheating, so sterile neutrinos remain decoupled from the thermal bath. The lightest of the three sterile neutrinos, N_1, is both massive and stable, and so is an ideal Feebly Interacting Massive Particle (FIMP) DM candidate. We will assume in our analysis that N_1 makes up the total DM energy density in the universe, thereby constraining its abundance using equation (4.6) [255]:

$$\Omega_{\text{DM},0} = \frac{1}{D}\frac{s_0}{\rho_{c,0}} M_1 Y_{1,f}(t) \sim 0.25. \tag{7.7}$$

The values of s_0 and $\rho_{c,0}$ are given in (2.101) and (2.88), and Y_1 is evaluated at the end of freeze-in DM production. We have an additional factor D to account for the entropy dilution

from heavier sterile neutrino decays. In section 7.7 we will show that this has a negligible impact on the DM abundance, i.e. $D \sim 1$. Constraining the coupling f_1 from the abundance, we can then evaluate the mass of DM, using (7.2), which has important consequences for structure formation [92].

7.3 Boltzmann equations for reheating and DM production

Three Boltzmann collision integral equations fully describe the dynamics of the system of particles during reheating and DM production [251, 252]:

$$\frac{\mathrm{d}f_\chi}{\mathrm{d}t} = C^{\chi}_{\chi\leftrightarrow hh/\varphi_i\varphi_i} + C_{\chi\chi\leftrightarrow hh/\varphi_i\varphi_i} + C^{\chi}_{\chi\leftrightarrow N\overline{N}} \tag{7.8}$$

$$\frac{\mathrm{d}f_N}{\mathrm{d}t} = C^{N}_{\chi\leftrightarrow N\overline{N}} \tag{7.9}$$

$$\frac{\mathrm{d}f_{\mathrm{SM}}}{\mathrm{d}t} = C^{\mathrm{SM}}_{\chi\leftrightarrow hh/\varphi_i\varphi_i} + C^{\mathrm{SM}}_{hh/\varphi_i\varphi_i\leftrightarrow \mathrm{SMSM}} + C^{\mathrm{SM}}_{h/\varphi_i\leftrightarrow \mathrm{SMSM}} \tag{7.10}$$

Equations (7.8) and (7.10) are simplified by the same assumptions stated in section 6.9.1, and additionally, the sterile neutrino collision integrals in equations (7.8) and (7.9) are simplified using the following:

- $\Gamma_{\mathrm{SM}} = O(10^6 - 10^8)\Gamma_N$, so $C^{\chi}_{\chi\leftrightarrow N\overline{N}}$ is neglected.
- Sterile neutrino density remains low during reheating, as Γ_N is much less than the Hubble expansion rate throughout the time of production; therefore the backward reaction $C^{N}_{N\overline{N}\to\chi}$ is neglected.

The above simplifications reduce the set of Boltzmann equations (7.8, 7.9, 7.10) to the following [253, 254]:

$$\frac{\partial f_\chi(k,t)}{\partial t} = \frac{am_\chi}{\sqrt{(am_\chi)^2 + k^2}}\Gamma_{\mathrm{SM}}\Big[f^{eq}_\chi(T_{\mathrm{SM}}) - f_\chi(k,t)\Big], \tag{7.11}$$

$$\frac{\partial f_N(k_N,t)}{\partial t} = \frac{m_\chi\Gamma_N a}{k_N^2}\int_{k'_{min}}^{\infty} dk' \frac{k'}{\sqrt{(am_\chi)^2 + k'^2}} f_\chi(k',t). \tag{7.12}$$

k and k_N are the conformal inflaton and sterile neutrino momenta respectively. In equation (7.12) we neglect the production of sterile neutrino DM via active-sterile neutrino oscillations, as for the range of parameters we are considering their production via inflaton decay is the dominant process. The lower bound on the integral is

$$k'_{\mathrm{min}} = \left|k_N - \frac{(am_\chi)^2}{4k_N}\right|. \tag{7.13}$$

As in section 6.9.1, the differential equation for $a(t)$, neglecting the contribution of the sterile neutrinos to the total energy density, is

$$H(t) = \frac{\dot{a}(t)}{a(t)} = \sqrt{\frac{\rho_\chi(t) + \rho_{\rm SM}(t)}{3M_P^2}}, \tag{7.14}$$

where the energy densities of the inflaton and SM are given by equations (6.77) and (6.78). We take the number of effective degrees of freedom of the SM as constant throughout reheating and DM production in the heavy inflaton parameter space, at $g_{\rm SM} = 100$. This is an acceptable approximation even for a lighter heavy inflaton, which produces sterile neutrinos at $(20 < T_{\rm SM} < 80)$ GeV; with $g_{\rm SM} = 86.25$ [67], the corresponding error on the inflaton-sterile neutrino coupling, f_1, is still less than 5%.

The differential equation for $T_{\rm SM}$ to replace the Boltzmann equation (7.10) is also the same as in section 6.9.1,

$$\frac{dT_{\rm SM}}{dt} = -HT_{\rm SM} - \frac{30}{g_{\rm SM}\pi(aT_{\rm SM})^3}\int_0^\infty dk\ k^2 m_\chi \Gamma_{\rm SM}\Big[f_\chi^{eq}(T_{\rm SM}) - f_\chi(k,t)\Big]. \tag{7.15}$$

(7.11), (7.14) and (7.15) form a closed set of differential equations; the solution for $f_\chi(k,t)$ will then be used in (7.12) to solve for $f_N(k_N,t)$.

7.4 Analytical treatment

The DM mass and momentum heavily depends on the inflaton distribution function at the time of production. At the extremities of the heavy inflaton parameter space, where the reheating temperature is much less/greater than the inflaton mass, the DM is produced via two different mechanisms; as we have done previously, we define the reheating temperature, $T_{\rm eq}$, as the temperature when the energy densities of the inflaton and the SM are equal. In these two regions we can use analytical approximations of the inflaton distribution functions to investigate the dependence of the DM properties on the inflaton parameters. In the parameter space between, the DM is produced via both mechanisms, so a more careful numerical analysis is required. Across the entire light inflaton parameter space the reheating temperatures are much less that the inflaton mass, and so we simply determine the DM properties in this window analytically.

7.4.1 Relativistic inflaton particles ($\mathbf{T_{eq} \gg m_\chi}$)

In the limit $T_{\rm eq} \gg m_\chi$, the inflaton has thermalised with the SM prior to the production of sterile neutrinos, at $T_{\rm prd} \sim \frac{m_\chi}{2}$. The thermal inflaton distribution function at the SM temperature, given by (6.75), is used in (7.12) to obtain the analytical approximation of the

sterile neutrino distribution. The sterile neutrino number density is given by [45]:

$$\begin{aligned} n_N(t) &= \frac{4\pi g_N}{a^3}\int_{k=0}^{\infty} dk_N\ k_N^2 f_N(k_N,t), \\ &= \frac{3\Gamma_N M_0 \zeta(5) T_{\rm SM}^3(t)}{2\pi m_\chi^2}, \end{aligned} \tag{7.16}$$

where the number of degrees of freedom of the sterile neutrino $g_N = 2$, and $M_0 \approx \frac{3M_{\rm P}}{\sqrt{g_{\rm SM}}}$. Having evaluated the entropy of the universe at the end of reheating,

$$s(t) = \frac{4}{3}\frac{\rho_{\rm SM}(t)}{T_{\rm SM}(t)} = \frac{2\pi^2}{45} g_{\rm SM} T_{\rm SM}^3(t), \tag{7.17}$$

the relative DM abundance (7.7), is calculated using (6.17), (7.2) and (7.6) for v_X, M_1 and Γ_{N_1} respectively, to obtain the following power-law relations between m_χ, β, f_1 and M_1:

$$\Omega_{\rm DM,0} \propto \frac{f_1^3}{\sqrt{\beta}}, \tag{7.18}$$

$$f_1 = (4.45\times 10^{-10})\left(\frac{\Omega_{\rm DM,0}}{0.25}\right)^{\frac{1}{3}}\left(\frac{\beta}{10^{-9}}\right)^{\frac{1}{6}}\left(\frac{g_{\rm SM}}{100}\right)^{\frac{1}{2}}, \tag{7.19}$$

$$M_1 = 9.94\ \text{keV}\left(\frac{\Omega_{\rm DM,0}}{0.25}\right)^{\frac{1}{3}}\left(\frac{10^{-9}}{\beta}\right)^{\frac{1}{3}}\left(\frac{g_{\rm SM}(T_{\rm prod})}{100}\right)^{\frac{1}{2}}\frac{m_\chi}{\text{GeV}}. \tag{7.20}$$

Here we have taken $D = 1$, which we will show is a reasonable estimate in section 7.7. The analytical approximation of the average sterile neutrino DM momentum on production is [45, 52]

$$\frac{\langle p_N\rangle}{T_{\rm prod}} = \frac{\pi^6}{378\zeta(5)} \approx 2.45. \tag{7.21}$$

Sterile neutrinos are therefore cooler than thermal fermions, which have $\langle p\rangle/T = 3.15$.

The DM mass and momentum in the light inflaton parameter space ($m_\chi \ll 2m_h$) are well approximated by the analytical results (7.20) and (7.21); this region of parameter space has been previously analysed in [45–47, 52]. Given the allowed range of light inflaton masses and self-couplings for successful inflation and reheating, stated in equation (6.65) and Table 6.1, we obtain the following range of DM masses:

$$M_1 \sim \begin{cases} \left(7\left(\frac{g_{\rm SM}(T_{\rm prod})}{60}\right)^{\frac{1}{2}} - 160\left(\frac{g_{\rm SM}(T_{\rm prod})}{100}\right)^{\frac{1}{2}}\right)\ \text{keV}, & \beta = 10^{-9} \\ \left(5\left(\frac{g_{\rm SM}(T_{\rm prod})}{10}\right)^{\frac{1}{2}} - 170\left(\frac{g_{\rm SM}(T_{\rm prod})}{80}\right)^{\frac{1}{2}}\right)\ \text{keV}. & \beta = 10^{-12} \end{cases} \tag{7.22}$$

Note that we have analytically evaluated (7.20) by taking $g_{\rm SM}(T_{\rm prod})$ as constant throughout DM production. However, $g_{\rm SM}(T_{\rm prod})$ is a rapidly changing function of temperature for $m_\chi \sim O(0.1-1)$ GeV and so the DM mass ranges in (7.22) should be taken as rough estimates. The

keV DM is classified as warm DM, then using equation (4.50), we calculate their free-streaming length to be

$$\begin{aligned}\lambda_{\rm FS} &\approx 3.64 \text{ Mpc } g_{*s}(T \approx M_1)^{-\frac{1}{3}} \left(\frac{1 \text{ keV}}{M_1}\right) \left(\frac{g_{*s}(T \approx M_1)}{g_{*s}(T_{\rm prod})}\right)^{\frac{1}{3}} \left(\frac{\langle p_N \rangle}{3.15 T_{\rm prod}}\right), \\ &\approx 3.64 \text{ Mpc } g_{*s}(T_{\rm prod})^{-\frac{1}{3}} \frac{2.45}{3.15} \left(\frac{1 \text{ keV}}{M_1}\right), \\ &= O(10^{-3} - 10^{-1}) \text{ Mpc}. \end{aligned} \tag{7.23}$$

In the first line we have used the conservation of entropy (2.22) to write the free-streaming as a function of the momentum on production, by rescaling the momentum at $T \approx M_1$ by the ratio of the number of degrees of freedom.

Figure 7.1, taken from [52], plots the inflaton-Higgs mixing angle against the inflaton mass. The black line plots the inflaton parameters that would lead to the production of 7 keV sterile neutrino DM, which is motivated by the anomalous x-ray emission [172, 184, 186, 192].

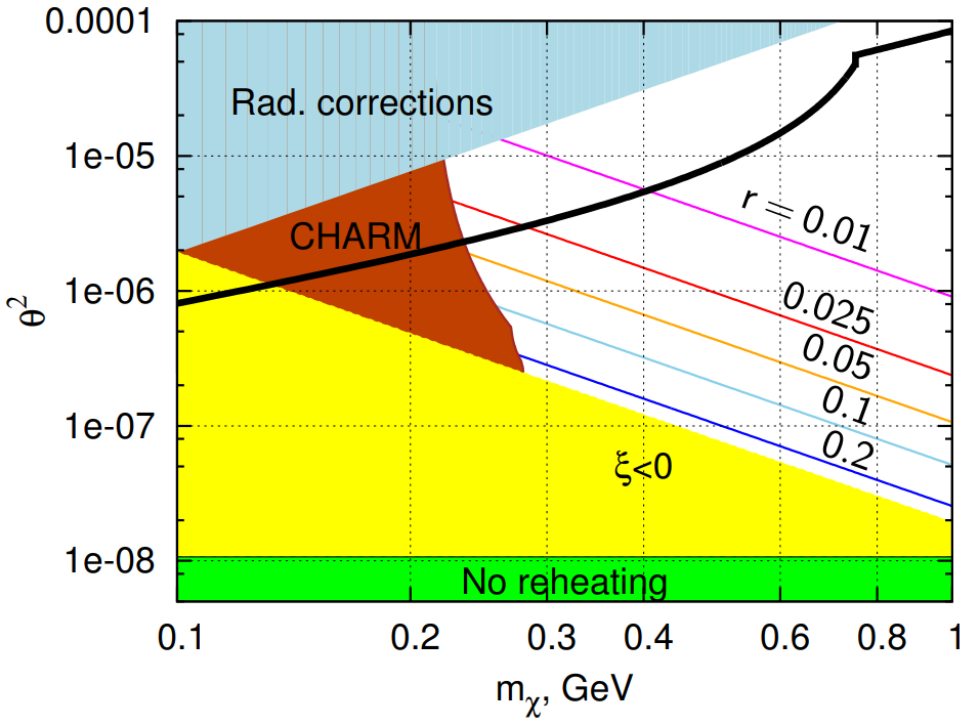

Figure 7.1: Exclusion plot of light inflaton parameter space with 7 keV sterile neutrino DM
Plot taken from [52] of the squared inflaton-Higgs mixing angle against inflaton mass. Shaded regions are forbidden: blue (top-left) region due to large radiative corrections to the inflationary potential; green (bottom) due to inefficient reheating; yellow (bottom-left) region due to tensor-to-scalar ratio, r, exceeding the CMB limit; and brown region is the experimental bound from the CHARM experiment [258]. The coloured lines are isocurves of constant r. The black curve corresponds to the inflaton parameters that would lead to the production of 7 keV sterile neutrino DM (motivated by the anomalous x-ray signal [186]) via inflaton decay.

We can see from Figure 6.7 that there is only a small region of the heavy inflaton ($m_\chi > 2m_h$) parameter space where $T_{\rm eq} \gg m_\chi$ and thus the thermal approximation is reasonable:

where the inflatons are relatively light, $m_\chi \lesssim 500$ GeV, and have self-couplings, $\beta \geq 10^{-10}$. In section 7.5 we will precisely analyse where the analytical approximations diverge from our numerical results.

7.4.2 Non-relativistic inflaton particles ($\mathbf{T_{eq} \ll m_\chi}$)

Heavier inflatons with smaller self-couplings have $T_{\rm eq} \ll m_\chi$, as shown in Figure 6.7. In this limit, sterile neutrinos are produced prior to thermalisation from a highly infra-red inflaton distribution resulting from turbulent preheating, given by equation (6.84), at the same time as SM production:

$$f_\chi(k,t) \sim e^{-\Gamma_{\rm SM} t} f_\chi(k,0) = \left(\frac{k}{k_0}\right)^{-\frac{3}{2}} e^{-\left(\frac{k}{k_0}+\Gamma_{\rm SM} t\right)}. \tag{7.24}$$

The sterile neutrino number density is obtained by solving the equation

$$\frac{\partial n_N(t) a^3}{\partial t} = 2\Gamma_N n_\chi(t) a^3, \tag{7.25}$$

where the inflaton number density is

$$n_\chi(t) = \frac{4\pi g_\chi}{a^3}\int_0^\infty dk\, k^2 f_\chi(k,t) = (2\sqrt{\pi})^{\frac{3}{2}} \left(\frac{k_0}{a}\right)^3 e^{-\Gamma_{\rm SM} t}. \tag{7.26}$$

This leads to

$$n_N(t) = 2(2\sqrt{\pi})^{\frac{3}{2}} \frac{\Gamma_N}{\Gamma_{\rm SM}} \left(\frac{k_0}{a}\right)^3. \tag{7.27}$$

Solving for the entropy in terms of k_0:

$$\begin{aligned} \frac{\partial n_{SM}(t) a^3}{\partial t} &= 2\Gamma_{\rm SM} n_\chi(t) a^3, \\ s(t) = \frac{2\pi^4 n_{SM}(t)}{45\zeta(3)} &= \frac{4\pi^4 (2\sqrt{\pi})^{\frac{3}{2}}}{45\zeta(3)} \left(\frac{k_0}{a}\right)^3, \\ Y_N &= \frac{45\zeta(3)}{4\pi^4} \frac{\Gamma_N}{\Gamma_{\rm SM}}. \end{aligned} \tag{7.28}$$

The relative DM abundance, (7.7), is calculated using (6.17), (7.2) and (7.6) for v_X, M_I and Γ_N, to obtain the following power-law relations between m_χ, β, f_1 and M_I:

$$\Omega^0_{\rm DM} \propto M_1 \frac{\Gamma_N}{\Gamma_{\rm SM}} \propto \frac{f_1^3 m_\chi^5}{\beta^{\frac{3}{2}}}, \tag{7.29}$$

$$M_1 \sim (1.05 \times 10^3)\ m_\chi^{-\frac{2}{3}}\ \text{MeV}. \tag{7.30}$$

Here we have also taken $D = 1$. Given that sterile neutrinos are produced at $T_{\rm SM} \sim T_{\rm eq}$, and presuming all the sterile neutrinos are created from inflaton particles at rest, their average

momentum on production is

$$\frac{\langle p_N \rangle}{T_{\rm prod}} \sim \frac{m_\chi}{2T_{\rm eq}}. \tag{7.31}$$

7.5 Numerical results

We set up our numerical analysis with the same initial conditions as stated in section 6.9.2, i.e. the universe filled with inflatons with a highly non-thermal infra-red distribution, given by equation (6.84). We proceed by numerically evolving the closed set of differential equations (7.11), (7.14) and (7.15). The solution for $f_\chi(k,t)$ is then used in (7.12) to solve for $f_N(k_N,t)$, and from which, we can determine the DM mass and momentum in the heavy inflaton window defined in section 6.9.2.

The reheating temperature relative to the inflaton mass determines when the DM sterile neutrinos are produced relative to the thermalisation of the inflaton distribution with the SM, and therefore the properties of the DM. This is demonstrated in Figure 7.2, which shows the time of sterile neutrino and SM production for a 260 GeV inflaton, as a function of the SM temperature. The temperature when the inflaton distribution thermalises is indicated by the vertical dotted lines.

Inflaton particles of mass 260 GeV and coupling $\beta = 10^{-9}$ have a reheating temperature of $T_{\rm eq} \sim 2400$ GeV. As shown by the red line in Figure 7.2, sterile neutrinos are produced from remnant thermalised inflaton particles post SM production. This is most efficient when the universe has cooled to $T_{\rm SM} \sim m_\chi/2$; at lower temperatures, production is inefficient as the inflaton occupation number is highly Boltzmann suppressed. However, non-relativistic inflatons most efficiently produce sterile neutrinos at the same time as the SM, at $T_{\rm SM} \sim T_{\rm eq}$; at this time, the inflaton distribution is non-thermal and the occupation number is at its largest. The orange line in Figure 7.2 demonstrates the non-thermal production of sterile neutrinos from inflaton particles of mass 260 GeV, coupling $\beta = 10^{-12}$, and a reheating temperature of $T_{\rm eq} \sim 240$ GeV. The intermediate couplings, $\beta = 10^{-10}/10^{-11}$, generate sterile neutrinos by both mechanisms that govern the highly relativistic/non-relativistic inflaton regions. The blue and green lines in Figure 7.2 show the increasing efficiency of sterile neutrino production at $T_{\rm eq}$ with decreasing β.

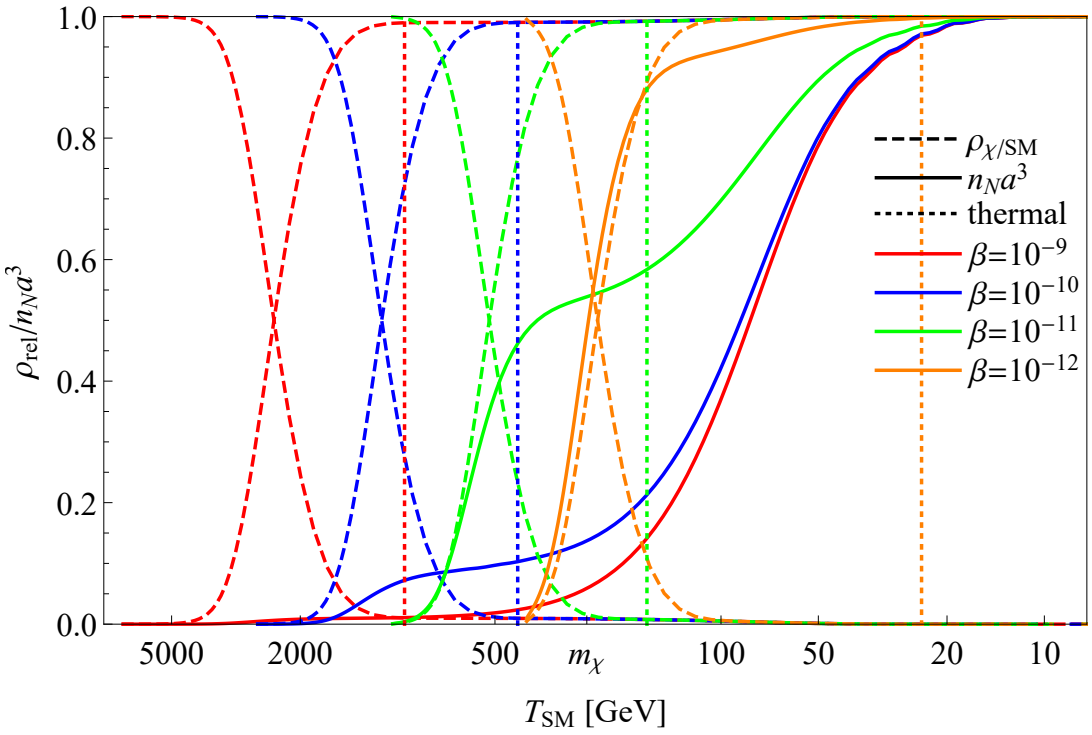

Figure 7.2: Evolution of inflaton decay and SM and DM sterile neutrino production, as a function of SM temperature

The plot gives numerical results for a 260 GeV inflaton, with self-coupling ($10^{-12} \leqslant \beta \leqslant 10^{-9}$), represented by different colours given in the legend. The dashed lines are the relative energy densities of inflaton/SM, $\rho_\chi/\rho_{\rm SM}$, and the full lines are the normalised conformal number densities of sterile neutrino, $n_N a^3$, plotted against the SM temperature, $T_{\rm SM}$. The label m_χ on the x-axis indicates where $T_{\rm SM}$ equals the inflaton mass. The vertical dotted lines give the SM temperature at which the inflaton distribution thermalises.

Analytical approximations of the sterile neutrino mass as a function of inflaton mass, that lead to the proper DM abundance, show a positive correlation for relativistic inflaton particles (7.20), and a negative correlation for non-relativistic inflaton particles (7.30). Plotting the sterile neutrino mass against the inflaton mass, shown in Figure 7.3, allows us to clearly identify which production mechanism dominates in different regions of the inflaton parameter space. The inflaton mass which produces the maximum sterile neutrino mass is analytically approximated, using (7.20) and (7.30), by

$$m_\chi \sim (5.1 \times 10^4)\beta^{\frac{1}{5}} \text{ GeV}. \tag{7.32}$$

The left/right of the peak in Figure 7.3 corresponds to the inflaton parameter space where the thermal/non-thermal production mechanism dominates. In agreement with Figure 7.3, (7.32) demonstrates that as β increases, the peak sterile neutrino mass moves to larger values of the inflaton mass; and (7.20) states that a relativistic inflaton with smaller β produces heavier

sterile neutrinos.

The numerical results in Figure 7.3 are given by the solid lines, and the analytical results by the dashed lines. The relativistic approximations (7.20), have a dependence on β, and are coloured accordingly; the non-relativistic approximation (7.30), has no dependence on β, so is given by the black line. The analytical and numerical results match to good accuracy for the lightest and heaviest inflaton particles with self-coupling $\beta = 10^{-9}$. The inflaton particles with smaller β do converge towards the analytical approximations, however numerical analysis is necessary for arbitrary values of the parameters.

Figure 7.4 plots the average sterile neutrino momentum over temperature at the end of reheating[1], $\langle p_N \rangle / T$, across the inflaton parameter space. The lightest inflaton particles, with coupling $\beta = 10^{-9}$, have $\langle p_N \rangle / T \sim 2.4$, which is in agreement with our analytical approximation for thermal production (7.21). Whilst $m_\chi < T_{\rm eq}$, increasing the inflaton mass increases the efficiency of sterile neutrino production at $T_{\rm eq}$, thereby decreasing $\langle p_N \rangle / T$ until a minimum is reached at $T_{\rm eq} = m_\chi$, corresponding to $\langle p_N \rangle / T \sim 1$. $\langle p_N \rangle / T$ rapidly increases once $m_\chi > T_{\rm eq}$, as $\langle p \rangle$ and $T_{\rm eq}$ are increasing and decreasing functions of m_χ, respectively. Analytical results are consistent with our numerical results for a heavy non-relativistic inflaton, given by (7.31); for example, the analytical estimate for 7600 GeV inflaton is $\langle p_N \rangle / T \sim 24$.

The model for NRP and RP DM sterile neutrino production from active neutrinos [178, 185] that we studied in section 5.2.1 produce keV sterile neutrinos; with an average momentum over temperature at $T \sim$ keV of $\langle p_N \rangle / T = O(1)$ (precise values are given in (5.35) and (5.41)), they are warm DM candidates. By comparison, production in heavy inflaton decays needs MeV sterile neutrinos, which are cold DM candidates with

$$\left(\frac{\langle p_N \rangle}{T} \right)_{T \sim \rm keV} = \left(\frac{g_{\rm SM}(T \sim \rm keV)}{g_{\rm SM}(T_{\rm prod})} \right)^{\frac{1}{3}} \frac{\langle p_N \rangle}{T_{\rm prod}} \sim 0.3 - 8, \tag{7.33}$$

where $g_{\rm SM}(T \sim \text{keV}) = 3.91$. Our model is therefore well within the constraints from the Lyman-α data with a free-streaming length, calculated from equation (4.50), of

$$\lambda_{\rm FS,0} = O(10^{-5} - 10^{-3}).$$

Sterile neutrinos with the largest free-streaming length are produced from a 7600 GeV inflaton with coupling $\beta = 10^{-9}$, and the smallest free-streaming length from an inflaton with coupling $\beta = 10^{-12}$.

[1] As we approximate the number of effective degrees of freedom to be constant throughout reheating, $g_{\rm SM} = 100$, the average DM momentum over temperature at the end of reheating, given in Figure 7.4, is equal to that on production, $\langle p_N \rangle / T_{\rm prod}$.

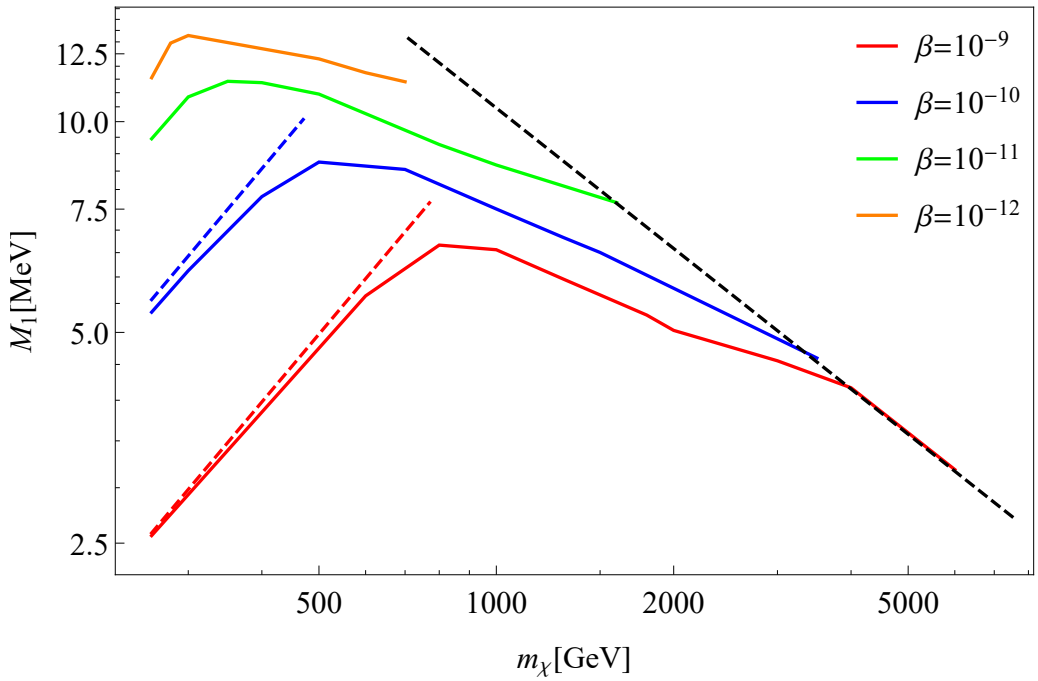

Figure 7.3: Sterile neutrino mass against inflaton mass

The solid lines are the numerical results and the dashed lines are the analytical approximations constrained by the observed DM abundance. The analytical results for thermal inflatons, given by (7.20), have a dependence on β so are colour-coded accordingly. The analytical result for non-relativistic inflatons, given by (7.30), has no dependence on β, so is given by the black dashed line.

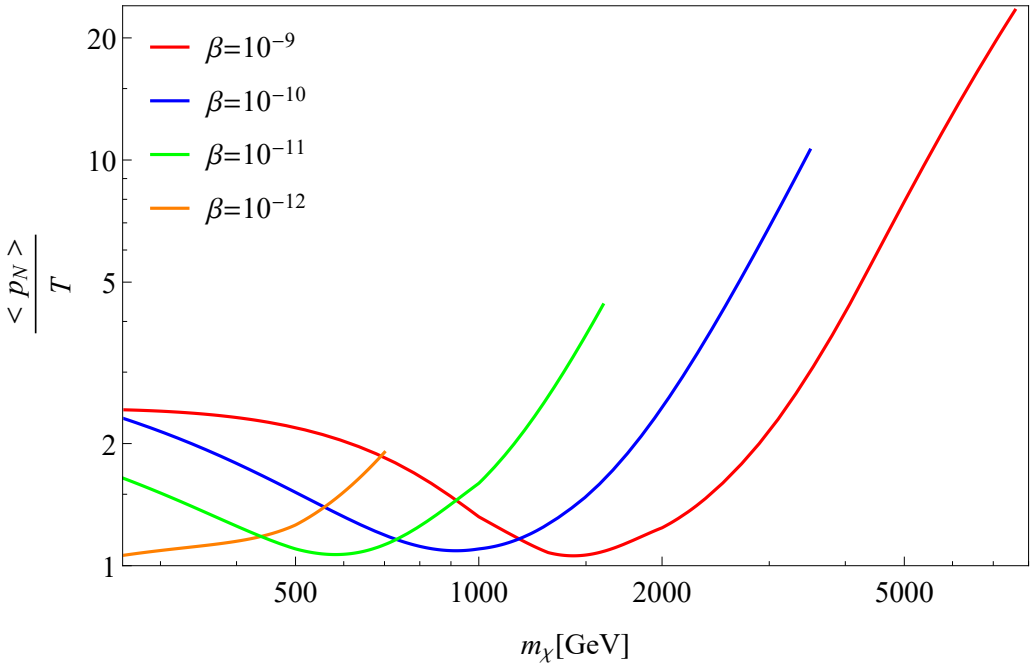

Figure 7.4: Average sterile neutrino momentum over temperature at the end of reheating, $\langle p_N \rangle / T$, against inflaton mass

Different colours represent inflatons with different self-coupling, β.

7.6 Leptogenesis

In section 5.3 we reviewed the mechanisms by which the νMSM model can generate a LA during the out-of-equilibrium production (freeze-in) and/or decay (freeze-out) of the two heavier sterile neutrinos, N_2 and N_3. The model is able to produce sufficient LA to explain the BAU for a wide range of sterile neutrino masses, $O(1-T_{\rm reh})$ GeV, if they are degenerate. The aim of this analysis is to check how the leptogenesis mechanisms are affected with the addition of the inflaton-sterile neutrino coupling in our model, and if this restricts the sterile neutrino's parameter space as a result.

In the νMSM model, the dominant process that thermalizes the sterile neutrino with the SM during the Higgs symmetric phase is $t\bar{t} \to N\overline{L}$, at a rate given in (5.83). If we take the typical value of the SM Yukawa coupling, $F_{\alpha I}$, that can generate the active neutrino masses via the Type 1 seesaw mechanism, as given in (5.85), the scattering rate is

$$\begin{aligned}\Gamma_{t\bar{t}\to N\overline{L}} &\sim \frac{9}{32\pi^3}\frac{m_{\rm atm}M_I}{v^2}T \\ &= O(10^{-13})\left(\frac{M_I}{10\ \text{GeV}}\right)\left(\frac{T}{10^3\ \text{GeV}}\right)\ \text{GeV}.\end{aligned} \tag{7.34}$$

The sterile neutrinos equilibrate with the SM via this process when $\Gamma_{t\bar{t}\to N\overline{L}}(T_{\rm eq}) \sim H(T_{\rm eq})$, at temperature

$$T_{\rm eq} \sim 5M_I. \tag{7.35}$$

As the sterile neutrinos equilibrate once they are non-relativistic, sterile neutrinos with masses large enough for $T_{\rm eq} > T_{\rm EW}$ can produce sufficient LA to generate the BAU during freeze-in, as the LA washout rate is Boltzmann suppressed. However, if the additional inflaton-sterile neutrino Yukawa coupling is large enough for sterile neutrinos to equilbriate whilst they are still relativisitic, the LA generated during freeze-in will be significantly washed-out.

The competing inflaton-sterile neutrino interaction in the symmetric Higgs phase is $\chi \to N_I\overline{N}_I$ for $M_N < m_\chi/2$, which has a rate given in equation (7.6) of

$$\Gamma_{N_I} = O(10^{-12})\left(\frac{\beta}{10^{-10}}\right)\left(\frac{M_I}{10\ \text{GeV}}\right)^2\left(\frac{10^2\ \text{GeV}}{m_\chi}\right)\ \text{GeV}. \tag{7.36}$$

The s-channel scattering process $hh/\varphi_i\varphi_i \to N_I\overline{N}_I$ mediated by an inflaton particle, and t-channel scattering process $\chi\chi \to N_I\overline{N}_I$ mediated by a sterile neutrino are sub-dominant. The equilibration temperature of the sterile neutrino decay process is

$$T_{\rm eq} \sim 200\left(\frac{\beta}{10^{-10}}\right)^{\frac{1}{2}}\left(\frac{10^2\ \text{GeV}}{m_\chi}\right)^{\frac{1}{2}}M_I. \tag{7.37}$$

Therefore in a large proportion of sterile neutrino parameter space, where $\beta = 10^{-9}/10^{-10}$ and $m_\chi \leq 10^2$ GeV, the sterile neutrinos freeze-out at $T_{\rm eq} \gg M_I$. As a result, there is a significant washout of the LA produced during freeze-in. For this reason, we will restrict our model to the parameter space of sterile neutrinos (N_2, N_3) that can produce sufficient LA only during freeze-out via the resonant leptogensis mechanism. Using the results obtained from [104, 164–166], our heavy sterile neutrino mass range is then restricted to $M_{2/3} \gtrsim 10^3$ GeV. This is a conservative bound, since variations of the resonant leptogenesis model [207–210] allow for $M_{2/3} \gtrsim 100$ GeV. A more relaxed lower mass bound still was argued in [201], in which $M_{2/3} \geq O(10)$ GeV; the results from [201] are summarised in section 5.3.4, where the parameter for resonant leptogenesis is given by the blue dashed line in Figure 5.10. Since resonant leptogenesis generates the LA at temperatures just below the sterile neutrino mass [104, 164–166, 208], its upper bound is limited by the maximum reheating temperature of our model, $T_{\rm reh} \leq O(10^{10})$ GeV. We may also want to restrict sterile neutrinos masses to $M_{2/3} \leq O(10^7)$ GeV in order to evade a hierarchy problem due to their large radiative corrections to the Higgs mass [11, 200], given by the term in (5.75).

7.7 Entropy dilution

The out-of-equilibrium decay of heavy, long-lived particles can release significant entropy. As the particles can be non-relativistic during radiation domination, their energy density increases by a factor of a relative to the radiation energy density, and can thus dominate the energy density of the universe by the time of its decay [56]. If we assume the heavy particles decay into SM particles, their entropy release effectively heats the SM relative to hidden sectors [56, 212, 259], such as DM. We define the entropy dilution factor, D, as the ratio of the entropy in the SM after and before the heavy particles decay [56],

$$D \equiv \frac{S_{\rm after}}{S_{\rm before}} = \left(\frac{T_{\rm after}}{T_{\rm before}}\right)^3 , \tag{7.38}$$

where entropy is $S_X = s(T_X)a^3$, and $T_{\rm after/before}$ is the SM temperature after/before the heavy particles decay. Note that as entropy release into the SM sector effectively cools the DM sector, it is a particularly beneficial process for very warm DM models [259, 260] that are strongly constrained by the Lyman-α free-streaming bound (4.52).

In this section we will evaluate the entropy dilution factor as a result of heavy sterile neutrino (N_2 and N_3) decays. This is an important part of our analysis as a large entropy release may significantly dilute the DM abundance (7.7), if N_2 and N_3 decay after DM production, and

the generated BA. The entropy dilution of our model is approximately given by [212, 261]

$$D \simeq \left(1 + 2.95 \left(\frac{2\pi^2 \tilde{g}_{*s}}{45}\right)^{\frac{1}{3}} \frac{(rM_I)^{\frac{4}{3}}}{(M_{\rm P}\Gamma_{N_I})^{\frac{2}{3}}}\right)^{\frac{3}{4}} \equiv (1+x)^{\frac{3}{4}}\,, \tag{7.39}$$

where $\tilde{g}_{*s}$ is the number of SM effective degrees of freedom at the time of N_I decay, and r is the ratio of N_I number density over the entropy density at the time of freeze-out.

In order to evaluate r, we first need to find the freeze-out temperature of N_I. Post EW symmetry breaking, sterile neutrinos are kept in equilibrium by their weak interactions with the thermal plasma, at a rate equal to the active neutrino rate suppressed by the squared active-sterile mixing angle [56],

$$\Gamma_I(T) \sim G_F^2 \theta_I^2 T^5. \tag{7.40}$$

The sterile neutrinos freeze-out once $\Gamma_I(T_f) \sim H(T_f)$, at temperature

$$T_f = 1.3 \left(\frac{g_{*\rho}}{100}\right)^{\frac{1}{6}} \left(\frac{10\ \text{GeV}}{M_I}\right)^{\frac{2}{3}} M_I, \tag{7.41}$$

which is evaluated using the typical value of a sterile neutrino Yukawa coupling, given in (5.85). $g_{*\rho}$ is the number of SM effective degrees of freedom at the time of N_I freeze-out. As sterile neutrinos are non-relativistic at freeze-out, their number density is Boltzmann suppressed, and r is given by

$$\begin{aligned} r \equiv \frac{n_N}{s} &= \frac{45}{8}\left(\frac{2}{\pi^7}\right)^{\frac{1}{2}} \frac{g_N}{g_{*\rho}} \left(\frac{M_I}{T_f}\right)^{\frac{3}{2}} \exp\left[-\frac{M_I}{T_f}\right], \\ &\sim 2\times 10^{-3} \left(\frac{100}{g_{*\rho}}\right)^{\frac{5}{4}} \left(\frac{M_I}{10\ \text{GeV}}\right) \exp\left[-0.8\left(\frac{100}{g_{*\rho}}\right)^{\frac{1}{6}} \left(\frac{M_I}{10\ \text{GeV}}\right)^{\frac{2}{3}}\right]. \end{aligned} \tag{7.42}$$

r is exponentially suppressed with increasing sterile neutrino mass, and so lighter sterile neutrinos produce a larger entropy dilution. In order to evaluate the maximum entropy dilution in our model, we will use the following decay width for light sterile neutrinos of mass $M_I < M_W$, given by equation (5.87),

$$\begin{aligned} \Gamma_{N_I} &\sim \frac{G_F^2 m_{\rm atm}}{192\pi^3} M_I^4, \\ &\sim \left(\frac{M_I}{10\ \text{GeV}}\right)^4 \times 10^{-20}\ \text{GeV}. \end{aligned} \tag{7.43}$$

We then use (7.42) and (7.43) to evaluate x in equation (7.39),

$$x \sim 0.3 \left(\frac{\tilde{g}_{*s}}{10}\right)^{\frac{1}{3}} \left(\frac{100}{g_{*\rho}}\right)^{\frac{5}{3}} \exp\left[-0.7\left(\frac{100}{g_{*\rho}}\right)^{\frac{2}{9}} \left(\frac{M_I}{10\ \text{GeV}}\right)^{\frac{8}{9}}\right]. \tag{7.44}$$

If we require sterile neutrinos to be within the mass range that generates sufficient LA to account for the BAU ($M_I > O(10)$ GeV), we can see from (7.44) that their decay does not produce significant entropy dilution, i.e. $D \sim 1$. This result is confirmed in [262], where a more detailed analysis is provided.

7.8 Discussion and conclusion

A mechanism for freeze-in DM production is realised in our model through the addition of a Yukawa coupling of the inflaton to sterile neutrinos, within the framework of the νMSM. We assume DM is made up entirely of the lightest sterile neutrino and is produced via inflaton decay. For an inflaton with $m_\chi \ll T_{\rm eq}$, DM is produced once the inflaton has thermalised and so the model parameters can be deduced analytically. The analytical analysis is applicable to the entire light inflaton ($m_\chi \ll m_h$) parameter space and to the heavy inflaton ($m_\chi > 2m_h$) parameter space where $m_\chi \lesssim 500$ GeV and $\beta \geq 10^{-10}$, in which DM is produced with $\langle p_N \rangle / T \sim 2.45$. For a heavy inflaton with $m_\chi \gtrsim T_{\rm eq}$, DM is produced simultaneously with the SM from a highly non-thermal infra-red inflaton distribution, and so it is necessary to solve the Boltzmann equations numerically. In the heavy inflaton parameter space the DM is strongly non-thermal with $\langle p_N \rangle / T \sim O(1-10)$ at the end of reheating. Using the known abundance of DM in the universe, the Yukawa coupling constrains the DM mass from a light inflaton to $O(10-100)$ keV and from a heavy inflaton to $O(1-10)$ MeV. The keV sterile neutrinos are classified as warm DM and the MeV sterile neutrinos are classified as cold DM, and both results are within the requirements for structure formation given by the Lyman-α data.

We constrain the mass range of the two heavier and degenerate sterile neutrinos in our model by requiring they produce sufficient LA to account for the BAU, and generate SM neutrino masses via the seesaw mechanism that are consistent with the neutrino mass splittings. We first evaluated the applicability of the leptogenesis mechanisms in the standard νMSM, in which LA can be generated during the freeze-in [11, 53, 105] and freeze-out [104, 164–166] of sterile neutrinos, to our modified νMSM. We compare the interaction rates of the sterile neutrinos with the SM and inflaton, as their equilibration rate impacts the final LA. In our model we find the sterile neutrino's interaction rate with the inflaton is greater than their interaction rate with the SM if $m_\chi > 2M_I$ and $\beta \geq 10^{-10}$. In this region of parameter space the sterile neutrinos equilibrate faster than those in the standard νMSM, resulting in a larger washout of LA that is produced during freeze-in production. We therefore choose the scenario where all the LA is efficiently generated via resonant leptogenesis during freeze-out. This conservatively limits the heavy sterile neutrino mass range to $M_{2/3} = O(10^3 - 10^{10})$ GeV, however the lower bound may be relaxed to $O(10)$ GeV according to the results presented in [201]. We find that the entropy dilution from the decay of sterile neutrinos within this mass range is Boltzmann

suppressed, with $D \sim 1$, and so it does not significantly dilute the DM abundance or generated BA.

Overall, the model provides a viable inflationary mechanism and DM generation, and is able to produce the SM neutrino masses via the see-saw mechanism and the BAU via leptogensis. The heavy inflaton parameter space evades all current experimental constraints, due to extremely low mixing of the inflaton with the Higgs sector, and strongly sterile neutrinos at cold DM velocity. A light inflaton is more likely to be detectable in future experiments, as it mixes more strongly with the Higgs sector. It produces sterile neutrinos at warm DM velocity, and so the light inflaton window may be constrained by the requirements for structure formation in the future.

A future study that could lead to potentially interesting detectable signatures would require extensions of the basic model studied here. In particular, it is possible to modify the potential so that the DM is warmer and therefore more visible. Mass terms for the Higgs doublet and sterile neutrino were removed from the Lagrangian so scale invariance is only broken in the inflaton sector, however these terms can be used to tune the sterile neutrino mass so the DM is lighter and therefore warmer. For example, the Majorana sterile neutrino mass term, $-\frac{M_I}{2}\bar{N}^c N$, can be tuned to have the opposite sign and have an equal magnitude to that acquired from the Yukawa coupling, thereby giving a smaller effective sterile neutrino mass. Alternatively, the inclusion of the symmetry breaking Higgs doublet mass term, $+\mu_\Phi^2 \Phi^\dagger \Phi$, would change the VEV of the inflaton field, and thus change the contribution to the sterile neutrino mass from the Yukawa term. Producing lighter and therefore warmer DM would allow the model to be constrained from the observation of the smallest DM structures formed in the universe.

In the following chapter we choose to re-analyse our model with the addition of the symmetry breaking Higgs doublet mass term. In this case, the Higgs quartic self-coupling, λ, is not fixed by the measurement of the Higgs boson mass, and so the EW vacuum may be stable or metastable. We argue that the universe with a positive cosmological constant should be metastable and reconstrain the parameter space of the model under this assumption, whilst evading all current cosmological and experimental constraints. If we incorporate sterile neutrino DM into our inflatonary model, we find that only inflaton with $m_\chi > O(0.1)$ GeV can produce DM that satisfies the requirements for structure formation.

Chapter 8

Light inflaton model in a metastable universe

8.1 Introduction

The SM is in excellent agreement with the experimental data at the present time. Moreover, the precision measurements of the Higgs boson mass, the top quark mass and the strong coupling constant indicate that the SM can be considered as a weakly coupled model up to the Planck scale. Intriguingly, the central measured values for the top and Higgs boson masses correspond to the situation of a metastable EW vacuum [39, 49, 263, 264]. The SM, however, does not include mechanisms for inflation [214–218], and should therefore be extended.

The experimental indication of the metastability of the EW vacuum is especially interesting in view of the theoretical expectations of the inconsistency of eternal de Sitter expansion of the universe, which would correspond to the present day dark energy domination [50, 51]. As far as it is argued that the eternal de Sitter expansion would lead to inconsistencies due to the quantum breakdown of the classical description from graviton-graviton scatterings [50, 51], it is required that the expansion finishes in some, possibly rather far, future. Therefore, we require a mechanism by which the universe can gracefully end before this critical time is reached. A universe in a false-vacuum state with a sufficiently long lifetime (a metastable vacuum) will eventually decay into the true vacuum state, thus providing us with a solution to this problem. At the same time, the inflationary scenario should lead in some way to the creation of the universe filled with this metastable state, to coincide with the current observations, in particular to our existence.

As in chapter 6, we extend the SM by an additional scalar inflaton field. Here, we study the most generic renormalizable Z_2 symmetric potential that allows the full model to be weakly coupled, which contains an additional massive parameter as compared to the previously studied model (6.3). The model can then provide us with both good inflationary behaviour while retaining metastability of the EW vacuum at present times. During inflation the Higgs direction

is stabilized by its positive mass generated by the interaction with the inflaton field [265, 266], while at late time the contribution of the inflaton is negligible, and the EW vacuum becomes metastable. In addition, by demanding that we have successful preheating with a reheating temperature at least above the EW phase transition, which is required for the generation of BA from leptogenesis, we arrive at a rather tightly constrained region of parameters for the inflaton field. In particular, this region will be largely explored by current and planned experiments on the high intensity frontier.

The chapter is organised as follows. In section 8.2 we outline the details of the model. Section 8.3 gives an overview of the metastable EW vacuum. Section 8.4 highlights the cosmological and observational constraints on the inflaton. In section 8.5 an analytical approximation of the allowed region for the experimentally observable parameters is given. Section 8.6 discusses the results. In section 8.7 we extend the model with νMSM dark matter, as in chapter 7, and evaluate the Lyman-α bound on the inflaton parameter space.

8.2 The model

In chapter 6 we minimally extended the SM with a single scalar (inflaton) field with a quartic self-coupling, serving as our scale-invariant inflationary potential; a scalar-Higgs portal coupling, which provides a mechanism for reheating; and a negative squared scalar mass term that leads to symmetry breaking in both sectors. We will now re-constrain that model with the most generic renormalizable Z_2 symmetric[1] potential, in which we have an additional negative squared mass term for the Higgs field, μ_Φ^2. The model assumes parameters that will lead to symmetry breaking of the Higgs field, tuned to the SM expected value, and of the inflaton field, to evade a relic abundance of stable particles:

$$V(X,\Phi) = \frac{\beta}{4}X^4 - \frac{1}{2}\mu_X^2 X^2 - \mu_\Phi^2 \Phi^\dagger\Phi + \lambda\left(\Phi^\dagger\Phi + \frac{\alpha}{\lambda}X^2\right)^2. \tag{8.1}$$

We consider both positive and negative α in our analysis.[2] As far as we are only interested in the situation where both fields have broken symmetry in order to correspond to observations, we can write the following formulas for μ_Φ and μ_X for any non-zero vacuum expectation values (VEVs) of the fields, $v \equiv \sqrt{2}\langle\Phi\rangle$ and $v_X \equiv \langle X\rangle$:

$$\mu_\Phi^2 = v^2\lambda + 2\alpha v_X^2, \tag{8.2}$$

$$\mu_X^2 = v_X^2\left(\beta + \frac{4\alpha^2}{\lambda}\right) + 2\alpha v^2. \tag{8.3}$$

[1] A small cubic term, μX^3, may solve the domain wall problem without influencing the dynamics of inflation and reheating, see section 6.6 for details.

[2] Note, that in equation (6.3) and previous works [43, 45–47] the sign convention for α was the opposite to (8.1), i.e. $\alpha \equiv -\alpha_{\text{present work}}$.

Going forward, we will work in the parameter space that trades μ_Φ and μ_X in favour of v and v_X, where v is the SM Higgs VEV, equal to 246 GeV. The 'vacuum angle', defined previously in equation (6.18), is

$$\tan\theta_{\rm V} \equiv \frac{v}{v_X}. \tag{8.4}$$

Spontaneous symmetry breaking of the fields gives mass to excitations of the fields on top of the vacua in the mass basis $(\tilde{h}, \tilde{\chi})$. Following the same formalism given in section 6.5 for the model given in (8.1), we find that the mass basis is rotated with respect to the gauge basis, $(h, \chi) \equiv (\sqrt{2}\Phi - v, X - \langle X\rangle)$, by the angle:

$$\tan\theta_{\rm m} = \begin{cases} +\left(\frac{2\alpha v_X}{v\lambda}\right)\frac{1}{1-\frac{m_\chi^2}{2v^2\lambda}}, & \alpha < 0 \\ -\left(\frac{2\alpha v_X}{v\lambda}\right)\frac{1}{1-\frac{m_\chi^2}{2v^2\lambda}}. & \alpha > 0 \end{cases} \tag{8.5}$$

As the angle $\theta_{\rm m}$ is a complicated expression in terms of v and v_X, in equation (8.5) we exceptionally use the mass of the physical inflaton state $\tilde{\chi}$, denoted by m_χ, for which an approximate analytical formula (8.37) is given later.

8.3 Metastability of the electroweak vacuum

The running of the Higgs quartic self-coupling, λ, to high energy scales determines the nature of the EW vacuum. If λ is positive at all energy scales, the EW vacuum is stable as it is the only vacuum state. However, if λ becomes negative at some energy scale (called the instability scale, μ_s), there exists an additional vacuum state with lower-energy that the EW vacuum will ultimately decay into. In this case, the EW vacuum is said to be metastable if its lifetime exceeds the age of the universe. Figures 8.1a and 8.1b below illustrate the renormalization group (RG) evolution of λ and the SM Higgs potential respectively, for a stable EW vacuum (blue curves) and metastable EW vacuum (red curves).

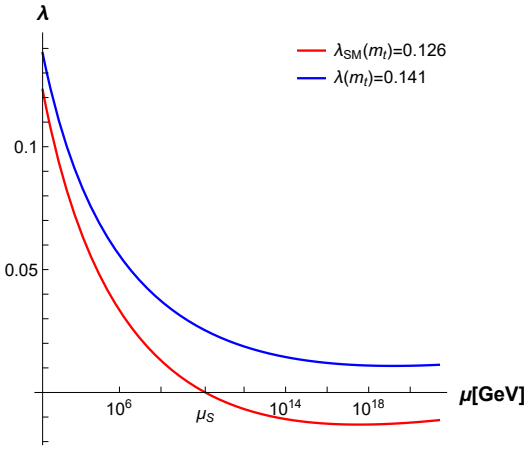

(a) 3-loop RG evolution of the Higgs self-coupling, λ, with energy scale, μ, evaluated at the SM value $\lambda_{\rm SM}(m_t) = 0.126$ in red and at $\lambda(m_t) = 0.141$ in blue. The instability scale, $\mu_S = O(10^{10})$ GeV, is the energy scale where $\lambda_{\rm SM}$ becomes negative.

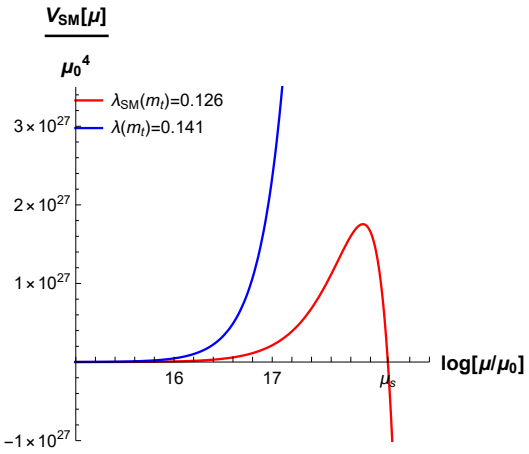

(b) The Higgs quartic potential, $V_{\rm SM}[\mu] = \frac{\lambda[\mu]}{4}\mu^4$, normalised at the reference scale $\mu_0 = m_t$.

Figure 8.1: RG evolution of the Higgs quartic self-coupling and the Higgs quartic potential

The running of λ is especially sensitive to experimental inputs of the top quark mass, m_t, and the strong coupling constant, α_s, due to the large negative contribution of the top Yukawa coupling, y_t, to λ's beta function. At 1-loop the beta functions of λ and y_t are[3] [267]:

$$\beta_\lambda = \frac{1}{16\pi^2}\left(12\lambda^2 + 6y_t^2\lambda - 3y_t^4\right), \tag{8.6}$$

$$\beta_{y_t} = \frac{1}{16\pi^2}\left(\frac{9}{4}y_t^3 - 4g_s^2 y_t\right). \tag{8.7}$$

Smaller m_t and larger α_s increase λ and therefore stabilise the EW vacuum. We use the following experimental values of the top quark's pole mass and $\alpha_s(m_Z)$, quoted with one standard deviation from their central value [39]:

$$m_t = 172.76 \pm 0.30 \text{ GeV}, \tag{8.8}$$

$$\alpha_s(m_Z) = 0.1179 \pm 0.0010. \tag{8.9}$$

The measurement of the Higgs boson mass in the SM fixes its self-coupling at the EW scale [$\lambda_{\rm SM}(m_h) = 0.1291 \pm 0.0003$ [39]]. The central values thus correspond to the metastable EW vacuum [49]. In our model, however, the value of λ is not uniquely fixed by the Higgs boson mass. Therefore, to assure the universe is in the metastable state at present, as outlined in the introduction, we just demand λ to be within the stability bound, $\lambda < \lambda_{\rm stab}$ [49]:

$$\lambda_{\rm stab}(m_t) = 0.134. \tag{8.10}$$

[3] Modification from the inflaton, X, is negligible; $\delta\beta_\lambda \sim \alpha^2 \lesssim 10^{-10}$.

Additionally λ is constrained by the instability bound, $\lambda > \lambda_{\text{instab}}$ [268, 269]:

$$\lambda_{\text{instab}}(m_t) = 0.1, \tag{8.11}$$

by the requirement that our universe exists at all; otherwise, the universe would decay faster than its lifetime. Both bounds (8.10) and (8.11) are evaluated at the central values of m_t (8.8) and α_s (8.9), with the renormalization scale equal to the top quark mass.

However, the bounds (8.10) and (8.11) alone do not ensure the survival of a mestable universe throughout the course of its history. In particular, periods of inflation and reheating could easily destabilise the metastable vacuum, and so additional model-dependent constraints are necessary. In addition to metastability constraints, those from cosmology and ensuring consistency of the model with current experimental measurements of the Higgs boson are the subjects of the following section.

8.4 Constraints

8.4.1 Cosmological constraints

8.4.1.1 Inflationary constraints

During the slow-roll inflationary epoch the classically evolving background fields converge towards the inflationary attractor solution, that is the direction along which the gradient of the potential is zero. Following the analysis carried out in section 6.3.1, the direction of the inflationary attractor solution in the field space is [43],

$$\tan\theta_{\text{inf}} \equiv \frac{\sqrt{2}\Phi_b}{X_b} \sim \sqrt{\frac{\beta - 2\alpha}{\lambda}}, \tag{8.12}$$

requiring that $|\alpha|, \beta \ll \lambda$. To establish if slow-roll inflation is compatible with a metastable universe, we evaluate Φ_b for $\alpha \lesssim 0$ and $2|\alpha| \lesssim \beta$) in Table 8.1.

	$\alpha > 0$	$\alpha < 0$
$2\lvert\alpha\rvert > \beta$	$\sqrt{2}\Phi_b = 0$	$\sqrt{2}\Phi_b \sim \sqrt{\frac{2\lvert\alpha\rvert}{\lambda[\mu]}} X_b$
$2\lvert\alpha\rvert < \beta$	$\sqrt{2}\Phi_b \sim \sqrt{\frac{\beta}{\lambda[\mu]}} X_b$	$\sqrt{2}\Phi_b \sim \sqrt{\frac{\beta}{\lambda[\mu]}} X_b$

Table 8.1: Φ_b evaluated from equation (6.12) for $\alpha \lesssim 0$ and $|\alpha| \lesssim \beta$

In regions of parameter space where $\theta_{\text{inf}} \neq 0$, we require the initial condition that $\Phi_b(0)$ starts from a point in field space where $\lambda[\Phi_b] > 0$. $\Phi_b(t)$ then evolves to larger field values as it converges towards the inflationary attractor solution, which simultaneously increases as λ

runs to higher energy scales. For most of the metastability parameter space, Φ_b evolves to field values of $O(10^{16} - 10^{18})$ GeV, which greatly exceed the instability scale, thus $\lambda[\Phi_b]$ becomes negative and the inflationary attractor breaks-down. Only λ within $\sim 1\%$ of the stability bound (8.10) gives $\Phi_b < \mu_s$ during inflation. Additionally for $\alpha < 0$, the negative cross-term is large enough to dominate the Higgs potential up to the scale of $O(M_{\rm P})$ if

$$\alpha \gtrsim O\left(10^{-10} \times \left(\frac{\mu_s[\text{GeV}]}{10^{16}}\right)^2\right). \tag{8.13}$$

In this region, the potential is unstable at the origin and so the Higgs field can only evolve towards the vacuum state beyond the scale of $M_{\rm P}$. We conclude that a non-zero inflationary attractor is only compatible with slow-roll inflation in a metastable universe for finely-tuned $\lambda \sim \lambda_{\rm stab}$ in the parameter space $\alpha > 0$ & $2|\alpha| < \beta$, and $\alpha < 0$ if $|\alpha|$ is smaller than the destabilising region defined in (8.13). The focus of our analysis going forward will therefore be on constraining the region $\alpha > 0$ & $2|\alpha| > \beta$, where for $\Phi_b = 0$, we evade the need to finely tune λ. Parameters within this region correspond to the light inflaton parameter space that was analysed in section 6.8. We can therefore apply the same inflationary and reheating constraints evaluated in section 6.8 to our model in sections 8.4.1.1 and 8.4.1.2.

The inflationary potential is constrained by the CMB measurement of the primordial scalar density perturbation amplitude [226], given in (3.103), and the tensor-to-scalar ratio limit [48, 219, 220], given in (3.105). Following the same procedure as in section 6.3, to ensure r is within the CMB limit, we require a non-minimal coupling of the scalar field to gravity $\left(\xi X^2 R/2\right)$ with $\xi \geq O(10^{-2})$. If we assume no new scales below the Planck scale ($\xi < 1$), we obtain the following range for the scalar field quartic self-coupling [46, 48]:

$$O(10^{-12}) \leq \beta \leq O(10^{-9}), \tag{8.14}$$

where the lower bound corresponds to the excessive production of tensor modes and the upper bound would require $\xi > 1$ and introduces additional scales below Planck.

Additionally, to ensure quantum corrections to the inflaton quartic self-coupling are sufficiently small and the inflationary analysis above holds, as in (6.62), we require [45]

$$\alpha < \alpha_{\rm max} = (0.1\beta)^{\frac{1}{2}}. \tag{8.15}$$

8.4.1.2 Constraints from preheating and reheating

For efficient sphaleron conversion of lepton to baryon asymmetry, we require the reheating temperature to exceed the EW symmetry breaking scale, $T_{\rm EW} = 160$ GeV [68]. The minimum reheating temperature requirement translates to a lower bound on α, which has been

established previously for the model with $\mu_\Phi^2 = 0$. The analyses are carried out separately for $m_\chi < 2m_h$ in section 6.8 [45–47] and $m_\chi > 2m_h$ in section 6.9 [43], as they reheat via different mechanisms: $\chi\chi \to hh$ and $\chi \to hh$ respectively. However, inflation requires our model to have $\alpha > 0$ & $2|\alpha| > \beta$ (for λ that is not finely-tuned), which limits us to light inflaton, $m_\chi \lesssim m_h$.

Following inflation is a preheating period, during which parametric resonance excites inflaton particles to occupy a highly infra-red distribution but does not efficiently transfer energy into the SM (due to $\alpha \ll \lambda$). The inflaton distribution slowly evolves self-similarly towards thermal equilibrium [232, 233] until perturbative reheating proceeds once the mean-free path is comparable to the Hubble expansion rate, $n_\chi \sigma_{\chi\chi\to hh} \sim H$ [46]. Assuming at this moment the inflatons have not yet thermalised, the minimum reheating temperature ($T_{\rm reh} > T_{\rm EW}$) imposes the following lower bound on α,

$$\alpha > \alpha_{\rm min} \sim (1.6 \times 10^{-9}) \left(\frac{\beta}{10^{-12}}\right)^{\frac{3}{7}}, \tag{8.16}$$

which we evaluated in section 6.8. Together with (8.15) this fully closes the $\beta - \alpha$ parameter space:

β	α
10^{-9}	$(3.1 \times 10^{-8}) - (1.0 \times 10^{-5})$
10^{-10}	$(1.1 \times 10^{-8}) - (3.2 \times 10^{-6})$
10^{-11}	$(4.2 \times 10^{-9}) - (1.0 \times 10^{-6})$
10^{-12}	$(1.6 \times 10^{-9}) - (3.2 \times 10^{-7})$

Table 8.2: Light inflaton $\beta - \alpha$ parameter space that allows for successful inflation and reheating

8.4.1.3 Big Bang Nucleosynthesis constraints

The measurement of primordial elemental abundances tightly constrains the number of additional relativistic degrees of freedom (evaluated in (2.83) to be approximately less than half a neutrino species) to the SM at this epoch [55]. A light inflaton should therefore preferably decay prior to Big Bang Nucleosynthesis (BBN), $\Gamma_\chi^{-1} \lesssim 1$ s, which constrains the mixing angle from below:

$$\Gamma_\chi = \sin^2\theta_{\rm m} \Gamma_h(m_\chi), \tag{8.17}$$

$$\theta_{\rm m} \gtrsim \sqrt{\frac{\Gamma_h^{-1}(m_\chi)}{1\ {\rm s}}}. \tag{8.18}$$

Here $\Gamma_h(m_\chi)$ is the SM Higgs boson decay width evaluated if its mass is equal to m_χ [48]. The lower bound on $\theta_{\rm m}$ is evaluated for $m_\chi \leq 1$ GeV in Table 8.3.

m_χ[GeV]	$(\theta_{\mathbf{m}}^{\mathbf{BBN}})^2$
10^{-4}	0.44
10^{-3}	3.3×10^{-4}
10^{-2}	3.9×10^{-10}
10^{-1}	3.8×10^{-11}

Table 8.3: Minimum $\theta_{\rm m}$ for a given inflaton mass, to ensure decay prior to BBN

Inflaton that are heavy enough to have hadronic decay modes ($m_\chi \gtrsim 2m_\pi \sim 0.3$ GeV), are more tightly constrained by BBN to have a lifetime $\Gamma_\chi^{-1} < O(0.01)$ s [94, 95]. However, inflatons with mass above the muon threshold ($m_\chi \gtrsim 2m_\mu \sim 0.2$ GeV) have a much shorter lifetime of $\Gamma_\chi^{-1} < O(10^{-5})$ s [47], and so there are no further BBN constraints in this region.

8.4.2 $\langle X \rangle = 0$ is excluded by overclosure of the universe

The relic inflaton with $\langle X \rangle = 0$, which cannot deplete via decay into the SM, freezes out with a large abundance. This could be a possible source of DM with the inflaton playing the role of a weakly interacting massive particle (WIMP), but this situation is fully excluded, as it leads to overclosure of the universe.

Post reheating the inflaton is in thermal equilibrium with the SM bath. However, as the universe expands and cools, the inflaton decouples and freezes out once its annihilation rate drops below the Hubble expansion rate. Using equation (4.23), we find that inflatons that are non-relativistic at the time of freeze-out, $T_f < m_\chi$, have a relic abundance today of [55]

$$\Omega_\chi \sim \frac{O(10^{-10})\ \text{GeV}^{-2}}{\langle \sigma_{\rm ann} v \rangle}. \tag{8.19}$$

The cross-section of the Higgs-mediated s-channel annihilation into SM particles is

$$\langle \sigma_{\rm ann} v \rangle_{\chi\chi \to \text{SM SM}} = \frac{1}{2} \frac{|M_{\chi\chi\to h}|^2}{\sqrt{s}} \frac{1}{|D_h(s)|^2} \Gamma_h(\sqrt{s}), \tag{8.20}$$

where $|M_{\chi\chi\to h}| = 4\alpha v$ and the invariant mass at $T \lesssim m_\chi$ is $\sqrt{s} \approx 2m_\chi$, and the propagator term is

$$|D_h(s)|^2 = \frac{1}{(s-m_h^2)^2 + m_h^2 \Gamma_h(m_h)^2} \sim \begin{cases} \frac{1}{m_h^4}, & m_\chi \ll m_h \\ \frac{1}{16 m_\chi^4}. & m_\chi \gg m_h \end{cases} \tag{8.21}$$

The Higgs-mediated s-channel annihilation into SM particles is the dominant contribution to

the light inflaton cross-section, $m_\chi \ll m_h$,

$$\langle \sigma_{\rm ann} v \rangle_{\chi\chi \to \rm SM\ SM} \sim \frac{4\alpha^2 v^2}{m_\chi m_h^4} \Gamma_h(2m_\chi) \lesssim O(10^{-20})\ \text{GeV}^{-2}, \tag{8.22}$$

for $m_\chi \leq 1$ GeV and $\alpha \leq 10^{-5}$. For a heavy inflaton, $m_\chi > m_h$, there is an additional contribution from the direct two-to-two inflaton-Higgs vertex,

$$\begin{aligned} \langle \sigma_{\rm ann} v \rangle_{\chi\chi \to \rm SM\ SM} + \langle \sigma_{\rm ann} v \rangle_{\chi\chi \to \rm hh} &\sim \frac{\alpha^2 v^2}{4m_\chi^5} \Gamma_h(2m_\chi) + \frac{\alpha^2}{16\pi m_\chi^2}, \\ &\lesssim O(10^{-17})\ \text{GeV}^{-2}, \end{aligned} \tag{8.23}$$

for $m_\chi \leq 10^3$ GeV and $\alpha \leq 10^{-5}$. In both cases, (8.22) and (8.23), the inflatons overclose the universe, $\Omega_\chi \gg \Omega_{\rm DM}$. Very light inflatons are relativistic at the time of freeze-out, $T_f \gg m_\chi$, and have a relic abundance today of [55, 147]

$$\Omega_\chi \sim \Omega_{\rm DM} \left(\frac{m_\chi}{O(10)\ \text{eV}} \right), \tag{8.24}$$

which we evaluated using equation (4.12), assuming 1 MeV $\lesssim T_f \lesssim$ 100 MeV that corresponds to $g_{*s}(T_f) = 10.75$ effective degrees of freedom. BBN constraints disfavour $m_\chi \ll T_{\rm BBN} \sim 1$ MeV, so we conclude that very light inflatons also overclose the universe. As a result of this analysis, our model is constrained by the requirement that $\langle X \rangle \neq 0$.

8.4.3 Particle physics constraints

8.4.3.1 Higgs measurement constraints

Our model must also be consistent with the current experimental measurement of the Higgs boson's signal strength and the invisible decay width bound. The signal strength, μ, is defined as the product of the Higgs boson production cross-section and its branching ratio ($\sigma \cdot BR$) observed, normalised to that of the SM. The result from combined ATLAS and CMS Run 1 data is [255]

$$\mu \equiv \frac{(\sigma \cdot BR)_{\rm obs}}{(\sigma \cdot BR)_{\rm SM}} = 1.09 \pm 0.11. \tag{8.25}$$

Given that for our model

$$(\sigma \cdot BR)_{\rm obs} = \cos^2\theta_{\rm m} (\sigma \cdot BR)_{\rm SM}, \tag{8.26}$$

we obtain the following 1σ upper bound on the mixing angle $\theta_{\rm m}$,

$$|\theta_{\rm m}| < |\theta_1| = 0.14. \tag{8.27}$$

In the parameter space $m_\chi < m_h/2$, there is an additional bound from the Higgs boson's invisible branching ratio, $BR_{\rm inv}$,

$$\Gamma_{h\to\chi\chi} \leq \left(\frac{1}{1-BR_{\rm inv}} - \cos^2\theta_{\rm m}\right)\Gamma_{SM}, \tag{8.28}$$

where $\Gamma_{\rm SM} = 4.1$ MeV is the theoretical SM Higgs boson width and

$$\Gamma_{h\to\chi\chi} \simeq \frac{\alpha^2 v^2}{2\pi m_h}\left(1 + 6\frac{(\lambda_{\rm SM}-\lambda)^{\frac{1}{2}}}{\lambda}\right)^2, \tag{8.29}$$

evaluated in the limit $\mu_\Phi^2 \gg v^2\lambda$ and $m_\chi \ll m_h$. The 95% C.L. limit on the invisible branching ratio from combined ATLAS Run 1 and Run 2 data is $BR_{\rm inv} = 0.26$ [270], which imposes a weaker bound on our parameter space than (8.27). Although this bound will not contribute to our results, this analysis may be useful for future reference.

8.4.3.2 Direct detection constraints

Furthermore, it is possible to directly constrain the inflaton particle created in high intensity experiments, which either escapes the detector (invisible mode) or decays later into a pair of observable particles. The constraints on a light scalar boson with the Higgs mixing angle, $\theta_{\rm m}$, and mass, m_χ, can readily be used [246, 271–280] and are shown in Figures 8.2a and 8.2b.

8.4.4 Stability Constraints

8.4.4.1 Inflation

To prevent the universe from being trapped in the true vacuum state, we require that the Higgs field value remains below the potential's instability scale, μ_V, defined as the energy scale where the Higgs potential is zero[4]. Although the inflationary attractor rapidly converges the Higgs background field to zero, we also need to ensure quantum fluctuations of the Higgs field, h, during inflation do not destabilise the EW vacuum.

The effective mass of h is dominated by the large inflaton field variance during slow-roll inflation. Evaluated at 60 e-foldings prior to the end of inflation, $X_{60} = O(10M_{\rm P})$, when the

[4]The energy scale that the Higgs potential is zero, μ_V, does not equal the SM instability scale, μ_s, for non-zero values of the inflaton field, due to the inflaton-Higgs quartic coupling. When the inflaton field value is zero, we just have $\mu_V = \mu_s$.

largest vacuum fluctuations are produced,

$$m_{\text{eff}} = \sqrt{3\lambda\langle\Phi_{60}^2\rangle + 2\alpha\langle X_{60}^2\rangle} \sim O(\sqrt{\alpha} \times 10^{19}) \text{ GeV}; \tag{8.30}$$

for simplicity we ignore the contribution from the backreaction of the Higgs field here. The large m_{eff} stabilisies the EW vacuum by pushing the potential's instability scale to higher energy scales with respect to the SM [265, 266]

$$\mu_V \sim \frac{m_{\text{eff}}}{\sqrt{|\lambda|}} \gtrsim O(10^{15} - 10^{17}) \text{ GeV}, \tag{8.31}$$

where $|\lambda| \leq O(0.01)$. As m_{eff} is greater than the Hubble expansion rate[5] [48],

$$H(X_{60}) = \sqrt{\frac{U(X_{60})}{3M_{\text{P}}^2}} = O(10^{13} - 10^{14}) \text{ GeV}, \tag{8.32}$$

the amplitude of inflationary enhanced quantum fluctuations of the Higgs field is [265, 266]

$$h = O\left(\frac{H(X_{60})}{10}\right) \sim O(10^{13} - 10^{12}) \text{ GeV}. \tag{8.33}$$

So we conclude that the EW vacuum is not destabilised during inflation, as we have shown $\mu_V > \Phi$ across the entire parameter space where $\alpha > 0$ & $2|\alpha| > \beta$.

8.4.4.2 Preheating and reheating

Post-slow-roll inflation, the oscillatory zero-mode inflaton transfer energy into excitations of the fields through parametric resonance, which could destabilize the EW vacuum if the Higgs fluctuations exceed the instability scale. However, this is evaded as the Higgs scattering rate greatly exceeds the production rate, $\lambda \gg \alpha$, thereby promptly halting the transfer of energy into excitations of the Higgs field [43].

In the perturbative reheating regime, we require temperatures to exceed the EW symmetry breaking scale. Assuming the inflatons are non-thermal, the range of reheating temperatures are

$$T_{\text{reh}} = O(T_{\text{EW}} - 10^{10}) \text{ GeV}, \tag{8.34}$$

which we evaluated in (6.64). Relatively low reheating temperatures stabilize the Higgs poten-

[5] $U(X_{60})$ is the conformally transformed potential given in equation (6.6), which is a decreasing function of β, evaluated in the range $\beta = O(10^{-12} - 10^{-9})$ [48].

tial due to the addition of the thermal Higgs mass [281],

$$V_{eff}(T,h) \approx V_{eff}(0,h) + \frac{m_{\rm T}^2}{2}h^2, \qquad (8.35)$$
$$m_{\rm T}^2 \sim \left(\frac{\lambda}{2} + \frac{g_t^2}{4}\right)T^2,$$

as positive thermal corrections increase the instability scale. However, very high temperatures induce local nucleation of bubbles that probe the instability region, either via quantum tunnelling from an excited state or classical excitation over the potential barrier. The bubbles then expand rapidly, close to the speed of light, and destroy everything in their way [264, 268, 282]. However, cutting the parameter space at the 1σ Higgs signal strength bound (8.27) restricts λ to the range $0.123 < \lambda(m_t) \leq \lambda_{\rm SM}$, and for

$$\lambda(m_t) > 0.120, \qquad (8.36)$$

the EW vacuum is sufficiently stable up to $T_{\rm reh} = O(M_{\rm P})$ [49, 268, 283]. We therefore assume the universe can safely reheat; however, if a less stringent Higgs signal strength bound was to be considered, cuts from reheating may be necessary to ensure thermal fluctuations do not destabilise the EW vacuum.

8.5 Analytical approximations

The analytical approximations for the inflaton and Higgs boson masses for $\alpha > 0$ & $2|\alpha| > \beta$ are:

$$m_\chi^2 \approx 2\beta v_X^2 - \frac{\beta^2 v_X^4}{2\lambda v^2} + O(\alpha,\beta,\alpha^2), \qquad (8.37)$$
$$m_h^2 \approx 2\lambda v^2 + \frac{\beta^2 v_X^4}{2\lambda v^2} + O(\alpha,\beta,\alpha^2) = 2\lambda_{\rm SM} v^2,$$

where the SM Higgs quartic coupling is $\lambda_{\rm SM}(m_h) = 0.129$. By fixing the Higgs mass, we obtain the $\lambda - v_X$ parameter space, for a given value of α and β,

$$\lambda_\pm = \frac{\lambda_{\rm SM}}{2}\left(1 \pm \sqrt{1 - \frac{4\beta^2 v_X^4}{m_h^4}}\right). \qquad (8.38)$$

In the limit $v_X \ll \frac{m_h}{\sqrt{2\beta}}$, the two solutions are

$$\begin{cases} \lambda_+ \sim \lambda_{\rm SM}\left(1 - \left(\frac{\beta v_X^2}{m_h^2}\right)^2\right), \\ \lambda_- \sim \lambda_{\rm SM}\left(\frac{\beta v_X^2}{m_h^2}\right)^2, \end{cases} \qquad (8.39)$$

however λ_+ is the only solution that lies within the metastability bounds (8.10) and (8.11). The maximum value of v_X is when $\lambda = \frac{\lambda_{\rm SM}}{2}$,

$$v_{X,\max} \approx \frac{m_h}{\sqrt{2\beta(1+Y)}} \tag{8.40}$$

where $Y = \frac{16\alpha^2}{\beta\lambda_{\rm SM}}$. For $Y < 1$, $v_{X,\max}$ is a decreasing function of β, and for $Y \gtrsim 1$, $v_{X,\max}$ is a decreasing function of α. Using approximations (8.37) and (8.40), we can then see that the maximum inflaton mass approaches the Higgs mass for the smallest Y and is suppressed for a larger Y,

$$m_{\chi,\max} \approx \frac{m_h}{\sqrt{1+Y}} \sim \begin{cases} m_h, & \text{if } Y \ll 1 \\ \sqrt{\frac{\beta}{8\alpha^2}}\lambda_{\rm SM} v. & \text{if } Y > 1 \end{cases} \tag{8.41}$$

8.6 Results

We obtain the $m_\chi - \theta_{\rm m}^2$ parameter space for a given value of the inflaton self-coupling, β, which is plotted in Figure 8.2 for $\beta = 10^{-9}$ (top) and $\beta = 10^{-12}$ (bottom). The shaded regions define theoretical bounds, while solid and dashed lines define current and future experimental bounds respectively. The dotted black curves are lines of constant α, and the solid green/blue lines define the boundaries for maximum/minimum α, which are given in Table 8.2. The parameter space is fully closed by the solid red line, which gives the 1σ bound from ATLAS and CMS measurements of the Higgs signal stength (8.27), and the shaded grey region, which eliminates the parameter space where $\Gamma_\chi^{-1} \leq 1$s to ensure inflaton decay prior to BBN (Table 8.3). The analytical approximation of the maximum inflaton mass (8.41) is in agreement with the results in Figure 8.2, which show that the maximum inflaton mass approaches the Higgs boson mass for smallest α and is suppressed for larger α.

Inflatons with $m_\chi \sim (1\text{ GeV} - m_h)$ have larger mixing angles and so future precision experiments may observe suppressed production cross-sections and tri-linear/quartic Higgs couplings with respect to the SM expectation. The (almost) horizontal dot-dashed lines in Figure 8.2 are isocurves of the tri-linear Higgs coupling, $\lambda v \cos^3\theta_{\rm m}$, which are suppressed by up to 2% with respect to the SM expected value ($\lambda_{\rm SM} v = 31.7$). However, fully disentangling the parameter space will require multiple particle physics observables, including the Higgs' couplings and signal strength, as well as a tighter bound on the invisible decay width, corresponding to $\Gamma_{h\to\chi\chi}$ (8.29) in our model. Additionally, a measurement of the tensor-to-scalar ratio would allow us to fix β.

Because of an increase in motivation to search for new physics in the hidden sector, i.e. particles with sub-EW mass that are very weakly-coupled to the SM, there are plans for a large

number of future experiments to probe regions beyond the reach of the Large Hadron Collider (LHC) [278]. The testability of our model would greatly benefit from these proposals, as with a combination of experiments, our parameter space could be accessible down to $\theta_{\rm m}^2 = O(10^{-11})$ for inflaton masses in the range $m_\chi \sim (0.03-5)$ GeV, as shown by the dashed coloured contours in Figure 8.2.

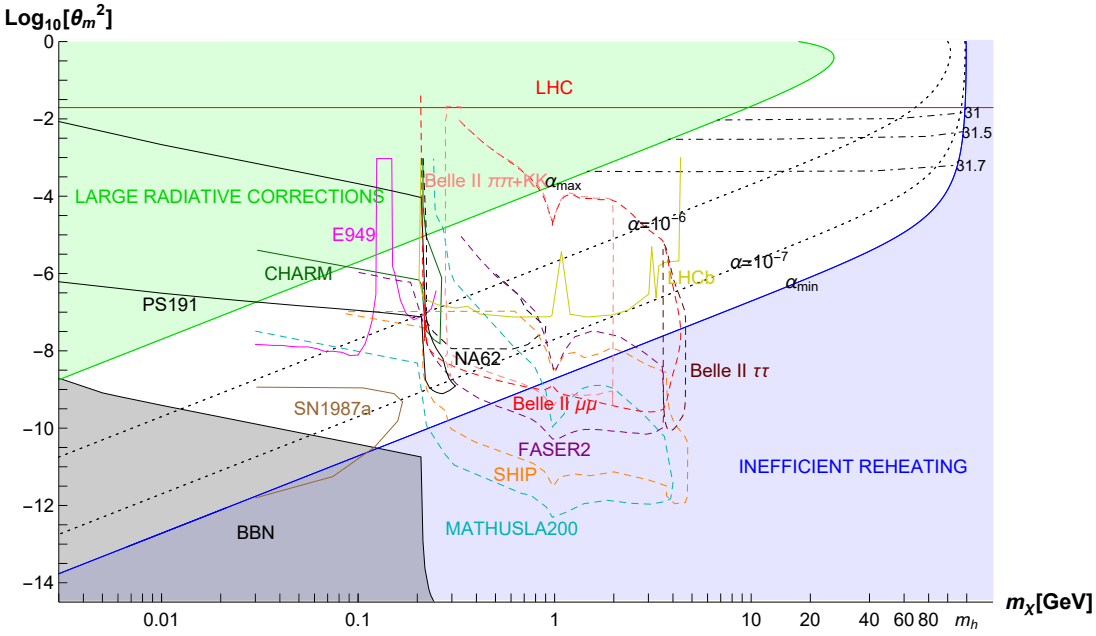

(a) $\beta = 10^{-9}$

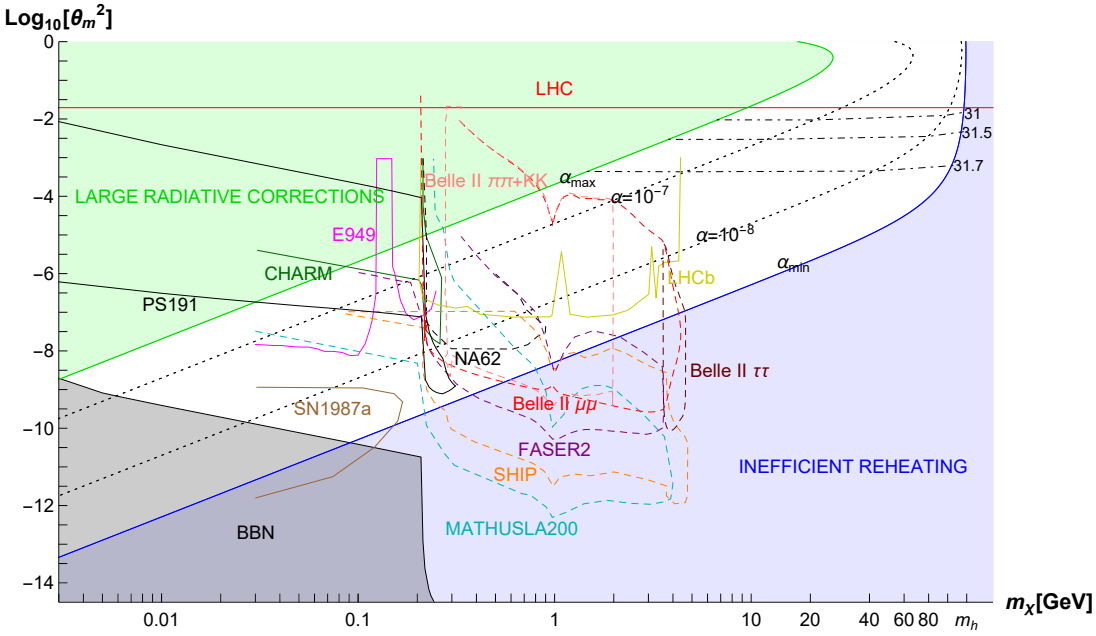

(b) $\beta = 10^{-12}$

Figure 8.2: Exclusion plot of light inflaton paramater space in a metastable universe

The plots give the parameter space of the squared mixing angle, $\mathrm{Log}_{10}[\theta_{\mathrm{m}}^2]$, against the inflaton mass m_χ, for $\beta = 10^{-9}$ (top) and $\beta = 10^{-12}$ (bottom). The shaded regions are theoretical bounds: (i) Bottom-right (blue): inefficient reheating, $T_{\mathrm{reh}} < T_{EW}$ (Table 8.2); (ii) Bottom-left (grey): inflaton decay after BBN, $\Gamma_\chi > t_{\mathrm{BBN}}$ where $t_{\mathrm{BBN}} \sim 1\mathrm{s}$ (Table 8.3); (iii) Top-left (green): large radiative corrections to the inflationary potential, $\alpha^2 > 0.1\beta$ (Table 8.2). The full and dashed lines are existing and future experimental bounds. The LHC bound is the 1σ bound from the ATLAS and CMS Higgs' signal strength measurements, given by (8.27). All other experimental bounds are taken from [246, 271–280]. Dotted lines are curves of constant α, and the (almost) horizontal dot-dashed lines are isocurves of the trilinear Higgs coupling, $\lambda v \cos^3\theta_{\mathrm{m}}$.

8.7 Sterile neutrino dark matter

As in chapter 7, we can incorporate DM production by extending our light inflaton model with a νMSM that is modified with the addition of a $N_I - X$ Yukawa coupling [43, 45, 46]:

$$L_{\nu MSM+X} = L_{\nu MSM} + \frac{1}{2}(\partial_\mu X)^2 - \frac{f_I}{2}\overline{N_I}^c N_I X + h.c. + V(X,\Phi), \tag{8.42}$$

where $V(X,\Phi)$ is the potential of our light scalar inflaton model given in (8.1). Spontaneous symmetry breaking in the inflaton sector, $X \to v_X + \chi$, initiates DM sterile neutrino production via inflaton decay in the early universe, $\chi \to N_1 N_1$, and generates the DM sterile neutrino mass,

$$M_1 = v_X f_1. \tag{8.43}$$

Our light inflaton model in chapters 6 and 7 assumes scale symmetry is only broken in the scalar sector (i.e. $\mu_\Phi = 0$). As inflation constrains the maximum value of α to be very small, within bound (6.62), the inflaton field has a very large VEV, given by equation (6.17), with $v_X \geq O(10^4)$ GeV. The results of our analysis on sterile neutrino DM production in sections 7.4 and 7.5 concluded that the DM sterile neutrinos are heavy and cool enough to be within the requirements for structure formation, given by the Lyman-α data. However, with the addition of the Higgs doublet massive parameter in (8.1), the model can have a much smaller inflaton VEV when $\mu_\Phi^2 \sim v^2\lambda$,

$$v_X = \sqrt{\frac{\mu_\Phi^2 - v^2\lambda}{2\alpha}} \ll \sqrt{\frac{v^2\lambda}{2\alpha}}. \tag{8.44}$$

As a result, model (8.1) is able to generate much lighter and warmer DM. Next we are going to evaluate the lowest inflaton mass that could generate DM consistent with Lyman-α data.

The Lyman-α free-streaming bound (4.52) constrains the lower mass of the DM particle,

$$M_1 > 36.4 \text{ keV } g_{\rm SM}(T_{\rm prod})^{-\frac{1}{3}} \left(\frac{\langle p\rangle}{3.15 T_{\rm prod}}\right). \tag{8.45}$$

Here we have used the conservation of entropy (2.22) to obtain the momentum at $T \approx M_1$ in equation (4.50) for the free-streaming length, by rescaling the momentum on production by the number of degrees of freedom. In section 7.4.1, we analytically evaluate the DM sterile neutrino mass for our $\mu_\Phi = 0$ model in the light inflaton parameter space, where relativistic inflatons have thermalised with the SM prior to DM production. The results of the analysis is applicable to our $\mu_\phi \neq 0$ model with $m_\chi \leq O(1)$ GeV, where $T_{\rm reh} \gg m_\chi$ and $m_\chi \approx \sqrt{2\beta} v_X$.

Then, equating the analytical approximation for M_1 in equation (7.20) with (8.45), we obtain a lower inflaton mass bound of

$$m_\chi > 36.6 \text{ GeV } g_{\text{SM}}(T_{\text{prod}})^{-\frac{5}{6}} \left(\frac{0.25}{\Omega_{\text{DM},0}}\right)^{\frac{1}{3}} \left(\frac{\beta}{10^{-9}}\right)^{\frac{1}{3}} \left(\frac{\langle p \rangle}{3.15 T_{\text{prod}}}\right), \tag{8.46}$$

where the DM sterile neutrinos are produced with an average momentum of $\langle p \rangle = 2.45 T_{\text{prod}}$ and $T_{\text{prod}} \sim m_\chi/2$. The Lyman-$\alpha$ inflaton mass bound for $\beta = 10^{-9}/10^{-12}$ is

$$m_\chi > \begin{cases} 0.7 \text{ GeV } \left(\frac{80}{g_{\text{SM}}(T_{\text{prod}})}\right)^{\frac{5}{6}}, & \beta = 10^{-9} \\ 0.4 \text{ GeV } \left(\frac{10}{g_{\text{SM}}(T_{\text{prod}})}\right)^{\frac{5}{6}}, & \beta = 10^{-12} \end{cases} \tag{8.47}$$

which corresponds to DM with $M_1 \geq O(10)$ keV. Note that we have analytically evaluated (8.46) in (8.47) by taking $g_{\text{SM}}(T_{\text{prod}})$ as constant throughout DM production. However, $g_{\text{SM}}(T_{\text{prod}})$ is a rapidly changing function of temperature for $m_\chi \sim O(0.1 - 1)$ GeV and so these bounds should be taken as rough estimates. Interestingly, the inflaton mass bounds are within the visible region of the inflaton parameter space, as shown by the current and future experimental sensitivity bounds in Figure 8.2. A measurement of the scalar particle would therefore allow us to predict the viability and properties of our DM model.

8.8 Discussion and conclusion

Our model minimally extends the SM via the addition of a single scalar inflaton field with a Z_2-symmetric potential. By doing so, we are able to incorporate mechanisms for inflation via the quartic scalar coupling, efficient reheating via the scalar-Higgs portal, and symmetry breaking in the Higgs and scalar sectors by the addition of two negative mass terms.

The addition of the scalar-Higgs portal rotates the mass basis of our model with respect to the gauge basis. As a result, the Higgs boson mass does not define uniquely its quartic coupling and so the stability of the EW vacuum is determined not only by the measurements of SM parameters, but also by the properties of the inflaton field. In order to constrain our model, we instead use the argument that an eternally accelerating universe is impossible [50, 51] to motivate the need of a metastable EW vacuum. However this is problematic during inflation, as here if λ becomes negative for an inflationary attractor that does not align along $\Phi_b = 0$, it will break down. Only if λ is finely tuned close to the stability bound can this be avoided. We therefore proceeded to analyse the case where fine-tuning is not necessary: in the parameter space where the inflationary attractor solution is $\Phi_b = 0$, given by $\alpha > 0$ & $2|\alpha| > \beta$. Additionally, this region of parameter space benefits from generating a large effective mass of the Higgs field during inflation, which exceeds the Hubble expansion rate. As a result, the

instability scale of the Higgs potential exceeds the amplitude of the Higgs inflationary-enhanced quantum fluctuations, thereby preventing the EW vacuum from being destabilized.

The range of the inflaton self-coupling, β, is determined by the CMB amplitude of scalar perturbations and the upper-bound on the tensor-to-scalar ratio. For a given value of β, the range of the inflaton-Higgs coupling, α, is bounded from below, to ensure reheating temperatures exceeds the EW symmetry breaking scale, and from above, so quantum corrections to the inflationary potential are sufficiently small. The maximum inflaton mass approaches m_h for $\alpha^2/\beta \leq O(10^{-4})$, and is suppressed for $\alpha^2/\beta \geq O(10^{-2})$. We require the inflatons to have a non-zero VEV so that post-reheating they are depleted via decay into SM particles. Inflatons with zero VEV are stable and would overclose the universe. We require inflatons to decay prior BBN due to the tightly constrained number of additional degrees of freedom at this epoch, thereby constraining inflatons with $m_\chi = O(0.001 - 0.1)$ GeV to have $\theta_{\rm m}^2 \geq O(10^{-9} - 10^{-11})$.

To be consistent with the observed Higgs signal strength results, there is an upper-bound on the inflaton-Higgs mixing angle, $\theta_{\rm m} \leq 0.14$, which translates to a lower bound on the Higgs self-coupling, $\lambda(m_t) \geq 0.123$. Within this bound, we evade additional cuts to the parameter space from reheating, as for $\lambda(m_t) > 0.120$ the EW vacuum is stable up to $T_{\rm reh} = O(M_{\rm P})$. Note that the interesting metastable region in our model ($0.123 \leq \lambda(m_t) \lesssim \lambda_{\rm SM}$) exists for any value of top quark mass within reasonable experimental errors given in (8.8). Even if the top quark is light enough for the SM to be stable, this would just reduce the stability bound (8.10) and only slightly shrink the allowed region in Figures 8.2a and 8.2b.

We can include freeze-in DM production in our model through the addition of a Yukawa coupling of the inflaton to sterile neutrinos, within the framework of the νMSM. In the parameter space $2|\alpha| > \beta$ and $m_\chi \leq O(1)$ GeV, DM is produced once the inflaton has thermalised and so the model parameters can be deduced analytically. A very light inflaton with $m_\chi = O(0.001 - 0.1)$ GeV has a small VEV and thus produces light and very warm DM with $M_1 < O(10)$ keV, which is excluded by the requirements for structure formation.

To conclude, the parameter space for $\alpha > 0$ & $2|\alpha| > \beta$, which evades all current experimental, cosmological and stability constraints required for a metastable vacuum, spans light inflaton with masses $O(10^{-3} - 125)$ GeV and mixing angles $\theta_{\rm m}^2 = O(10^{-11} - 10^{-2})$. We have a rich set of experimental probes from particle physics and cosmology to study our model, which requires a multitude of observables: from measurements of the Higgs couplings, invisible decay width and production cross-section, and a measurement of the tensor-to-scalar ratio. Future upgrades of current experiments may be sensitive enough to observe suppressed linear and trilinear couplings Higgs couplings with respect to the SM in the parameter space of larger mixing angles, $\theta_{\rm m}^2 \geq O(10^{-4})$, where inflatons have masses $m_\chi \gtrsim 1$ GeV. However, accessibility to the parameter space of very weakly-coupled inflatons is dependent on the planned proposals

of new experiments [278] that target the hidden sector (namely MATHUSLA200, SHIP, and FASER2). The experimental testability of our model would greatly benefit from a combination of these experiments, which can probe mixing angles down to $\theta_{\rm m}^2 = O(10^{-11})$ and inflatons with masses $m_\chi \sim (0.03-5)$ GeV. A measurement of the inflaton within the visible mass range would allow us to predict the viability and properties of our DM model, where for an inflaton with $m_\chi \leq O(0.1)$ GeV, our DM model would be excluded by constraints from Lyman-α data.

Chapter 9

Conclusions and outlook

In this thesis we analyse cosmological models that aim to solve some of the fundamental problems in cosmology and the SM: explaining the homogeneity and isotropy of the universe, SM and DM production, large scale structure formation, and the generation of the BAU and SM neutrino masses. We study three variations of a minimal single-field inflationary model. First we constrain the basic model, with one scalar mass term, which provides mechanisms for inflation and reheating. We then extend the basic model with a modified νMSM that provides a mechanism for DM production, and generates the SM neutrino masses and the BAU. Finally, we re-constrain a generic Z_2 symmetric inflationary model with two mass terms, under the assumption that our universe is metastable. We will now summarise the results and the limitations of our models, noting where we have made assumptions and approximations, where improvements and extensions to our analysis could be made in the future, and the prospects of experimental searches.

Our basic inflationary model incorporates mechanisms for inflation and reheating through minimally extending the SM with a single scalar inflaton field. The model has a Z_2 symmetric potential, with a quartic scalar self-coupling (β), a negative scalar mass term (μ_X^2) and an inflaton-Higgs portal coupling (α). The quartic inflaton term dominates the energy density of the universe during inflation, when inflaton field values are $X > O(M_{\rm P})$. In order for our model to be within the tensor-to-scalar ratio, we are required to introduce a non-minimal coupling of the inflaton field to gravity. Using the slow-roll formalism, the inflaton quartic self-coupling is constrained by the CMB's measurement of the amplitude of scalar perturbations to the range $\beta = O(10^{-12} - 10^{-9})$, where the lower bound corresponds to the excessive production of tensor modes and the upper bound introduces additional scales below Planck. The negative scalar mass term gives rise to symmetry breaking in the inflaton sector. The inflaton-Higgs portal coupling then allows for the transfer of symmetry breaking into the Higgs sector, with parameters tuned to the SM Higgs VEV, as well as providing a mechanism for reheating.

Following the inflationary epoch is a period of preheating, in which inflationary energy is non-perturbatively transferred into excitations of the fields via parametric resonance. Energy is inefficiently transferred into the SM, as excitations of the Higgs field promptly re-scatter

from their resonance bands due to their large self-coupling, $\lambda \sim 0.1$. As the inflaton field has a relatively small self-coupling, energy is efficiently transferred into excitations of the field, which populate a highly non-thermal infra-red distribution function. The inflaton particles then enter a period of free-turbulence, during which three and four particle scatterings evolve the inflaton distribution self-similarly towards thermalization.

Once the Hubble expansion rate is of the order of the inflaton decay/scattering rate, the perturbative reheating period proceeds, during which inflatons can efficiently transfer their energy into the SM. We define two regions of the inflaton parameter space that reheat via different mechanisms. First we review the previously analysed [45–48] light inflaton parameter space ($m_\chi \ll 2m_h \equiv \alpha \gg \beta$), in which the universe reheats via $\chi\chi \to hh$. The light inflaton mass is constrained to ($0.16 \lesssim m_\chi \lesssim 16$) GeV, where the lower bound ensures radiative corrections from the inflaton-Higgs coupling do not spoil the inflationary potential, and the upper bound ensures reheating temperatures exceed the EW symmetry breaking scale, $T_{\rm EW} = 160$ GeV, so that the BAU can be produced via EW sphaleron processes. Experimental searches of scalars in meson decays [235, 244–250] further constrains the light inflaton mass range to $m_\chi > 1$ GeV. I then present my original work [43] on the heavy inflaton parameter space ($m_\chi > 2m_h \equiv \alpha < \beta/8$), in which the universe reheats via $\chi \to hh$. The heavy inflaton parameter space is constrained to ($250 < m_\chi \lesssim 7600$) GeV, where the lower bound is necessary for the kinematics of the decay, and the upper bound is also provided by the minimum reheating temperature, $T_{\rm EW}$. Heavy inflaton evade direct observational constraints, due to their small mixing with the Higgs sector.

Now we turn to the limitations of our model, and the approximations and assumptions we made in our analysis. Firstly, our maximum quartic scalar self-coupling is not a stringent theoretical bound, but ensures our model is UV complete up to the Planck scale without complicating the theory. We may have $\beta > O(10^{-9})$ if modifications to our model are made to ensure unitarity up to the Planck scale, for example, by adding additional particles to our theory. Note that a measurement of the tensor-to-scalar ratio in the future would fix β in our model. The heavy inflaton distribution function is highly non-thermal at the time of reheating, and so the parameter space is constrained by numerically solving the Boltzmann equations, assuming that 3-particle scatterings drive the turbulent evolution towards thermal equilibrium, as suggested in [232, 233]. We found a relatively weak dependence on the initial distribution function, with a $(10-20)\%$ difference between 3- and 4-particle scattering functions. We ignored the details of symmetry restoration in the EW sector after preheating in our analysis, and our results for inflaton masses approaching the kinematic limit of decay into two Higgs bosons may be modified by the full thermal quantum treatment of the evolution. The light inflaton distribution function is closer to thermal equilibrium at the time of reheating, due to their larger

coupling with the SM, and so we approximate the reheating bounds analytically. We assume 4-particle scatterings drive the turbulent evolution towards thermal equilibrium, as we obtain a more conservative bound than the 3-particle scattering function. In our reheating analysis for both light and heavy inflaton, we made the approximation that the SM instantaneously thermalises on production, which is reasonable at $T_{\rm reh} \geq O(100)$ GeV, as the SM interaction rate greatly exceeds the Hubble expansion rate.

Future work on this model may include adding the renormalisable trilinear inflaton-Higgs coupling, $\chi\Phi^\dagger\Phi$, which would lead to more efficient reheating and thus extend the upper mass bound on the inflaton. Additionally, a significant increase in the inflaton-Higgs mixing angle is motivated by particle physics experiments, as detection channels, such as $\chi \to q\bar{q}$, may become accessible. Alternatively, if we are able to generate the BAU at temperatures below the EW scale, we could relax the minimum reheating bound and thus the inflaton upper mass bound would be increased. This may be possible if we are able to produce sphaleron configurations non-thermally during the preheating epoch [284, 285]. Note that at low reheating temperatures it may then be necessary to study non-equilibrating SM dynamics. The light inflaton parameter space would particularly benefit from these alterations, as the mass range is tightly constrained from below by particle physics experiments.

Next we study our inflationary model extended by the νMSM, modified with an additional inflaton-sterile neutrino Yukawa coupling. The model contains three sterile neutrinos: the lightest is our DM candidate (N_1), and two heavier (N_2, N_3), which generate the SM neutrino masses via the see-saw mechanism and the BAU via leptogenesis. Our model produces freeze-in DM via inflaton decay in the early universe, $\chi \to N_1 N_1$, and we constrain the mass of N_1 assuming it makes up the total DM abundance. We neglect the contribution of active-sterile neutrino oscillations to DM production, as the active-sterile neutrino coupling is strongly constrained by the absence of x-ray emissions from the radiative decay of sterile neutrinos [106, 187]. Relativistic light inflaton produce DM after they have thermalised with the SM at $T_{\rm prod} \sim m_\chi/2$ and with an average momentum of $\langle p_N \rangle / T \sim 2.45$. We can constrain the DM parameter space analytically in this region, in which light inflaton produce warm DM with mass $O(10 - 100)$ keV. Non-relativisitic inflaton produce DM simultaneously with the SM from a highly non-thermal distribution, and so a numerical analysis is necessary to constrain the DM parameter space in this region. Heavy inflaton produce strongly non-thermal cold DM with an average momentum of $\langle p_N \rangle / T \sim O(1 - 10)$ and mass $O(1 - 10)$ MeV. Both regions of the DM parameter space currently satisfy the requirements for structure formation. However in the future, more stringent bounds from Lyman-α data may increase the lower mass bound of the warm DM and thus constrain the light inflaton window. Two degenerate heavier sterile neutrinos can produce the BAU via resonant leptogenesis during freeze-out,

and the SM neutrino masses via the see-saw mechanism, with masses in the range $M_{2/3} = O(10^3 - 10^{10})$ GeV.

In our DM study we make the approximation that the number of effective SM degrees of freedom ($g_{\rm SM}$) during DM production is constant. However in the light inflaton parameter space, where $T_{\rm prod} \sim O(0.1 - 1)$ GeV, $g_{\rm SM}$ is a rapidly changing function of temperature. In future studies, we may want to perform a numerical analysis with $g_{\rm SM}$ as a function of temperature, in order to make higher precision bounds on the DM parameter space. Other future studies include extentions to the model so that the DM is lighter and therefore warmer, which could lead to potentially detectable signatures from structure formation. For example, the Majorana sterile neutrino mass term, $-\frac{M_I}{2}\bar{N}^c N$, can be tuned to have the opposite sign and have an equal magnitude to that acquired from the Yukawa coupling, thereby giving a smaller effective sterile neutrino mass. Alternatively, we could modify the sterile neutrino mass with the addition of the symmetry breaking Higgs doublet mass term, $+\mu_\Phi^2 \Phi^\dagger \Phi$, which we studied in chapter 8. Producing warmer DM then allows our model to be constrained by Lyman-α data.

Our final model [44] extends the basic inflationary model with a negative Higgs doublet mass term (μ_Φ^2), so we have symmetry breaking in both the Higgs and scalar sectors. We require the Higgs VEV to correspond to the SM expected value and the inflaton VEV to be non-zero, so that the universe is not overclosed with inflaton particles. As a result of the additional massive parameter, the Higgs boson mass does not fix the Higgs quartic self-coupling ($\lambda \neq m_h^2/2v^2$), and so the stability of the EW vacuum is dependent on the parameters of the inflationary model. We assume that a universe with a positive cosmological constant is metastable, based on Dvali's argument that an eternal de Sitter universe would lead to quantum inconsistencies [50, 51], and constrain our model accordingly. The metastable region constrains the Higgs self-coupling to the range $0.1 < \lambda(m_t) < 0.134$. However, additional model-dependent bounds from inflation and reheating are necessary, as during these periods the Higgs field value can exceed the instability scale and thus destabilise the EW vacuum. For $\lambda(m_t) > 0.120$, the EW vacuum is stable up to reheating temperatures $T = O(M_{\rm P})$ against thermal fluctuations of the Higgs field.

In most regions of our model's parameter space the universe inflates along a non-zero angle in the inflaton-Higgs field space, inversely proportional to $\sqrt{\lambda}$. As a result, the inflationary attractor will break down if λ runs to negative values. This can be evaded if λ is finely tuned close to the stability scale, however, we choose to analyse the case where fine-tuning is not necessary: the parameter space region $\alpha > 0$ & $2|\alpha| > \beta$, where the inflationary attractor solution is $\Phi_b = 0$. Additionally, the large effective Higgs mass from the positive α term in the potential stabilizes the EW vacuum against inflationary enhanced quantum fluctuations of the

Higgs field.

The region of parameter space where $\alpha > 0$ & $2|\alpha| > \beta$ corresponds to the light inflaton region, in which the universe reheats via $\chi\chi \to hh$. The model's $\beta - \alpha$ parameter space is constrained from inflation and reheating by the same bounds previously evaluated for the basic model. Additionally the model is constrained by the requiring the inflaton particles decay prior to BBN, which bounds the inflaton-Higgs mixing angle to $\theta_{\rm m}^2 \geq O(10^{-9} - 10^{-11})$ for inflatons with $m_\chi = O(0.001-0.1)$ GeV. Finally, we require the model to be consistent with experimental observations. The measurement of the Higgs signal strength constrains the Higgs self-coupling to $\lambda(m_t) \geq 0.123$, which is within the bound for EW stability during reheating. The interesting metastable region of our model is then confined to $0.123 \leq \lambda(m_t) \leq \lambda_{\rm SM}$.

We conclude that in the region of parameter space where $\alpha > 0$ & $2|\alpha| > \beta$, inflaton with $m_\chi = O(10^{-3} - 125)$ GeV and $\theta_{\rm m}^2 = O(10^{-11} - 10^{-2})$ evade all current experimental, cosmological and stability constraints required for a metastable vacuum. If we extend the model with our sterile neutrino DM model we would have further constraints from Lyman-α data. The addition of the Higgs mass term results in small inflaton VEVs when $\mu_\Phi^2 \sim \lambda v^2$, and thus lighter and warmer DM compared to the previously analysed $\mu_\Phi = 0$ model. As a result, a measurement of inflaton with $m_\chi \leq O(0.1)$ GeV would exclude our DM model by the requirements for structure formation. The model has a number of experimental probes from particle physics and cosmology: measuring the Higgs' couplings, invisible decay width and production cross-section, and the tensor-to-scalar ratio. Future upgrades of current experiments may be sensitive enough to probe the parameter space of larger mixing angles, $\theta_{\rm m}^2 \geq O(10^{-4})$, where inflatons have $m_\chi \gtrsim 1$ GeV, through the observation of suppressed linear and trilinear Higgs couplings. The experimental testability of very weakly coupled inflaton is dependent on the planned proposals of future experiments [278] (MATHUSLA200, SHIP, and FASER2), that are able to probe inflatons with $m_\chi \sim (0.003-5)$ GeV and mixing angles down to $\theta_{\rm m}^2 = O(10^{-11})$. A measurement of the inflaton within this mass range would allow us to predict the viability and properties of our sterile neutrino DM model.

Chapter 10

Appendix

In this chapter we calculate the amplitude of $K^+ \to \pi^+\chi$, due to a discrepancy between the results in [236] and [47, 237–239]. We begin by evaluating the amplitude of the flavour-changing neutral current ($s \to d$) in the free-quark approximation. Then we utilize the low-energy effective field theory of QCD, chiral perturbation theory, to find the amplitude of the hadronic states. We will begin with a short introduction to chiral perturbation theory in section 10.1, before calculating the decay width of $K^+ \to \pi^+\chi$ in section 10.2.

10.1 Chiral perturbation theory

QCD is a theory of the strong force, involving interactions between gluons and quarks. As the strong force coupling, α_s, increases at low energies, gluons and quarks can not be approximated to asymptotic states in the low-energy regime. Therefore an effective field theory of QCD is built using hadronic states, called chiral perturbation theory [286, 287].

In the low-energy regime, only the three lightest quarks (u, d, s) are considered. In the limit that the quark masses are taken to zero, the QCD Lagrangian is

$$\mathcal{L}_{\text{QCD}} = \sum_f \bar{q}_{f,i}(i\gamma^\mu(D_\mu)_{ij}q_{f,j} - \frac{1}{4}G_{\mu\nu,a}G_a^{\mu\nu}, \tag{10.1}$$

where $q_{f,i}$ are quark fields of flavour f ($f = u, d, s$) and colour i ($i =$ red, blue, green), γ^μ are the Dirac matrices, and $G^a_{\mu\nu}$ ($a = 1...8$) are the gluon field strength tensors. The gauge covariant derivative is

$$(D_\mu)_{ij} = \partial_\mu\delta_{ij} - ig(T_a)_{ij}A^a_\mu, \tag{10.2}$$

where T_a are the SU(3) generators, which are related to the Gell-Mann matrices by $T_a = \lambda_a/2$, A^a_μ are the gluon fields, and g is the quark-gluon coupling strength. In the chiral limit of zero quark masses, the QCD Lagrangian has a $SU(3)_L \times SU(3)_R \times U(1)_V$ symmetry, where $SU(3)_L \times SU(3)_R$ corresponds to chiral symmetry (i.e. invariance under parity transformation)

and $U(1)_V$ corresponds to baryon number conservation. The generators of $SU(3)_L \times SU(3)_R$ are Q_L^a and Q_R^a, which for the purpose of investigating chiral symmetry breaking, are more conveniently written as vector and axial-vector operators [286, 287],

$$\begin{aligned} Q_V^a &= Q_R^a + Q_L^a, \\ Q_A^a &= Q_R^a - Q_L^a, \end{aligned} \tag{10.3}$$

that have parity $P = -1$ and $P = +1$ respectively.

Spontaneous symmetry breaking occurs when a global symmetry of the theory is broken under the global transformation of the ground state, ϕ_0, i.e. the generators of the theory do not annihilate the ground state [288],

$$T^a \phi_0 \neq 0. \tag{10.4}$$

Goldstone's thoerem states that for each generator of the symmetry that is broken, a massless scalar particle called a Goldstone boson is produced.

To conserve symmetry currents, we require the following commutation relation to hold [286, 287],

$$[H_{\mathrm{QCD}}^0, Q_{A,V}^a] = 0, \tag{10.5}$$

where H_{QCD}^0 is the Hamiltonian operator. We would therefore expect any state of negative parity to have a degenerate state of positive parity. However, in the low-energy hadronic spectrum there is a pseudoscalar meson octet $(K^{\pm}, K^0, \pi^{\pm}, \pi^0, \eta, \eta^{'})$, which have much lower masses than the rest of the hadronic spectrum, and no pseudoscalar baryon octet. The asymmetry of the hadronic spectrum hints at the spontaneous breakdown of chiral symmetry $SU(3)_L \times SU(3)_R \rightarrow SU(3)_V$, where for every axial operator that breaks the chiral symmetry, a massless meson ($P = -1$) is produced in the limit of zero quark masses [286, 287]. The pseudoscalar meson octet are therefore realised as the Goldstone bosons, which form the asymptotic states used to construct chiral perturbation theory [286, 287].

The lowest order effective Lagrangian for chiral perturbation theory, which obeys $SU(3)_L \times SU(3)_R$ global symmetries and has a ground state invariant under $U(1)_V$, is [286, 287]

$$\mathcal{L}_{eff} = \frac{F_0^2}{4} \mathrm{Tr}\left(\partial_\mu U \partial_\mu U^\dagger\right). \tag{10.6}$$

U transforms under global $SU(3)_L \times SU(3)_R$ transformations as [286, 287]

$$U \to RUL^\dagger, \tag{10.7}$$

$$U^\dagger \to LU^\dagger R^\dagger, \tag{10.8}$$

where $LL^\dagger = RR^\dagger = \mathbb{I}$, and U is invariant under $U(1)_V$ transformations as mesons have a baryon number of zero. U is given by [286, 287]

$$U(x) = \exp\left(i\frac{\phi(x)}{F_0}\right), \tag{10.9}$$

where F_0 is the pion decay constant and matrix ϕ is [286, 287]

$$\phi(x) = \sum_{a=1}^{8} \lambda_a \phi_a(x) = \begin{bmatrix} \pi^0 + \frac{1}{\sqrt{3}}\eta_8 & \sqrt{2}\pi^+ & \sqrt{2}K^+ \\ \sqrt{2}\pi^- & -\pi^0 + \frac{1}{\sqrt{3}}\eta_8 & \sqrt{2}K^0 \\ \sqrt{2}K^- & \sqrt{2}\bar{K}^0 & -\frac{2}{\sqrt{3}}\eta_8 \end{bmatrix}, \tag{10.10}$$

where ϕ_a are the Goldstone bosons. The factor $\frac{F_0^2}{4}$ in (10.6) is required to give the standard kinetic term of the field, $\frac{1}{2}\partial_\mu\phi_a\partial^\mu\phi_a$, in the first order expansion of the Lagrangian [286, 287].

The Goldstone boson masses are incorporated into the QCD Lagrangian with the addition of the explicit chiral symmetry breaking term [286, 287],

$$\mathcal{L}_{\text{QCD}} = -\bar{q}_R M q_L - \bar{q}_L M^\dagger q_R. \tag{10.11}$$

In order to incorporate Goldstone masses into our effective fied theory, we include the following additional term [286, 287]

$$\mathcal{L}_{S.B.} = \frac{F_0^2 B_0}{2}\text{Tr}\left(MU^\dagger + UM^\dagger\right), \tag{10.12}$$

where B_0 is a constant related to the chiral quark condensate by $3F_0^2B_0 = -\langle q\bar{q}\rangle$, and [286, 287]

$$M = \begin{bmatrix} m_u & 0 & 0 \\ 0 & m_d & 0 \\ 0 & 0 & m_s \end{bmatrix}, \tag{10.13}$$

where m_i $(i = u, d, s)$ are the quark masses. We can then predict the masses of the Goldstone bosons of the theory, the pseudoscalar meson octet, by expanding (10.12) to second-order in

the fields,

$$\begin{aligned}\mathcal{L}_{S.B} \supset & -\frac{B_0}{2}\mathrm{Tr}\left(M\phi^2\right), \\ & = -\frac{B_0}{2}\Big(2(m_u+m_d)\pi^+\pi^- + 2(m_u+m_s)K^+K^- + 2(m_d+m_s)K^0\bar{K}^0, \\ & + (m_u+m_d)\pi^0\pi^0 + \frac{(m_u+m_d+4m_s)}{3}\eta^2\Big). \end{aligned} \tag{10.14}$$

The masses of the Goldstone bosons are then given by [286, 287]

$$\begin{aligned} m^2_{\pi^\pm} &= B_0(m_u+m_d), \quad & m^2_{K^\pm} &= B_0(m_u+m_s), \\ m^2_{K^0} &= B_0(m_d+m_s), \quad & m^2_{\eta} &= \frac{B_0}{3}(m_u+m_d+4m_s). \end{aligned} \tag{10.15}$$

10.2 Decay width of $K^+ \to \pi^+\chi$

Particle physics experiments can search for invisible scalars, such as our light inflaton, in rare meson decays [47], the largest amplitude of which is from $K^+ \to \pi^+\chi$. To calculate the amplitude of $K^+ \to \pi^+\chi$ we first take the free-quark approximation. We evaluate the weak contributions to the flavour-changing neutral quark current $\overline{s} \to \overline{d}$ from a W boson (W^+) and Faddeev-Popov unphysical scalar (Φ^+) loop with an internal quark line [239]. A Higgs boson is radiated from the internal quark line, and mixes to produce an inflaton field [47, 239], as shown in Figure 10.1. We presume a soft Higgs boson emission, i.e. we take the Higgs momentum to zero and the internal quark momentum to $p-q$. In this limit, the amplitude is approximately given by the weak contribution to the quark self-energy with an external Higgs field, multiplied by the Higgs-inflaton mixing angle [47, 239]. The internal quark line has contributions from top, charm and up flavours, however as the charm and up quarks' contributions are suppressed by their small masses, only the top quark contribution is significant. Finally we implement chiral perturbation theory to find the meson interaction amplitude.

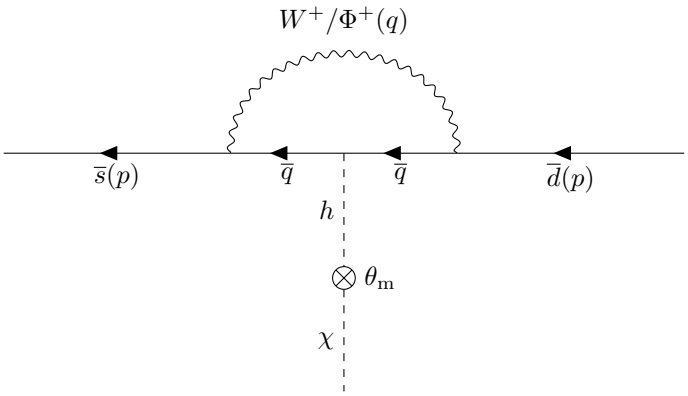

Figure 10.1: Flavour-changing neutral current $\overline{s} \to \overline{d}$

Quark-level process of $K^+ \to \pi^+\chi$. The neutral quark current ($\overline{s} \to \overline{d}$) changes flavour via the W boson (W^+) or unphysical scalar (Φ^+) loop. The Higgs boson (h) is emitted from the internal quark, which then mixes to produce an inflaton particle (χ). p is the momentum of the external quarks and q is the loop momentum of W^+/Φ^+.

10.2.1 Feynman Rules in Feynman-'t Hooft Gauge ($\xi = 1$)

- W^+ propagator:

$$G_{\mu\nu}(q) = \frac{-i}{q^2 - m_W^2 + i\epsilon}[g_{\mu\nu} - (1-\xi)\frac{q_\mu q_\nu}{q^2 - \xi m_W^2}] = \frac{-ig_{\mu\nu}}{q^2 - m_W^2 + i\epsilon}, \tag{10.16}$$

  where q is the momentum and m_W is the mass of the W boson.

- ϕ^+ propagator:

$$G(q) = \frac{-i}{q^2 - \xi m_W^2 + i\epsilon} = \frac{-i}{q^2 - m_W^2 + i\epsilon}. \tag{10.17}$$

- q_f propagator[1]:

$$G(p) = \frac{i(\not{p} + m_f)}{p^2 - m_f^2 + i\epsilon}, \tag{10.18}$$

  where p is the momentum and m_f is the mass of quark ($f = u, d, c, s, t, b$).

- $u_\alpha W^+ d_\beta$ interaction vertex:

$$\frac{ig_W}{\sqrt{2}}\gamma_\mu P_L V_{\alpha\beta}, \tag{10.19}$$

  where g_W is the SU(2) gauge coupling constant, u_α are 'up'-type quarks ($\alpha = u, c, t$), d_β are 'down'-type quarks ($\beta = d, s, b$), and $V_{\alpha\beta}$ is the CKM matrix element for quark-mixing of flavours α and β.

- $u_\alpha \phi^+ d_\beta$ interaction vertex:

$$\frac{ig_W}{\sqrt{2}}\left(\frac{m_\alpha}{m_W}P_L - \frac{m_\beta}{m_W}P_R\right)V_{\alpha\beta} = \frac{i\sqrt{2}}{v}(m_\alpha P_L - m_\beta P_R)V_{\alpha\beta}, \tag{10.20}$$

  where $v = \frac{2m_W}{g_W}$ is the Higgs VEV.

[1] We use the notation $\not{X} \equiv \gamma^\mu X_\mu$.

P_L and P_R are the left- and right-handed projection operators,

$$P_L = \frac{1-\gamma_5}{2}, \quad P_R = \frac{1+\gamma_5}{2}. \tag{10.21}$$

P_L and P_R project out the left- and right-handed components of a particle,

$$\begin{aligned} u_{L/R} &= P_{L/R}u, \quad v_{L/R} = P_{R/L}v, \\ \bar{u}_{L/R} &= \bar{u}P_{R/L}, \quad \bar{v}_{L/R} = \bar{v}P_{L/R}, \end{aligned} \tag{10.22}$$

where $u(\bar{u})$ is an incoming (outgoing) particle, $\bar{v}(v)$ is an incoming (outgoing) antiparticle.

Next we will evaluate the W^+ and Φ^+ contributions to the amplitude of the flavour changing neutral current,

$$M(p) = \bar{s}(p)[-i\Sigma(p)]d(p), \tag{10.23}$$

where $\Sigma(p)$ is the polarisation operator.

10.2.2 W^+ boson contribution

In the Feynman-'t Hooft gauge, the polarisation operator of the quark self-energy with a W^+ boson loop is

$$-i\Sigma(p) = \int \frac{\mathrm{d}^4 q}{(2\pi)^4} \left[\frac{-ig_W}{\sqrt{2}}\gamma^\mu P_L V_{ts}^*\right] \left[\frac{i(\not{p}-\not{q}+m_t)}{(p-q)^2-m_t^2}\right] \left[\frac{ig_W}{\sqrt{2}}\gamma^\nu P_L)V_{td}\right] \left[\frac{-ig_{\mu\nu}}{q^2-m_W^2}\right]. \tag{10.24}$$

The term proportional to m_t does not contribute to the amplitude of the quark self-energy:

$$-i\Sigma(p) \supset \gamma^\mu P_L \gamma_\mu P_L = \gamma^\mu P_L P_R \gamma_\mu = 0. \tag{10.25}$$

The term proportional to $(\not{p}-\not{q}) = \gamma^\rho(p-q)_\rho$ does contribute to the amplitude of the quark self-energy:

$$-i\Sigma(p) \supset \gamma^\mu P_L \gamma^\rho \gamma_\mu P_L - \gamma^\mu \gamma^\rho \gamma_\mu P_L = -2\gamma^\rho P_L. \tag{10.26}$$

Here we have used the anti-commutation relation

$$\{\gamma^5, \gamma^\mu\} = \gamma^5\gamma^\mu + \gamma^\mu\gamma^5 = 0, \tag{10.27}$$

and identities

$$\begin{aligned} (\gamma^5)^2 &= \mathbb{I}_4, \\ \gamma^\mu\gamma^\rho\gamma_\mu &= -2\gamma^\rho. \end{aligned} \tag{10.28}$$

However, the correct result for the calculation of the off-diagonal quark self-energy amplitude in [239] states that the only contribution in the Feynman-'t Hooft gauge is from the unphysical scalar loop. Unfortunately we have failed to show that the contribution from the W^+ boson loop is zero here. Nevertheless, we continue our attempt to calculate the $K^+ \to \pi^+\chi$ amplitude from the ϕ^+ loop contribution to the quark self-energy in the following section.

10.2.3 ϕ^+ contribution

In the Feynman-'t Hooft gauge, the polarisation operator of the quark self-energy with a ϕ^+ boson loop is

$$-i\Sigma(p) = \int \frac{\mathrm{d}^4 q}{(2\pi)^4} \left[\frac{-i\sqrt{2}}{v}(m_s P_L - m_t P_R)V_{ts}^*\right]\left[\frac{i(\not{p}-\not{q}+m_t)}{(p-q)^2-m_t^2}\right] \left[\frac{i\sqrt{2}}{v}(m_t P_L - m_d P_R)V_{td}\right]\left[\frac{-i}{q^2-m_W^2}\right]. \tag{10.29}$$

In order to evaluate the above expression, we implement the following tricks to simplify the integral.

Feynman parameterisation

Applying the Feynman parameterisation,

$$\frac{1}{AB} = \int_0^1 dx \frac{1}{[Ax+(1-x)B]^2}, \tag{10.30}$$

to the denominator of equation (10.29) with $A = (p-q)^2 - m_t^2$ and $B = q^2 - m_W^2$, we obtain the following expression,

$$\frac{1}{[q^2-m_W^2][(p-q)^2-m_t^2]} = \int_0^1 dx \frac{1}{[l^2-\Delta]^2}, \tag{10.31}$$

with $l = (q - xp)$ and $\Delta = (1-x)(m_W^2 - xp^2) + xm_t^2$.

Wick rotation

We re-express our integral over q as an integral over l, and perform the Wick rotation $l^0 \to il_E^0$,

$$\int \frac{\mathrm{d}^4 q}{(2\pi)^4} \frac{\not{p}-\not{q}+m_t}{[q^2-m_W^2][(p-q)^2-m_t^2]} = \int \frac{\mathrm{d}^4 l_E}{(2\pi)^4} \int_0^1 dx \frac{(1-x)\not{p}+m_t}{[l_E^2+\Delta]^2}. \tag{10.32}$$

As l is anti-symmetric about the integrand, linear terms in l are dropped.

Dimensional regularisation and $\overline{MS}$ Scheme

To dimensionally regularise the logarithmic divergent loop integral over l_E, we infinitesimally shift the number of dimensions from $D = 4$ to $D = 4 - 2\epsilon$, which gives the following finite result,

$$\begin{aligned}\int \frac{\mathrm{d}^{4-2\epsilon} l_E}{(2\pi)^{4-2\epsilon}} \frac{1}{[l_E^2 + \Delta]^2} &= \frac{1}{(4\pi)^2} \left(\frac{4\pi\mu^2}{\Delta}\right)^{\epsilon} \frac{\Gamma(\epsilon)}{\Gamma(2)}, \\ &= \frac{1}{(4\pi)^2} \left(\frac{1}{\epsilon} + \ln(4\pi) + \ln\left(\frac{\mu^2}{\Delta}\right) - \gamma_E + O(\epsilon)\right), \end{aligned} \tag{10.33}$$

where μ is the ultraviolet cutoff and $\Gamma(x)$ is the Gamma function. In the second line we have expanded the following terms in orders of ϵ,

$$\begin{aligned}\Gamma(\epsilon) &= \frac{1}{\epsilon} - \gamma_E + O(\epsilon), \\ \left(\frac{4\pi\mu^2}{\Delta}\right)^{\epsilon} &= 1 + \epsilon \ln\left(\frac{4\pi\mu^2}{\Delta}\right) + O(\epsilon^2), \end{aligned} \tag{10.34}$$

where $\gamma_E \sim 0.58$ is the Euler-Mascheroni constant.

The $\overline{MS}$ scheme subtracts the terms $\frac{1}{\epsilon} + \ln(4\pi) - \gamma_E$ from equation (10.33),

$$\to \frac{1}{(4\pi)^2} \ln\left(\frac{\mu^2}{\Delta}\right). \tag{10.35}$$

Then putting the external momentum on-shell, $p^2 = m_{s/d}^2$, and expanding about the Higgs VEV, $\sqrt{2}\Phi \to v + h(x)$, integral (10.32) becomes[2]

$$\int_0^1 dx[(1-x)\not{p} + m_t] \ln\left(\frac{\mu^2}{\Delta}\right) \supset -\frac{h}{v}[\not{p} - 2m_t]. \tag{10.36}$$

We only retain the terms linear in h in order to calculate the effective amplitude of a soft Higgs emission from the internal quark line, which has a polarization operator of

$$-i\Sigma(p) = \frac{2\sqrt{2}G_F}{16\pi^2} \frac{h}{v} V_{ts}^* V_{td} \left(m_t^2 \not{p} P_L + m_s m_d \not{p} P_R + 2m_t^2 m_d P_R + 2m_t^2 m_s P_L\right). \tag{10.37}$$

[2]There is some uncertainty around producing the result given in (10.36).

Wavefunction renormalisation

In order renormalize the wavefunction, we first define the Lagrangian for the s and d quarks, expressed in terms of the propagator operator $\hat{P}$, and mass matrix, $\hat{M}$,

$$\mathcal{L} = \bar{\psi}\hat{P}\psi + \bar{\psi}\hat{M}\psi, \tag{10.38}$$

$$= \begin{pmatrix} \bar{s}_L \\ \bar{s}_R \\ \bar{d}_L \\ \bar{d}_R \end{pmatrix}^T \begin{bmatrix} \not{p} & 0 & \delta z_1 \not{p} & 0 \\ 0 & \not{p} & 0 & \delta z_2 \not{p} \\ \delta z_1^* \not{p} & 0 & \not{p} & 0 \\ 0 & \delta z_2^* \not{p} & 0 & \not{p} \end{bmatrix} \begin{pmatrix} s_L \\ s_R \\ d_L \\ d_R \end{pmatrix} + \begin{pmatrix} \bar{s}_L \\ \bar{s}_R \\ \bar{d}_L \\ \bar{d}_R \end{pmatrix}^T \begin{bmatrix} 0 & m_s & 0 & \delta m_1 \\ m_s & 0 & \delta m_2 & 0 \\ 0 & \delta m_2^* & 0 & m_d \\ \delta m_1^* & 0 & m_d & 0 \end{bmatrix} \begin{pmatrix} s_L \\ s_R \\ d_L \\ d_R \end{pmatrix}.$$

The mixed quark terms correspond to the effective propagators and masses of the flavour changing neutral current:

$$\mathcal{L} \supset \bar{s}\big[\delta z_1 \not{p} P_L + \delta z_2 \not{p} P_R + \delta m_1 P_R + \delta m_2 P_L\big] d + c.c. \tag{10.39}$$

Then equating the terms in (10.39) with the terms in the amplitude calculated in (10.37),

$$M(p) = \bar{s}[-i\Sigma(p)]d = A\bar{s}\big[m_t^2 \not{p} P_L + m_s m_d \not{p} P_R + 2m_t^2 m_d P_R + 2m_t^2 m_s P_L\big] d, \tag{10.40}$$

where $A = \frac{2\sqrt{2}G_F}{16\pi^2} V_{ts}^* V_{td} \frac{h}{v}$, we obtain the following for the effective propagators and masses for the quark-mixing terms,

$$\begin{aligned} \delta z_1 &= A m_t^2, \qquad \delta z_2 = A m_d m_s \to 0, \\ \delta m_1 &= 2A m_t^2 m_d, \qquad \delta m_2 = 2A m_t^2 m_s. \end{aligned} \tag{10.41}$$

The renormalised wavefunction is given by $\tilde{\psi} = \hat{D}\psi$,

$$\tilde{\psi} = \begin{pmatrix} \tilde{s}_L \\ \tilde{s}_R \\ \tilde{d}_L \\ \tilde{d}_R \end{pmatrix} = \begin{bmatrix} 1 & 0 & \delta z_1 & 0 \\ 0 & 1 & 0 & \delta z_2 \\ \delta z_1^* & 0 & 1 & 0 \\ 0 & \delta z_2^* & 0 & 1 \end{bmatrix}^{\frac{1}{2}} \begin{pmatrix} s_L \\ s_R \\ d_L \\ d_R \end{pmatrix}, \tag{10.42}$$

where $\hat{D}$ diagonalises the kinetic terms in the Lagrangian. In order to obtain the renormalised mass matrix, $\hat{\tilde{M}}$, we evaluate the mass term in (10.38) of the renormalised wavefunction,

$$\mathcal{L} \supset \bar{\psi}\hat{M}\psi = \bar{\tilde{\psi}}\hat{\tilde{M}}\tilde{\psi}, \tag{10.43}$$

where $\hat{\tilde{M}} = (\hat{D})^{-1}\hat{M}(\hat{D})^{-1}$ and

$$\hat{D}^{-1} \approx \begin{bmatrix} 1 & 0 & -\frac{\delta z_1}{2} & 0 \\ 0 & 1 & 0 & -\frac{\delta z_2}{2} \\ -\frac{\delta z_1^*}{2} & 0 & 1 & 0 \\ 0 & -\frac{\delta z_2^*}{2} & 0 & 1 \end{bmatrix} \tag{10.44}$$

to first order in δz. The renormalised masses of the flavour changing quark current to first order in δz and δm are

$$\mathcal{L} \supset \bar{\tilde{s}}_L \Big[-\frac{\delta z_2}{2} m_s + \delta m_1 - \frac{\delta z_1}{2} m_d \Big] \tilde{d}_R + \bar{\tilde{s}}_R \Big[-\frac{\delta z_1}{2} m_s + \delta m_2 - \frac{\delta z_2}{2} m_d \Big] \tilde{d}_L + c.c. \tag{10.45}$$

Then by substituting in the expressions for δz and δm from (10.41), we obtain the contribution of a Φ^+ loop with a soft Higgs emission to the radiative corrections of the quark masses,

$$\mathcal{L} \supset \frac{3\sqrt{2}G_F}{16\pi^2} V_{ts}^* m_t^2 V_{td} \frac{h}{v} \Big[m_d \bar{\tilde{s}}_L \tilde{d}_R + m_s \bar{\tilde{s}}_R \tilde{d}_L \Big] + c.c. \tag{10.46}$$

Implementing chiral perturbation theory

In order to obtain the amplitude of the meson decay $K^+ \to \pi^+ \chi$ from the free quark approximation, we need to implement the chiral perturbation theory that we studied in section 10.1. In the low energy effective field theory, K^+ and π^+ are Goldstone bosons of the spontaneously broken chiral symmetry $SU(3)_L \times SU(3)_R \to SU(3)_V$. The Goldstone boson masses are incorporated into the theory with the addition of an explicit symmetry breaking term [286, 287] given by equation (10.12),

$$\mathcal{L}_{S.B.} = \frac{F_0^2 B_0}{2} \mathrm{Tr}\left(M U^\dagger + U M^\dagger \right), \tag{10.47}$$

where M is the 3×3 light quark (u, d, s) mass matrix and U is the matrix of Goldstone bosons, defined in (10.9) and (10.10). The off-diagonal quark mass elements due to the radiative corrections given in (10.46) are expressed in matrix form by [239]

$$M_{\mathrm{rad}} = \gamma_3 M = \begin{bmatrix} 0 & 0 & 0 \\ 0 & 0 & m_s \xi \\ 0 & m_d \xi^* & 0 \end{bmatrix}, \tag{10.48}$$

where

$$\gamma_3 = \begin{bmatrix} 0 & 0 & 0 \\ 0 & 0 & \xi \\ 0 & \xi^* & 0 \end{bmatrix}, \tag{10.49}$$

and $\xi = \frac{3\sqrt{2}G_F}{16\pi^2}\frac{h}{v}V_{ts}^* m_t^2 V_{td}$. Then by expanding (10.47) to second order of the fields, we extract the terms proportional to $\pi^\pm K^\pm$ in order to obtain the amplitude of $K^\pm \to \pi^\pm h$,

$$\begin{aligned}
\mathcal{L}_{\text{S.B.}} - \frac{F_0^2 B_0}{2}\text{Tr}\left(M_{\text{rad}}U^\dagger + UM_{\text{rad}}^\dagger\right) &\supset \frac{B_0}{8}\text{Tr}\left(M_{\text{rad}}\phi^2 + \phi^2 M_{\text{rad}}^\dagger\right), \\
&= \frac{B_0}{2}\text{Tr}\left(\begin{bmatrix} 0 & 0 & 0 \\ 0 & \xi m_s \pi^+ K^- & \xi m_s K^+ K^- \\ 0 & \xi^* m_d \pi^+\pi^- & \xi^* m_d \pi^- K^+ \end{bmatrix} + \begin{bmatrix} 0 & 0 & 0 \\ 0 & \xi^* m_s \pi^- K^+ & \xi m_d \pi^+\pi^- \\ 0 & \xi^* m_s K^+ K^- & \xi m_d \pi^+ K^- \end{bmatrix}\right), \\
&= \frac{B_0}{2}\left(\xi(m_s+m_d)\pi^+K^- + \xi^*(m_s+m_d)\pi^-K^+\right), \\
&= \frac{m_K^2}{2}\left(\xi\pi^+K^- + \xi^*\pi^-K^+\right),
\end{aligned} \tag{10.50}$$

where $m_K^2 = B_0(m_s + m_d)$. Then with the addition of the inflaton-Higgs mixing angle, θ_{m}, we obtain the amplitude for

$$M(K^+ \to \pi^+\chi) = \frac{m_K^2\theta_{\text{m}}}{v}\frac{3\sqrt{2}G_F}{32\pi^2}V_{ts}m_t^2V_{td}^*, \tag{10.51}$$

which is agreement with the results given in [47, 237–239]. The corresponding branching fraction is [47]

$$\begin{aligned}
\text{Br}(K^+ \to \pi^+\chi) &= \frac{\Gamma(K^+ \to \pi^+\chi)}{\Gamma_{\text{total}}(K^+)}, \\
&= \frac{1}{\Gamma_{\text{total}}(K^+)}\frac{|M(K^+ \to \pi^+\chi)|^2}{16\pi M_K}\frac{2|\mathbf{p}_\chi|}{M_K}, \\
&\approx 1.3 \times 10^{-3}\left(\frac{2|\mathbf{p}_\chi|}{M_K}\right)\theta_{\text{m}}^2,
\end{aligned} \tag{10.52}$$

where $\mathbf{p}_\chi$ is the inflaton momentum in the centre of mass frame, M_K is the kaon mass and $\Gamma_{\text{total}}(K_+)$ is the total decay width of K^+.

Bibliography

[1] A. Einstein. "Die Feldgleichungen der Gravitation". In: *Sitzungsberichte der Königlich Preußischen Akademie der Wissenschaften (Berlin* (Jan. 1915), pp. 844–847.

[2] A. D. Sakharov. "Violation of CP in variance, asymmetry, and baryon asymmetry of the universe". In: *JETP* 5.24-27 (1967).

[3] M. Kobayashi and T. Maskawa. "CP-Violation in the Renormalizable Theory of Weak Interaction". In: *Progress of Theoretical Physics* 49.2 (Feb. 1973), pp. 652–657. ISSN: 0033-068X. DOI: 10.1143/PTP.49.652. eprint: https://academic.oup.com/ptp/article-pdf/49/2/652/5257692/49-2-652.pdf. URL: https://doi.org/10.1143/PTP.49.652.

[4] V. Fanti et al. "A new measurement of direct CP violation in two pion decays of the neutral kaon". In: *Physics Letters B* 465.1-4 (Oct. 1999), pp. 335–348. DOI: 10.1016/s0370-2693(99)01030-8. URL: https://doi.org/10.1016%2Fs0370-2693%2899%2901030-8.

[5] K. Abe et al. "Observation of Large CP Violation in the Neutral B Meson System". In: *Physical Review Letters* 87.9 (Aug. 2001). DOI: 10.1103/physrevlett.87.091802. URL: https://doi.org/10.1103%2Fphysrevlett.87.091802.

[6] B. Aubert et al. "Measurement of CP Asymmetries in $B_0 \to \Phi K_0$ and $B_0 \to K^+K^-K^0_S$ Decays". In: *Physical Review D* 71.9 (May 2005). DOI: 10.1103/physrevd.71.091102. URL: https://doi.org/10.1103%2Fphysrevd.71.091102.

[7] F. Betti. "Observation of CP violation in charm decays at LHCb". In: (2019). DOI: 10.48550/ARXIV.1905.05428. URL: https://arxiv.org/abs/1905.05428.

[8] G. R. Farrar and M. E. Shaposhnikov. "Baryon asymmetry of the Universe in the standard model". In: *Physical Review D* 50.2 (July 1994), pp. 774–818. DOI: 10.1103/physrevd.50.774. URL: https://doi.org/10.1103%2Fphysrevd.50.774.

[9] M.B. Gavela et al. "Standard model CP-violation and baryon asymmetry (I). Zero temperature". In: *Nuclear Physics B* 430.2 (Nov. 1994), pp. 345–381. DOI: 10.1016/0550-3213(94)00409-9. URL: https://doi.org/10.1016%2F0550-3213%2894%2900409-9.

[10] Patrick Huet and Eric Sather. "Electroweak baryogenesis and standard model CP violation". In: *Physical Review D* 51.2 (Jan. 1995), pp. 379–394. DOI: 10.1103/physrevd.51.379. URL: https://doi.org/10.1103%2Fphysrevd.51.379.

[11] M. Shaposhnikov. "Baryon Asymmetry of the Universe and Neutrinos". In: *Progress of Theoretical Physics* 122 (July 2009). DOI: 10.1143/PTP.122.185.

[12] Q. R. Ahmad et al. "Measurement of the Rate of $\nu_e + d \rightarrow p + p + e^-$ Interactions Produced by ^8B Solar Neutrinos at the Sudbury Neutrino Observatory". In: *Phys. Rev. Lett.* 87 (7 July 2001), p. 071301. DOI: 10.1103/PhysRevLett.87.071301. URL: https://link.aps.org/doi/10.1103/PhysRevLett.87.071301.

[13] Q. R. Ahmad et al. "Direct Evidence for Neutrino Flavor Transformation from Neutral-Current Interactions in the Sudbury Neutrino Observatory". In: *Phys. Rev. Lett.* 89 (1 June 2002), p. 011301. DOI: 10.1103/PhysRevLett.89.011301. URL: https://link.aps.org/doi/10.1103/PhysRevLett.89.011301.

[14] V. C. Rubin and Jr. W. K. Ford. "Rotation of the Andromeda Nebula from a Spectroscopic Survey of Emission Regions". In: 159 (Feb. 1970), p. 379. DOI: 10.1086/150317.

[15] L. Scholz-Diaz, I. Martin-Navarro, and J. Falcon-Barroso. "The dark side of galaxy stellar populations I: The stellar-to-halo mass relation and the velocity dispersion - halo mass relation". In: (2022). arXiv: 2202.03441 [astro-ph.GA].

[16] D. Clowe, A. Gonzalez, and M. Markevitch. "Weak-Lensing Mass Reconstruction of the Interacting Cluster 1E 0657558: Direct Evidence for the Existence of Dark Matter". In: *The Astrophysical Journal* 604.2 (Apr. 2004), pp. 596–603. ISSN: 1538-4357. DOI: 10.1086/381970. URL: http://dx.doi.org/10.1086/381970.

[17] A. G. Sánchez et al. "Cosmological parameters from cosmic microwave background measurements and the final 2dF Galaxy Redshift Survey power spectrum". In: 366.1 (Feb. 2006), pp. 189–207. DOI: 10.1111/j.1365-2966.2005.09833.x. arXiv: astro-ph/0507583 [astro-ph].

[18] Planck Collaboration. "Planck 2018 results". In: *Astronomy & Astrophysics* 641 (Sept. 2020), A1. DOI: 10.1051/0004-6361/201833880. URL: https://doi.org/10.1051%2F0004-6361%2F201833880.

[19] G. de Vaucouleurs, A. de Vaucouleurs, and J. R. Corwin. "Second reference catalogue of bright galaxies". In: *Second reference catalogue of bright galaxies* 1976 (Jan. 1976), p. 0.

[20] I. Zehavi et al. "Galaxy clustering in the completed SDSS redshift survey: the dependence on color and luminosity". In: 736.1 (July 2011), p. 59. DOI: 10.1088/0004-637x/736/1/59. URL: https://doi.org/10.1088%2F0004-637x%2F736%2F1%2F59.

[21] Planck Collaboration. "Planck 2018 results". In: *Astronomy & Astrophysics* 641 (Sept. 2020), A6. DOI: 10.1051/0004-6361/201833910. URL: https://doi.org/10.1051%2F0004-6361%2F201833910.

[22] T. Cohen et al. "Asymmetric dark matter from a GeV hidden sector". In: *Physical Review D* 82.5 (Sept. 2010). ISSN: 1550-2368. DOI: 10.1103/physrevd.82.056001. URL: http://dx.doi.org/10.1103/PhysRevD.82.056001.

[23] B. Dutta and J. Kumar. "Asymmetric dark matter from hidden sector baryogenesis". In: *Physics Letters B* 699.5 (May 2011), pp. 364–367. ISSN: 0370-2693. DOI: 10.1016/j.physletb.2011.04.036. URL: http://dx.doi.org/10.1016/j.physletb.2011.04.036.

[24] J. Preskill, M. B. Wise, and F. Wilczek. "Cosmology of the Invisible Axion". In: *Phys. Lett. B* 120 (1983). Ed. by M. A. Srednicki, pp. 127–132. DOI: 10.1016/0370-2693(83)90637-8.

[25] L. F. Abbott and P. Sikivie. "A Cosmological Bound on the Invisible Axion". In: *Phys. Lett. B* 120 (1983). Ed. by M. A. Srednicki, pp. 133–136. DOI: 10.1016/0370-2693(83)90638-X.

[26] M. Dine and W. Fischler. "The Not So Harmless Axion". In: *Phys. Lett. B* 120 (1983). Ed. by M. A. Srednicki, pp. 137–141. DOI: 10.1016/0370-2693(83)90639-1.

[27] P. W. Graham, D. E. Kaplan, and S. Rajendran. "Cosmological Relaxation of the Electroweak Scale". In: *Phys. Rev. Lett.* 115 (22 Nov. 2015), p. 221801. DOI: 10.1103/PhysRevLett.115.221801. URL: https://link.aps.org/doi/10.1103/PhysRevLett.115.221801.

[28] A. Banerjee et al. "Probing the relaxed relaxion at the luminosity and precision frontiers". In: *Journal of High Energy Physics* 2020.7 (July 2020). ISSN: 1029-8479. DOI: 10.1007/jhep07(2020)153. URL: http://dx.doi.org/10.1007/JHEP07(2020)153.

[29] S. Dodelson and L. M. Widrow. "Sterile neutrinos as dark matter". In: *Physical Review Letters* 72.1 (Jan. 1994), pp. 17–20. ISSN: 0031-9007. DOI: 10.1103/physrevlett.72.17. URL: http://dx.doi.org/10.1103/PhysRevLett.72.17.

[30] X. Shi and G. M. Fuller. "New Dark Matter Candidate: Nonthermal Sterile Neutrinos". In: *Physical Review Letters* 82.14 (Apr. 1999), pp. 2832–2835. ISSN: 1079-7114. DOI: 10.1103/physrevlett.82.2832. URL: http://dx.doi.org/10.1103/PhysRevLett.82.2832.

[31] A. G. Riess et al. "Observational Evidence from Supernovae for an Accelerating Universe and a Cosmological Constant". In: *The Astronomical Journal* 116.3 (Sept. 1998), pp. 1009–1038. DOI: 10.1086/300499. URL: https://doi.org/10.1086%2F300499.

[32] S. Perlmutter et al. “Measurements of Ω and Λ from 42 High-Redshift Supernovae”. In: *The Astrophysical Journal* 517.2 (June 1999), pp. 565–586. DOI: 10.1086/307221. URL: https://doi.org/10.1086%2F307221.

[33] Y. Akrami et al. “Planck2018 results”. In: *Astron. Astrophys.* 641 (Sept. 2020), A10. ISSN: 1432-0746. DOI: 10.1051/0004-6361/201833887. URL: http://dx.doi.org/10.1051/0004-6361/201833887.

[34] C. L. Bennett et al. “First-Year Wilkinson Microwave Anisotropy Probe (WMAP) Observations: Preliminary Maps and Basic Results”. In: *The Astrophysical Journal Supplement Series* 148.1 (Sept. 2003), pp. 1–27. DOI: 10.1086/377253. URL: https://doi.org/10.1086%2F377253.

[35] P. A. R. Ade et al. “Planck2013 results. XVI. Cosmological parameters”. In: *Astronomy Astrophysics* 571 (Oct. 2014), A16. ISSN: 1432-0746. DOI: 10.1051/0004-6361/201321591. URL: http://dx.doi.org/10.1051/0004-6361/201321591.

[36] P. A. R. Ade et al. “Planck2013 results. I. Overview of products and scientific results”. In: *Astronomy Astrophysics* 571 (Oct. 2014), A1. ISSN: 1432-0746. DOI: 10.1051/0004-6361/201321529. URL: http://dx.doi.org/10.1051/0004-6361/201321529.

[37] R. Esmailzadeh, G. D. Starkman, and S. Dimopoulos. “Primordial Nucleosynthesis without a Computer”. In: 378 (Sept. 1991), p. 504. DOI: 10.1086/170452.

[38] V. Mukhanov. “Nucleosynthesis Without Computer”. In: *International Journal of Theoretical Physics* 43.3 (Mar. 2004), pp. 669–693. DOI: 10.1023/b:ijtp.0000048169.69609.77. URL: https://doi.org/10.1023%2Fb%3Aijtp.0000048169.69609.77.

[39] P.A. Zyla et al. “Review of Particle Physics”. In: *Prog. Theor. Exp. Phys.* 2020 (8 Aug. 2020), p. 083C01. URL: https://doi.org/10.1093/ptep/ptaa104.

[40] Planck Collaboration. “Planck 2015 results. XIII. Cosmological parameters”. In: *Astronomy &amp Astrophysics* 594 (Sept. 2016), A13. DOI: 10.1051/0004-6361/201525830. URL: https://doi.org/10.1051%2F0004-6361%2F201525830.

[41] G. R. Blumenthal et al. “Formation of galaxies and large-scale structure with cold dark matter.” In: 311 (Oct. 1984), pp. 517–525. DOI: 10.1038/311517a0.

[42] J. Richard Bond, L. Kofman, and D. Pogosyan. “How filaments of galaxies are woven into the cosmic web”. In: *Nature* 380.6575 (Apr. 1996), pp. 603–606. DOI: 10.1038/380603a0. URL: https://doi.org/10.1038%2F380603a0.

[43] F. Bezrukov and A. Keats. “Heavy light inflaton and dark matter production”. In: *Physical Review D* 102.11 (Dec. 2020). ISSN: 2470-0029. DOI: 10.1103/physrevd.102.115011. URL: http://dx.doi.org/10.1103/PhysRevD.102.115011.

[44] Fedor Bezrukov and Abigail Keats. "Light inflaton model in a metastable universe". In: *Phys. Rev. D* 104 (7 Oct. 2021), p. 075020. DOI: 10.1103/PhysRevD.104.075020. URL: https://link.aps.org/doi/10.1103/PhysRevD.104.075020.

[45] M. Shaposhnikov and I. Tkachev. "The νMSM, inflation, and dark matter". In: *Physics Letters B* 639.5 (Aug. 2006), pp. 414–417. ISSN: 0370-2693. DOI: 10.1016/j.physletb.2006.06.063. URL: http://dx.doi.org/10.1016/j.physletb.2006.06.063.

[46] Y. Bartocci A. Anisimov and F. L. Bezrukov. "Inflaton mass in the νMSM inflation". In: *Physics Letters B* 671.2 (Jan. 2009), pp. 211–215. ISSN: 0370-2693. DOI: 10.1016/j.physletb.2008.12.028. URL: http://dx.doi.org/10.1016/j.physletb.2008.12.028.

[47] F. Bezrukov and D. Gorbunov. "Light inflaton hunter's guide". In: *Journal of High Energy Physics* 2010.5 (May 2010). ISSN: 1029-8479. DOI: 10.1007/jhep05(2010)010. URL: http://dx.doi.org/10.1007/JHEP05(2010)010.

[48] F. Bezrukov and D. Gorbunov. "Light inflaton after LHC8 and WMAP9 results". In: *Journal of High Energy Physics* 2013.7 (July 2013). ISSN: 1029-8479. DOI: 10.1007/jhep07(2013)140. URL: http://dx.doi.org/10.1007/JHEP07(2013)140.

[49] A. V. Bednyakov et al. "Stability of the Electroweak Vacuum: Gauge Independence and Advanced Precision". In: *Physical Review Letters* 115.20 (Nov. 2015). ISSN: 1079-7114. DOI: 10.1103/physrevlett.115.201802. URL: http://dx.doi.org/10.1103/PhysRevLett.115.201802.

[50] G. Dvali and C. Gomez. "Quantum Exclusion of Positive Cosmological Constant?" In: (2014). arXiv: 1412.8077 [hep-th].

[51] G. Dvali, C. Gómez, and S. Zell. "Quantum break-time of de Sitter". In: *Journal of Cosmology and Astroparticle Physics* 2017.06 (June 2017), pp. 028–028. ISSN: 1475-7516. DOI: 10.1088/1475-7516/2017/06/028. URL: http://dx.doi.org/10.1088/1475-7516/2017/06/028.

[52] F.L. Bezrukov and D.S. Gorbunov. "Relic gravity waves and 7 keV dark matter from a GeV scale inflaton". In: *Physics Letters B* 736 (Sept. 2014), pp. 494–498. ISSN: 0370-2693. DOI: 10.1016/j.physletb.2014.07.060. URL: http://dx.doi.org/10.1016/j.physletb.2014.07.060.

[53] T. Asaka and M. Shaposhnikov. "The νMSM, dark matter and baryon asymmetry of the universe". In: *Physics Letters B* 620.1-2 (July 2005), pp. 17–26. ISSN: 0370-2693. DOI: 10.1016/j.physletb.2005.06.020. arXiv: hep-ph/0505013. URL: http://dx.doi.org/10.1016/j.physletb.2005.06.020.

[54] T. Asaka, S. Blanchet, and M. Shaposhnikov. "The νMSM, dark matter and neutrino masses". In: *Phys. Lett. B* 631 (2005), pp. 151–156. DOI: 10.1016/j.physletb.2005.09.070. arXiv: hep-ph/0503065.

[55] D. S. Gorbunov and V. A. Rubakov. *Introduction to the Theory of the Early Universe : Hot Big Bang Theory*. Second. Singapore: World Scientific, 2017.

[56] E. W. Kolb and M. S. Turner. *The Early Universe*. Vol. 69. 1990. ISBN: 978-0-201-62674-2. DOI: 10.1201/9780429492860.

[57] S. Weinberg. *Cosmology*. 2008. ISBN: 978-0-19-852682-7.

[58] V. M. Slipher. "The radial velocity of the Andromeda Nebula". In: *Lowell Observatory Bulletin* 2.8 (Jan. 1913), pp. 56–57.

[59] V. M. Slipher. "Spectrographic Observations of Nebulae". In: *Popular Astronomy* 23 (Jan. 1915), pp. 21–24.

[60] E. Hubble. "A relation between distance and radial velocity among extra-galactic nebulae". In: *Proceedings of the National Academy of Sciences* 15.3 (1929), pp. 168–173. DOI: 10.1073/pnas.15.3.168. eprint: https://www.pnas.org/doi/pdf/10.1073/pnas.15.3.168. URL: https://www.pnas.org/doi/abs/10.1073/pnas.15.3.168.

[61] A. Einstein. "Kosmologische Betrachtungen zur allgemeinen Relativitätstheorie". In: *Sitzungsberichte der Königlich Preußischen Akademie der Wissenschaften (Berlin* (Jan. 1917), pp. 142–152.

[62] W. de Sitter. "On the relativity of inertia. Remarks concerning Einstein's latest hypothesis". In: *Koninklijke Nederlandse Akademie van Wetenschappen Proceedings Series B Physical Sciences* 19 (Mar. 1917), pp. 1217–1225.

[63] A. Friedmann. "Über die Krümmung des Raumes". In: *Zeitschrift fur Physik* 10 (Jan. 1922), pp. 377–386. DOI: 10.1007/BF01332580.

[64] G. Lemaıtre. "Un Univers homogène de masse constante et de rayon croissant rendant compte de la vitesse radiale des nébuleuses extra-galactiques". In: *Annales de la Société Scientifique de Bruxelles* 47 (Jan. 1927), pp. 49–59.

[65] G. Lemaitre. "L'Hypothése de l'Atome Primitif". In: *Publications du Laboratoire d'Astronomie et de Geodesie de l'Universite de Louvain* 12 (Jan. 1949), pp. D1–D19.

[66] F. Bernardeau, C. Grojean, and J. Dalibard. *Particle Physics and Cosmology: the Fabric of Spacetime*. Elsevier Science, 2007.

[67] L. Husdal. "On Effective Degrees of Freedom in the Early Universe". In: *Galaxies* 4.4 (2016), p. 78. DOI: 10.3390/galaxies4040078. arXiv: 1609.04979 [astro-ph.CO].

[68] M. D'Onofrio and K. Rummukainen. "Standard model cross-over on the lattice". In: *Physical Review D* 93.2 (Jan. 2016). ISSN: 2470-0029. DOI: 10.1103/physrevd.93.025003. URL: http://dx.doi.org/10.1103/PhysRevD.93.025003.

[69] C. Yanagisawa. "Looking for cosmic neutrino background". In: *Frontiers in Physics* 2 (2014). ISSN: 2296-424X. DOI: 10.3389/fphy.2014.00030. URL: https://www.frontiersin.org/articles/10.3389/fphy.2014.00030.

[70] B. Follin et al. "First Detection of the Acoustic Oscillation Phase Shift Expected from the Cosmic Neutrino Background". In: *Physical Review Letters* 115.9 (Aug. 2015). DOI: 10.1103/physrevlett.115.091301. URL: https://doi.org/10.1103%2Fphysrevlett.115.091301.

[71] J Bernstein, L. S. Brown, and G. Feinberg. "Cosmological helium production simplified". In: *Rev. Mod. Phys.* 61 (1 Jan. 1989), pp. 25–39. DOI: 10.1103/RevModPhys.61.25. URL: https://link.aps.org/doi/10.1103/RevModPhys.61.25.

[72] S. Sarkar. "Big bang nucleosynthesis and physics beyond the standard model". In: *Reports on Progress in Physics* 59.12 (Dec. 1996), pp. 1493–1609. DOI: 10.1088/0034-4885/59/12/001. URL: https://doi.org/10.1088%2F0034-4885%2F59%2F12%2F001.

[73] P. J. E. Peebles and J. T. Yu. "Primeval Adiabatic Perturbation in an Expanding Universe". In: 162 (Dec. 1970), p. 815. DOI: 10.1086/150713.

[74] W. Hu and N. Sugiyama. "Anisotropies in the cosmic microwave background: an analytic approach". In: *The Astrophysical Journal* 444 (May 1995), p. 489. ISSN: 1538-4357. DOI: 10.1086/175624. URL: http://dx.doi.org/10.1086/175624.

[75] S. W. Hawking. "The development of irregularities in a single bubble inflationary universe". In: *Physics Letters B* 115.4 (1982), pp. 295–297. ISSN: 0370-2693. DOI: https://doi.org/10.1016/0370-2693(82)90373-2. URL: https://www.sciencedirect.com/science/article/pii/0370269382903732.

[76] J. M. Bardeen, P. J. Steinhardt, and M. S. Turner. "Spontaneous creation of almost scale-free density perturbations in an inflationary universe". In: *Phys. Rev. D* 28 (4 Aug. 1983), pp. 679–693. DOI: 10.1103/PhysRevD.28.679. URL: https://link.aps.org/doi/10.1103/PhysRevD.28.679.

[77] A. D. Sakharov. "The Initial Stage of an Expanding Universe and the Appearance of a Nonuniform Distribution of Matter". In: *Soviet Journal of Experimental and Theoretical Physics* 22 (Jan. 1966), p. 241.

[78] D. S. Gorbunov and V. A. Rubakov. *Introduction to the theory of the early universe : cosmological perturbations and inflationary theory*. Singapore: World Scientific, 2011.

[79] P. J. E. Peebles. “Recombination of the Primeval Plasma”. In: 153 (July 1968), p. 1. DOI: 10.1086/149628.

[80] Y. B. Zeldovich, V. G. Kurt, and R. A. Syunyaev. “Recombination of Hydrogen in the Hot Model of the Universe”. In: *Zhurnal Eksperimentalnoi i Teoreticheskoi Fiziki* 55 (July 1968), pp. 278–286.

[81] D. J. Fixsen. “The temperature of the cosmic microwave background”. In: *The Astrophysical Journal* 707.2 (Nov. 2009), pp. 916–920. ISSN: 1538-4357. DOI: 10.1088/0004-637x/707/2/916. URL: http://dx.doi.org/10.1088/0004-637X/707/2/916.

[82] A. G. Doroshkevich, Y. B. Zel’dovich, and R. A. Syunyaev. “Fluctuations of the microwave background radiation in the adiabatic and entropic theories of galaxy formation”. In: 22 (Oct. 1978), pp. 523–528.

[83] N. W. Halverson et al. “Degree Angular Scale Interferometer First Results: A Measurement of the Cosmic Microwave Background Angular Power Spectrum”. In: *The Astrophysical Journal* 568.1 (Mar. 2002), pp. 38–45. ISSN: 1538-4357. DOI: 10.1086/338879. URL: http://dx.doi.org/10.1086/338879.

[84] P. D. Mauskopf et al. “Measurement of a Peak in the Cosmic Microwave Background Power Spectrum from the North American Test Flight of Boomerang”. In: *The Astrophysical Journal* 536.2 (June 2000), pp. L59–L62. DOI: 10.1086/312743. URL: https://doi.org/10.1086%2F312743.

[85] P. de Bernardis et al. “A flat Universe from high-resolution maps of the cosmic microwave background radiation”. In: *Nature* 404.6781 (Apr. 2000), pp. 955–959. DOI: 10.1038/35010035. URL: https://doi.org/10.1038%2F35010035.

[86] W. Hu and N. Sugiyama. “Small-Scale Cosmological Perturbations: An Analytic Approach”. In: *The Astrophysical Journal* 471.2 (Nov. 1996), pp. 542–570. ISSN: 1538-4357. DOI: 10.1086/177989. URL: http://dx.doi.org/10.1086/177989.

[87] J. Silk. “Cosmic Black-Body Radiation and Galaxy Formation”. In: 151 (Feb. 1968), p. 459. DOI: 10.1086/149449.

[88] S. Weinberg. “Entropy Generation and the Survival of Protogalaxies in an Expanding Universe”. In: 168 (Sept. 1971), p. 175. DOI: 10.1086/151073.

[89] A. Klypin et al. “Where Are the Missing Galactic Satellites?” In: 522.1 (Sept. 1999), pp. 82–92. DOI: 10.1086/307643. arXiv: astro-ph/9901240 [astro-ph].

[90] M. Miranda and A. V. Macciò. “Constraining Warm Dark Matter using QSO gravitational lensing”. In: (2007). DOI: 10.48550/ARXIV.0706.0896. URL: https://arxiv.org/abs/0706.0896.

[91] A. Garzilli, A. Boyarsky, and O. Ruchayskiy. "Cutoff in the Lyman- forest power spectrum: Warm IGM or warm dark matter?" In: *Physics Letters B* 773 (2017), pp. 258–264. ISSN: 0370-2693. DOI: https://doi.org/10.1016/j.physletb.2017.08.022. URL: https://www.sciencedirect.com/science/article/pii/S0370269317306445.

[92] M. Viel et al. "How cold is cold dark matter? Small scales constraints from the flux power spectrum of the high-redshift Lyman-alpha forest". In: *Phys. Rev. Lett.* 100 (2008), p. 041304. DOI: 10.1103/PhysRevLett.100.041304. arXiv: 0709.0131 [astro-ph].

[93] M. Viel et al. "Warm dark matter as a solution to the small scale crisis: New constraints from high redshift Lyman-α forest data". In: *Phys. Rev. D* 88 (4 Aug. 2013), p. 043502. DOI: 10.1103/PhysRevD.88.043502. URL: https://link.aps.org/doi/10.1103/PhysRevD.88.043502.

[94] M. Pospelov and J. Pradler. "Metastable GeV-scale particles as a solution to the cosmological lithium problem". In: *Phys. Rev. D* 82 (10 Nov. 2010), p. 103514. DOI: 10.1103/PhysRevD.82.103514. URL: https://link.aps.org/doi/10.1103/PhysRevD.82.103514.

[95] A. Boyarsky et al. "Improved big bang nucleosynthesis constraints on heavy neutral leptons". In: *Phys. Rev. D* 104 (2 July 2021), p. 023517. DOI: 10.1103/PhysRevD.104.023517. URL: https://link.aps.org/doi/10.1103/PhysRevD.104.023517.

[96] A.D. Dolgov et al. "Heavy sterile neutrinos: bounds from big-bang nucleosynthesis and SN 1987A". In: *Nuclear Physics B* 590.3 (2000), pp. 562–574. ISSN: 0550-3213. DOI: https://doi.org/10.1016/S0550-3213(00)00566-6. URL: https://www.sciencedirect.com/science/article/pii/S0550321300005666.

[97] P. Ntelis. "The Homogeneity Scale of the universe". In: (2016). DOI: 10.48550/ARXIV.1607.03418. URL: https://arxiv.org/abs/1607.03418.

[98] A. R. Liddle and D. H. Lyth. *Cosmological Inflation and Large-Scale Structure*. Cambridge University Press, 2000. DOI: 10.1017/CBO9781139175180.

[99] D. Baumann. "TASI Lectures on Inflation". In: (Nov. 2019).

[100] E. Komatsu and C. L. Bennett et al. "Results from the Wilkinson Microwave Anisotropy Probe". In: *Progress of Theoretical and Experimental Physics* 2014.6 (June 2014), 6B102–. DOI: 10.1093/ptep/ptu083. URL: https://doi.org/10.1093%2Fptep%2Fptu083.

[101] Planck Collaboration. "Planck 2013 results. XXII. Constraints on inflation". In: *Astronomy &amp Astrophysics* 571 (Oct. 2014), A22. DOI: 10.1051/0004-6361/201321569. URL: https://doi.org/10.1051%2F0004-6361%2F201321569.

[102] M. Viel et al. "Constraining warm dark matter candidates including sterile neutrinos and light gravitinos with WMAP and the Lyman-forest". In: *Physical Review D* 71.6 (Mar. 2005). ISSN: 1550-2368. DOI: 10.1103/physrevd.71.063534. URL: http://dx.doi.org/10.1103/PhysRevD.71.063534.

[103] L. Covi, E. Roulet, and F. Vissani. "CP violating decays in leptogenesis scenarios". In: *Physics Letters B* 384.1-4 (Sept. 1996), pp. 169–174. ISSN: 0370-2693. DOI: 10.1016/0370-2693(96)00817-9. URL: http://dx.doi.org/10.1016/0370-2693(96)00817-9.

[104] A. Pilaftsis. "Baryogenesis through mixing of heavy Majorana neutrinos". In: (1998). arXiv: hep-ph/9810211 [hep-ph]. URL: https://doi.org/10.22323/1.001.0075.

[105] E. K. Akhmedov, V. A. Rubakov, and A. Y. Smirnov. "Baryogenesis via Neutrino Oscillations". In: *Physical Review Letters* 81.7 (Aug. 1998), pp. 1359–1362. ISSN: 1079-7114. DOI: 10.1103/physrevlett.81.1359. URL: http://dx.doi.org/10.1103/PhysRevLett.81.1359.

[106] M. Drewes et al. "A White Paper on keV Sterile Neutrino Dark Matter". In: *JCAP* 01 (2017), p. 025. DOI: 10.1088/1475-7516/2017/01/025. arXiv: 1602.04816 [hep-ph].

[107] J. Binney and S. Tremaine. *Galactic Dynamics*. Second. Princeton: Princeton University Press, 1987.

[108] F. Zwicky. "The redshift of extragalactic nebulae". In: *Helv. Phys. Acta* 6 (1933), pp. 110–127. DOI: 10.1007/s10714-008-0707-4.

[109] V. C. Rubin et al. "Extended rotation curves of high-luminosity spiral galaxies. IV. Systematic dynamical properties, Sa → Sc." In: 225 (Nov. 1978), pp. L107–L111. DOI: 10.1086/182804.

[110] J. P. Ostriker and P. J. E. Peebles. "A Numerical Study of the Stability of Flattened Galaxies: or, can Cold Galaxies Survive?" In: 186 (Dec. 1973), pp. 467–480. DOI: 10.1086/152513.

[111] J. P. Ostriker, P. J. E. Peebles, and A. Yahil. "The Size and Mass of Galaxies, and the Mass of the Universe". In: 193 (Oct. 1974), p. L1. DOI: 10.1086/181617.

[112] J. Einasto et al. "Missing mass around galaxies - Morphological evidence". In: 252 (Nov. 1974), pp. 111–113. DOI: 10.1038/252111a0.

[113] K. Freese. "Review of Observational Evidence for Dark Matter in the Universe and in upcoming searches for Dark Stars". In: *EAS Publications Series* 36 (2009), pp. 113–126. ISSN: 1638-1963. DOI: 10.1051/eas/0936016. URL: http://dx.doi.org/10.1051/eas/0936016.

[114] J. K. Adelman-McCarthy et al. (The SDSS Collaboration). "The Fourth Data Release of the Sloan Digital Sky Survey". In: *The Astrophysical Journal Supplement Series* 162.1 (Jan. 2006), pp. 38–48. ISSN: 1538-4365. DOI: 10.1086/497917. URL: http://dx.doi.org/10.1086/497917.

[115] M.J. Jee and H. Ford. *NASA Hubble Space Telescope Detects Ring of Dark Matter*. https://www.nasa.gov/mission_pages/hubble/news/dark_matter_ring_mm.html. Accessed: 2022-02-15. 2015.

[116] X-ray: NASA/CXC/CfA/M. Markevitch et al.; Optical: NASA/STScI; Magellan/U. Arizona/ D. Clowe et al.; Lensing Map: NASA/STScI; ESO WFI; Magellan/U. Arizona/D. Clowe et al. *Composite image of the galaxy cluster 1E 0657-56*. https://chandra.harvard.edu/photo/2006/1e0657/. Accessed: 2022-02-15. 2006.

[117] D. Clowe et al. "A Direct Empirical Proof of the Existence of Dark Matter". In: *The Astrophysical Journal* 648.2 (Aug. 2006), pp. L109–L113. ISSN: 1538-4357. DOI: 10.1086/508162. URL: http://dx.doi.org/10.1086/508162.

[118] L. J. Hall et al. "Freeze-in production of FIMP dark matter". In: *Journal of High Energy Physics* 2010.3 (Mar. 2010). ISSN: 1029-8479. DOI: 10.1007/jhep03(2010)080. URL: http://dx.doi.org/10.1007/JHEP03(2010)080.

[119] D. G. Cerdeño. "DARK MATTER 101 From production to detection". In: 2016.

[120] SDSS Collaboration. "The Seventeenth Data Release of the Sloan Digital Sky Surveys: Complete Release of MaNGA, MaStar, and APOGEE-2 Data". In: 259.2, 35 (Apr. 2022), p. 35. DOI: 10.3847/1538-4365/ac4414. arXiv: 2112.02026 [astro-ph.GA].

[121] C. B. Netterfield et al. "A Measurement by BOOMERANG of Multiple Peaks in the Angular Power Spectrum of the Cosmic Microwave Background". In: *The Astrophysical Journal* 571.2 (June 2002), pp. 604–614. DOI: 10.1086/340118. URL: https://doi.org/10.1086%2F340118.

[122] Y. B. Zel'dovich. "Gravitational instability: An approximate theory for large density perturbations." In: 5 (Mar. 1970), pp. 84–89.

[123] P. J. E. Peebles. *Physical cosmology*. 1971.

[124] Y. Zeldovich, J. Einasto, and S. Shandarin. "Giant voids in the Universe". In: *Nature* 300 (Dec. 1982). DOI: 10.1038/300407a0.

[125] J. M. Uson and D. T. Wilkinson. "New limits on small-scale anisotropy in the microwave background". In: 277 (Feb. 1984), pp. L1–L3. DOI: 10.1086/184188.

[126] Planck Collaboration. "Planck 2018 results". In: *Astronomy & Astrophysics* 641 (Sept. 2020), A10. DOI: 10.1051/0004-6361/201833887. URL: https://doi.org/10.1051%2F0004-6361%2F201833887.

[127] J. Lesgourgues and S. Pastor. "Massive neutrinos and cosmology". In: *Physics Reports* 429.6 (July 2006), pp. 307–379. DOI: 10.1016/j.physrep.2006.04.001. URL: https://doi.org/10.1016%2Fj.physrep.2006.04.001.

[128] J. Lesgourgues and S. Pastor. "Neutrino Mass from Cosmology". In: *Advances in High Energy Physics* 2012 (2012), pp. 1–34. DOI: 10.1155/2012/608515. URL: https://doi.org/10.1155%2F2012%2F608515.

[129] A. G. Doroshkevich, V. N. Lukash, and E. V. Mikheeva. "A solution to the problems of cusps and rotation curves in dark matter halos in the cosmological standard model". In: *Uspekhi Fizicheskih Nauk* 182.1 (2012), p. 3. ISSN: 1996-6652. DOI: 10.3367/ufnr.0182.201201a.0003. URL: http://dx.doi.org/10.3367/UFNr.0182.201201a.0003.

[130] A. Boyarsky et al. "Lyman-α constraints on warm and on warm-plus-cold dark matter models". In: 2009.5, 012 (May 2009), p. 012. DOI: 10.1088/1475-7516/2009/05/012. arXiv: 0812.0010 [astro-ph].

[131] J. N. Bahcall, J. L. Greenstein, and W. L. W. Sargent. "The Absorption-Line Spectrum of the Quasi-Stellar Radio Source PKS 0237-23". In: 153 (Aug. 1968), p. 689. DOI: 10.1086/149696.

[132] G. Burbidge and A. Hewitt. "A Catalog of Quasars Near and Far". In: 88.6 (Dec. 1994), p. 32.

[133] R. Lynds. "The Absorption-Line Spectrum of 4c 05.34". In: 164 (Mar. 1971), p. L73. DOI: 10.1086/180695.

[134] M. Rauch. "The Lyman Alpha Forest in the Spectra of QSOs". In: *Annual Review of Astronomy and Astrophysics* 36.1 (Sept. 1998), pp. 267–316. DOI: 10.1146/annurev.astro.36.1.267. URL: https://doi.org/10.1146%2Fannurev.astro.36.1.267.

[135] P. McDonald et al. "The Ly Forest Power Spectrum from the Sloan Digital Sky Survey". In: *The Astrophysical Journal Supplement Series* 163.1 (Mar. 2006), pp. 80–109. DOI: 10.1086/444361. URL: https://doi.org/10.1086%2F444361.

[136] G. D. Becker, M. Rauch, and W. L. W. Sargent. "The Evolution of Optical Depth in the Ly Forest: Evidence Against Reionization atiz/i∼6". In: *The Astrophysical Journal* 662.1 (June 2007), pp. 72–93. DOI: 10.1086/517866. URL: https://doi.org/10.1086%2F517866.

[137] M. Viel. "The Lyman-α Forest as a Probe of the Coldness of Dark Matter". In: *IFAE 2007*. Ed. by Gianpaolo Carlino et al. Milano: Springer Milan, 2008, pp. 255–260. ISBN: 978-88-470-0747-5.

[138] A. Garzilli et al. "The Lyman- forest as a diagnostic of the nature of the dark matter". In: *Monthly Notices of the Royal Astronomical Society* 489.3 (Aug. 2019), pp. 3456–3471. DOI: 10.1093/mnras/stz2188. URL: https://doi.org/10.1093%2Fmnras%2Fstz2188.

[139] J. P. E. Peebles. "Primeval adiabatic perturbations - Effect of massive neutrinos". In: 258 (July 1982), pp. 415–424. DOI: 10.1086/160094.

[140] T. Quinn, N. Katz, and G. Efstathiou. "Photoionization and the formation of dwarf galaxies". In: *Monthly Notices of the Royal Astronomical Society* 278.4 (Feb. 1996), pp. L49–L54. ISSN: 0035-8711. DOI: 10.1093/mnras/278.4.L49. eprint: https://academic.oup.com/mnras/article-pdf/278/4/L49/18199824/278-4-L49.pdf. URL: https://doi.org/10.1093/mnras/278.4.L49.

[141] M. S. Bovill and M. Ricotti. "Pre-reionization Fossils, Ultra-faint Dwarfs and the Missing Galactic Satellite Problem". In: *The Astrophysical Journal* 693.2 (Mar. 2009), pp. 1859–1870. DOI: 10.1088/0004-637x/693/2/1859. URL: https://doi.org/10.1088%2F0004-637x%2F693%2F2%2F1859.

[142] M. McQuinn. "The Evolution of the Intergalactic Medium". In: *Annual Review of Astronomy and Astrophysics* 54.1 (Sept. 2016), pp. 313–362. DOI: 10.1146/annurev-astro-082214-122355. URL: https://doi.org/10.1146%2Fannurev-astro-082214-122355.

[143] K. Petraki and A. Kusenko. "Dark-matter sterile neutrinos in models with a gauge singlet in the Higgs sector". In: *Physical Review D* 77.6 (Mar. 2008). ISSN: 1550-2368. DOI: 10.1103/physrevd.77.065014. URL: http://dx.doi.org/10.1103/PhysRevD.77.065014.

[144] A. Garzilli et al. "How to constrain warm dark matter with the Lyman- forest". In: *Monthly Notices of the Royal Astronomical Society* 502.2 (Jan. 2021), pp. 2356–2363. ISSN: 0035-8711. DOI: 10.1093/mnras/stab192. eprint: https://academic.oup.com/mnras/article-pdf/502/2/2356/36218015/stab192.pdf. URL: https://doi.org/10.1093/mnras/stab192.

[145] D. N. Schramm and M. S. Turner. "Big-bang nucleosynthesis enters the precision era". In: *Reviews of Modern Physics* 70.1 (Jan. 1998), pp. 303–318. ISSN: 1539-0756. DOI: 10.1103/revmodphys.70.303. URL: http://dx.doi.org/10.1103/RevModPhys.70.303.

[146] S. Schael et al. "Precision electroweak measurements on the Z resonance". In: *Phys. Rept.* 427 (2006), pp. 257–454. DOI: 10.1016/j.physrep.2005.12.006. arXiv: hep-ex/0509008.

[147] P. A. Zyla et al. "Review of Particle Physics". In: *PTEP* 2020.8 (2020), p. 083C01. DOI: 10.1093/ptep/ptaa104.

[148] R. Davis, D. S. Harmer, and K. C. Hoffman. "Search for Neutrinos from the Sun". In: *Phys. Rev. Lett.* 20 (21 May 1968), pp. 1205–1209. DOI: 10.1103/PhysRevLett.20.1205. URL: https://link.aps.org/doi/10.1103/PhysRevLett.20.1205.

[149] J. N. Bahcall, N. A. Bahcall, and G. Shaviv. "Present Status of the Theoretical Predictions for the ^{37}Cl Solar-Neutrino Experiment". In: *Phys. Rev. Lett.* 20 (21 May 1968), pp. 1209–1212. DOI: 10.1103/PhysRevLett.20.1209. URL: https://link.aps.org/doi/10.1103/PhysRevLett.20.1209.

[150] J. N. Bahcall and S. C. Frautschi. "Lepton non-conservation and solar neutrinos". In: *Physics Letters B* 29.10 (1969), pp. 623–625. ISSN: 0370-2693. DOI: https://doi.org/10.1016/0370-2693(69)90090-2. URL: https://www.sciencedirect.com/science/article/pii/0370269369900902.

[151] L. Wolfenstein. "Neutrino oscillations in matter". In: *Phys. Rev. D* 17 (9 May 1978), pp. 2369–2374. DOI: 10.1103/PhysRevD.17.2369. URL: https://link.aps.org/doi/10.1103/PhysRevD.17.2369.

[152] S. P. Mikheyev and A. Y. Smirnov. "Resonance Amplification of Oscillations in Matter and Spectroscopy of Solar Neutrinos". In: *Sov. J. Nucl. Phys.* 42 (1985), pp. 913–917.

[153] Z. Maki, M. Nakagawa, and S. Sakata. "Remarks on the Unified Model of Elementary Particles". In: *Progress of Theoretical Physics* 28.5 (Nov. 1962), pp. 870–880. ISSN: 0033-068X. DOI: 10.1143/PTP.28.870. eprint: https://academic.oup.com/ptp/article-pdf/28/5/870/5258750/28-5-870.pdf. URL: https://doi.org/10.1143/PTP.28.870.

[154] P. B. Pal. "Particle physics confronts the solar neutrino problem". In: *Int. J. Mod. Phys. A* 7 (1992), pp. 5387–5460. DOI: 10.1142/S0217751X92002465.

[155] E. Majorana. "Teoria simmetrica dell'elettrone e del positrone". In: *Il Nuovo Cimento* 14.4 (Apr. 1937), pp. 171–184. DOI: 10.1007/BF02961314.

[156] J. D. Vergados, H. Ejiri, and F. Šimkovic. "Theory of neutrinoless double-beta decay". In: *Reports on Progress in Physics* 75.10 (Sept. 2012), p. 106301. ISSN: 1361-6633. DOI: 10.1088/0034-4885/75/10/106301. URL: http://dx.doi.org/10.1088/0034-4885/75/10/106301.

[157] J. Garayoa and T. Schwetz. "Neutrino mass hierarchy and Majorana CP phases within the Higgs triplet model at the LHC". In: *Journal of High Energy Physics* 2008.03 (Mar. 2008), pp. 009–009. DOI: 10.1088/1126-6708/2008/03/009. URL: https://doi.org/10.1088%2F1126-6708%2F2008%2F03%2F009.

[158] P. Minkowski. "$\mu \to e\gamma$ at a rate of one out of 10^9 muon decays?" In: *Physics Letters B* 67.4 (1977), pp. 421–428. ISSN: 0370-2693. DOI: https://doi.org/10.1016/0370-2693(77)90435-X. URL: https://www.sciencedirect.com/science/article/pii/037026937790435X.

[159] T. Yanagida. "Horizontal gauge symmetry and masses of neutrinos". In: *Conf. Proc. C* 7902131 (1979). Ed. by Osamu Sawada and Akio Sugamoto, pp. 95–99.

[160] S. Dodelson and L. M. Widrow. "Sterile neutrinos as dark matter". In: *Phys. Rev. Lett.* 72 (1 Jan. 1994), pp. 17–20. DOI: 10.1103/PhysRevLett.72.17. URL: https://link.aps.org/doi/10.1103/PhysRevLett.72.17.

[161] X. Shi and G. M. Fuller. "New Dark Matter Candidate: Nonthermal Sterile Neutrinos". In: *Phys. Rev. Lett.* 82 (14 Apr. 1999), pp. 2832–2835. DOI: 10.1103/PhysRevLett.82.2832. URL: https://link.aps.org/doi/10.1103/PhysRevLett.82.2832.

[162] M. Plümacher. "Baryogenesis and lepton number violation". In: *Zeitschrift für Physik C Particles and Fields* 74 (1997), pp. 549–559. DOI: 10.1007/s002880050418. URL: https://doi.org/10.1007/s002880050418.

[163] M. Fukugita and T. Yanagida. "Barygenesis without grand unification". In: *Physics Letters B* 174.1 (1986), pp. 45–47. ISSN: 0370-2693. DOI: https://doi.org/10.1016/0370-2693(86)91126-3. URL: https://www.sciencedirect.com/science/article/pii/0370269386911263.

[164] L. Covi and E. Roulet. "Baryogenesis from mixed particle decays". In: *Physics Letters B* 399.1-2 (Apr. 1997), pp. 113–118. ISSN: 0370-2693. DOI: 10.1016/s0370-2693(97)00287-6. URL: http://dx.doi.org/10.1016/S0370-2693(97)00287-6.

[165] A. Pilaftsis. "CP violation and baryogenesis due to heavy Majorana neutrinos". In: *Physical Review D* 56.9 (Nov. 1997), pp. 5431–5451. ISSN: 1089-4918. DOI: 10.1103/physrevd.56.5431. URL: http://dx.doi.org/10.1103/PhysRevD.56.5431.

[166] A. Pilaftsis and T. E. J. Underwood. "Resonant leptogenesis". In: *Nuclear Physics B* 692.3 (Aug. 2004), pp. 303–345. ISSN: 0550-3213. DOI: 10.1016/j.nuclphysb.2004.05.029. URL: http://dx.doi.org/10.1016/j.nuclphysb.2004.05.029.

[167] V. Brdar et al. "Type I seesaw mechanism as the common origin of neutrino mass, baryon asymmetry, and the electroweak scale". In: *Physical Review D* 100.7 (Oct. 2019). ISSN: 2470-0029. DOI: 10.1103/physrevd.100.075029. URL: http://dx.doi.org/10.1103/PhysRevD.100.075029.

[168] A. Boyarsky, O. Ruchayskiy, and M. Shaposhnikov. "The Role of Sterile Neutrinos in Cosmology and Astrophysics". In: *Annual Review of Nuclear and Particle Science* 59.1 (Nov. 2009), pp. 191–214. ISSN: 1545-4134. DOI: 10.1146/annurev.nucl.010909.083654. URL: http://dx.doi.org/10.1146/annurev.nucl.010909.083654.

[169] A. Boyarsky, D. Iakubovskyi, and O. Ruchayskiy. "Next decade of sterile neutrino studies". In: *Physics of the Dark Universe* 1 (June 2013). DOI: 10.1016/j.dark.2012.11.001.

[170] A. Dolgov. "Massive sterile neutrinos as warm dark matter". In: *Astroparticle Physics* 16.3 (Jan. 2002), pp. 339–344. ISSN: 0927-6505. DOI: 10.1016/s0927-6505(01)00115-3. URL: http://dx.doi.org/10.1016/S0927-6505(01)00115-3.

[171] A. Boyarsky et al. "Constraints on sterile neutrinos as dark matter candidates from the diffuse X-ray background". In: *Monthly Notices of the Royal Astronomical Society* 370.1 (July 2006), pp. 213–218. ISSN: 1365-2966. DOI: 10.1111/j.1365-2966.2006.10458.x. URL: http://dx.doi.org/10.1111/j.1365-2966.2006.10458.x.

[172] J. Alvey et al. "New constraints on the mass of fermionic dark matter from dwarf spheroidal galaxies". In: *Monthly Notices of the Royal Astronomical Society* 501.1 (Nov. 2020), pp. 1188–1201. ISSN: 1365-2966. DOI: 10.1093/mnras/staa3640. URL: http://dx.doi.org/10.1093/mnras/staa3640.

[173] R. Barbieri and A. Dolgov. "Bounds on sterile neutrinos from nucleosynthesis". In: *Physics Letters B* 237.3 (1990), pp. 440–445. ISSN: 0370-2693. DOI: https://doi.org/10.1016/0370-2693(90)91203-N. URL: https://www.sciencedirect.com/science/article/pii/037026939091203N.

[174] D. Notzold and G. Raffelt. "Neutrino dispersion at finite temperature and density". In: *Nucl. Phys.* B307 (1988), pp. 924–936.

[175] A. Y. Smirnov. "The MSW Effect and Matter Effects in Neutrino Oscillations". In: *Physica Scripta* T121 (Jan. 2005), pp. 57–64. DOI: 10.1088/0031-8949/2005/t121/008. URL: https://doi.org/10.1088%2F0031-8949%2F2005%2Ft121%2F008.

[176] V. Avila-Reese P. Colin and O. Valenzuela. "Substructure and Halo Density Profiles in a Warm Dark Matter Cosmology". In: *The Astrophysical Journal* 542.2 (Oct. 2000), pp. 622–630. ISSN: 1538-4357. DOI: 10.1086/317057. URL: http://dx.doi.org/10.1086/317057.

[177] J. Sommer-Larsen and A. Dolgov. "Formation of Disk Galaxies: Warm Dark Matter and the Angular Momentum Problem". In: *The Astrophysical Journal* 551.2 (Apr. 2001), pp. 608–623. ISSN: 1538-4357. DOI: 10.1086/320211. URL: http://dx.doi.org/10.1086/320211.

[178] M. Laine and M. Shaposhnikov. "Sterile neutrino dark matter as a consequence of MSM-induced lepton asymmetry". In: *Journal of Cosmology and Astroparticle Physics* 2008.06 (June 2008), p. 031. ISSN: 1475-7516. DOI: 10.1088/1475-7516/2008/06/031. URL: http://dx.doi.org/10.1088/1475-7516/2008/06/031.

[179] M. Shaposhnikov. "The MSM, leptonic asymmetries, and properties of singlet fermions". In: *Journal of High Energy Physics* 2008.08 (Aug. 2008), pp. 008–008. ISSN: 1029-8479. DOI: 10.1088/1126-6708/2008/08/008. URL: http://dx.doi.org/10.1088/1126-6708/2008/08/008.

[180] A. Boyarsky, O. Ruchayskiy, and D. Iakubovskyi. "A lower bound on the mass of dark matter particles". In: *Journal of Cosmology and Astroparticle Physics* 2009.03 (Mar. 2009), pp. 005–005. ISSN: 1475-7516. DOI: 10.1088/1475-7516/2009/03/005. URL: http://dx.doi.org/10.1088/1475-7516/2009/03/005.

[181] S. Tremaine and J. E. Gunn. "Dynamical Role of Light Neutral Leptons in Cosmology". In: *Phys. Rev. Lett.* 42 (6 Feb. 1979), pp. 407–410. DOI: 10.1103/PhysRevLett.42.407. URL: https://link.aps.org/doi/10.1103/PhysRevLett.42.407.

[182] S. H. Hansen et al. "Constraining the window on sterile neutrinos as warm dark matter". In: *Monthly Notices of the Royal Astronomical Society* 333.3 (July 2002), pp. 544–546. ISSN: 1365-2966. DOI: 10.1046/j.1365-8711.2002.05410.x. URL: http://dx.doi.org/10.1046/j.1365-8711.2002.05410.x.

[183] K. Kohri, M. Kawasaki, and K. Sato. "Big Bang Nucleosynthesis and Lepton Number Asymmetry in the Universe". In: *The Astrophysical Journal* 490.1 (Nov. 1997), pp. 72–75. ISSN: 1538-4357. DOI: 10.1086/512793. URL: http://dx.doi.org/10.1086/512793.

[184] J. Baur et al. "Constraints from Ly- forests on non-thermal dark matter including resonantly-produced sterile neutrinos". In: *Journal of Cosmology and Astroparticle Physics* 2017.12 (Dec. 2017), pp. 013–013. ISSN: 1475-7516. DOI: 10.1088/1475-7516/2017/12/013. URL: http://dx.doi.org/10.1088/1475-7516/2017/12/013.

[185] A. Boyarsky et al. "Sterile neutrino Dark Matter". In: *Progress in Particle and Nuclear Physics* 104 (2019), pp. 1–45. ISSN: 0146-6410. DOI: https://doi.org/10.1016/j.ppnp.2018.07.004. URL: https://www.sciencedirect.com/science/article/pii/S0146641018300711.

[186] A. Boyarsky et al. "Unidentified Line in X-Ray Spectra of the Andromeda Galaxy and Perseus Galaxy Cluster". In: *Physical Review Letters* 113.25 (Dec. 2014). ISSN: 1079-7114. DOI: 10.1103/physrevlett.113.251301. URL: http://dx.doi.org/10.1103/PhysRevLett.113.251301.

[187] K. Abazajian, G. M. Fuller, and W. H. Tucker. "Direct detection of warm dark matter in the X-ray". In: *Astrophys. J.* 562 (2001), pp. 593–604. DOI: 10.1086/323867. arXiv: astro-ph/0106002.

[188] A. Boyarsky, J. Nevalainen, and O. Ruchayskiy. "Constraints on the parameters of radiatively decaying dark matter from the dark matter halos of the Milky Way and Ursa Minor". In: *Astronomy Astrophysics* 471.1 (May 2007), pp. 51–57. ISSN: 1432-0746. DOI: 10.1051/0004-6361:20066774. URL: http://dx.doi.org/10.1051/0004-6361:20066774.

[189] A. Boyarsky, O. Ruchayskiy, and M. Markevitch. "Constraints on Parameters of Radiatively Decaying Dark Matter from the Galaxy Cluster 1E 065756". In: *The Astrophysical Journal* 673.2 (Feb. 2008), pp. 752–757. ISSN: 1538-4357. DOI: 10.1086/524397. URL: http://dx.doi.org/10.1086/524397.

[190] B. W. Lee and R. E. Shrock. "Natural suppression of symmetry violation in gauge theories: Muon- and electron-lepton-number nonconservation". In: *Phys. Rev. D* 16 (5 Sept. 1977), pp. 1444–1473. DOI: 10.1103/PhysRevD.16.1444. URL: https://link.aps.org/doi/10.1103/PhysRevD.16.1444.

[191] P. B. Pal and L. Wolfenstein. "Radiative decays of massive neutrinos". In: *Phys. Rev. D* 25 (3 Feb. 1982), pp. 766–773. DOI: 10.1103/PhysRevD.25.766. URL: https://link.aps.org/doi/10.1103/PhysRevD.25.766.

[192] Esra Bulbul et al. "Detection of An Unidentified Emission Line in the Stacked X-ray spectrum of Galaxy Clusters". In: *The Astrophysical Journal* 789.1 (June 2014), p. 13. DOI: 10.1088/0004-637X/789/1/13. URL: https://dx.doi.org/10.1088/0004-637X/789/1/13.

[193] M. Kawasaki and K. Murai. "Lepton Asymmetric Universe". In: (2022). DOI: 10.48550/ARXIV.2203.09713. URL: https://arxiv.org/abs/2203.09713.

[194] A. Strumia. "Baryogenesis via leptogenesis". In: (Aug. 2006), pp. 655–680. arXiv: hep-ph/0608347.

[195] M. Laine and M. Shaposhnikov. "Remark on sphaleron erasure of baryon asymmetry". In: *Physical Review D* 61.11 (May 2000). ISSN: 1089-4918. DOI: 10.1103/physrevd.61.117302. URL: http://dx.doi.org/10.1103/PhysRevD.61.117302.

[196] V. A. Kuzmin, V. A. Rubakov, and M. E. Shaposhnikov. "On anomalous electroweak baryon-number non-conservation in the early universe". In: *Physics Letters B* 155.1 (1985), pp. 36–42. ISSN: 0370-2693. DOI: https://doi.org/10.1016/0370-2693(85)91028-7. URL: https://www.sciencedirect.com/science/article/pii/0370269385910287.

[197] M. A. Luty. "Baryogenesis via leptogenesis". In: *Phys. Rev. D* 45 (2 Jan. 1992), pp. 455–465. DOI: 10.1103/PhysRevD.45.455. URL: https://link.aps.org/doi/10.1103/PhysRevD.45.455.

[198] S. Y. Khlebnikov and M. E. Shaposhnikov. "Melting of the Higgs vacuum: conserved numbers at high temperature". In: *Physics Letters B* 387.4 (Oct. 1996), pp. 817–822. ISSN: 0370-2693. DOI: 10.1016/0370-2693(96)01116-1. URL: http://dx.doi.org/10.1016/0370-2693(96)01116-1.

[199] S. Davidson and A. Ibarra. "A lower bound on the right-handed neutrino mass from leptogenesis". In: *Physics Letters B* 535.1-4 (May 2002), pp. 25–32. ISSN: 0370-2693. DOI: 10.1016/s0370-2693(02)01735-5. URL: http://dx.doi.org/10.1016/S0370-2693(02)01735-5.

[200] F. Vissani. "Do experiments suggest a hierarchy problem?" In: *Physical Review D* 57.11 (June 1998), pp. 7027–7030. ISSN: 1089-4918. DOI: 10.1103/physrevd.57.7027. URL: http://dx.doi.org/10.1103/PhysRevD.57.7027.

[201] J. Klaric, M. Shaposhnikov, and I. Timiryasov. "Reconciling resonant leptogenesis and baryogenesis via neutrino oscillations". In: *Physical Review D* 104.5 (Sept. 2021). ISSN: 2470-0029. DOI: 10.1103/physrevd.104.055010. URL: http://dx.doi.org/10.1103/PhysRevD.104.055010.

[202] A. D. Simone and A. Riotto. "On resonant leptogenesis". In: *Journal of Cosmology and Astroparticle Physics* 2007.08 (Aug. 2007), pp. 013–013. ISSN: 1475-7516. DOI: 10.1088/1475-7516/2007/08/013. URL: http://dx.doi.org/10.1088/1475-7516/2007/08/013.

[203] M. Garny, A. Kartavtsev, and A. Hohenegger. "Leptogenesis from first principles in the resonant regime". In: *Annals of Physics* 328 (Jan. 2013), pp. 26–63. ISSN: 0003-4916. DOI: 10.1016/j.aop.2012.10.007. URL: http://dx.doi.org/10.1016/j.aop.2012.10.007.

[204] P. S. B. Dev et al. "Flavour covariant transport equations: An application to resonant leptogenesis". In: *Nuclear Physics B* 886 (Sept. 2014), pp. 569–664. ISSN: 0550-3213. DOI: 10.1016/j.nuclphysb.2014.06.020. URL: http://dx.doi.org/10.1016/j.nuclphysb.2014.06.020.

[205] P. S. B. Dev et al. "Flavour Covariant Formalism for Resonant Leptogenesis". In: *Nuclear and Particle Physics Proceedings* 273-275 (Apr. 2016), pp. 268–274. ISSN: 2405-6014. DOI: 10.1016/j.nuclphysbps.2015.09.037. URL: http://dx.doi.org/10.1016/j.nuclphysbps.2015.09.037.

[206] S. Davidson, E. Nardi, and Y. Nir. "Leptogenesis". In: *Physics Reports* 466.4-5 (Sept. 2008), pp. 105–177. ISSN: 0370-1573. DOI: 10.1016/j.physrep.2008.06.002. URL: http://dx.doi.org/10.1016/j.physrep.2008.06.002.

[207] A. Pilaftsis. "Resonant Leptogenesis with Observable Lepton Number Violation". In: *Physical Review Letters* 95.8 (Aug. 2005). ISSN: 1079-7114. DOI: 10.1103/physrevlett.95.081602. URL: http://dx.doi.org/10.1103/PhysRevLett.95.081602.

[208] A. Pilaftsis and T. E. J. Underwood. "Electroweak-scale resonant leptogenesis". In: *Physical Review D* 72.11 (Dec. 2005). ISSN: 1550-2368. DOI: 10.1103/physrevd.72.113001. URL: http://dx.doi.org/10.1103/PhysRevD.72.113001.

[209] F. F. Deppisch and A. Pilaftsis. "Lepton flavor violation and13in minimal resonant leptogenesis". In: *Physical Review D* 83.7 (Apr. 2011). ISSN: 1550-2368. DOI: 10.1103/physrevd.83.076007. URL: http://dx.doi.org/10.1103/PhysRevD.83.076007.

[210] F. F. Deppisch and A. Pilaftsis. "Minimal resonant leptogenesis and lepton flavour violation". In: *AIP Conference Proceedings* (2012). ISSN: 0094-243X. DOI: 10.1063/1.4742094. URL: http://dx.doi.org/10.1063/1.4742094.

[211] L. Duarte, J. Peressutti, and O. A. Sampayo. "Majorana neutrino decay in an effective approach". In: *Physical Review D* 92.9 (Nov. 2015). ISSN: 1550-2368. DOI: 10.1103/physrevd.92.093002. URL: http://dx.doi.org/10.1103/PhysRevD.92.093002.

[212] F. Bezrukov, H. Hettmansperger, and M. Lindner. "keV sterile neutrino Dark Matter in gauge extensions of the Standard Model". In: *Phys. Rev. D* 81 (2010), p. 085032. DOI: 10.1103/PhysRevD.81.085032. arXiv: 0912.4415 [hep-ph].

[213] P.S. Bhupal Dev et al. "Kadanoff–Baym approach to flavour mixing and oscillations in resonant leptogenesis". In: *Nuclear Physics B* 891 (Feb. 2015), pp. 128–158. DOI: 10.1016/j.nuclphysb.2014.12.003. URL: https://doi.org/10.1016%2Fj.nuclphysb.2014.12.003.

[214] A. A. Starobinsky. "A New Type of Isotropic Cosmological Models Without Singularity". In: *Phys. Lett. B* 91 (1980). Ed. by I.M. Khalatnikov and V.P. Mineev, pp. 99–102. DOI: 10.1016/0370-2693(80)90670-X.

[215] V. F. Mukhanov and G. V. Chibisov. "Quantum Fluctuations and a Nonsingular Universe". In: *JETP Lett.* 33 (1981), pp. 532–535.

[216] A. H. Guth. "The Inflationary Universe: A Possible Solution to the Horizon and Flatness Problems". In: *Phys. Rev. D* 23 (1981). Ed. by Li-Zhi Fang and R. Ruffini, p. 347. DOI: 10.1103/PhysRevD.23.347.

[217] Andrei D. Linde. "A New Inflationary Universe Scenario: A Possible Solution of the Horizon, Flatness, Homogeneity, Isotropy and Primordial Monopole Problems". In: *Phys. Lett. B* 108 (1982). Ed. by L. Fang and R. Ruffini, p. 389. DOI: 10.1016/0370-2693(82)91219-9.

[218] A. Albrecht and P. J. Steinhardt. "Cosmology for Grand Unified Theories with Radiatively Induced Symmetry Breaking". In: *Phys. Rev. Lett.* 48 (1982). Ed. by Li-Zhi Fang and R. Ruffini, pp. 1220–1223. DOI: 10.1103/PhysRevLett.48.1220.

[219] D. I. Kaiser. "Primordial spectral indices from generalized Einstein theories". In: *Physical Review D* 52.8 (Oct. 1995), pp. 4295–4306. ISSN: 0556-2821. DOI: 10.1103/physrevd.52.4295. URL: http://dx.doi.org/10.1103/PhysRevD.52.4295.

[220] E. Komatsu and T. Futamase. "Complete constraints on a nonminimally coupled chaotic inflationary scenario from the cosmic microwave background". In: *Physical Review D* 59.6 (Feb. 1999). ISSN: 1089-4918. DOI: 10.1103/physrevd.59.064029. URL: http://dx.doi.org/10.1103/PhysRevD.59.064029.

[221] A. R. Liddle and D. H. Lyth. "The cold dark matter density perturbation". In: *Physics Reports* 231.1–2 (Aug. 1993), pp. 1–105. ISSN: 0370-1573. DOI: 10.1016/0370-1573(93)90114-s. URL: http://dx.doi.org/10.1016/0370-1573(93)90114-S.

[222] J. L. F. Barbón and J. R. Espinosa. "On the Naturalness of Higgs inflation". In: *Physical Review D* 79.8 (Apr. 2009). DOI: 10.1103/physrevd.79.081302. URL: https://doi.org/10.1103%2Fphysrevd.79.081302.

[223] C. P. Burgess, H. M. Lee, and M. Trott. "On Higgs inflation and naturalness". In: *Journal of High Energy Physics* 2010.7 (July 2010). DOI: 10.1007/jhep07(2010)007. URL: https://doi.org/10.1007%2Fjhep07%282010%29007.

[224] M. P. Hertzberg. "On inflation with non-minimal coupling". In: *Journal of High Energy Physics* 2010.11 (Nov. 2010). DOI: 10.1007/jhep11(2010)023. URL: https://doi.org/10.1007%2Fjhep11%282010%29023.

[225] F. Bezrukov et al. "Higgs inflation: consistency and generalisations". In: *Journal of High Energy Physics* 2011.1 (Jan. 2011). DOI: 10.1007/jhep01(2011)016. URL: https://doi.org/10.1007%2Fjhep01%282011%29016.

[226] D. H. Lyth and A. Riotto. "Particle physics models of inflation and the cosmological density perturbation". In: *Physics Reports* 314.1-2 (June 1999), pp. 1–146. ISSN: 0370-1573. DOI: 10.1016/s0370-1573(98)00128-8. URL: http://dx.doi.org/10.1016/S0370-1573(98)00128-8.

[227] S. E. Larsson, S. Sarkar, and P. L. White. "Evading the cosmological domain wall problem". In: *Physical Review D* 55.8 (Apr. 1997), pp. 5129–5135. ISSN: 1089-4918. DOI: 10.1103/physrevd.55.5129. URL: http://dx.doi.org/10.1103/PhysRevD.55.5129.

[228] G. Dvali and G. Senjanović. "Is There a Domain Wall Problem?" In: *Physical Review Letters* 74.26 (June 1995), pp. 5178–5181. ISSN: 1079-7114. DOI: 10.1103/physrevlett.74.5178. URL: http://dx.doi.org/10.1103/PhysRevLett.74.5178.

[229] S. A. Abel, S. Sarkar, and P. L. White. "On the cosmological domain wall problem for the minimally extended supersymmetric standard model". In: *Nuclear Physics B* 454.3 (Nov. 1995), pp. 663–681. ISSN: 0550-3213. DOI: 10.1016/0550-3213(95)00483-9. URL: http://dx.doi.org/10.1016/0550-3213(95)00483-9.

[230] P. B. Greene, A. Linde L. Kofman, and A. A. Starobinsky. "Structure of resonance in preheating after inflation". In: *Physical Review D* 56.10 (Nov. 1997), pp. 6175–6192. ISSN: 1089-4918. DOI: 10.1103/physrevd.56.6175. URL: http://dx.doi.org/10.1103/PhysRevD.56.6175.

[231] L. Kofman, A. D. Linde, and A. A. Starobinsky. "Towards the theory of reheating after inflation". In: *Phys. Rev. D* 56 (1997), pp. 3258–3295. DOI: 10.1103/PhysRevD.56.3258. arXiv: hep-ph/9704452.

[232] R. Micha and I. I. Tkachev. "Turbulent thermalization". In: *Physical Review D* 70.4 (Aug. 2004). ISSN: 1550-2368. DOI: 10.1103/physrevd.70.043538. URL: http://dx.doi.org/10.1103/PhysRevD.70.043538.

[233] R. Micha and I. I. Tkachev. "Relativistic Turbulence: A Long Way from Preheating to Equilibrium". In: *Phys. Rev. Lett.* 90 (12 Mar. 2003), p. 121301. DOI: 10.1103/PhysRevLett.90.121301. URL: https://link.aps.org/doi/10.1103/PhysRevLett.90.121301.

[234] I. Boiarska et al. "Phenomenology of GeV-scale scalar portal". In: *Journal of High Energy Physics* 2019.11, 162 (Nov. 2019), p. 162. DOI: 10.1007/JHEP11(2019)162. arXiv: 1904.10447 [hep-ph].

[235] The NA62 Collaboration. "Measurement of the very rare $K^+ \to \pi^+\nu\overline{\nu}$ decay". In: *Journal of High Energy Physics* 2021.6 (June 2021). ISSN: 1029-8479. DOI: 10.1007/jhep06(2021)093. URL: http://dx.doi.org/10.1007/JHEP06(2021)093.

[236] G. Krnjaic. "Probing light thermal dark matter with a Higgs portal mediator". In: *Physical Review D* 94.7 (Oct. 2016). DOI: 10.1103/physrevd.94.073009. URL: https://doi.org/10.1103%2Fphysrevd.94.073009.

[237] M. J. Dolan et al. "A taste of dark matter: flavour constraints on pseudoscalar mediators". In: *Journal of High Energy Physics* 2015.3 (Mar. 2015). DOI: 10.1007/jhep03(2015)171. URL: https://doi.org/10.1007%2Fjhep03%282015%29171.

[238] N.G. Deshpande, G. Eilam, and J. Jiang. "On the possibility of a new boson X0(214MeV) in +→p+". In: *Physics Letters B* 632.2 (2006), pp. 212–214. ISSN: 0370-2693. DOI: https://doi.org/10.1016/j.physletb.2005.10.050. URL: https://www.sciencedirect.com/science/article/pii/S037026930501539X.

[239] H. Leutwyler and M. A. Shifman. "Light Higgs Particle in Decays of K and η Mesons". In: *Nucl. Phys. B* 343 (1990), pp. 369–397. DOI: 10.1016/0550-3213(90)90475-S.

[240] Hai-Yang Cheng and Hoi-Lai Yu. "Are there really no experimental limits on a light Higgs boson from kaon decay?" In: *Phys. Rev. D* 40 (9 Nov. 1989), pp. 2980–2986. DOI: 10.1103/PhysRevD.40.2980. URL: https://link.aps.org/doi/10.1103/PhysRevD.40.2980.

[241] S. Weinberg. "Nonlinear Realizations of Chiral Symmetry". In: *Phys. Rev.* 166 (5 Feb. 1968), pp. 1568–1577. DOI: 10.1103/PhysRev.166.1568. URL: https://link.aps.org/doi/10.1103/PhysRev.166.1568.

[242] J. A. Cronin. "Phenomenological Model of Strong and Weak Interactions in Chiral $U(3) \bigotimes U(3)$". In: *Phys. Rev.* 161 (5 Sept. 1967), pp. 1483–1494. DOI: 10.1103/PhysRev.161.1483. URL: https://link.aps.org/doi/10.1103/PhysRev.161.1483.

[243] J. Wess and B. Zumino. "Lagrangian Method for Chiral Symmetries". In: *Phys. Rev., 163: 1727-35(Nov. 25, 1967).* (Jan. 1967). DOI: 10.1103/PhysRev.163.1727. URL: https://www.osti.gov/biblio/4492657.

[244] NA62 Collaboration. "Search for π_0 decays to invisible particles". In: *Journal of High Energy Physics* 2021.2 (Feb. 2021). ISSN: 1029-8479. DOI: 10.1007/jhep02(2021)201. URL: http://dx.doi.org/10.1007/JHEP02(2021)201.

[245] A. V. Artamonov et al. "Study of the decay $K^+ \to \pi^+ \nu\bar{\nu}$ in the momentum region $140 < P_\pi < 199$ MeV/c". In: *Phys. Rev. D* 79 (2009), p. 092004. DOI: 10.1103/PhysRevD.79.092004. arXiv: 0903.0030 [hep-ex].

[246] M. W. Winkler. "Decay and detection of a light scalar boson mixing with the Higgs boson". In: *Physical Review D* 99.1 (Jan. 2019). ISSN: 2470-0029. DOI: 10.1103/physrevd.99.015018. URL: http://dx.doi.org/10.1103/PhysRevD.99.015018.

[247] J. R. Batley et al. "Searches for lepton number violation and resonances in $K^\pm \to \pi\mu\mu$ decays". In: *Phys. Lett. B* 769 (2017), pp. 67–76. DOI: 10.1016/j.physletb.2017.03.029. arXiv: 1612.04723 [hep-ex].

[248] R. Aaij et al. "Search for long-lived scalar particles in $B^+ \to K^+\chi(\mu^+\mu^-)$ decays". In: *Phys. Rev. D* 95 (7 Apr. 2017), p. 071101. DOI: 10.1103/PhysRevD.95.071101. URL: https://link.aps.org/doi/10.1103/PhysRevD.95.071101.

[249] R. Aaij et al. "Search for Hidden-Sector Bosons in $B^0 \to K^{*0}\mu^+\mu^-$ Decays". In: *Phys. Rev. Lett.* 115 (16 Oct. 2015), p. 161802. DOI: 10.1103/PhysRevLett.115.161802. URL: https://link.aps.org/doi/10.1103/PhysRevLett.115.161802.

[250] J.-T. Wei et al. "Measurement of the Differential Branching Fraction and Forward-Backward Asymmetry for $B \to K^{(*)}l^+l^-$". In: *Phys. Rev. Lett.* 103 (17 Oct. 2009), p. 171801. DOI: 10.1103/PhysRevLett.103.171801. URL: https://link.aps.org/doi/10.1103/PhysRevLett.103.171801.

[251] G. Steigman M. Kawasaki and H. Kang. "Cosmological evolution of an early decaying particle". In: *Nucl. Phys. B* 403 (1993), pp. 671–706. DOI: 10.1016/0550-3213(93)90366-W.

[252] H. Kang, M. Kawasaki, and G. Steigman. "Cosmological evolution of generic early decaying particles and their daughters". In: *Nucl. Phys. B* 402 (1993), pp. 323–348. DOI: 10.1016/0550-3213(93)90645-6.

[253] J. König, A. Merle, and M. Totzauer. "keV Sterile Neutrino Dark Matter from Singlet Scalar Decays: The Most General Case". In: *JCAP* 11 (2016), p. 038. DOI: 10.1088/1475-7516/2016/11/038. arXiv: 1609.01289 [hep-ph].

[254] A. Merle and M. Totzauer. "keV Sterile Neutrino Dark Matter from Singlet Scalar Decays: Basic Concepts and Subtle Features". In: *JCAP* 06 (2015), p. 011. DOI: 10.1088/1475-7516/2015/06/011. arXiv: 1502.01011 [hep-ph].

[255] M. Tanabashi et al. "Review of Particle Physics". In: *Phys. Rev. D* 98 (3 Aug. 2018), p. 030001. DOI: 10.1103/PhysRevD.98.030001. URL: https://link.aps.org/doi/10.1103/PhysRevD.98.030001.

[256] G. Bertone and D. Hooper. "History of dark matter". In: *Rev. Mod. Phys.* 90.4 (2018), p. 045002. DOI: 10.1103/RevModPhys.90.045002. arXiv: 1605.04909 [astro-ph.CO].

[257] F. Bezrukov and D. Gorbunov. "Applicability of approximations used in calculations of the spectrum of dark matter particles produced in particle decays". In: *Phys. Rev. D* 93.6 (2016), p. 063502. DOI: 10.1103/PhysRevD.93.063502. arXiv: 1412.1341 [hep-ph].

[258] F. Bergsma et al. "Search for axion-like particle production in 400 GeV proton-copper interactions". In: *Physics Letters B* 157.5 (1985), pp. 458–462. ISSN: 0370-2693. DOI: https://doi.org/10.1016/0370-2693(85)90400-9. URL: https://www.sciencedirect.com/science/article/pii/0370269385904009.

[259] J. A. Evans et al. "Light Dark Matter from Entropy Dilution". In: *Journal of High Energy Physics* 2020.2 (Feb. 2020). DOI: 10.1007/jhep02(2020)151. URL: https://doi.org/10.1007%2Fjhep02%282020%29151.

[260] J. Hasenkamp and J. Kersten. "Leptogenesis, gravitino dark matter, and entropy production". In: *Physical Review D* 82.11 (Dec. 2010). DOI: 10.1103/physrevd.82.115029. URL: https://doi.org/10.1103%2Fphysrevd.82.115029.

[261] R. J. Scherrer and M. S. Turner. "Decaying particles do not "heat up" the Universe". In: *Phys. Rev. D* 31 (4 Feb. 1985), pp. 681–688. DOI: 10.1103/PhysRevD.31.681. URL: https://link.aps.org/doi/10.1103/PhysRevD.31.681.

[262] S. Eijima, M. Shaposhnikov, and I. Timiryasov. "Freeze-in generation of lepton asymmetries after baryogenesis in the νMSM". In: (2020). arXiv: 2011.12637 [hep-ph].

[263] F. Bezrukov et al. "Higgs Boson Mass and New Physics". In: *JHEP* 10 (2012). Ed. by Gudrid Moortgat-Pick, p. 140. DOI: 10.1007/JHEP10(2012)140. arXiv: 1205.2893 [hep-ph].

[264] J. Elias-Miró et al. "Higgs mass implications on the stability of the electroweak vacuum". In: *Physics Letters B* 709.3 (Mar. 2012), pp. 222–228. ISSN: 0370-2693. DOI: 10.1016/j.physletb.2012.02.013. URL: http://dx.doi.org/10.1016/j.physletb.2012.02.013.

[265] K. Kohri and H. Matsui. "Electroweak vacuum instability and renormalized Higgs field vacuum fluctuations in the inflationary universe". In: *Journal of Cosmology and Astroparticle Physics* 2017.08 (Aug. 2017), pp. 011–011. ISSN: 1475-7516. DOI: 10.1088/1475-7516/2017/08/011. URL: http://dx.doi.org/10.1088/1475-7516/2017/08/011.

[266] O. Lebedev and A. Westphal. "Metastable electroweak vacuum: Implications for inflation". In: *Physics Letters B* 719.4-5 (Feb. 2013), pp. 415–418. ISSN: 0370-2693. DOI: 10.1016/j.physletb.2012.12.069. URL: http://dx.doi.org/10.1016/j.physletb.2012.12.069.

[267] K. G. Chetyrkin and M. F. Zoller. "Three-loop β-functions for top-Yukawa and the Higgs self-interaction in the standard model". In: *Journal of High Energy Physics* 2012.6 (June 2012). ISSN: 1029-8479. DOI: 10.1007/jhep06(2012)033. URL: http://dx.doi.org/10.1007/JHEP06(2012)033.

[268] J. R. Espinosa, G. F. Giudice, and A. Riotto. "Cosmological implications of the Higgs mass measurement". In: *Journal of Cosmology and Astroparticle Physics* 2008.05 (May 2008), p. 002. ISSN: 1475-7516. DOI: 10.1088/1475-7516/2008/05/002. URL: http://dx.doi.org/10.1088/1475-7516/2008/05/002.

[269] G. Isidori, G. Ridolfi, and A. Strumia. "On the metastability of the Standard Model vacuum". In: *Nuclear Physics B* 609.3 (Aug. 2001), pp. 387–409. ISSN: 0550-3213. DOI: 10.1016/s0550-3213(01)00302-9. URL: http://dx.doi.org/10.1016/S0550-3213(01)00302-9.

[270] M. Aaboud et al. "Combination of Searches for Invisible Higgs Boson Decays with the ATLAS Experiment". In: *Physical Review Letters* 122.23 (June 2019). ISSN: 1079-7114. DOI: 10.1103/physrevlett.122.231801. URL: http://dx.doi.org/10.1103/PhysRevLett.122.231801.

[271] R. Aaij et al. "Search for long-lived scalar particles in $B^+ \to K^+\chi(\mu^+\mu^-)$ decays". In: *Phys. Rev. D* 95.7 (2017), p. 071101. DOI: 10.1103/PhysRevD.95.071101. arXiv: 1612.07818 [hep-ex].

[272] R. Aaij et al. "Search for hidden-sector bosons in $B^0 \to K^{*0}\mu^+\mu^-$ decays". In: *Phys. Rev. Lett.* 115.16 (2015), p. 161802. DOI: 10.1103/PhysRevLett.115.161802. arXiv: 1508.04094 [hep-ex].

[273] A. V. Artamonov et al. "New measurement of the $K^+ \to \pi^+\nu\bar{\nu}$ branching ratio". In: *Phys. Rev. Lett.* 101 (2008), p. 191802. DOI: 10.1103/PhysRevLett.101.191802. arXiv: 0808.2459 [hep-ex].

[274] M. S. Turner. "Axions from SN 1987a". In: *Phys. Rev. Lett.* 60 (1988), p. 1797. DOI: 10.1103/PhysRevLett.60.1797.

[275] J. A. Frieman, S. Dimopoulos, and M. S. Turner. "Axions and stars". In: *Phys. Rev. D* 36 (8 Oct. 1987), pp. 2201–2210. DOI: 10.1103/PhysRevD.36.2201. URL: https://link.aps.org/doi/10.1103/PhysRevD.36.2201.

[276] A. Burrows, M. S. Turner, and R. P. Brinkmann. "Axions and SN 1987A". In: *Phys. Rev. D* 39 (4 Feb. 1989), pp. 1020–1028. DOI: 10.1103/PhysRevD.39.1020. URL: https://link.aps.org/doi/10.1103/PhysRevD.39.1020.

[277] R Essig et al. "Discovering new light states at neutrino experiments". In: *Phys. Rev. D* 82 (11 Dec. 2010), p. 113008. DOI: 10.1103/PhysRevD.82.113008. URL: https://link.aps.org/doi/10.1103/PhysRevD.82.113008.

[278] J. Beacham et al. "Physics beyond colliders at CERN: beyond the Standard Model working group report". In: *Journal of Physics G: Nuclear and Particle Physics* 47.1 (Dec. 2019), p. 010501. ISSN: 1361-6471. DOI: 10.1088/1361-6471/ab4cd2. URL: http://dx.doi.org/10.1088/1361-6471/ab4cd2.

[279] A. Filimonova, R. Schäfer, and S. Westhoff. "Probing dark sectors with long-lived particles at Belle II". In: *Physical Review D* 101.9 (May 2020). ISSN: 2470-0029. DOI: 10.1103/physrevd.101.095006. URL: http://dx.doi.org/10.1103/PhysRevD.101.095006.

[280] D. Gorbunov, I. Krasnov, and S. Suvorov. "Constraints on light scalars from PS191 results". In: *Physics Letters B* 820 (Sept. 2021), p. 136524. ISSN: 0370-2693. DOI: 10.1016/j.physletb.2021.136524. URL: http://dx.doi.org/10.1016/j.physletb.2021.136524.

[281] A. Salvio et al. "On gravitational and thermal corrections to vacuum decay". In: *Journal of High Energy Physics* 2016.9 (Sept. 2016). ISSN: 1029-8479. DOI: 10.1007/jhep09(2016)054. URL: http://dx.doi.org/10.1007/JHEP09(2016)054.

[282] L. D. Rose, C. Marzo, and A. Urbano. "On the fate of the Standard Model at finite temperature". In: *Journal of High Energy Physics* 2016.5 (May 2016). ISSN: 1029-8479. DOI: 10.1007/jhep05(2016)050. URL: http://dx.doi.org/10.1007/JHEP05(2016)050.

[283] J. R. Espinosa and M. Quirós. "Improved metastability bounds on the Standard Model Higgs mass". In: *Physics Letters B* 353.2-3 (June 1995), pp. 257–266. ISSN: 0370-2693. DOI: 10.1016/0370-2693(95)00572-3. URL: http://dx.doi.org/10.1016/0370-2693(95)00572-3.

[284] L. M. Krauss and M. Trodden. "Baryogenesis below The Electroweak Scale". In: *Physical Review Letters* 83.8 (Aug. 1999), pp. 1502–1505. DOI: 10.1103/physrevlett.83.1502. URL: https://doi.org/10.1103%2Fphysrevlett.83.1502.

[285] M. Trodden. "Making Baryons Below the Electroweak Scale". In: (Sept. 2000). DOI: 10.1142/9789812792129_0062. URL: https://doi.org/10.1142%2F9789812792129_0062.

[286] A. Pich. "Chiral perturbation theory". In: *Reports on Progress in Physics* 58.6 (June 1995), pp. 563–609. DOI: 10.1088/0034-4885/58/6/001. URL: https://doi.org/10.1088%2F0034-4885%2F58%2F6%2F001.

[287] S. Scherer. "Introduction to Chiral Perturbation Theory". In: (2002). DOI: 10.48550/ARXIV.HEP-PH/0210398. URL: https://arxiv.org/abs/hep-ph/0210398.

[288] M. E. Peskin and D. V. Schroeder. *An Introduction to quantum field theory*. Reading, USA: Addison-Wesley, 1995. ISBN: 978-0-201-50397-5.